

SYNTHESIS AND BIOLOGICAL EVALUATION OF PENTAFLUOROPHOSPHATES AS AMPHIPHILIC NON-CLEAVABLE PHOSPHATASE INHIBITORS

Inaugural-Dissertation

to obtain of the academic degree

Doctor rerum naturalium (Dr. rer. nat.)

submitted to the Department of Biology, Chemistry, Pharmacy

of Freie Universität Berlin

by

Matteo Accorsi

2022

The present work is part of the research that has been conducted under the supervision of Prof. Dr. Jörg Rademann in the time between March 2015 and April 2021 at the Institut für Pharmazie of the Freie Universität Berlin.

1st reviewer: Prof. Dr. Jörg Rademann

2nd reviewer: Prof Dr. Bettina Keller

date of defense: 09/09/22

To my parents

“Study hard what interests you the most
in the most undisciplined, irreverent and original manner possible.”

- Richard Feynmann

Part of this work has been already published:

[1] S. Wagner, M. Accorsi, J. Rademann, "Benzyl Mono-*P*-Fluorophosphonate and Benzyl Penta-*P*-Fluorophosphate Anions Are Physiologically Stable Phosphotyrosine Mimetics and Inhibitors of Protein Tyrosine Phosphatases" *Chemistry* **2017**, *23*, 15387-15395. <https://doi.org/10.1002/chem.201701204>

[2] J. Rademann, S. Wagner, M. Accorsi "Pentafluorophosphate derivative, its uses and an appropriate manufacturing method" Europäische Patentanmeldung, 13.09.2017, 17190937.7

[3] W. Hoffmann, J. Langenhan, S. Huhmann, J. Moschner, R. Chang, M. Accorsi, J. Seo, J. Rademann, G. Meijer, B. Kokschi, M. T. Bowers, G. von Helden, K. Pagel, "An Intrinsic Hydrophobicity Scale for Amino Acids and Its Application to Fluorinated Compounds" *Angew. Chem. Int. Ed. Engl.* **2019**, *58*, 8216-8220. <https://doi.org/10.1002/anie.201813954>

Manuscripts in preparation:

[4] M. Accorsi, M. Tiemann, L. Wehrhan, L. M. Finn, R. Cruz, M. Rautenberg, F. Hemmerling, J. Heberle, B. G. Keller, J. Rademann, *Angewandte Chemie* **2022**, *submitted*

[5] H. Qianzhu, M. Accorsi, M. Tiemann, T. Huber, J. Rademann, *in preparation*

.

Acknowledgements

The preparation of this work was possible thanks to the support of many different people that encouraged and accompanied me in this journey with patience and determination.

I would like to thank Prof. Dr. Jörg Rademann for giving me the chance to work in his research group on interesting and challenging project, for allowing me to investigate autonomously and mentoring me at critical stages of the research. Also, I am grateful to Prof. Dr. Keller for accepting to be the second reviewer.

My gratitude goes to Ms. Regina Allner, Dr. Annette Kietzmann and Dr. Christoph Arkona, Thomas Rudolf, Silke Bergemann, Eleonore Christmann as well as the analytic department for the precious support I received in many different aspects during this experience, scientifically and emotionally.

I would like to thank all the lab colleagues encountered during these years: Christina Fischer, Mike Jaegle, Sebastian Kohling, Eric Nawrotzky, EeLin Wong, Joana Blaszkiewicz, Franziska Gottschalk, Lisa Redl, Stefan Wagner, Caroline Tauber, Rebekka Wamser, Damian Klemczak, Jan Dürig, Barbara Schröder, Enaam Masri, Xinning Wang, Juwen Jia, Wei Song, Peter Demirel, Peter Varga, Saan Voss, Umar Aziz and Ali Saoud, as well as Doğuş Işık, Alexandra Gruber and Phuong Tran for the friendly atmosphere and the support, for the pleasant working atmosphere and the collaborative spirit that I have experienced during my stay. A special acknowledgement goes to Timon Kurzawa, Tommaso Pecchioli, Matthias Henrot, Gabriella Ambrosio, Massimo Rigo and Markus Tiemann, for the many fruitful discussions and for the valuable help inside and outside the lab.

Last but not least, I would like to thank my friends in Italy, in Berlin (viva i fioi), the ones now all over the world, and my family for the unconditional and endless support I received during these challenging years.

All of you are, and will stay, in my heart.

Declaration of Independence

Herewith I certify that I have prepared and written my thesis independently and that I have not used any sources and aids other than those indicated by me.

This manuscript was not submitted to any other institution.

Table of Contents

1	Introduction	1
1.1	Post-translational modifications of proteins	1
1.2	Phosphorylation	2
1.3	Protein tyrosine phosphatase 1B	10
1.4	Fluorine: a peculiar element.....	27
2	Aim of the project.....	38
3	Results and Discussion	40
3.1	Early chemical synthesis of pentafluorophosphates.....	40
3.2	Extension of the strategic plan to PF ₅ amino acid.....	51
3.3	Optimization of the perfluorination reaction.....	61
3.4	Preparation of the building block for Fmoc-based solid phase peptide synthesis (SPPS).....	74
3.5	Computational Analysis.....	77
3.6	Determination of lipophilicity.....	82
3.7	Stability of aryl <i>gem</i> difluoromethylen pentafluorophosphate towards commonly employed SPPS conditions	86
3.8	Peptide synthesis.....	91
3.9	Determination of inhibitory potential.....	103
4	Summary and Outlook and future perspectives	108
5	Zusammenfassung und Ausblick	112
6	Experimental Part	116
6.1	Materials and methods.....	116
6.2	Chemical Synthesis.....	120
7	NMR spectra.....	139
8	References	157

Abbreviations

Abbreviations

ACN	Acetonitrile
ADP	Adenosine diphosphate
ATP	Adenosine triphosphate
CNS	Central nervous system
DAST	Dimethylaminosulfur trifluoride
DBU	1,8-Diazabicyclo[5.4.0]undec-7-ene
DCM	Dichloromethane
DIC	N,N'-Diisopropylcarbodiimide
DiFMUP	6,8-Difluoro-4-Methylumbelliferyl Phosphate
DIPEA	Diisopropyl ethyl amine
Dme	dimethoxyethane
DMF	N,N-Dimethylformamide
DMSO	Dimethyl sulfoxide
DNA	Deoxyribonucleic acid
Dppp	1,3-Bis(diphenylphosphino)propane
EDCI	1-Ethyl-3-(3-dimethylaminopropyl)carbodiimid
GABA	γ -aminobutyric acid
GSK3	Glycogen synthase 3
HFIP	Hexafluoro-2-propanol
HOBt	N-Hydroxybenzotriazole
IC ₅₀	Inhibitory concentration 50%
IM-MS	Ion mobility mass spectrometry
IR	Infrared

Abbreviations

Jak2	Janus-Kinase 2
LC - MS	Liquid chromatography - Mass spectrometry
MAP	Mitogen activated protein
NMR	Nuclear magnetic resonance
NfF	Perfluorobutanesulfonyl fluoride
<i>p</i> -NPP	<i>para</i> -nitrophenyl phosphate
PDB	Protein data bank
PET	Positron emission tomography
PKB	Protein kinase B
PTB	Phosphotyrosine binding domains
PTK	Protein tyrosine kinase(s)
PTM	Post translational modification
PTP	Protein tyrosine phosphatase(s)
PTP1B	Protein tyrosine phosphatase 1B
PVP-HF	Poly-[4-vinylpyridinium-poly-(hydrogenfluoride)]
ROS	Reactive oxygen species
SEIRA	Surface enhanced infrared absorption spectroscopy
SH2	Src-homology 2 domain
SPPS	Solid phase peptide synthesis
SSRI	Selective serotonin reuptake inhibitors
STAT	Signal transduced and activator of transcription
Src	abbreviation for "sarcoma"
SUMO	Small ubiquitine related modifier
TBTU	2-(1H-Benzotriazole-1-yl)-1,1,3,3-tetramethylamminium tetrafluoroborate

Abbreviations

TCEP	Tris-(2-carboxyethyl)-phosphin
TFA	Trifluoroacetic acid
TMACl	Tetramethylammonium chloride
TMAF	Tetramethylammonium fluoride
TMSBr	Trimethylsilyl bromide
TMSCl	Trimethylsilyl chloride
TMSI	Trimethylsilyl iodide
TOF	Time of flight
UV	Ultraviolet
WHO	World health organization

Abstract

Phosphorylation is known to regulate a myriad of vital biological processes in cells and misregulation is associated with several diseases that include cancer, multiple sclerosis and diabetes. Scientific research has demonstrated that phosphatases have a high potential as pharmaceutical targets, and phosphatase inhibitors can ideally be designed to selectively modulate enzyme activities in order to achieve a therapeutic effect. The value of *gem*-difluoromethylen phosphonic acids as hydrophilic non-cleavable phosphate mimetics is well known in literature but their inability to penetrate cell membranes is a strong limiting factor for *in vivo* applications.

The aim of this work was the identification and the subsequent fine tuning of a convenient synthetic route from commercially available phenylalanine to pentafluorophosphates, as well as the incorporation of these fluorine-rich, amphiphilic phosphotyrosine mimetics in peptides. Although acid sensibility of pentafluorophosphates hampered the identification of a protocol compatible with solid phase peptide synthesis (SPPS), this was ultimately achieved using an excess of fluorides that allowed the synthesis of mono and bivalent model peptides. After the synthesis on solid support, the determination of the inhibitory potential against protein tyrosine phosphatase 1B (PTP1B) was determined in a photometric assay.

Furthermore, in a joint research work it was possible to further investigate properties and potential of this moiety, including the crystal structure and the lipophilicity of the first pentafluorinated amino acid.

Abstract

1 Introduction

1.1 Post-translational modifications of proteins

Living organisms rely on a highly complex and interconnected network of biochemical reactions which regulate fundamental processes of cellular life.

Post-translational modifications (PTM) of proteins play a key role in the regulation of functions such as cell mobility, protein synthesis, replication and cell death; among the possible changes that a protein can undergo, phosphorylation is one of the most common. Other common modifications via attachments of small chemical groups are acetylation reactions and methylation. Bigger molecules or even other proteins can be attached to proteins. Examples on this regard are glycosylation or isoprenylation for the former, and sumoylation and ubiquitylation for the latter. These last two modifications can influence protein activity by allosteric inhibition or tagging the protein for degradation via proteolysis, respectively. ^[1]

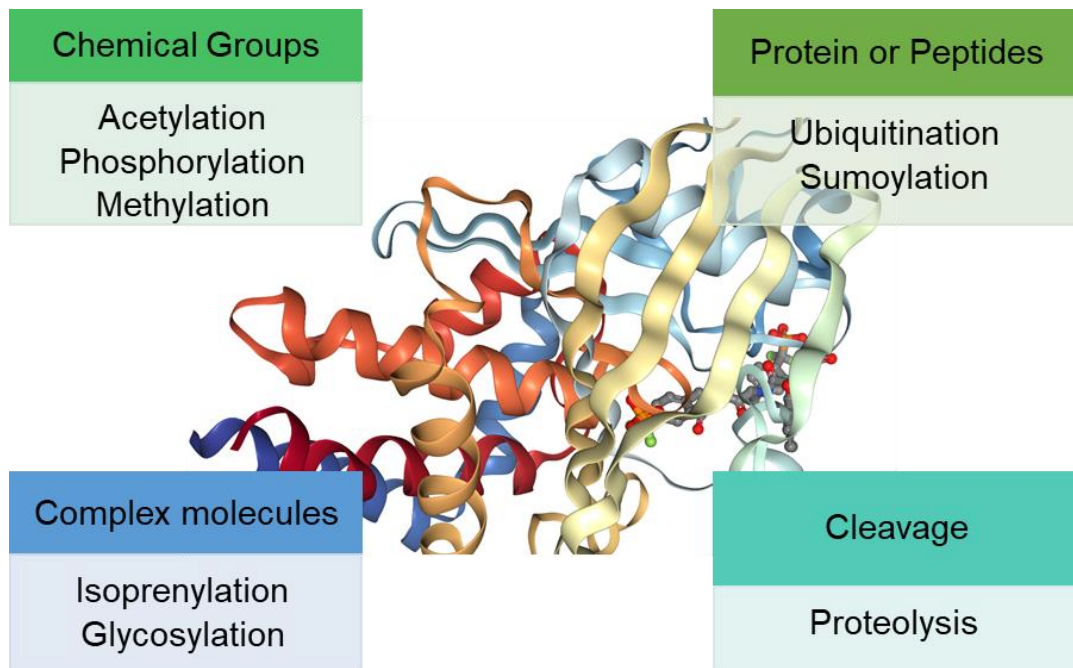


Figure 1: Protein activity can be influenced after translation by a variety of modifications, which can alter their structure in both reversible or irreversible fashion. Adapted from [1]

1.2 Phosphorylation

The attachment of a polar phosphate group (PO_4^{2-}) by protein kinases to the side chain of suitable amino acids of the protein backbone produces a phosphorylated protein. This modification is counterbalanced by protein phosphatases, which are able to cleave it. Phosphorylation consumes one molecule of adenosine triphosphate (ATP), which is converted into ADP (adenosine diphosphate) and the whole process is literally of vital importance. (Figure 2).

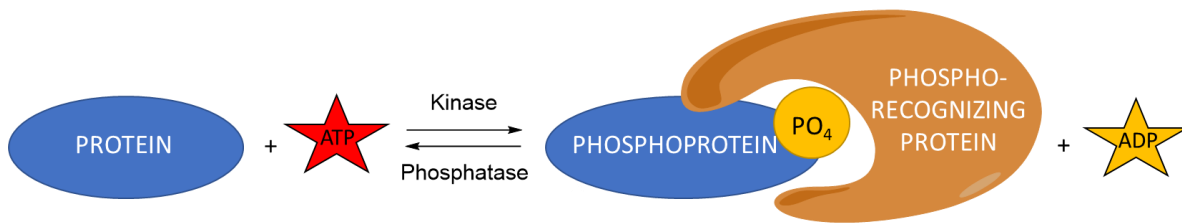


Figure 2: Phosphorylation of suitable protein residues is ensured by kinases and counterbalanced by phosphatases

The change in polarity induced by the introduction of the bulky and negatively charged phosphate group can cause relevant structural changes that can influence the shape and activity of proteins as well as the interaction that proteins can have with each other. Phosphorylation was first observed in 1906 by Phoebus Levene after hydrolysis of vitelline.^[1] In 1933, serine phosphoric acid was obtained from vitellinic acid.^[2] Almost 20 years later, in 1954, the first enzymatic phosphorylation of proteins was described by Kennedy, who reported the transfer of a phosphate group to proteins in rat liver mitochondria.^[3] Last but not least, in 1992 Fischer and Krebs received the Nobel prize for the identification of protein phosphorylation as a major regulatory mechanism.^[4]

A recent analysis of the regulatory sites database in PhosphoSitePlus, Needham et al. shows highlights how crucial phosphorylation is in biological processes such as transcription, which is a fundamental activity for cell life and tightly associated with healthy living cells. (Figure 3)^[5]

Introduction

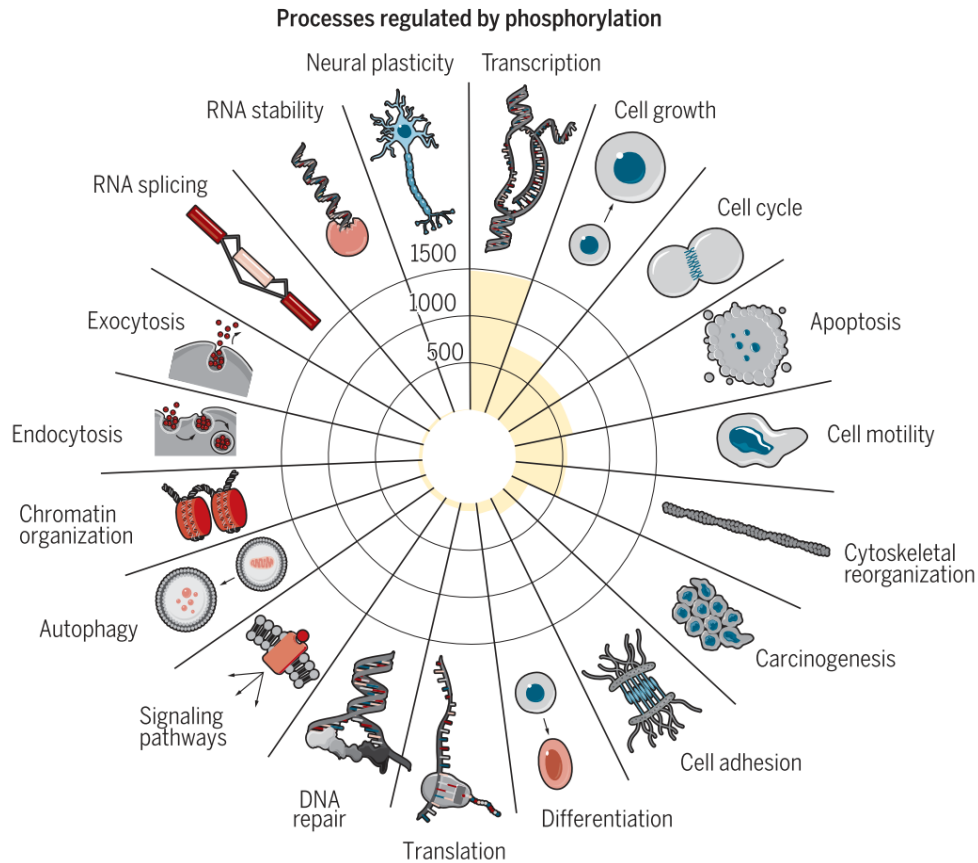


Figure 3: Overview of biological processes relying on phosphorylation, from [5]

Furthermore, this study highlights how among the variety of biological functions affected by phosphorylation, molecular association and protein activity appear to be the most heavily involved.^[5] (Figure 4)

A good example of these phospho-induced effects, such as molecular association and transcription can be well observed in the dimerization of STAT5 after phosphorylation by JAK (Janus Kinases). The phosphorylated STAT5 dimer is then ready for translocation in the nucleus where it triggers transcription of genes responsible for cell proliferation, apoptosis, cell differentiation or response to inflammation.^[6]

Protein phosphorylation can occur at multiple sites^[7] or at a single site of a particular protein that act as an initiator for the next events.^[8] The precise position of a phosphorylation site is not always easy to predict: in contrast to acetylation, which often is carried out in structured domains, phosphorylation can occur in disordered regions, with overall low conservation.^[9]

Introduction

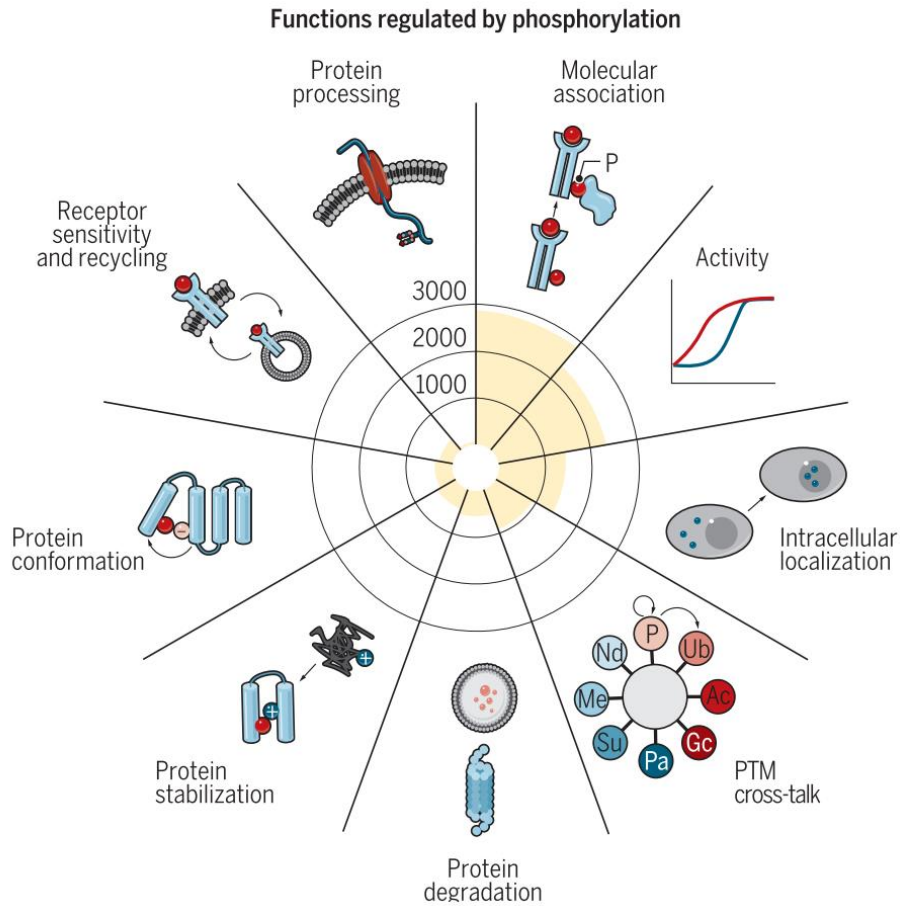


Figure 4: Overview of biological functions where phosphorylation plays a key role, from [5]

The importance of a correct phosphorylation pattern for a healthy cell is reflected by the consequences observed when this equilibrium is misregulated: in this case, cancer, defined as a group of illnesses related to abnormal cell growth and regulation, is one of the most observed outcomes. (Figure 5)

Introduction

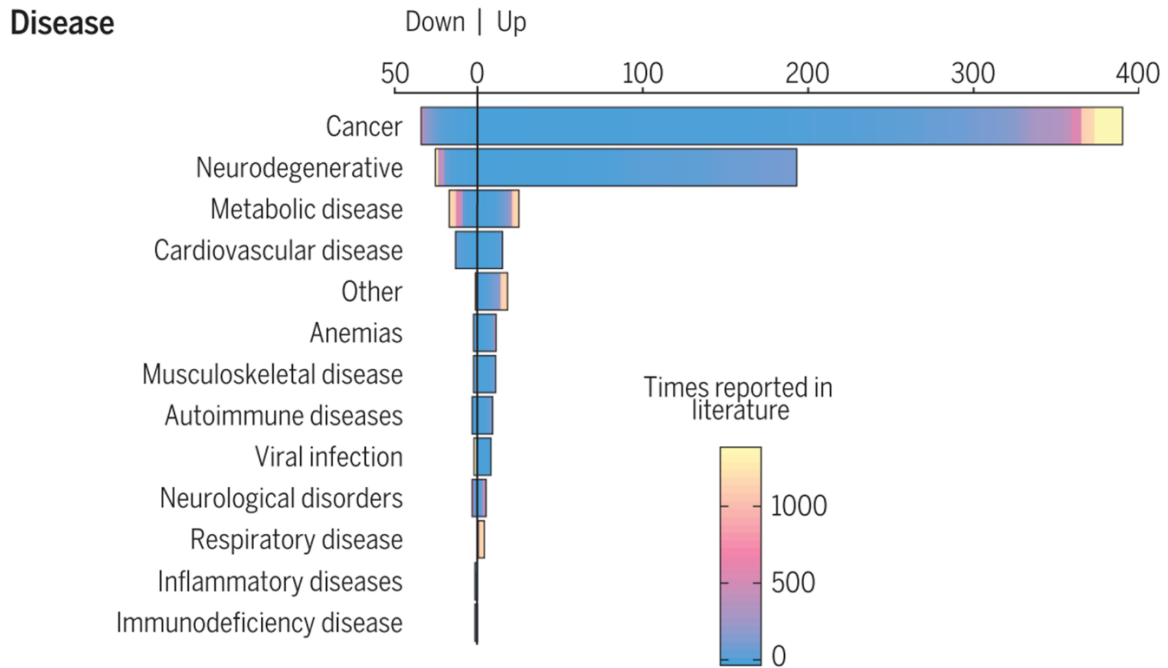


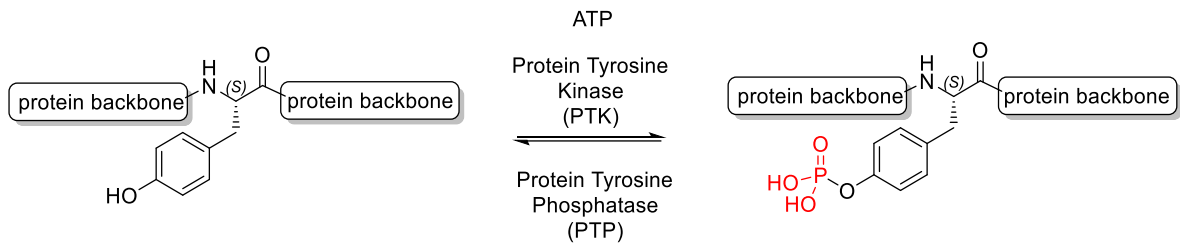
Figure 5: Misregulations in phosphorylation event cause many human diseases, among which cancer is the most prominent.^[5]

Most of the phosphorylation events in mammalian cells occurs on serine (85%), threonine (15%), and tyrosine (1%) residues,^[10] and is regarded as O-phosphorylation. Phosphorylation of other amino acid residues is reported as well but these modifications are less stable.^[11] It is estimated that 30% of all proteins may be phosphorylated in eukaryotes.^[12]

This work will focus on tyrosine phosphorylation, by investigating new inhibitors of protein tyrosine phosphatase.

1.2.1 Protein tyrosine phosphorylation

Phosphorylation on tyrosine residues was first discovered by Hunter and colleagues on polyoma virus middle T antigen in 1979^[13] and since then a steadily increasing number of tyrosine phosphorylated proteins have been identified.



Scheme 1: Phosphorylation of tyrosine residues in proteins is regulated by kinases and phosphatases

The majority of protein tyrosine kinases (PTKs) are phosphorylated themselves, allowing them to obtain an active conformation, that in turn make them capable to phosphorylate their substrate proteins in presence of a molecule of ATP.^[14]

Down on the signaling cascade, a second group of proteins domains that can read the previously conducted phosphorylation is responsible for the propagation of the stimulus. They includes the Src homology 2 (SH2) and phosphotyrosine-binding (PTB) domains.^[15]

A third group of proteins, protein tyrosine phosphatases (PTPs), are capable of erasing the phospho-tag terminating the signal.^[16] The level of PTP activity is very high in cells, ensuring prompt pTyr dephosphorylation if required by the cell state.^[17]

The crucial role of tyrosine phosphorylation is indeed reflected in the human genome, which encodes for at least 90 PTKs,^[18] hundreds of pTyr-recognition domains including 121 members of the Src homology 2 (SH2) domain family,^[19] and almost 10,000 known tyrosine phosphorylation sites.^[20]

1.2.2 SH2 Domain

One archetypical domain which recognizes a phosphorylated tyrosine residue is the Src-homology 2 (SH2) domain and it represent the largest group of pTyr binding modules.^[19a, 21] This highly conserved non-catalytic module composed by a sequence of approximately 100 amino acids was first reported by Pawson in the Fujinami sarcoma virus in 1986.^[22]

Few years later, in 1992, the crystal structure complexed with a tyrosine phosphorylated peptide was determined by Waksman et al.^[23] (Figure 6)

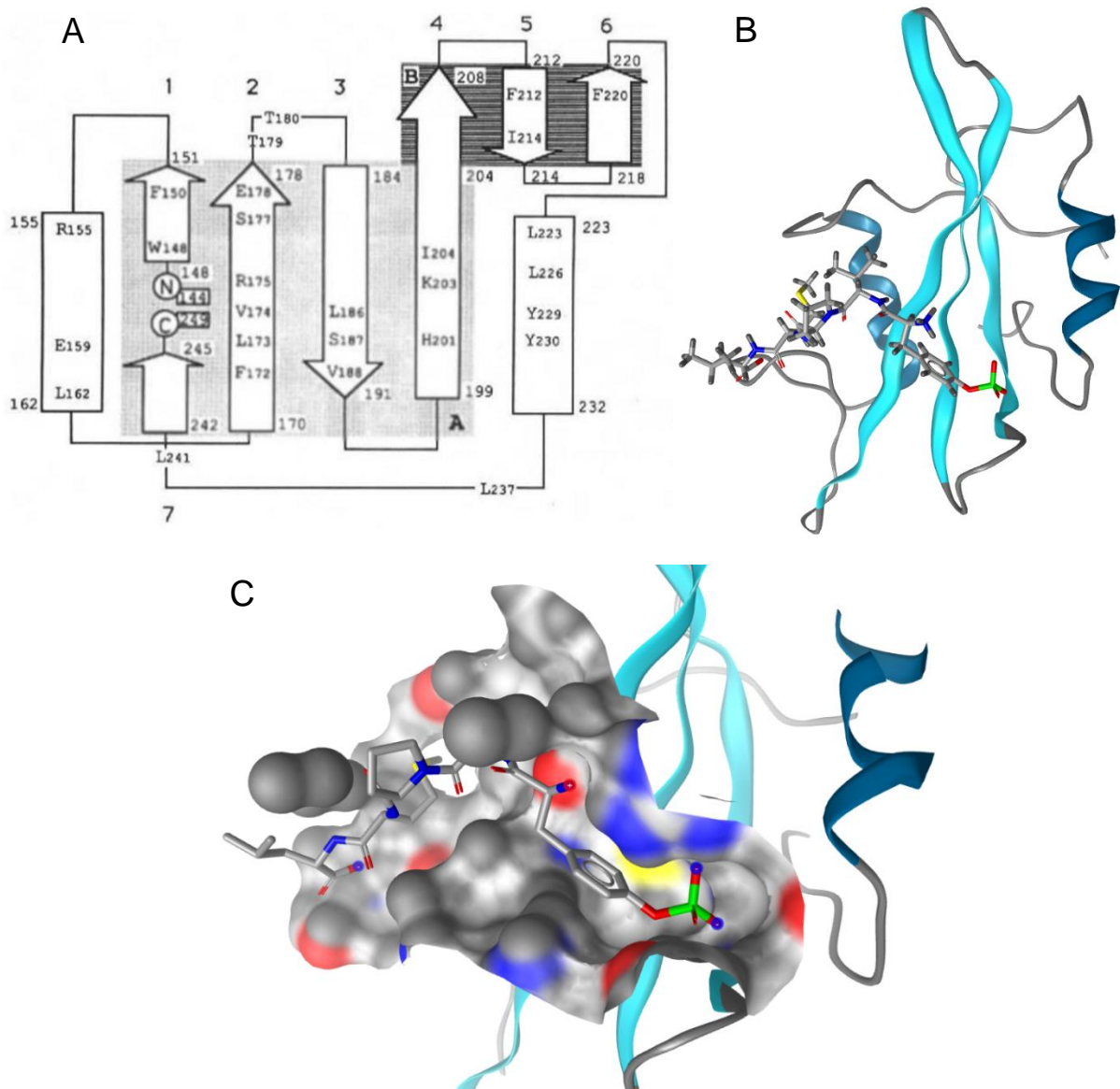


Figure 6: A) Tertiary structure of SH2 domain as originally reported by Waksman [23]; B) Crystal structure with a phosphopeptide ligand obtained with Ligand Scout (from original

Introduction

electron density file from Waksman [23] PDB = 1SHA); C) Closer look on the active site surface with bound substrate.

Introduction

This domain, composed by two α -helices and 7 β -sheets, allows many different kinds of proteins such as kinases, phosphatases, ligase and transcription factors to perform their action.^[24] SH2 domain allow proteins to recognize suitable substrates, but also permit autoinhibition of their catalytic activity.^[25] In Figure 7 it is shown how the intramolecular interaction between the phosphorylated tyrosine residue and the SH2 domain as docking site leads to autoinhibition of Src activity. On the contrary, dephosphorylation of the substrate leads to the release of the substrate from the binding site of the enzyme and restoration of the activity. A similar autoregulation mechanism is observed in glycogen synthase kinase 3 (GSK3), which is involved in insulin signaling. Phosphorylation of the serine residue results in autoinhibition of the protein but in this case SH2 domain is not responsible for substrate recognition because of the different amino acid involved.

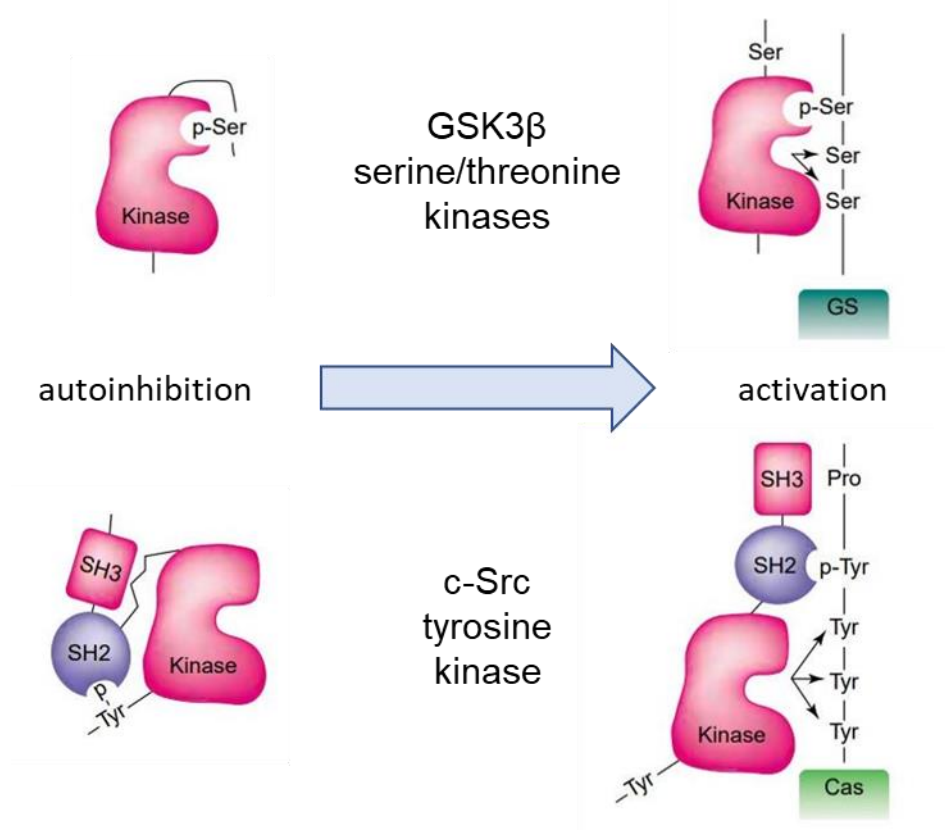


Figure 7: Kinases can be inactivated by autophosphorylation and reactivated upon dephosphorylation, adapted from [25]

1.3 Protein tyrosine phosphatase 1B

Genomics is a branch of molecular biology which studies the function, evolution, and mapping of genomes and in April 2003 scientists achieved the sequencing of the human genome. This major step forward allowed the identification of genes encoding for 108 phosphatases, which were subsequently classified in the protein tyrosine phosphatase super family, characterized by the presence of the signature motif in the active center known as **C(X)₅R**, indicating the amino acids present after the cysteine residue.^[26]

Phosphotyrosine phosphatases are sub-classified in the four groups shown in Figure 8:

<p>A: Class I Cys-based PTPs (99 Genes)</p> <p>Classical (38)</p> <ul style="list-style-type: none"> Transmembrane Receptor-like, (RPTPs) (21) Intracellular non receptor, (NRPTPs) (17) <p>Dual specificity VH1-like phosphatase (DSP) (61)</p> <ul style="list-style-type: none"> MAP kinase phosphatase, (MKPs) (11) Atypical DSPs (19) Slingshots (3) Phosphatase of regenerating liver (PRLs) (3) Cell division cycle phosphatases (CDC14) (4) Phosphatase and tensin homolog (PTENs) (5) Myotubularine (16) 	<p>Substrate specificity</p> <p>PTyr</p> <p>PTyr</p> <p>Ptyr, PThr</p> <p>Ptyr, Pthr, mRNA</p> <p>PSer</p> <p>PTyr</p> <p>PTyr</p> <p>D3-phosphoinositides</p> <p>PI(3)P</p> <p>PTyr</p> <p>Ptyr, PThr</p> <p>PTyr, PSer</p>
<p>B: Class II Cys-based PTPs (1)</p> <p>Low Molecular Weight phosphatases (LMPTPs) (1)</p>	
<p>C: Class III Cys-based PTPs 3)</p> <p>Cell division cycle phosphatases (CDC25) (3)</p>	
<p>D: ASP-based PTPs (4)</p> <p>Eyes Absent proteins (EyA) (4)</p>	

Figure 8: Classification of protein tyrosine phosphatases super family, adapted from Alonso et al.^[27]

Introduction

As summarized in the following picture, classical PTPs have been further categorized as receptor-like (R) and non-transmembrane (NT) proteins. Although the distinction is not always absolute, most of the R-PTP present two PTP domains, while the NT are present in the cytosolic environment, where they are responsible for a plethora of cellular functions. This work will address the first NT-PTP, known as PTPN1 or PTP1B, considered a model phosphatase.

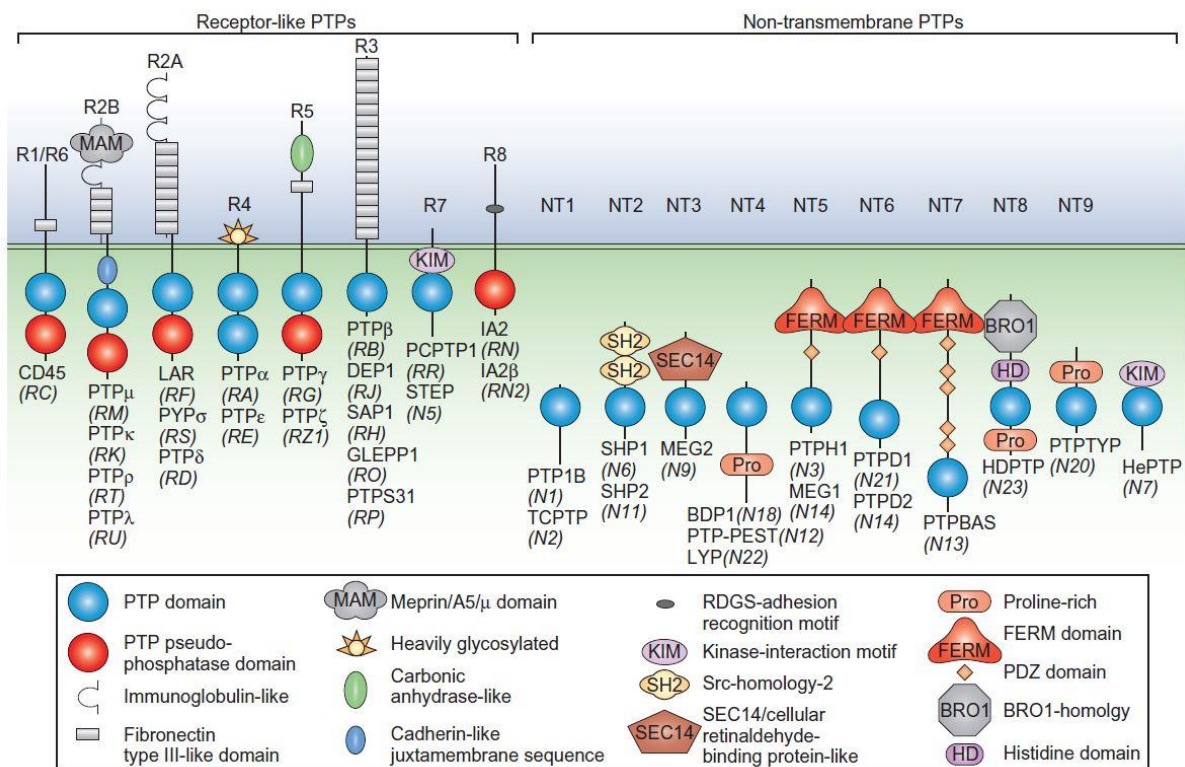


Figure 9: Overview of classical PTPs: receptor-like and non-transmembrane PTPs as reported by Tonks.^[28]

PTP1B was first characterized and purified in 1988 from human placenta by Tonks et al;^[29] the suffix 1B was given considering the chromatographic behavior and it was purified as a protein of 321 amino acid. This enzyme represents a fundamental example for its class of enzymes, sharing highly conserved sequences with other PTPs. The protein is expressed ubiquitously and its abundance strongly supports its important and general role in controlling cellular functions.^[30] The structure was elucidated by Barford et al. in 1994 by obtaining a crystal structure with sodium tungstate.^[31] The 37-kDa form is composed of a single domain, organized into 8 α helix and 12 β sheets. The conserved catalytic domain is located to the COOH

Introduction

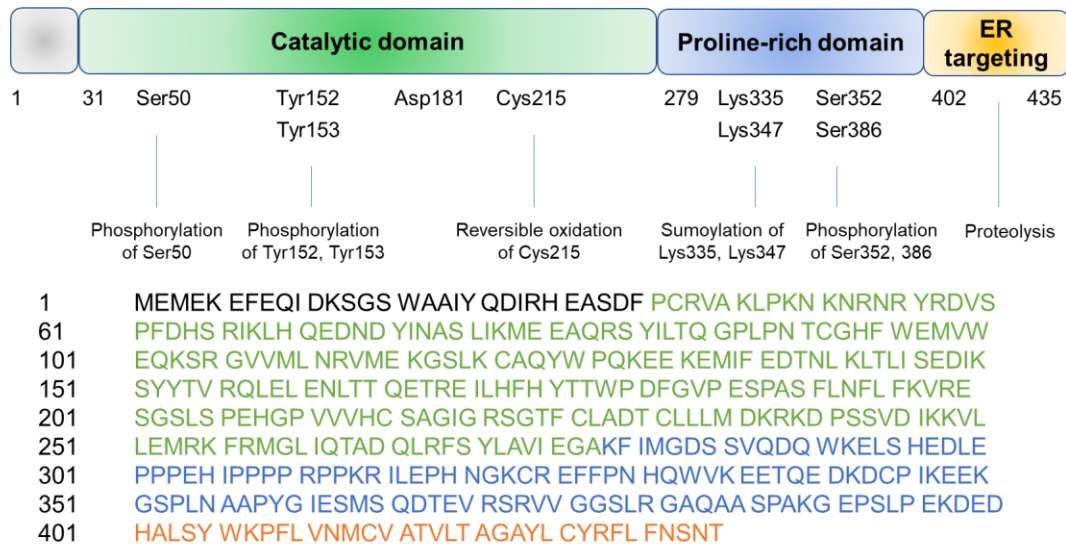


Figure 11: Structural domains of PTP1B and key amino acids regulating its activity, adapted from Yip et al.^[32]

The catalytic domain is located between residue 30 and 278 and the active site, also called P-loop and identified between residue 214 and 221, is composed of the sequence His-Cys-Ser-Ala-Gly-Ile-Gly-Arg and is 8 to 9 Å deep. It is surrounded by the Q-loop (Gln262-Phe269), a phosphotyrosine recognition loop (Asn40-Tyr46) and the R loop (Leu110-Cys121). The protein structure can shift between an open and a closed conformation, depending on the position of a portion called WPD loop 177-185, composed of the amino acid sequence Try179-Pro180-Asp181. An allosteric site is also present and it is composed of the α -helices 6,3 and 7 (Figure 12).^[33]

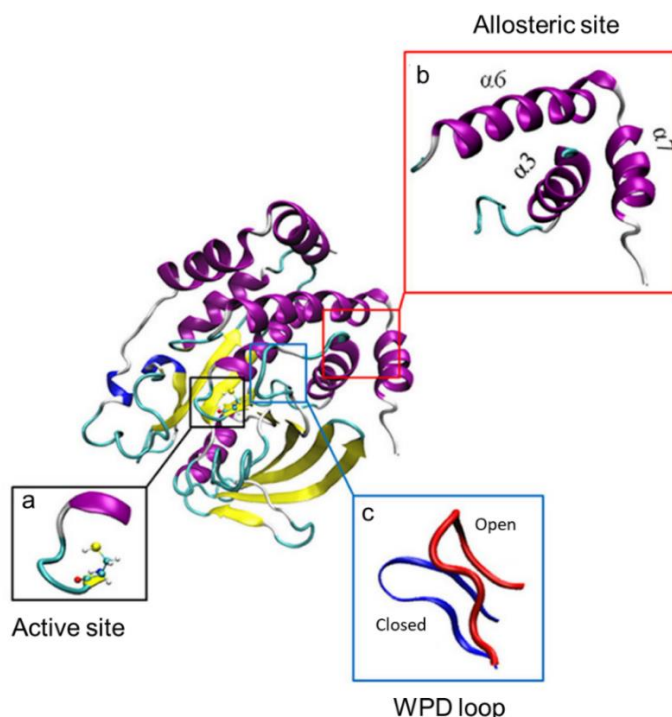


Figure 12: Quaternary structure of PTP1B with highlights on the active site, the allosteric site and the WPD loop as reported by Jin et al.^[33]

The allosteric region distance from the active center is quantified in about 20 Å and via x-ray crystallography it was possible to observe changes in the conformation of this site during catalytic activity.^[34] Although being catalytically inactive and more exposed to the solvent, the allosteric site offers a possibility to design potent and selective inhibitors due to the fact that this portion is not highly conserved in most PTP's.^[35] Furthermore, its structural adaptability can be exploited for drug discovery.^[36]

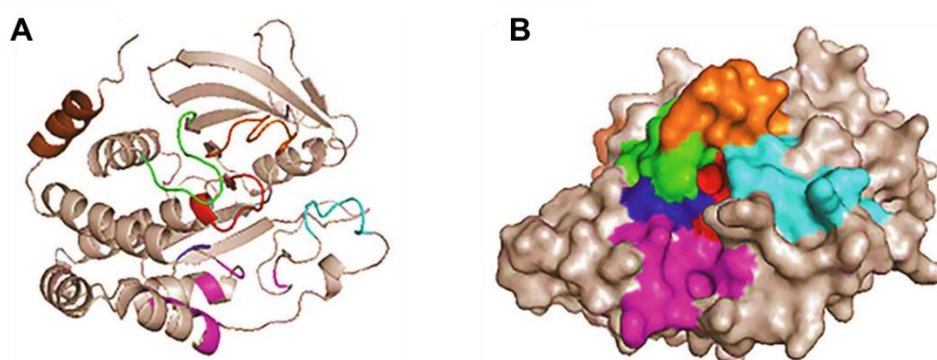


Figure 13: A) Active site of PTP1B and surrounding areas shown as cartoon (A) and as protein surface (B) showing: active site (red), WPD loop (green), phosphotyrosine recognizing loop (light blue), Q loop residue (blue), second aryl phosphate binding site (magenta), R loop (orange) and helix Ser285-Ser295.^[37]

Introduction

The catalytic mechanism relies on the nucleophilic attack of Cys215 to the phosphorus, held in position by the arginine residue (Step 1). Cleavage of the P-O bond yield a phosphorylated thiol which is then hydrolyzed regenerating the active center (Step 2).^[38]

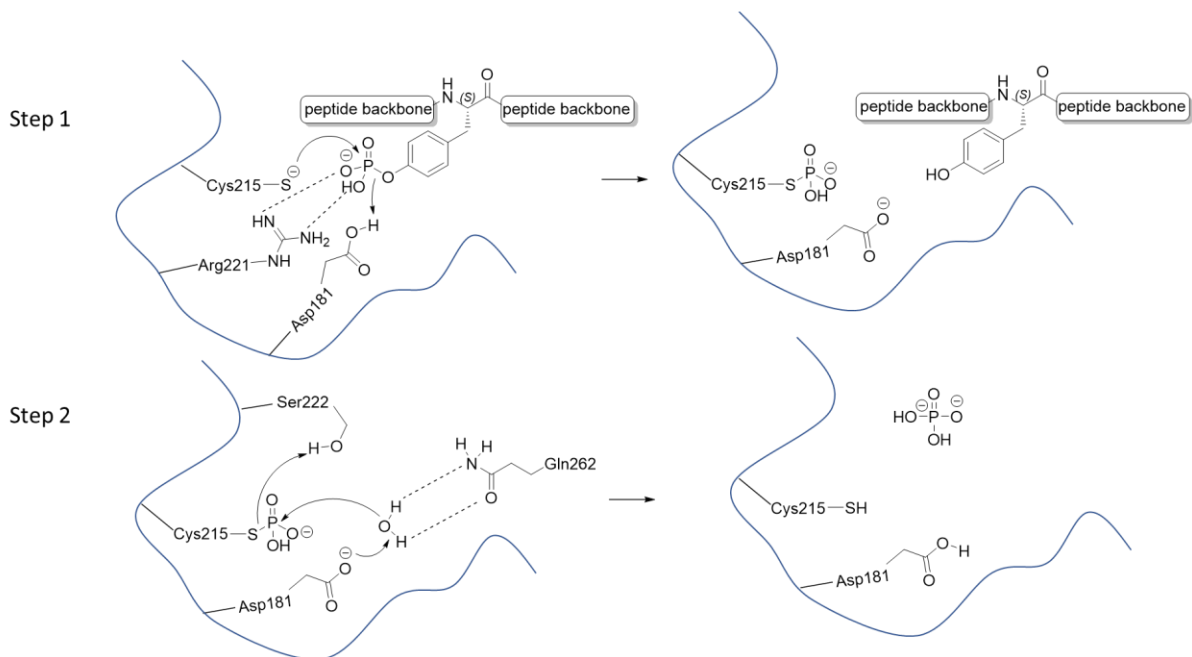


Figure 14: Cysteine-mediated catalytic mechanism of PTP1B, adapted from Brandão et al.^[39]

The 35 carboxy-terminal residues help targeting and anchoring the enzyme to the endoplasmatic reticulum (ER) of the cell. This ER-tethering imposes certain restrictions on the activity of PTP1B and questions about how it can dephosphorylate substrates located on the membrane or in the cytoplasmatic environment are legit. Currently, there are four rational explanations for this phenomenon. The first is that activated receptors are internalized via vesicle mediated endocytosis, which brings them in close contact with the enzyme on the ER. ^[40] The second it based on experimental live imagine analysis, is that the ER-bound PTP1B can dephosphorylated the insure receptor (IR) during its biosynthesis. ^[40b, 41] The third scenario describes PTP1B as attached to a stretchable ER portion which allow to reach substrate at the plasma membrane.^[42] Last but not least, PTP1B can reach its substrates via adaptor proteins (phospholipases or N-cadherin), physically binding the enzyme to its target.^[43]

Introduction

The implication of the phosphatase in the regulation of insulin signaling became evident in mice experiments conducted by Elchebly in 1999.^[44] Disruption of the gene encoding for PTP1B yielded healthy animals with lower blood sugar concentration and half of the concentration of insulin in circulation when compared to unmodified littermates. When subjected to a high fat diet, the latter showed a marked weight gain and become insulin resistant, while the former were untouched by these effects.

PTP1B catalyzes dephosphorylation of the insulin receptor (IR) and IR substrates, negatively regulating insulin stimulation. Overexpression of PTP1B in cell cultures decreases phosphorylation stimulated by insulin of IR and/or IRS-1; on the contrary a reduction in the level of PTP1B favors insulin-initiated signaling.^[45]

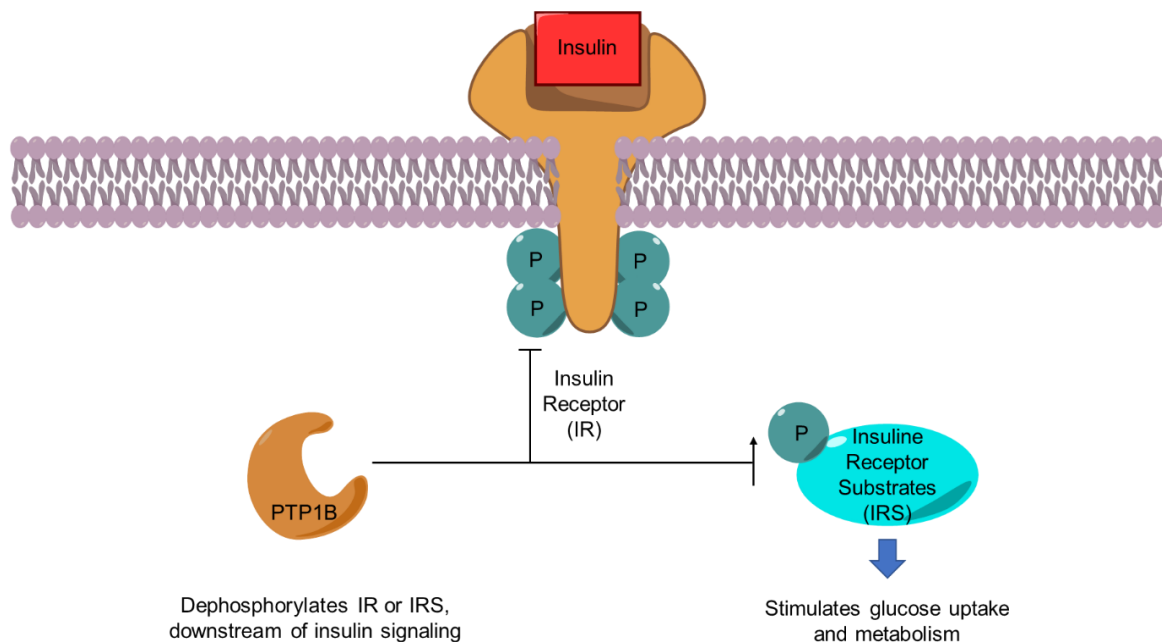


Figure 15: Role of PTP1B in insulin signaling. Adapted from [43]

It also dephosphorylates Jak2 (Janus kinase 2) involved in leptin signaling, acting therefore as a negative regulator of this metabolic hormone.^[45]

Introduction

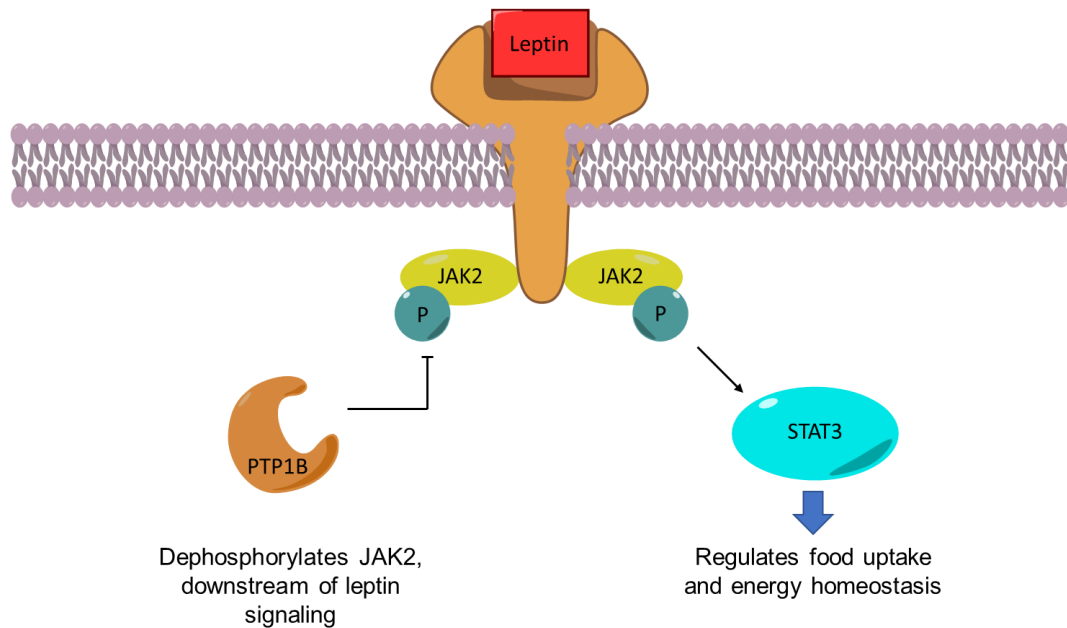


Figure 16: Role of PTP1B in leptin signaling. Adapted from [43]

PTP1B activity can be inhibited by small molecules, that can be used as insulin mimetics and insulin sensitizers.^[46] These results supported the identification of PTP1B as a potential therapeutic target in the treatment of diabetes type 2 and obesity.^[47]

Although the role of PTP1B in metabolism is consolidated, the same cannot be said for its involvement in cancer. Intuitively, overexpression of the phosphatase should protect against an excess of phosphorylation by constitutively active kinases, and this idea was verified by v-src expressing cells^[30b] and by several reports suggesting that PTP1B promotes apoptosis through different mechanisms.^[48] On the other hand, mice lacking of PTP1B were not showing any increase in tumor formation. Instead, the protein was reported to promote growth and invasion of cancer cells in a c-src-dependent manner. In colon cancer cells, the overexpression of PTP1B is associated with accelerated colony formation as well as increased tumor growth.^[49] Similarly, in breast cancer cells, over-activated PTP1B is correlated with the activation of c-src and the formation of invadopodia,^[50] defined as protrusions of the cellular membrane which results in degradation of the extracellular matrix and is associated with cancer invasiveness and metastasis.^[51]

1.3.1 Regulation of PTP1B activity

PTP1B enzymatic activity is known to be tightly regulated by different mechanisms, that can work in parallel:

- Phosphorylation
- Oxidation
- Sumoylation
- Proteolysis

Phosphorylation as a mean to modify PTP1B activity can occur at serine or tyrosine residues, at multiple locations. Several studies have focused on clarifying whether the phosphorylation site is be associated with an increase or decrease of activity but results have been difficult to rationalize. Although phosphorylation at S50 by PKB (Protein Kinase B) decreased activity and compromised the capability to dephosphorylate the IR (Insulin Receptor),^[52] data showed that dual specificity protein kinase 1 and 2 (CLK1 and CLK2) can increase the activity two-fold when operating on the same residue.^[53]

Being a cysteine residue, the sulfur center is susceptible of oxidation. This happens in a controlled manner *in vivo* and modulates PTP1B activity.^[54] The thiol, when deprotonated, shows enhanced nucleophilicity and catalytic efficiency, but its susceptible to inactivation. Reactive oxygen species (ROS) can oxidize it to the sulfenic acid, causing a domino effect that results in the formation of a cyclic sulfenamide, that temporarily inhibits enzyme activity.^[55] The reversibility of this process is not retained when the oxidation of the cysteine residue proceeds to sulfinic (SOOH) or sulfonic (SO₂OH) acid.^[56]

Sumoylation is defined as the protein modification involving proteins of the small-ubiquitin-related modifier proteins (SUMO) family. Sumo conjugation allows to dynamically control protein stability, activity, and localization.^[57] Recently it was demonstrated that PTP1B is SUMO-modified upon interaction with SUMO E3 ligase, a protein inhibitor of activated STAT-1, reducing the enzymatic activity of the phosphatase.^[58]

Introduction

Although sumoylation eventually leads to proteolysis, this process was observed directly *in vitro* with calpain-1, which was able to digest PTP1B into small fragments.^[59]

In vivo, PTP1B can be cleaved from its anchoring point on the ER, leading to the release of the solubilized protein into the cytosolic environment. This is part of the mechanism by which platelets are stimulated to aggregate irreversibly as a response to a *in vivo* stimulus.^[30a] The release of phosphatase from its natural location is used in its virulence mechanism by *Yersinia*, a gram negative genus of bacteria: phosphatases enter in the cytosol of the mammalian target cells and promiscuously dephosphorylate proteins inducing cell death.^[60]

1.3.2 PTP1B Inhibition

After demonstrating the importance of tyrosine phosphorylation in living systems, and more precisely the role of PTP1B in chronic metabolic diseases and cancer, an important challenge was the development of inhibitors with a high degree of potency and selectivity. The main issue is the high degree of sequence conservation among phosphatases, which strongly disfavors drugs selectivity, and the charge of the active site, which interact with charged molecules, which in turn are not able to cellular membrane limiting their *in vivo* activity. Unfortunately, so far PTP1B inhibitors are still not available on the market as drugs, and only a few compounds have been tested in clinical trials as prodrugs: Ertiprotafib and Trodusquemine.

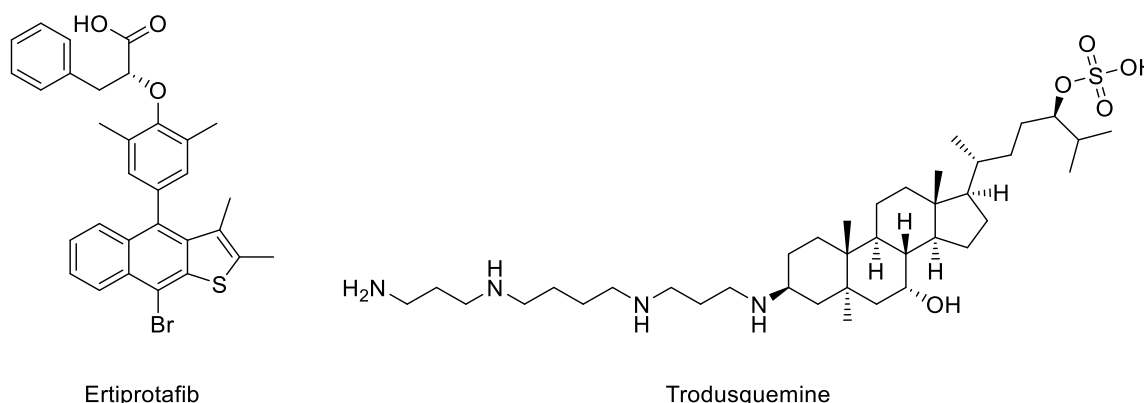


Figure 17: Structure of prodrugs PTP1B inhibitors Ertiprotafib and Trodusquemine which made to clinical trial. ^{[59][60]}

Introduction

The first one, developed by Wyeth-Ayerst Labs, is a synthetic mono carboxylic acid that proceeded up to Phase II clinical trials, where it was stopped due to insufficient activity and dose limiting side effect produced by inducing PTP1B aggregation.^[61]

On the other hand, Trodusquemine, also known as MSI-1436, is a natural product obtained from the liver of dogfish shark, *Squalus acanthias*.^[62] It was well tolerated by patients in phase I clinical trials, but the proprietary company, Genaera Corporation, went bankrupt and the studies were interrupted.^[63] Nonetheless, research about this compound started again showing promising results.^[64] Quite interestingly, none of these drug candidates presented a phosphorus atom.

Of course, these are not the only examples of PTP1B inhibitors: intense research in both synthetic and natural fields allowed the identification of a plethora of molecules showing different degree of selectivity, potency and core structures.

Within the synthetic development, the so-called gold standard for phosphotyrosine mimetic is represented by non-cleavable methylene phosphonic acids. Already in early 1990, it was clear that in order to inhibit PTP activity, a phosphotyrosine analogue resistant to hydrolysis was required. This idea led to the synthesis of phosphonates as first class of tyrosine mimetics, by replacing the oxygen bridge between the phenyl ring and the phosphorus center with a methylene group. This building block was then incorporated in a peptide sequence and the inhibitory potential evaluated.^[65]

The decreased affinity observed with these early pTyr mimetic was improved by investigating with more elaborated analogues, with the difluorinated analogue presenting the best profile in terms of pKa, bio isosteric character and the inhibitory PTP1B potential.^[66] Non-cleavable Ac-DADE(pY)L-H hexapeptide containing the F₂Pmp rest resulted in a 1000-fold increase compared to its non-fluorinated analogue Pmp (Figure 18)

Introduction

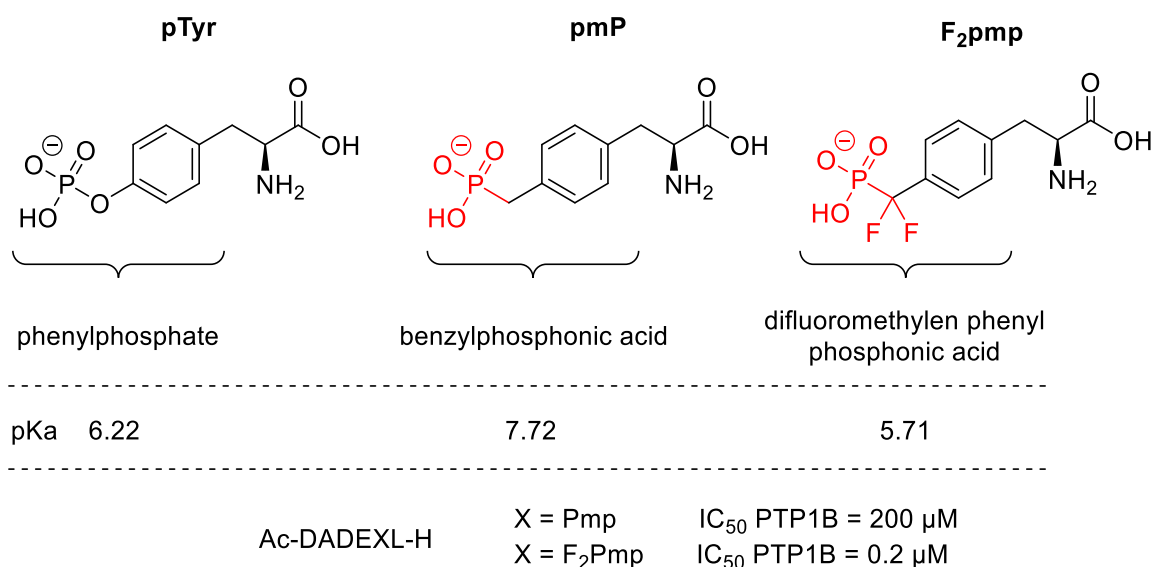


Figure 18: Natural phosphotyrosine and the first class of non-cleavable phosphotyrosine mimetics with pKa value of corresponding simplified phosphonic acid.^[67] Peptidic inhibitors containing these phosphomimetics inhibits PTP1B with a 3 orders of magnitude of difference as reported by Akamatsu et al.^[68]

These encouraging results were unfortunately toned down by the inability of these structures to cross the cellular membrane, which pushed the scientific community to further elaborate strategies to overcome this crucial issue. Selectivity was also to be addressed, because the residue around pTyr mimetic have been found crucial for substrate recognition by the protein.^[38b, 69]

Few years after the development of difluoromethylen phosphonic acids as phosphotyrosine mimetics, deeper studies on PTP1B crystal structure allowed the identification of an allosteric site located adjacent to the active site.^[70] This second aryl phosphate-binding site, although being more solvent exposed, appears to not be conserved among PTPs and consequently can represent an additional target for the development of highly selective and potent inhibitors. Indeed this assumption was verified by Shen et al. in 2001, in a combinatorial library and screening procedure. With this method, the authors were able to identify a bivalent inhibitor targeting simultaneously the active site and the secondary aryl phosphate binding site resulting in a great level of potency and selectivity.^[71] (Figure 19A) Despite these promising results, the bisphosphonate's inability to cross cellular membrane polarity was still a critical issue, which Boutselis et al. addressed by preparing a prodrug of the inhibitor and evaluate it in a cellular based assay.^[72] (Figure 19B)

Introduction

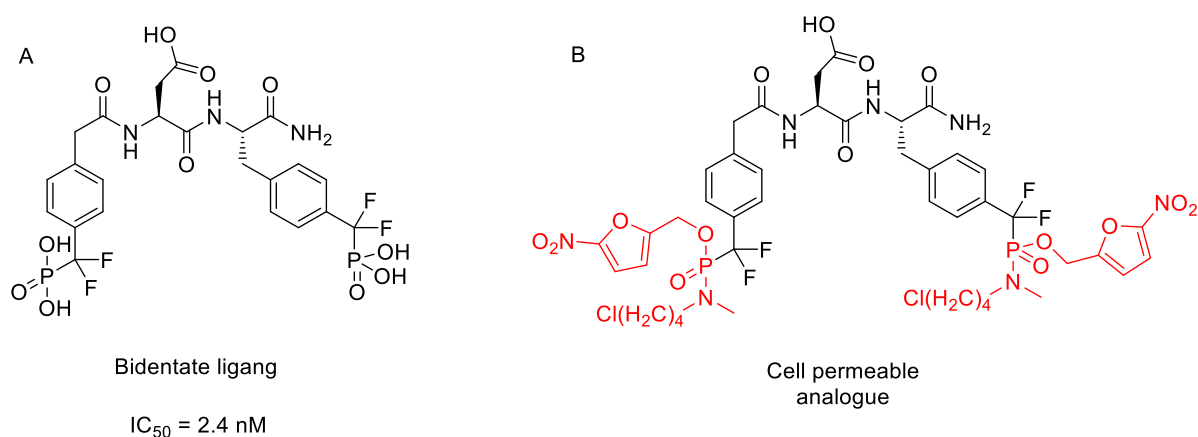


Figure 19: A: the most potent *in vitro* PTP1B inhibitor to date reported by Shen et al.^[71]; B: its cellular active prodrug analog by Boutselis et al.^[72]

The compound was active in HepG2 cellular assays, where it potentiated the insulin signaling pathway, after removal of the masking groups in the cytosolic environment via sequential enzymatic and spontaneous transformations, generating the free phosphonic acid.

In order to mask the polarity of the phosphonic acid and increase lipophilicity, sulfonamides have been considered as possible alternatives. Chen et al. in 2003 rationalized that their sterical hindrance would be similar to the phosphate group, but with a reduced charge, and investigated the inhibitory potential of peptidic sulfonamides as PTP inhibitors.^[73] Unfortunately, the main compound (reported in Figure 20), turned out to be inactive towards PTP1B.

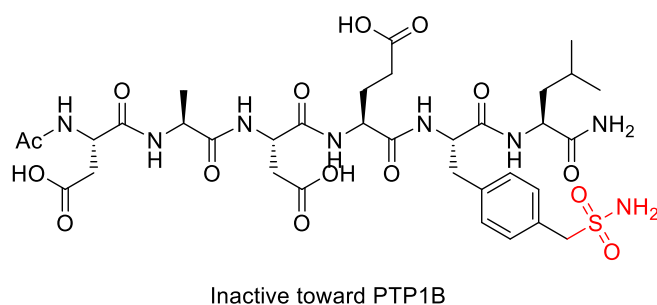


Figure 20: Hexapeptide containing the sulfonamide as phosphomimetic moiety is inactive towards PTP1B

In the same years, Leung et al. showed that difluoromethylen sulfonic acids can be used as phosphate surrogate for PTP1B inhibitors, presenting comparable but higher IC₅₀ values (Figure 21).^[74] Consequently, although they cannot be regarded as direct replacement for difluorophosphonates in peptidomimetic inhibitors, difluoro sulfonates can still represent an interesting surrogate.^[74]

Introduction

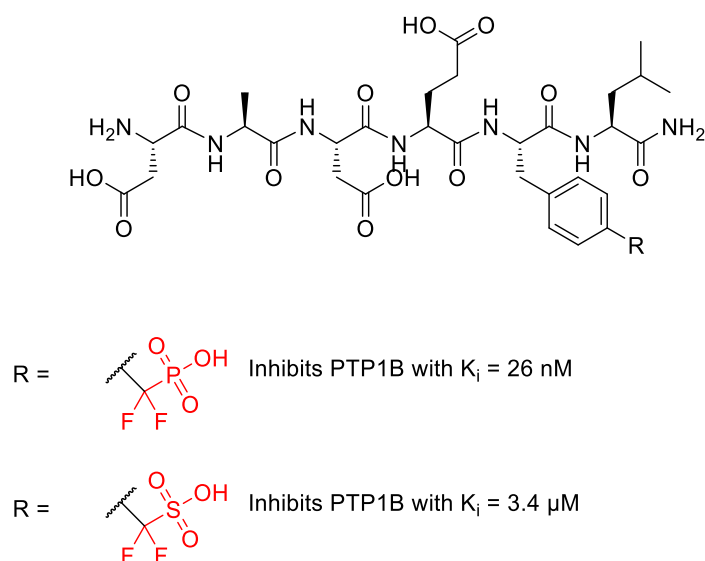


Figure 21: Peptidomimetic containing the $F_2Smp^{[74]}$ as analogue of $F_2Pmp^{[75]}$

As previously shown in the case of Ertiprotafib, phosphonic acids or related analogues are not the only moiety to inhibit PTP1B. In order to increase lipophilicity, recent medicinal chemistry efforts evaluated 3-carboxy-4-(O-carboxymethyl) tyrosine as pTyr alternative in the construction of small peptidomimetics, yielding sub to micromolar potency.^[76] (Figure 22)

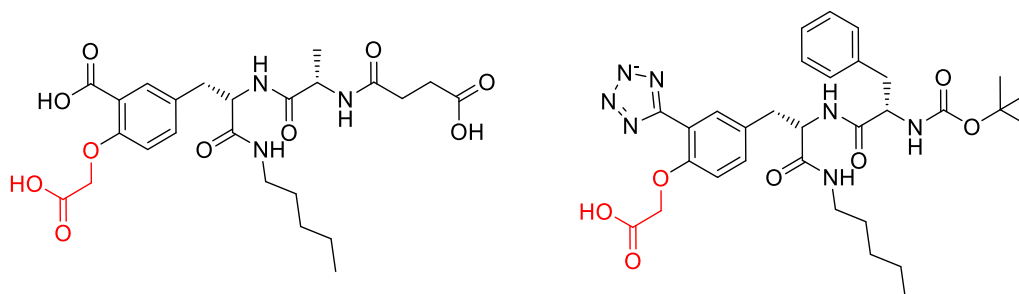


Figure 22: Example of inhibitors containing 3-carboxy-4-(O-carboxymethyl) tyrosine as pTyr mimetic

More research work was carried out also trying to address the secondary aryl binding site by adding substituents branching out from already known core structures of PTP1B: Novo Nordisk developed non-phosphorus, non-peptidic highly selective inhibitors using a structure-based molecular design, allowing to achieve a K_i of 600 nM and a degree of selectivity from an otherwise low affinity and non-selective compound.^[77] (Figure 23)

Introduction

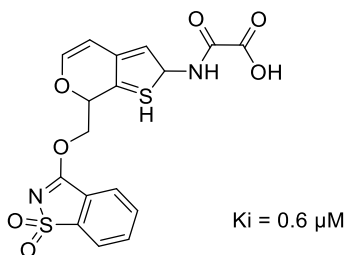


Figure 23: Novo Nordisk selective inhibitor targeting the secondary aryl binding site results in increase in potency and selectivity.

Researchers across the world tried to find the correct declination of a lipophilic molecule, therefore able to penetrate the cell membrane, but also capable to interact with a charged active site and to achieve selectivity among different PTPs by reaching a secondary aryl phosphate binding site adjacent to the catalytic pocket of the enzyme, and this challenge is still ongoing.

As showed previously in the case of Trodusquemine, a potent inhibitor obtained from a dogfish shark, the possibilities offered by natural products should not be underestimated. In the attempt to propose a tool for PTP1B drug discovery, a recent review by Zhao et al. classifies more than 500 natural compounds showing phosphatase inhibition according to their molecular structure. From this research emerges that the phosphatase inhibitory potential is not restricted to the previously reported phosphonic acids, sulfonic acids, sulfonamides or carboxylic acids. As a matter of facts, a very big number of naturally occurring molecules can be useful in the developments of advanced and pharmaceutically acceptable PTP1B inhibitors: the structure of few relevant examples is reported in the following picture.

Introduction

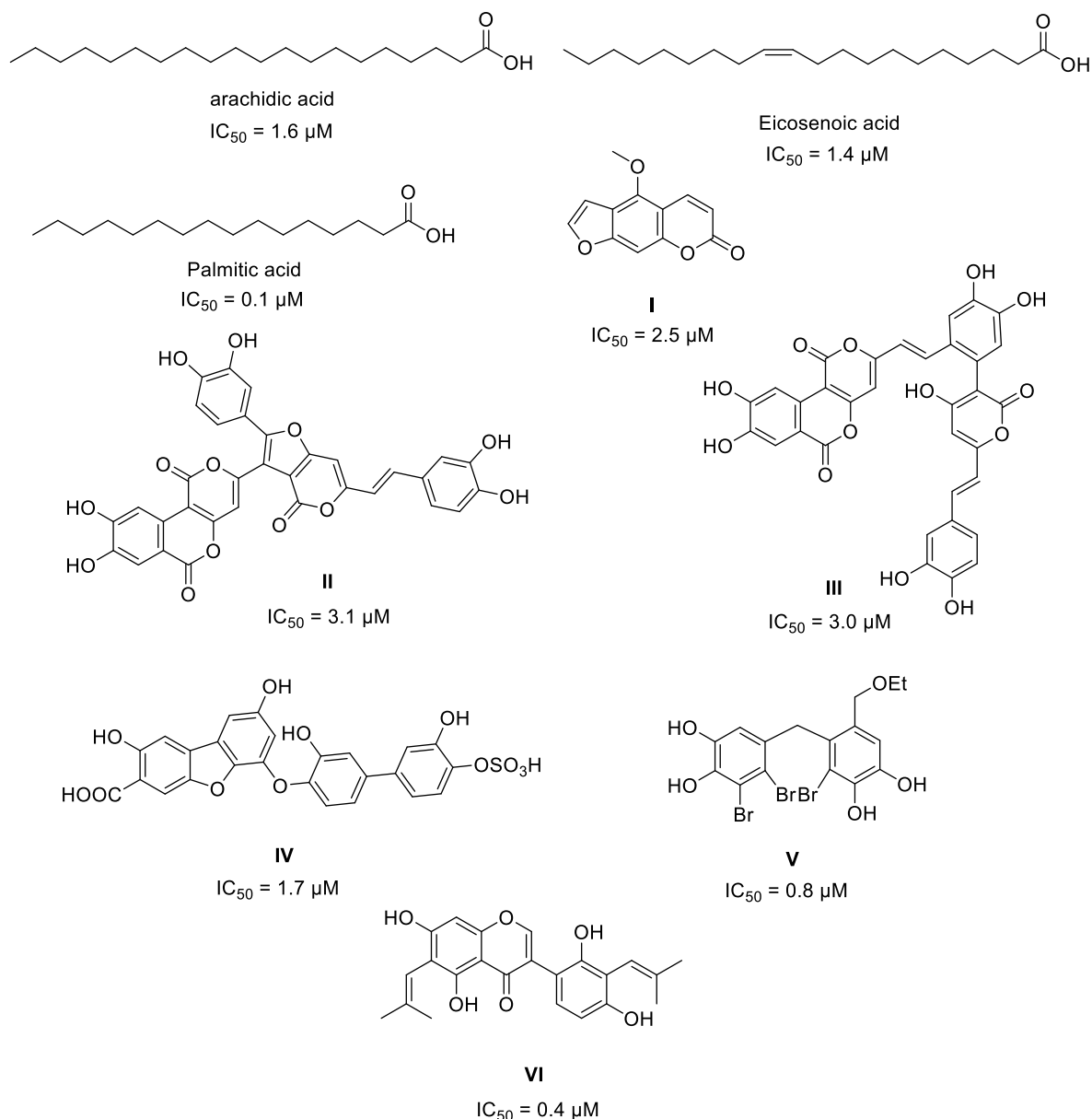


Figure 24 Examples of naturally occurring PTP1B inhibitors

Fatty acids play an important role in insulin resistance and metabolism by reducing the obesity facilitating weight loss, and many of them have been identified as PTP1B inhibitors.^[78] Arachidic acid showed strong bioactivity, as well as the eicosenoic acid, as its mono, cis unsaturated analogue (IC_{50} : 1.6 μM and 1.4 μM respectively).^[79] This last compound can be obtained from the bark of *Phellodendron amurense*, a plant known in traditional Chinese medicine for its beneficial effect and recently showed encouraging results in preventing prostate tumor.^[80] Originally discovered in 1842 in saponified palm oil,^[81] palmitic acid is another strong PTP1B inhibitor (IC_{50} : 0.1 μM) that can be also found in *Agrimonia Pilosa*, a common perennial herb in Eastern Europe and Asia.^[82] From the Japanese herb *Angelica*

Introduction

keiskei, Li et al. reported the isolation of **I** and determined an IC₅₀ toward PTP1B of 2.5 μM.^[83]

Fungi can be a source of PTP1B inhibitors too: Wang et al. isolated compound **II** and **III** from *Phellinus igniarius*, reporting an IC₅₀ of 3.1 and 3.0 μM respectively.^[84]

From *Cladophora socialis*, a species of green algae found all over the world, Feng et al. isolated the sulfonated vanillic acid derivative **IV**, showing an IC₅₀ of 1.7 μM.^[85]

Quite interestingly, very bulky substrates can achieve potent inhibition of the protein tyrosine phosphate 1B as well. Many polybrominated phenols obtained from the extract of different algae have been investigated regarding their bioactivity and compound **V**, isolated from red marine algae showed sub-micromolar PTP1B with a IC₅₀ of 0.84 μM.^[86]

Flavonoids are compounds ubiquitous in plants, presenting a core structure composed by 15 carbon atoms and a skeleton of two phenyl rings, A and B, connected by a three-carbon bridge. Isoflavones have been reported to inhibit PTP1B in low micromolar range,^[87] and compound **VI** is one of the most active; extracted from *Glycyrrhiza uralensis* (Licorice), showed a IC₅₀ of 0.4 μM.^[88]

As mentioned before, the number of compounds found in nature acting as PTP1B inhibitors is very high and an exhaustive analysis is out of the scope of this work. In addition to the previously reported class of compounds, phenolic acids, tannins, terpenoids, steroids and alkaloids have been studied and biologically evaluated. A more detailed analysis can be found in literature.^[89]

1.4 Fluorine: a peculiar element

Fluorine atoms present specific characteristics that differentiate it from other elements of the periodic table. When comparing atoms sizes from the periodic table of elements, the fluorine atom is similar to that of hydrogen (van der Waals radius of 1.47 Å vs 1.10 Å)^[90] but the electronegativity is almost doubled (4.0 vs 2.1 on the Pauling scale)^[91] and the consequent perturbation of the electron density influences molecular properties described later. Furthermore, the C-F bond is one of the strongest in organic chemistry (116 kcal/mol),^[92] resulting in an enhanced stability towards thermal and oxidative stress, and is slightly longer than the corresponding C-H (1.40 vs 1.09 Å).^[93]

Table 1: Physico-chemical properties of hydrogen and fluorine compared. From [87-90]

Atom	Van der Waals radius [Å]	Electronegativity	C-X bond energy [kcal/mol]	C-X bond length [Å]
H	1.10	2.1	99	1.09
F	1.47	4.0	116	1.40

The profound changes in chemical and physical properties induced by fluorine insertion into molecules, such as chemical and metabolic stability, electronic localization, dipole, lipophilicity, or H-bonds capability just to name a few, have been of great benefit for numerous applications in many different scientific fields such as material science, agrochemical and pharmaceutical industries.

In a study conducted by Raines et al, computational analysis showed how the electrostatic potential surface of aromatic compounds is strongly affected by the substitution of the proton normally present in the benzene ring with fluorine atoms.^[94]

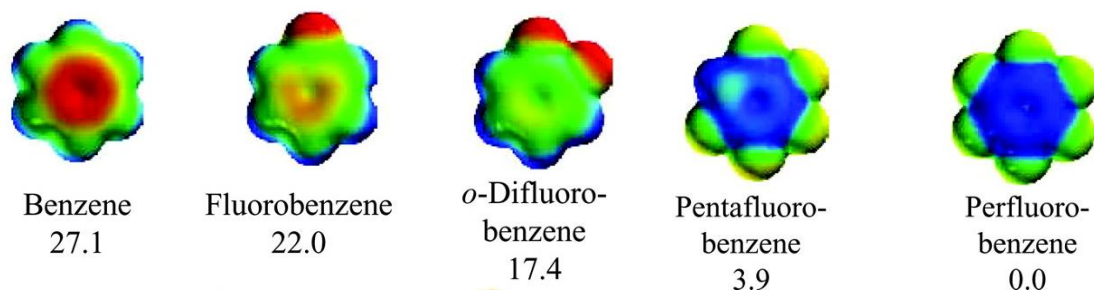


Figure 25: Electrostatic potential surfaces of aromatic inhalants and their cation- π interaction strengths. From [91]

The series of pictures visualizes benzene's electron density and how it shifts from the inside of the ring towards the fluorine substituents, along with the hydrogen/fluorine exchange. The energy was defined as the negative binding energy of a cation to the π electron cloud of benzene. The color code used is explained as follows: blue was used to identify an electrostatic potential equal to or more positive than 20 kcal/mol, while red on the contrary indicates a potential equal to or more negative than -20 kcal/mol.

1.4.1 Fluorine in medicinal chemistry

The analysis of the property changes induced by a single fluorine atom, if located in a crucial position of a bioactive molecule, was pioneered in 1970's by Fried et al. with studies on fluorinated derivatives of cortisone.^[95] Since then, methods for the introduction and exploitation of fluorine in medicinal chemistry have been the topic of profound and intense research and it is now clear how important this element is in the field of drug research. Nowadays, it is estimated that about 20% of market drugs are fluorinated pharmaceuticals and current trends in globally registered drugs suggest a promising future for this class of compounds.^[96] The excitement that can arise from this analysis is further endorsed by the fact that fluorine-containing compounds constitute over 50% of blockbuster drugs.^[97]

The reason for such success is to be attributed to both its physicochemical and pharmacokinetic properties.

Despite it is slightly larger than hydrogen, fluorine can be a reasonable hydrogen mimetic, with minimal steric impact on the binding mode to a receptor or enzyme and the greater stability of the C-F bond compared to C-H bond, allowing strategic H - F

Introduction

exchange in metabolically known attack sites. This allows to improve stability, inhibit oxidative metabolism and increase the bioavailability.^[98] The isosteric character of a *gem*difluoromethylen group compared to oxygen was investigated with computational methods^[99] and was verified by numerous reports of phosphotyrosine mimetics based on this strategy, as well as in the development of hydrolytically stable analogues of nucleosides,^[100] phosphoserine,^[99, 101] and phosphorylated sugars, such as arabinose.^[102]

Fluorine addition is known to influence the lipophilicity of a compound. This effect was well observed in a recent study from Hoffmann et al., where a new hydrophobicity scale for canonical amino acids and fluorinated counterparts was reported.^[103]

Interesting is also to observe the interaction the fluorinate compounds can have with the active site of enzymes. If it is inserted near a reactive center, this can lead to irreversible inhibition due to formation of a covalent bond between the enzyme and the substrate, with a fluorine acting as a leaving group. This knowledge was used in the development of warfare gas,^[104] as well as with more scientific purposes, for example in the identification of new reactive sites.^[105]

The pKa and the reactivity of neighboring functional groups can be modulated in order to achieve a favorable pharmaceutical profile. Van Niel et al. in 1999 demonstrated how the insertion of fluorine atoms allowed to reduce the pKa and obtain a selective human 5HT_{1D} receptor ligands with improved pharmacokinetic profiles, following the discovery of sumatriptan, a drug used against migraine.^[106] Fluorine can be introduced to increase acidity as well, as demonstrated by studies on methotrexate, a drug against rheumatoid arthritis, and its corresponding fluorinated analogue. The latter presents a decreased toxicity due to the presence of a single fluorine atom in γ to a carboxy group by increasing its acidity. This effect inhibits the formation of poly γ -glutamate metabolites, which are responsible for the adverse effects observed in the non-fluorinated analogue.^[107]

Last but not least, the dipole induced by fluorine atoms can result in electrostatic repulsion within a molecule, which in turns stabilizes a specific conformation. This effect was nicely observed in by DeBernardis et al., who found that specificity of 6-

Introduction

fluoronorepinefrine may result from conformational bias due to repulsive effect of fluorine to a vicinal hydroxy group.^[108]

The development of new API's require the analysis of their pharmacokinetics. Understanding the impact of fluorine atoms on the physico-chemical properties of polyfunctionalized molecules allowed the development of new potent drugs with optimal values in terms of potency, tissue distribution, clearance, and metabolic stability. A clear example is represented by the research on drugs acting on the central nervous system (CNS). The biological activity of such molecules depends on the ability to penetrate the lipophilic obstacle of the BBB (blood brain barrier) and ultimately reach the brain, where they can exert their bioactivity. One of the greatest advances of 20th century psychiatry has been the discovery of haloperidol as an antipsychotic drug acting by blocking dopamine receptors by Janssen Pharmaceutica. This compound represents the standard compound for butyrophenons, one of the most important class of neuroleptics^[109] and is included in the list of WHO (World Health Organization) of essential medicines.^[110] The fluorine in *para* position of the phenyl group turned out to be optimal for neuroleptic activity and along the research for more potent analogues, it was discovered that pimozide, containing 2 *para*fluorophenyl groups, was acting longer than haloperidol.^[111]

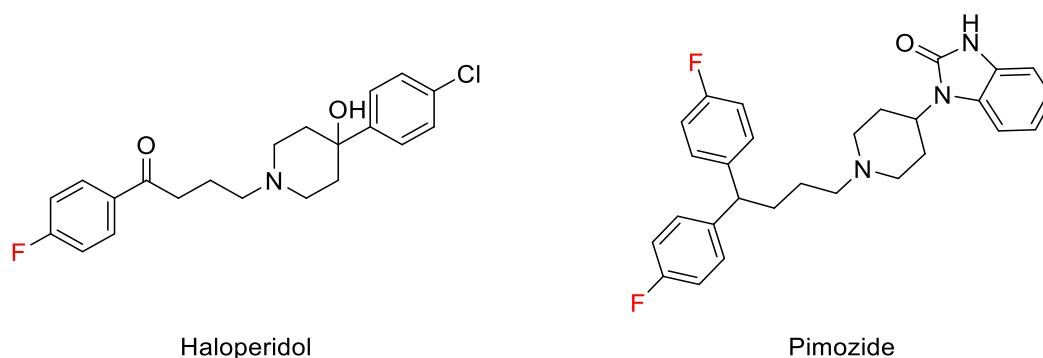


Figure 26: Neuroleptic drug Haloperidol and its longer lasting analogue Pimozide

Serotonin uptake inhibitors are another prominent class of CNS-acting drugs exerting an antidepressant effect. Currently, in the UK, there are 8 SSRI (Selective Serotonin Reuptake Inhibitors) that can be prescribed, 6 contain at least one halogen and 5 of them presents at least 1 fluorine atom; the structures are shown in Figure 27.^[112] Quite interestingly, sertraline shows one of the shortest half-life of the previously mentioned drugs, it is very slowly absorbed and undergoes extensive

Introduction

metabolic hydroxylation before excretion.^[113] All these properties may be associated with the lack of fluorine.^[114]

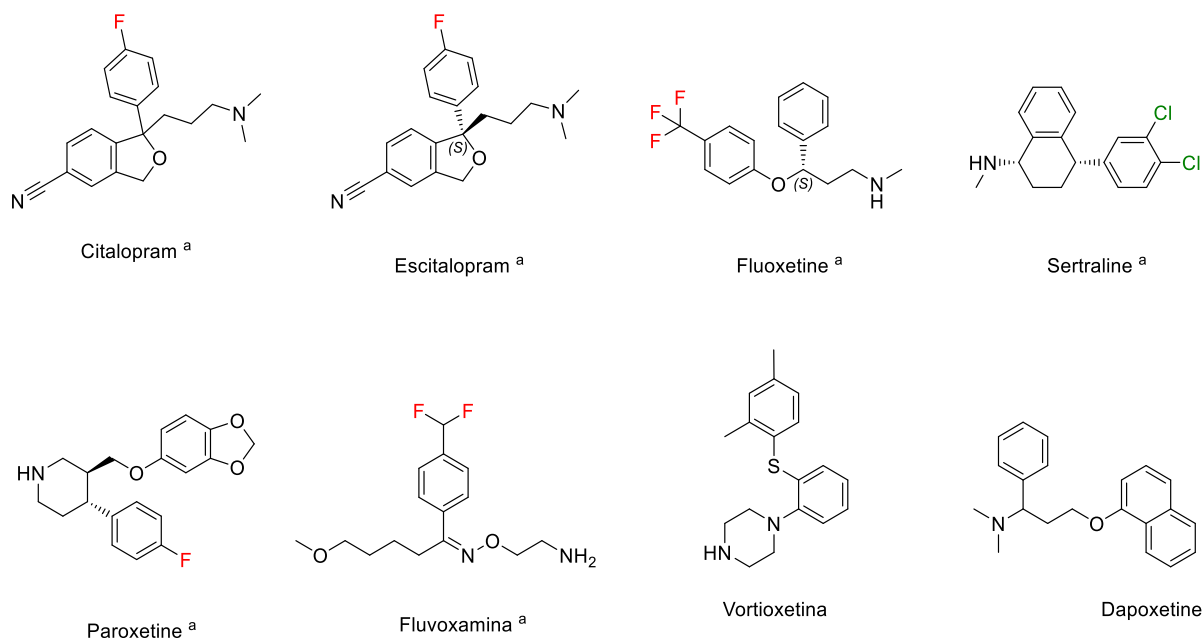


Figure 27: Selective serotonin reuptake inhibitors available in the UK. From [109] a: drugs authorized in Germany.^[115]

Another nice example of the incredible versatility of fluorine in medicinal chemistry is represented by fluoroestrogens. Despite the fact that estrogens can induce tumors in several animal species, a study from Liehr et al. proved that the addition of a fluorine atom in position 2 is able to prevent oxidation of that position, consequently impeding the formation of reactive species that would bind covalently to proteins and DNA. The study reveals the highly estrogenic yet non carcinogenic effect of 2-fluoroestrogen.^[116]

Furthermore, fluorine can be used as radioligand as well. In another study, it was demonstrated how fluorine is used to inhibit the extensive metabolic oxidation that would promote variations in the concentrations of 16α -[^{18}F]fluoroestradiol- 17β in the body. This molecule can then be used as a probe in PET imaging techniques, which would allow the visualization of primary breast tumors where it accumulates ^[117].

The beneficial effect of fluorine is of course not limited to these examples, many different drugs have been developed or investigated, for example in the case of the

famous Celecoxib, a selective cyclooxygenase inhibitor,^[118] or the development of Ezetimide, a drug that reduces the absorption of cholesterol in the intestine.^[119]

The role of fluorine in medicinal chemistry is so noteworthy that many reviews on this topic can be found in literature.^[98, 120]

1.4.2 Pentafluorophosphate

Within the elements belonging to the semi or non-metals that can be inserted in organic molecules and can be perfluorinated, such as boron, carbon, sulfur or phosphorus as a central atom, the latter is relatively under investigated when compared to the others. Boron trifluoride (BF_3), trifluoromethyl ($-\text{CF}_3$), or even the less common pentafluorosulfanyl ($-\text{SF}_5$) are known to be very stable groups with broad applications: Boron trifluoride is widely used as coordinating reagent, CF_3 is commonly encountered in different chemical industries and the SF_5 moiety is effectively used in agrochemistry, medicinal chemistry and material chemistry.^[121]

On the other hand, literature about pentafluorophosphates (PF_5^-) is limited, not only regarding the synthesis and complexity of molecules containing it, but also on the application and properties of this interesting moiety.

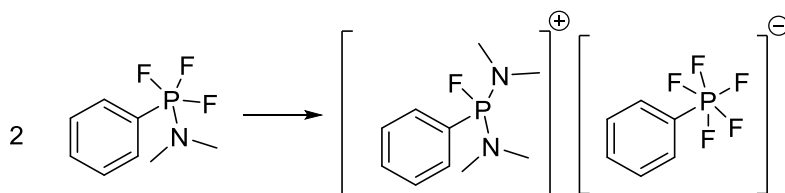
The utility of fluorine substitution in medicinal chemistry is very well demonstrated. As we saw, many pharmaceuticals present in their structure one atom of fluorine, which can be increased up to three yielding the trifluoromethyl group. This group has a broad application including medicinal chemistry^[122] or chemical synthesis. A small but meaningful example on how different a methyl group from a trifluoromethyl group can be observed in the strong increase in acidity of trifluoroacetic acid (TFA) when compared to acetic acid. ($\text{pK}_a_{\text{TFA}} = 0.52$, $\text{pK}_a_{\text{acetic acid}} = 4.76$).^[123]

Despite being less investigated than the trifluoromethyl group, pentafluorosulfanyl moiety proved to be a very interesting and pharmaceutically promising substituent and bioisosteric replacement.^[121b, 124] In 2017, Zhang et al. reported the synthesis of different pentafluorosulfanyl benzopyran derivatives as novel cyclooxygenase 2 (COX-2) inhibitors, producing highly potent and selective inhibitors with demonstrated efficacy in murine models for the treatment of inflammations.^[125]

Introduction

In order to investigate the application of any specific group, a synthetic method granting its availability is clearly fundamental. The introduction of trifluoromethyl groups^[126] or pentafluorosulfanyl^[127] is well established and the chemicals needed to insert them are commercially available. The situation is somehow different for pentafluorophosphates: despite the chemical analogy of these two perfluorinated group with the phosphate analogue, experimental data that strongly support the usefulness and the big potential in medicinal chemistry is somehow lacking in the case of latter, most likely due to synthetic issues.

Although an early report from 1963 on the synthesis of fluorophosphoranes (general formula PR_5) via reaction of chlorophosphines and group V fluorides does not mention pentafluorophosphates,^[128] the same authors one year later observed a “new phosphorus containing species” forming from a stored sample of phenyl dimethylamino trifluoro phosphorane over several weeks at room temperature.^[129] Spontaneous formation of a crystalline solid soluble only in acetonitrile or dimethylsulfoxide, was observed, despite no change in the elemental composition occurred. The observed reaction is reported in the following scheme.



Scheme 2: Isomerization of phenyl dimethylamino trifluoro phosphorane observed in 1964 by Schmutzler et al.^[129]

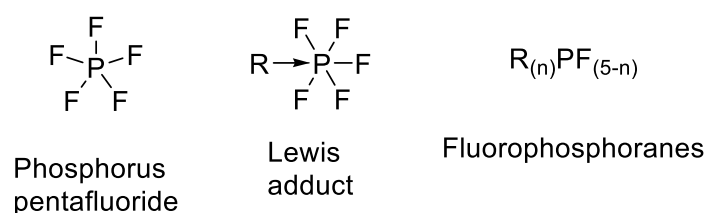
Back then, the authors reported hexacoordinated phosphorus species to be noteworthy for their paucity and claimed that there are no other well established precedents but the long known PF_6^- and PCl_6^- (from $PCl_4^+ PCl_6^-$). More studies published between 1960 and 1970 included spectroscopic characterization of fluorinated phosphoranes and characterization of the $R \rightarrow PF_5$ complex, formed reacting phosphorus pentafluoride (Lewis acid) with donor molecules (amines, alkyl phosphines or ethers).^[129-130]

Phosphorus pentafluoride reacts immediately with water yielding fluorophosphonic acids; it was first prepared in 1876 through fluorination of PCl_5 using AsF_3 but it can be obtained as well by treating PCl_5 with other fluorinating agents such as HF, AgF,

Introduction

SbF_3 , PbF_2 ^[131] or Me_3SnF .^[132] Decomposition and subsequent hydrolysis of lithium phosphorus hexafluoride is a problem in lithium batteries, yielding to increased degradation and loss of capacity. ^[133] Octahedral geometry of Na^+PF_6^- ^[134] and pyridine adduct of PF_5 ^[135] was confirmed via X-ray crystallography.

These initial studies characterized physically and spectroscopically phosphorus pentafluoride as a single molecule or in Lewis adducts, as well as different fluorinated phosphoranes, but a general method to introduce pentafluorophosphates without relying on the Lewis adduct in stable molecules was yet not well defined.

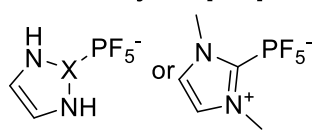
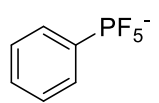
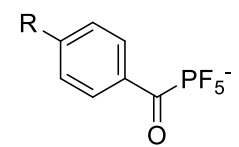
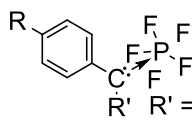


Scheme 3: Fluorine-containing pentacoordinated phosphorus species

Investigations on hexacoordinated pentafluorophosphates are quite recent and the few synthetic methods that have been reported are summarized in the following table.

Introduction

Table 2: Synthesis of pentafluorophosphates reported in the literature

Entry	Perfluoroalkyl chain with length from 1 to 12	Accessible via	Drawbacks
1.	$\text{F}_3\text{C}-\text{PF}_5^-$ [136]	a) Phosphine dichloride oxidation $\text{CF}_3\text{PCl}_2 + \text{N}_2\text{O}_4$ <i>then</i> b) Phosphonic acid dichloride fluorination $\text{CF}_3\text{P}(\text{O})(\text{Cl})_2 + \text{TMAF}$	Inconvenient preparation s.m.
2.	R_f-PF_5^- [137]	Phosphonic acid fluorination $\text{R}'\text{P}(\text{O})(\text{OH}) + \text{HF}_2^- + \text{H}^+$	Harsh conditions Glass incompatible
Heterocycle [138]			
3.	 $\text{X} = \text{CH}, \text{CHCH}_2$	Thermolysis of corresponding PF_6^- salt	High Temperature (400 °C)
Phenyl [139]			
4.		One-pot phosphine dichloride oxidation + fluorination $\text{PhPCl}_2 + \text{Br}_2 + \text{KF}$	fast hydrolysis in open atmosphere
Benzoyl [140]			
5.	 $\text{R} = \text{Cl}, \text{CF}_3$	Hydrolysis of corresponding carbene  $\text{R}' \text{ R}' = \text{morpholine}$	- only Cl isolated - no yield reported

Introduction

Entry 1 summarize the investigations of Pavlenko et al. regarding the preparation of trifluoromethyl pentafluorophosphate.^[136] The compound was obtained oxidizing trifluoromethyl phosphine dichloride and fluorinating the resulting phosphonic acid dichloride with substoichiometric amounts (<5 equivalents) of tetramethyl ammonium fluoride. The reaction yielded equimolar amounts of monofluoro and pentafluorophosphates. The less soluble and consequently less reactive cesium fluoride was successfully tested as well, and allowed the preparation of trifluoromethyl pentafluorophosphate as cesium salt. Drawbacks of these two methods are the inconvenient access to the precursors (phosphonic acid dichloride), the experimental set up in order to use N₂O₄ and the reaction time (dismutation of phosphoryl trifluoride to monofluoro and pentafluorophosphate occurs slowly and at low temperature). The cost of anhydrous tetramethyl ammonium fluoride was indeed an additional limiting factor and no generally applicable purification method was proposed, since the product was obtained via recrystallization.

Entry 2 described the work of Ignatyev et al, where perfluoroalkylated chains functionalized with a phosphonic acid were converted into their pentafluorophosphate analogue by reaction with concentrated sulfuric acid and bifluoride salt at 100 °C. These anhydrous very harsh conditions eliminated the problem of the cost of the fluorinating agent, but the use of HF requires a specific HF-resistant set up, beside the high health hazard. Furthermore, these reaction conditions precluded perfluorination of molecules with acid- and temperature-sensitive functional groups.^[137]

The work of Tian et al. from 2012 is described in Entry 3. Here, pentafluorophosphates were obtained starting from N-heterocyclic carbene (NHC) and hexafluorophosphate salt via thermolysis at 400 °C of the salt. The mechanism used here relies on the thermal decomposition of the very stable hexafluorophosphate salt into phosphorus pentafluoride, followed by its reaction with the carbene. This synthesis exploit once again the formation of a Lewis adduct between PF₅, and an electron donor (the NHC), using harsh conditions with restricted application in organic chemistry.^[138]

Introduction

An interesting one-pot procedure was described by Vabre et al in 2017 (Entry 4). Starting from phosphine dichloride, the oxidation with molecular bromine and fluorination with KF allowed the preparation of phenyl pentafluorophosphates. Beside the limited versatility of using phosphine dichlorides as starting materials, unfortunately this compound showed fast hydrolysis in open atmosphere. Nonetheless, this research work shows potentially very interesting *in vivo* pharmaceutical application as radiotracer for ^{18}F -PET imaging of the NHC-pentafluorophosphates, previously reported by Tian et al. ^{18}F radiolabeled pentafluorophosphono NHC was injected in a murine model and PET scans showed accumulation of the compound in the urinary track. Very importantly, no bone uptake was observed, indicating no ^{18}F release after 3 hours. Further research on the medical applicability of this adduct is reported to be ongoing.^[139]

Research on benzoyl pentafluorophosphates (Entry 5) was reported by Guzyr in 2013 via hydrolysis of the corresponding carbene, which was obtained with reaction of aryl keto phosphonate and MOST (morpholino sulfur trifluoride). The spectroscopic characterization of this compound is unfortunately not accompanied by a synthetic protocol, a purification method and a final yield.^[140]

Difficulties in the synthesis of pentafluorophosphates were also reported by Michael Könnner in his bachelor thesis at Freie Universität Berlin under the guidance of Prof. Rademann.^[141] In the attempt of producing monofluorophosphonates, after fluorination of the phosphonic acid dichloride with a KF and RP-HPLC purification, a fraction containing a sample phenyl *gem*-difluoromethylen pentafluorophosphate was identified. Despite subsequent attempts with different fluorinating reagents such as NaF or even the more exotic XeF_2 , super dry conditions (addition of molecular sieves or sulfuric acid), and controlling the reaction via ^{19}F and ^{31}P NMR, the product could not be detected again.

2 Aim of the project

Few methods for the preparation of small molecules containing the pentafluorophosphate moiety were reported in the literature. However, an efficient synthetic protocol compatible with different functional group, which was not relying on expensive reagents or harsh conditions and was glass-compatible, was still missing. Stability issues were also observed with specific compounds such as PhPF_5^- or the acyl pentafluorophosphate reported in entry 5 of Table 2.

Although non-cleavable fluorinated phosphotyrosine mimetics are good inhibitors of phosphatases *in vitro*, they failed *in vivo* based assays due to their high hydrophilicity and subsequent inability to cross the cellular membrane.

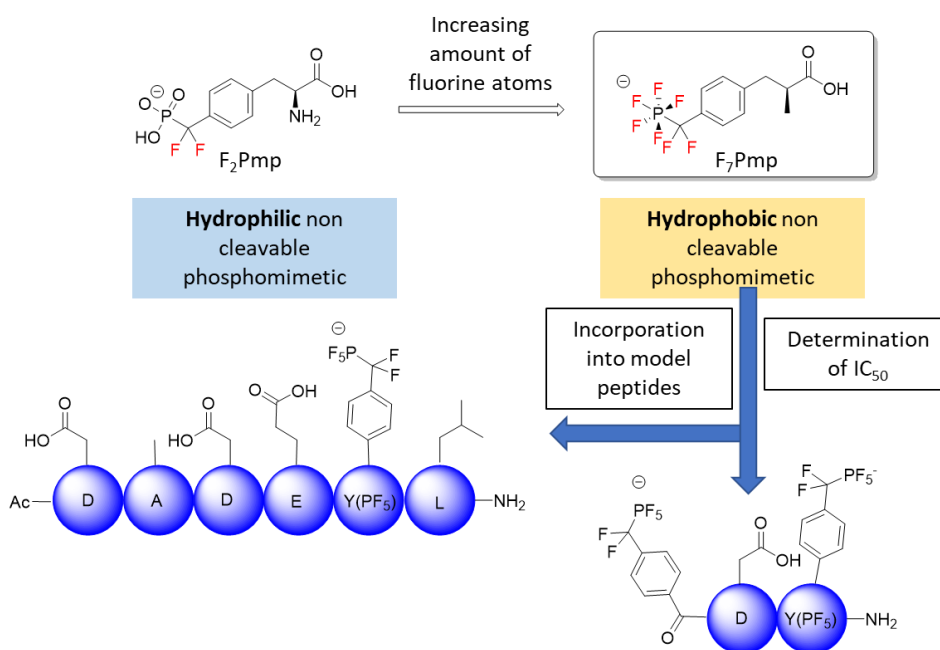
Considering the interesting properties and wide application of trifluoromethyl or pentafluorosulfanyl group, analogous investigations on pentafluorophosphates were still missing and compounds bearing it remained relatively unexplored. One of the reasons for this lack of knowledge, in addition to the specific instability of some structure, might have been the absence of a versatile synthetic procedure compatible with the presence of other functional group in the molecule.

The proven efficacy of CF_3 and promising results of the SF_5 derivatives, respectively in lead optimization or drug discovery, stimulates the interest and support efforts to validate pentafluorophosphates as pharmaceutically useful entities as phosphate mimetic in biological processes.

In order to address this challenge, the first crucial objective was the identification of a reproducible protocol, allowing functionalization of complex scaffolds with mild conditions. Its identification led to the availability of the first fragments, the potency of which was evaluated as phosphatase inhibitor. The encouraging *in vitro* results supported efforts in the process development phase, aiming to optimize important reaction parameters, such as time, cost, overall yield, number of steps, and last but not least, ease of execution. Achieving this important objective granted easy access to big amounts of pentafluorinated building block and allowed to further expand the aim of the project from small fragments to more complex ligands such as peptides. The

Aim of the project

increased lipophilicity of pentafluorinated fragments offered a possibility to overcome the previously mentioned limitation of the polar *gem*-difluoromethylen phosphonic acid as tyrosine mimetics. Consequently, final objectives of this research work was the biological evaluation of pentafluorophosphates as phosphotyrosine peptidomimetics, a deeper evaluation of pharmaceutically relevant physical properties such as lipophilicity and cell permeability of this interesting and under investigated moiety and a final comparison with the known *gem*-difluoromethylen phosphonate.



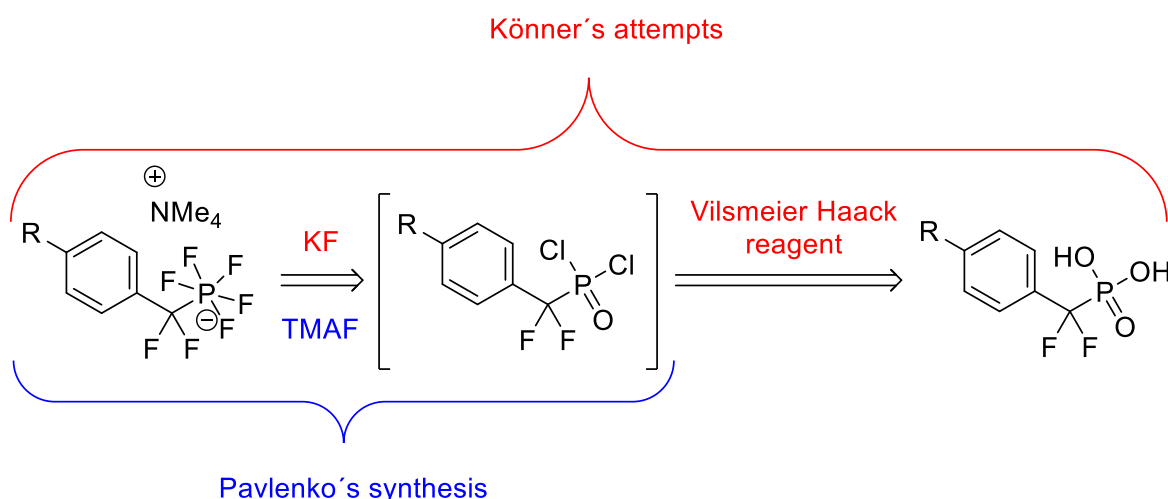
3 Results and Discussion

3.1 Early chemical synthesis of pentafluorophosphates

3.1.1 Overview of the strategic plan

After analyzing the previous works and having identified their drawbacks, early investigations on pentafluorophosphates started combining the successful but not reproducible Könner attempt (based on phosphonic acid chlorination with oxalyl chloride and subsequent reaction with fluoride salts) with the results reported by Pavlenko et al. (fluorination of phosphonic acid dichloride with TMAF).

Consequently, instead of following the previously described published oxidation of dichlorophosphine with N_2O_4 or Br_2 , the phosphonic acid dichloride was obtained via chlorination of the phosphonic acid with a combination of oxalyl chloride and DMF, also known as the Vilsmeier Haack reagent. The fluorinating step was carried out using commercially available anhydrous TMAF instead of KF.



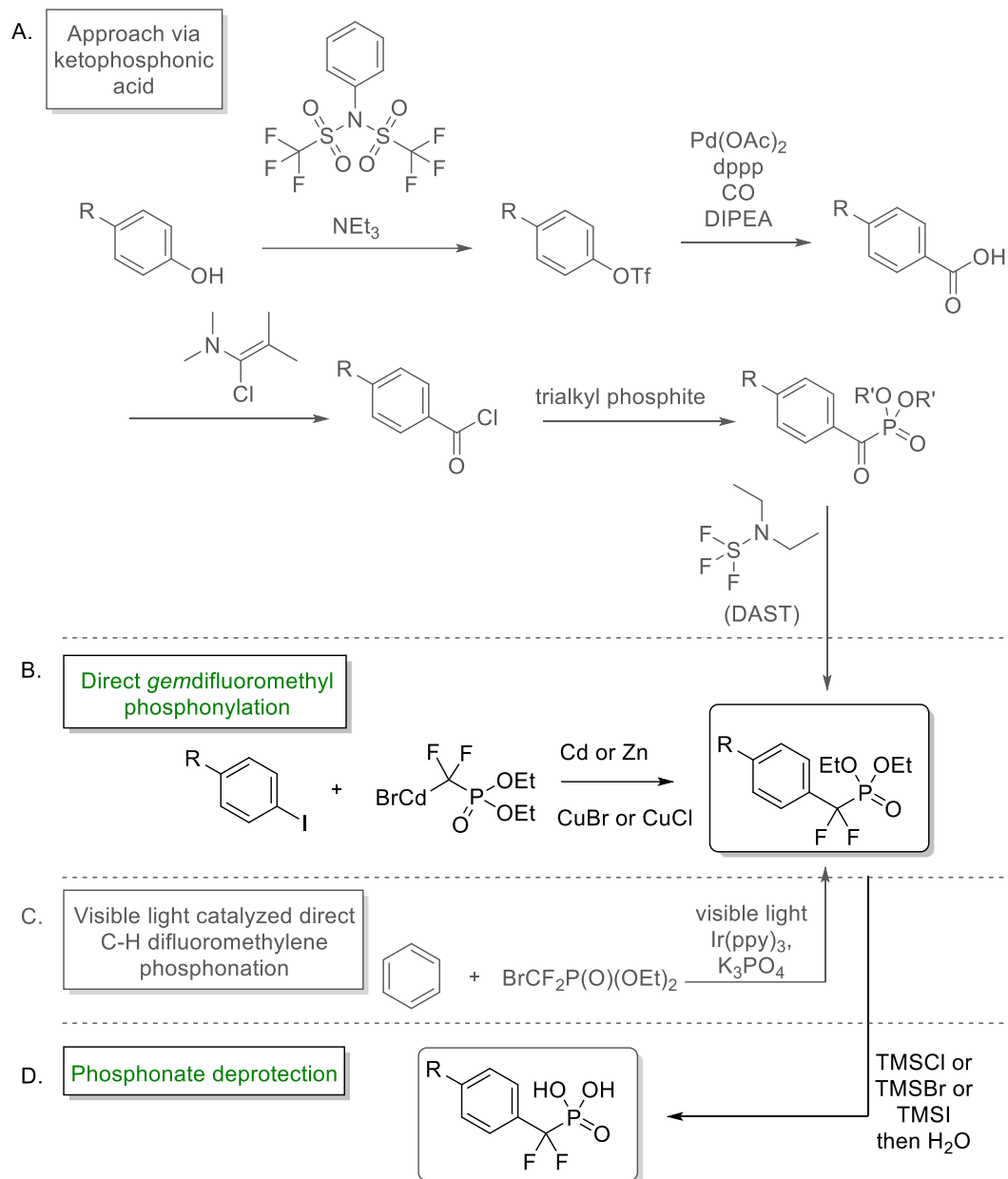
Scheme 4: Initial approach for the synthesis of pentafluorophosphates using phosphonic acid dichloride, obtained from the corresponding acid, and reacting it with TMAF.

In order to obtain a non-cleavable phosphotyrosine mimetic, the presence of CF_2 bridge between the phosphorus and the phenyl ring is crucial. There are different ways to obtain gemdifluoromethylen phosphonic acid derivatives. One possible synthetic pathway was reported by Dr. Wagner in his doctoral dissertation.^[142] As

Results and Discussion

shown in Scheme 5A, the transformation of phenolic OH into a good leaving group (triflate in this case) was followed by carbonylation reaction yielding the carboxylic acid derivative. Chlorination with the Ghosez reagent was followed by reaction with a trialkyl phosphite, yielding the ketophosphonic acid via a mechanism similar to the Arbuzov reaction. The keto group could then be fluorinated with diethylamino sulfur trifluoride (DAST), yielding the gemdifluoromethylen phosphonic acid. Since the present work was not focused on benzoyl phosphonates, the synthesis could be shortened following the previously mentioned pioneering studies of Burton et al. using the now commercially available diethyl bromo *gem*difluoromethylen phosphonate building block. This useful building block was inserted in only one step onto a iodinated arene as shown in the second part of the scheme (Scheme 5B).

Results and Discussion

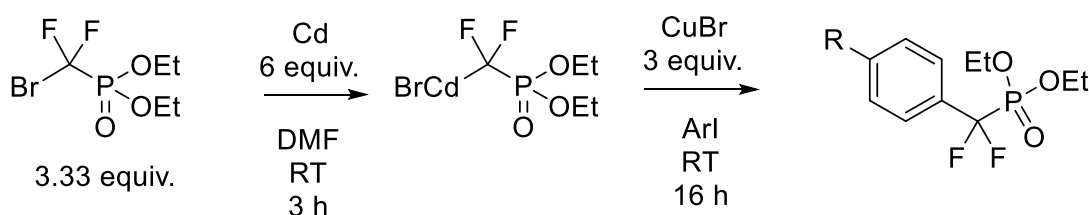


Scheme 5: Possible synthetic strategies for the synthesis of gemdifluoromethylene phosphonic acids

An interesting improvement for such transformation is the recently reported photochemical reaction reported by Wang et al in 2014.^[143] Using a photosensitizer *fac*-Ir(ppy)₃ in presence of a base and LED light, the researchers could synthesize a *gem*difluoromethylen phosphonic acid starting from benzene. (Scheme 5C) Nonetheless, the route according to scheme 5B was chosen. Ultimately, phosphonic acid deprotection was carried out with standard silylating reagent such as silyl halides, followed by hydrolysis of the silyl ester resulting in the free phosphonic acid (Scheme 5D)

3.1.2 *Gem*difluoromethylen phosphorylation of iodo arenes

The Cu (I) mediated coupling of organocadmium reagent with iodo arene was pioneered by Burton et al.,^[144] who reported reactions of bromo *gem*difluoromethylen phosphonate with zinc as well. ^[145] and investigated the use of different copper (I) halides, such as CuBr or CuCl.^[146] This this research work, cadmium and CuBr were chosen because of the higher yield associated to their use. Hence, commercially available bromo *gem*difluoromethylene ethyl phosphonate was reacted with metallic cadmium in a polar aprotic solvent under dry conditions and transformed into the corresponding organometal; subsequent coupling to a iodo arene in presence of CuBr yielded ethyl protected phenyl phosphonic acid. The general reaction scheme is summarized below.



Scheme 6: General synthesis of CuBr-mediated cadmium coupling of bromo *gem*-difluoromethylen phosphonate with iodo arenes

The activation of metallic cadmium was carried out using aqueous solution of HCl followed by washing with water and acetone. The activated shiny metal was then covered in DMF and reacted with the bromo *gem*difluorophosphonate in a Grignard-like reaction. After gentle heating, the reaction is triggered and by releasing energy, it proceeds readily without additional heating. After 3 hours, the solution was added

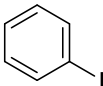
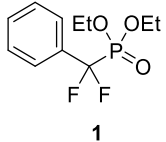
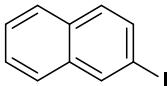
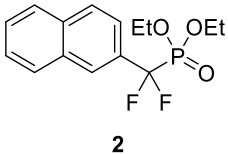
Results and Discussion

dropwise to a mixture of iodo are and copper salt in DMF and left stirring for 16 hours.

Critical to this reaction is water exclusion. All reagents, chemicals solvents and glassware need to be thoroughly dried. The formation of the organocadmium is obviously crucial and depends on the temperature. Too little heat and the reaction will not proceed well. Furthermore, it is reported that once formed, the organozinc $(\text{EtO})_2\text{P}(\text{O})\text{CF}_2\text{ZnBr}$ in presence of the copper halide in the second step decomposes slowly but spontaneously to yield both geometrical isomers of the 1,2-difluoroethendiyl *bis*phosphonate.^[147] Consequently, the addition of the organo cadmium to the mixture of iodo arene and copper bromide was carried out in small portions over a prolonged period of time, in order to avoid decomposition. The expected conversion to the final compound avoiding the formation of the side products was verified by the procedure reported by Meyer in 2011, where in the crude mixture 93% conversion to the desired phosphonate was observed.^[148]

Following the reaction condition described above, the synthesis of phenyl and naphthyl *gem*difluoromethylen diethyl phosphonate was achieved. The results are summarized in the following table.

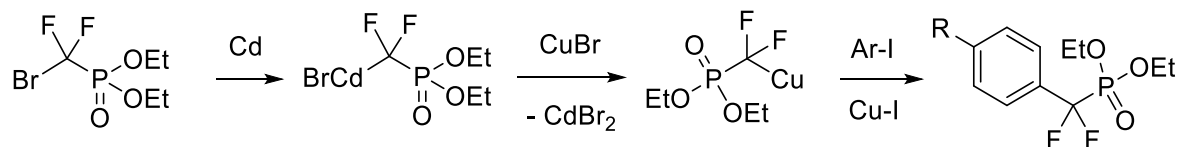
Table 3: Synthesis of *gem*difluoromethylen phosphonic acid diethyl ester

Entry	Starting material	Final product	Yield
1		 1	84%
2		 2	91%

After an aqueous workup with ammonium chloride to quench reactive species, to remove metal ions from the mixture and to wash away water soluble byproduct, the organic layer was dried and subjected to column chromatography, yielding the desired product in very good yield.

Results and Discussion

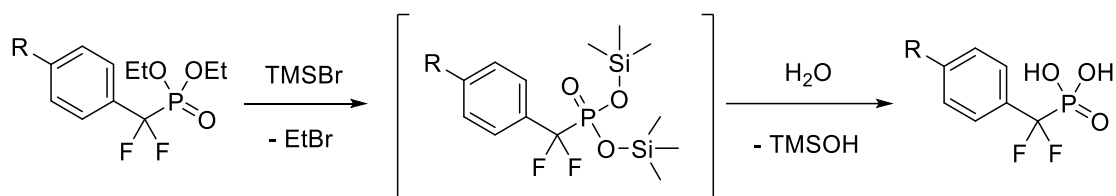
The reaction mechanism reported in the following scheme was suggested by Burton: the formation of the organocadmium is followed by the formation of the organocuprate, which react with the iodinated arene yielding the coupling product.



Scheme 7: Reaction mechanism as reported by Qiu.^[146a]

3.1.3 Deprotection of phosphonic acid esters

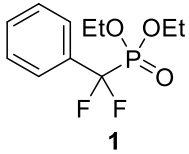
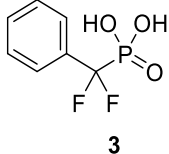
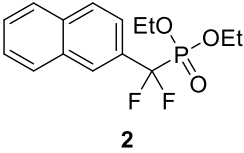
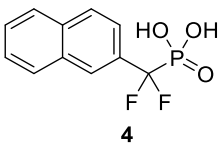
Reaction of phosphonic acid esters with a trimethylsilyl halide, such TMSBr or TMSI yields the corresponding silyl esters, which undergo hydrolysis to the free phosphonic acids, as summarized by the following reaction scheme.^[149]



Scheme 8: General synthesis of phosphonic acid

As described in the scheme above, the halogen of the silyl halide attacks the protecting alkyl chain of the phosphonate, resulting in the formation of gaseous bromoethane and the monosilyl ester; the second equivalent of TMSBr complete the silylation reaction. This product can then be hydrolyzed in a mixture of MeOH and water. This reaction was performed using TMSBr comparing two slightly different conditions. The reaction in DCM proceeded slowly but after 16 hours it was complete. In order to speed up the process by increasing the temperature, a higher boiling solvent was chosen. For this purpose, ACN was used and the reaction stirred in a microwave reaction and warmed up to 70°C proceeded steadily in 3 hours. The conditions tested are reported in the following table, which includes the experiment conducted by Dr. Wagner.^[150] Purification of these phosphonic acid was performed on MPLC using C18 silica cartridges of suitable size and H₂O/ACN (5 to 99%) as mobile phase. Lyophilization yielded the phosphonic acid as a white powder.

Table 4: Synthesis of phosphonic acids

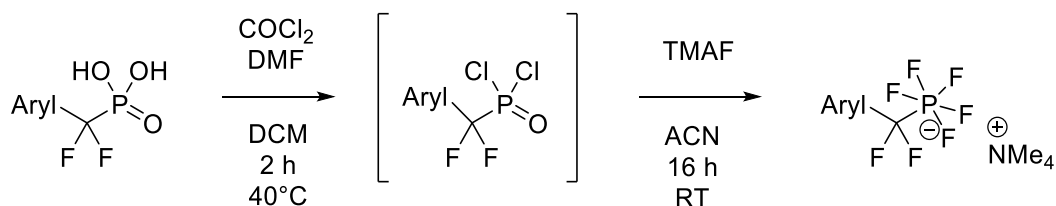
Entry	Starting material	Conditions	Final product	Yield
1		TMSBr DCM, 16 h, RT		98%
2		TMSBr ACN, 3 h, 70 °C		78% ^a

Results and Discussion

a: *performed* *by* *Dr.* *Stefan* *Wagner.*^[150]

3.1.4 First pentafluorinated fragments

As anticipated, the first investigation on small fragments containing the pentafluorophosphate moiety was achieved using as a starting point the chlorination protocol described by Michael Könnner and Stefan Wagner plus the investigations of Pavlenko et al.^[136] and is summarized in Scheme 9.



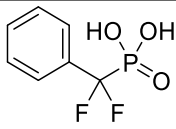
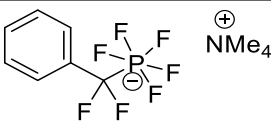
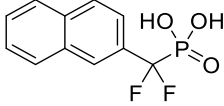
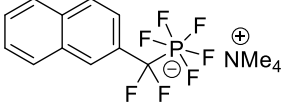
Scheme 9: Early synthesis of pentafluorophosphates from phosphonic acid

According to the scheme, the phosphonic acid was converted into the labile dichloride in DCM with the Vilsmeier Haack reagent, a combination of oxalyl chloride and DMF yielding the chloroiminium ion as reactive species. Formation of dichloride was accompanied by a change in the color of the reaction mixture, turning from colorless to yellow. Removal of DCM plus the excess of reagents under high vacuum was followed by redissolution of the crude product in dry ACN and the addition of stoichiometric amounts of anhydrous TMAF at RT. After 16 hours, the reaction was concentrated at rotary evaporator and the precipitate was collected and dried under vacuo. This reaction protocol was not reproducible but allowed the successful synthesis of the two target compounds even if the isolated yields were very low.

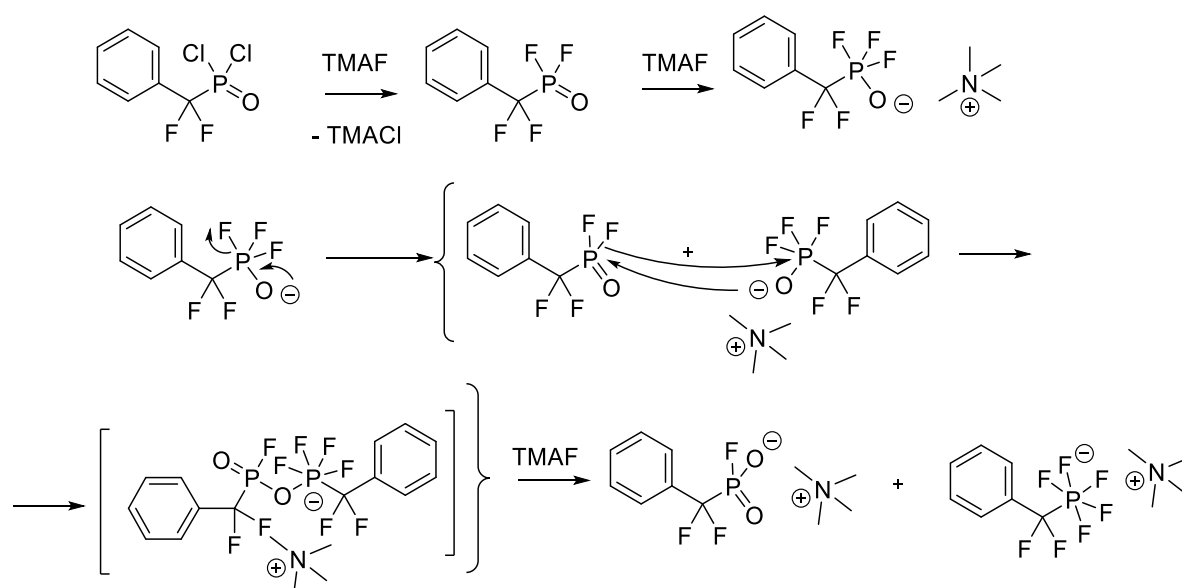
Summarizing, in such experiments 2.5 equivalents of oxalyl chloride and 4.1 equivalents of TMAF were used; despite the application of the same reaction conditions to the phenyl and naphthyl substrate, the isolated yield dropped from 21% to 6%.^[150] These results are summarized in the following table.

Results and Discussion

Table 5: Early synthesis of pentafluorophosphates

Entry	Starting material	Final product	Yield
1			21%
2			6%

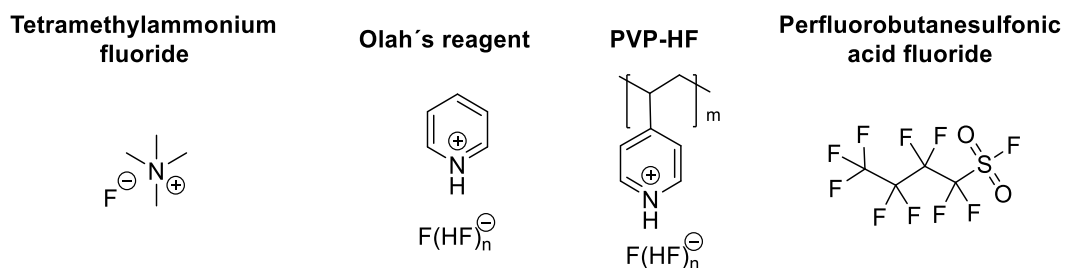
The mechanism, described in the following scheme, was proposed by Pavlenko and is based on the intermolecular reaction between phosphonic trifluoride and difluoride into monofluoro phosphonates and pentafluorophosphates upon formal addition of another equivalent of TMAF. According to this study, the reaction was carried out at -17 °C in DME (dimethoxyethane) overnight.



Scheme 10: Mechanism of perfluorination reaction reported by Pavlenko.^[136]

Due to the high cost of the anhydrous TMAF, other fluorinating agents were tested as well and their structures are shown in the following scheme (Scheme 11).

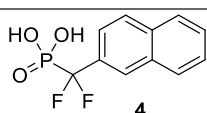
Results and Discussion



Scheme 11: Tested fluorinating agents

The use of pyridinium poly hydrogen fluoride, both in solution and on solid support (known as poly-(4-vinylpyridinium poly-(hydrogen fluoride)) or PVP-HF), with and without and external source of fluoride, was investigated without success. Due to the necessity to formally remove the oxygens from the phosphorus center and substitute them with fluoride, the use of the nonafluorobutanesulfonyl fluoride (NfF) was considered a possible alternative. Unfortunately, in this case the desired reaction was not observed either. The results are summarized in the following table.

Table 6: Perfluorination attempts with alternative fluorinating reagent: a) monitored by LC-MS (DI) b) monitored by TLC (SiO₂); c) monitored by NMR;

Entry	Starting material	Reaction conditions	PF ₅ conversion
1		Olah's reagent (10 eq.) RT, 24 h, ACN	0 ^a
2	4	Olah's reagent (10 eq.) + NaF (5 eq.) RT, 24 h, ACN	0 ^{a,b}
3	4	NfF (7 eq.) + DBU (10 eq.) RT, 24 h, ACN	0 ^b
4	4	NfF (7 eq.) + DBU (10 eq.) + NaF (4 eq.) RT, 24 h, ACN	0 ^b
5	4	PVP-HF 60 °C, 16 h, ACN	0 ^c

The only suitable reagent for a mild conversion to the pentafluorophosphate appeared therefore to be the anhydrous tetramethylammonium fluoride but its high cost (92 €/g from Sigma Aldrich) united with the stoichiometric excess needed was still a relevant and limiting factor. Furthermore, its extremely high hygroscopicity was complicating its handling, with increasing doubts about its reliability over the time.

3.2 Extension of the strategic plan to PF₅ amino acid

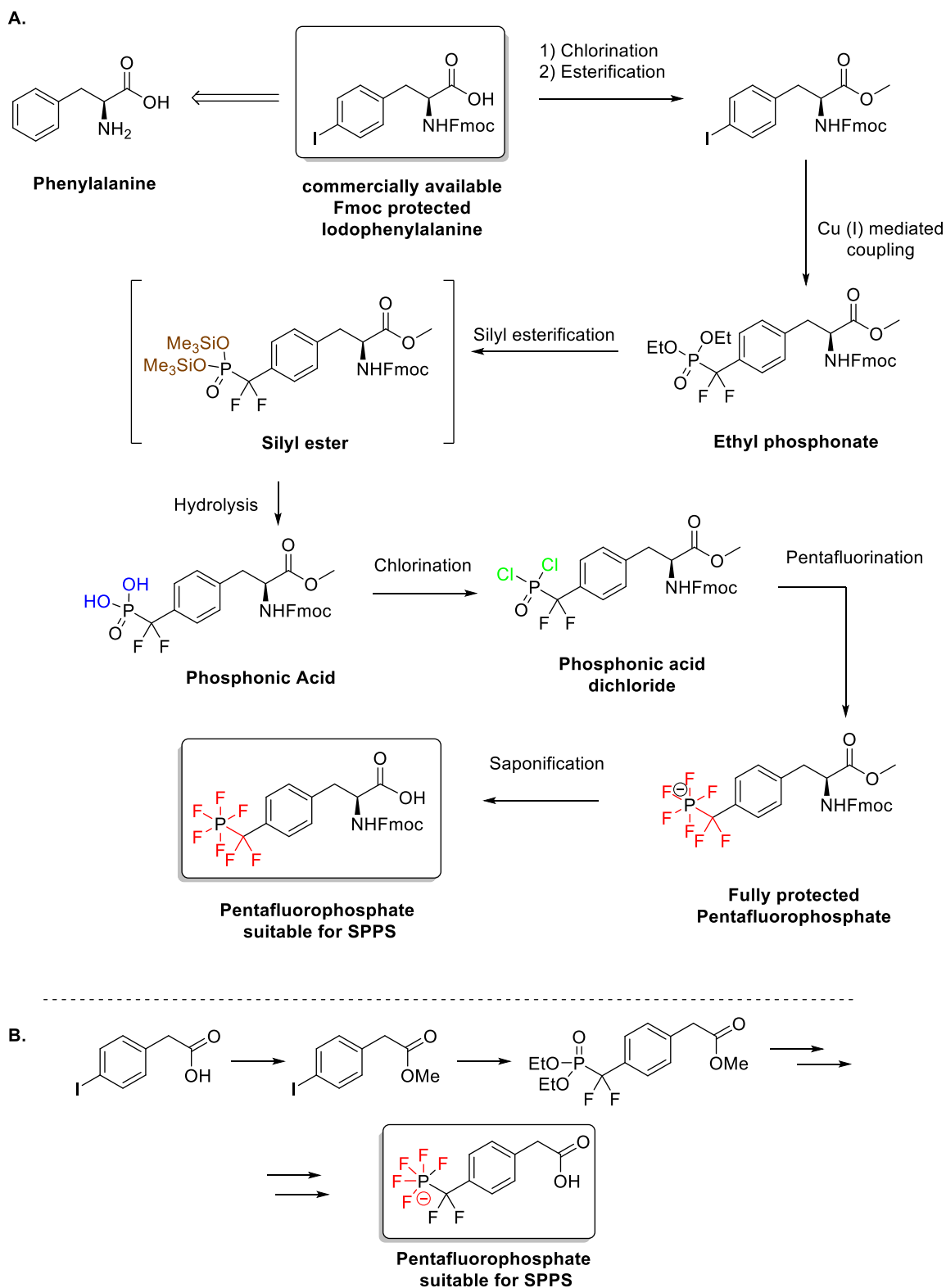
After the success represented by the first synthesis, the research work proceeded focusing on the preparation of the first pentafluorinated phosphotyrosine mimetic.

In order to continue with the strategy highlighted in the previous chapter, *gem*difluoromethylen phosphonates were needed as starting material. The synthesis of non-cleavable phosphotyrosine mimetic was very well reported in the literature, and the synthesis of CH₂, CHF and CF₂ was accurately described by Burke et al.^[151] A more recent synthesis that take advantage of the commercial availability of BrCF₂P(O)(OEt)₂ was reported by Meyer et al. and was used with slight modifications. Instead of protecting the carboxylic acid of the amino acid with a silyl group, the methyl ester was chosen and the consequent methods for its introduction and cleavage were changed accordingly. The synthetic pathway from commercially available Fmoc protected iodophenylalanine to the pentafluorinated amino acid is summarized in the following scheme 12A.

The commercially available Fmoc protected iodophenylalanine was protected at its carboxylic acid functionality via formation of the methyl ester in a standard organic chemistry reaction. The protected amino acid was then converted into its corresponding diethyl phosphonate with the same Cu mediated organocadmium coupling described for the case of phenyl and naphthyl halides. The deprotection the phosphonic acid was performed via formation of the silyl ester and subsequent hydrolysis as previously discussed. The so formed *gem*difluoromethylen phosphonic acid was then converted into the corresponding dichloride and perfluorinated using reaction conditions that allowed the aforementioned successful preparation of the early pentafluorinated fragments.

Considering that the ultimate goal was the synthesis of two peptide sequences, one of which was composed by a phenylacetic acid derivative (see Chapter 2: Aim of the project), the preparation of this last building block deriving from iodophenyl acetic acid was rationalized without crucial modifications to the protocols used so far. (Scheme 12B)

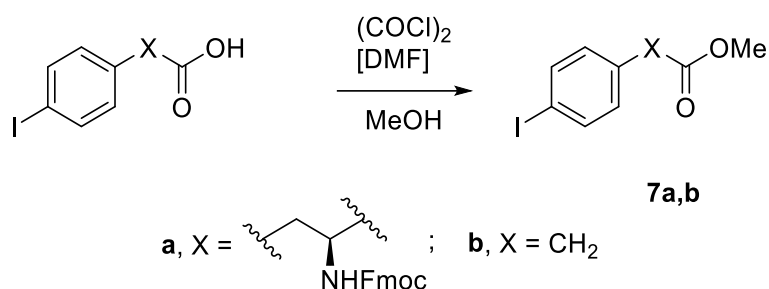
Results and Discussion



Scheme 12: A. Synthetic pathway from commercially available Fmoc-(4-I)-Phe-OH to Fmoc-(4-PF₅CF₂)-Phe-OH. B. Analogue approach using iodophenyl acetic acid as scaffold to 4-PF₅CF₂-phenylacetic acid.

3.2.1 Synthesis of methyl ester

In order to prepare the building blocks for subsequent reactions, it was necessary to convert the carboxylic acid into the corresponding ester. This well-known modification was carried out using the standard protocol involving activation of the carboxylic acid as a carboxylic acid chloride with Vilsmeier-Haack reagent in MeOH, yielding the related methyl ester, as summarized in the following scheme.



Scheme 13: General reaction of methyl esterification

The Fmoc-(4-I)Phe-OH was converted in the corresponding methyl ester **7a** in 92% yield. The iodophenyl acetic acid was subjected to the same reaction conditions and methyl ester **7b** was obtained in 70% yield as summarized in the table below.

Table 7: Overview of methyl esterification reaction

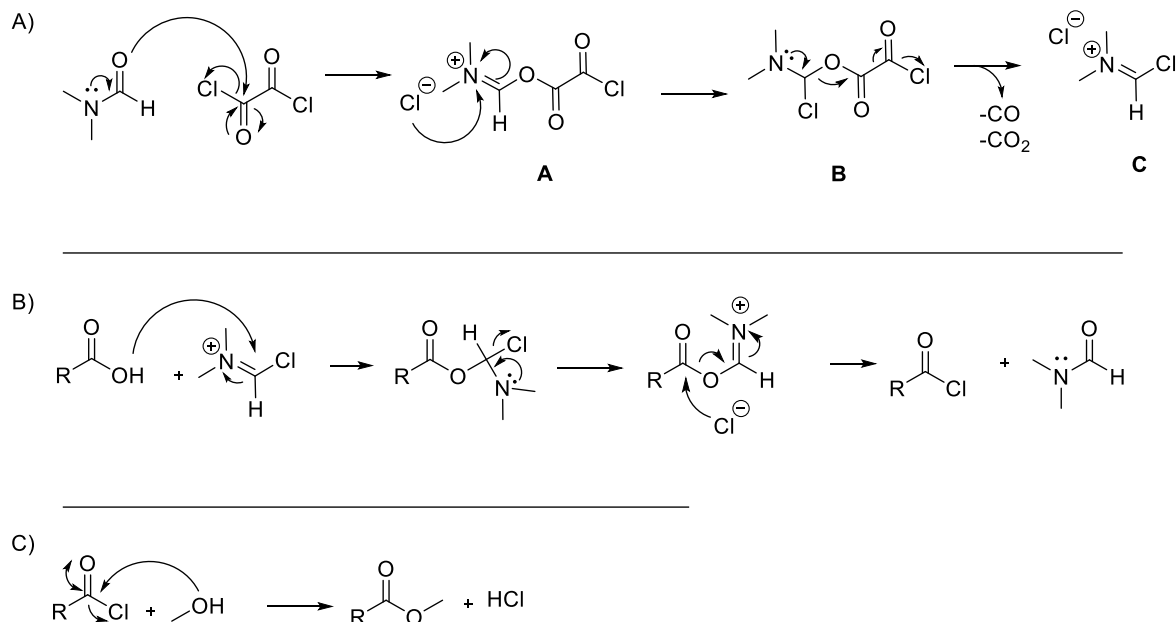
Entry	Starting material	Final product	Yield
1			92%
2			70%

The chlorination reaction proceeds via the mechanisms summarized in the following scheme.

The nucleophilic attack of DMF on the oxalyl chloride yields the intermediate **A** that reacts again with the chloride anion released producing the instable intermediate **B**. The electronic rearrangement produces the gaseous byproducts carbon monoxide,

Results and Discussion

carbonic anhydride and hydrochloride acid (which conveniently escape the reaction flask), ultimately yielding the chloroiminium cation **C**, known as Vilsmeier-Haack reagent, as stable product. (Scheme 14A)

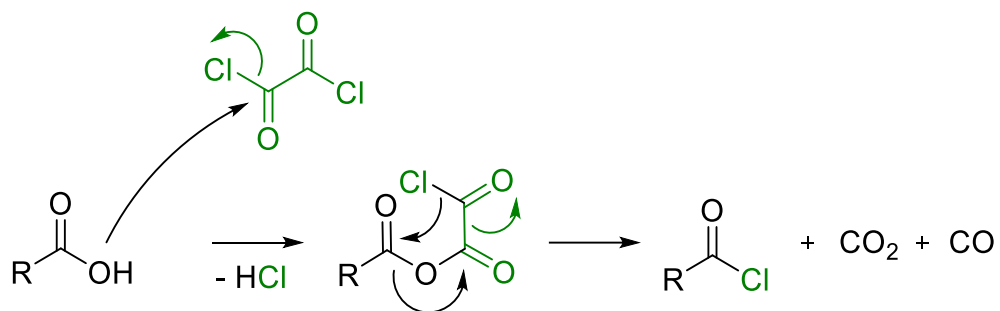


Scheme 14: Mechanism of chlorination and subsequent esterification: A) Preparation of Vilsmeier-Haack reagent; B) Chlorination of a carboxylic acid; C) Methyl esterification of the acyl chloride

The in-situ prepared chlorinating agent **C** react with the carboxylic acid yielding the acyl chloride and regenerating DMF which can reenter the catalytic cycle. (Scheme 14B).

Ultimately, the acyl chloride reacts with the solvent, in this case methanol via nucleophilic attack, producing the desired ester together with one equivalent of hydrochloric acid (Scheme 14C).

Although oxalyl chloride alone is a good chlorination reagent, it was found that Vilsmeier reagent is stronger and more active.^[152] The chlorination mechanism in absence of DMF is reported in the following scheme.^[153]

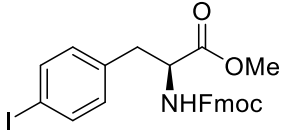
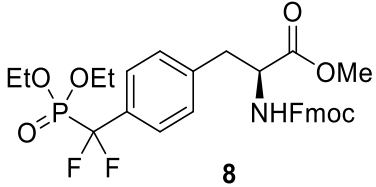
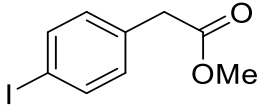
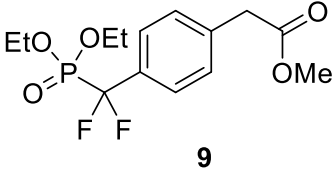


Scheme 15: Chlorination of carboxylic acid with oxalyl chloride in absence of DMF^[153]

3.2.2 Synthesis of diethyl *gem*difluoromethylen phosphonates

In order to obtain the protected phosphono amino acid, the method previously described for phenyl and naphthyl phosphonate was used. Hence, the formation of the organocadmium phosphonate was followed by slow reaction with CuBr and the iodinated arene.

Table 8: Synthesis of *gem*difluoromethylen phosphonic acid diethyl ester

Entry	Starting material	Final product	Yield
1			>99%
2			>99%

With the few precautions highlighted previously when discussing this reaction, the synthesis didn't present any particular problems; it proceeded smoothly and after an aqueous work up, the purification of the crude on column chromatography allowed the isolation of the desired product.

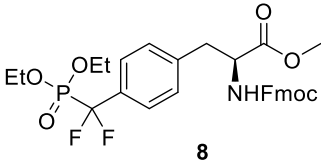
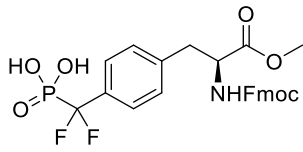
3.2.3 Deprotection of phenylalanine phosphonic acid

The preparation of phosphonic acids from the related diethyl ester was achieved as previously described using trimethylsilyl halide^[149] and the resulting silyl ester was subsequently hydrolyzed with H₂O yielding the corresponding free phosphonic acid. Excluding the stable trimethylsilyl fluoride and TMSCl, reported to cleave phosphonic acid esters only at temperature above 130 °C over long period of time (>8 h)^[154], the performances of TMSBr and TMSI were analyzed and reflected the relationship between reactivity and the atomic number of the halogen.

The results are summarized in the following table.

Results and Discussion

Table 9: Synthesis of phosphonic acids

Entry	Starting material	Conditions	Final product	Yield
2	 8	TMSBr DCM 16 h RT	 10	91%
3	8	TMSI DCM 3h 0 °C	10	95%

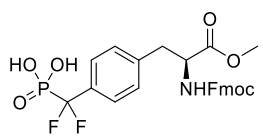
A three-fold excess (6 equivalents) of the brominated reagent reacting at room temperature for 16 hours were needed to completely hydrolyze the substrate. On the other hand, TMSI took only two fold excess (4 equivalents) reacting at 0 °C for 3 hours to complete the conversion. In the literature, this appears the reagent of choice for the rapid and deprotection of phosphonates.^[155] The superiority in the performances were somehow counterbalanced by the decomposition of the reagent observed within storage at -25° C. Following the storage conditions suggested by Blackburn et al. in a detailed study on the reagent was not sufficient to avoid corrosion of the cap and coloration of the reagent, with consequent arising doubts upon its future use.^[156] Since an effective deprotection of the diethyl ester could be achieved with TMSBr as well, with reasonable reaction times (overnight) at room temperature, this reagent was chosen for the deprotection steps in following experiments.

Results and Discussion

3.2.4 Early synthesis of phenylalanine pentafluorophosphate

The research on the synthesis of pentafluorophosphates continued using the conditions used to pentafluorinate the phenyl and naphthyl phosphonic acid. Results are summarized in the following Table 10.

Table 10: Synthesis of 4-(Pentafluorophosphato-difluoromethylen)-phenylalanine **11** with TMAF from phosphonic acid; a) monitored by NMR; b) C18 RP-Silica, H₂O/ACN; c) SiO₂, EtOAc/MeOH/H₂O (12:1.5:1)

Entry	Starting material	(COCl) ₂ + DMF	Reaction conditions	Crude Conv.	Workup	Yield of 11
1	 10	2.5 eq. + 3 drops 40 °C, 2 h DCM	TMAF anh. (4.1 eq.), 0 °C to RT, 16 h, ACN	40% ^a	conc. in vacuo	8% ^b
2	10	10 eq + 1 mL 40 °C, 6 h DCM	TMAF anh. (13 eq.) 0 °C to RT, 18 h, ACN	94% ^a	Celite filtration	53% ^c
3	10	2.5 eq. + 3 drops 40 °C, 5 h DCM	TMAF dried (13 eq.) 0 °C to RT, 18 h, ACN	4% ^a	/	/

The phosphonic acid was consequently dissolved in DCM, a slight excess of the fluorinating agent was added. After 2 hours the crude was evaporated at reduced pressure to remove all the volatile components, the substoichiometric amounts of TMAF were added to the residue redissolved in ACN and the reaction was stirred for

Results and Discussion

16 hours. The conversion in the crude could be quantified as 40% from the F NMR; concentration in vacuo of the crude and purification of the residue on reverse phase silica yielded 8% of the product. (Entry 1)

The reason for the low yield in the crude and the subsequent marked decrease in the isolated yield could be attributed to:

- 1) an incomplete dichlorination;
- 2) the substoichiometric amount of the precious fluorinating agent;
- 3) possible decomposition during workup and purification.

All these points were addressed but an additional difficulty in the interpretation of the data, consisted in the decomposition of the pentafluorinated moiety observed when left in the reaction mixture or in the crude mixture. Consequently, even with a complete dichlorination and quantitative perfluorination, the final yield could have been 0 if the crude was left untreated. This strongly hampered data rationalization and problem identification, until the decomposition process could be understood and avoided.

Investigating the reason expected to be responsible for the low yield reported in Entry 1 allowed a considerable improvement in terms of crude and isolated yield.

Entry 2 summarized the condition used: the chlorination reaction was increased to 6 hours and the amount of chlorination reagent was increase to 10 equivalents. After removing the volatile components at high vacuum, the crude was dissolved in ACN and reacted with an excess of TMAF (13 equivalents) overnight. In this case, NMR analysis of the crude showed almost quantitative conversion to the desired pentafluorophosphate. The residue was then filtrated on celite and purified on column chromatography on silica gel. In this case as well, the yield dropped quite sensibly between the work up and purification step and therefor this point was still be resolved. Furthermore, the cost of the fluorinating agent associated with the big excess used and the long reaction times left some possibilities for further optimizations.

The first issue addressed was the cost of anhydrous TMAF. The corresponding tetrahydrate is noticeably cheaper (~ 6 €/g) and according to the literature can be

Results and Discussion

dried to a high extent even if not completely due to strong interactions with the solvent. Hence, for this attempt the tetrahydrate was subjected to the treatment described by Klanberg et al.^[157] Accordingly, it was dissolved in MeOH and concentrated on rotary evaporator for three times. The obtained syrup was then dried under high vacuum at 150 °C for a couple of days, resulting in a fishy smelling (trimethylamine) white powder which was stored under inert atmosphere in a Schlenk flask. After a 5 h long chlorination, removal of the volatile components under vacuo and subsequent fluorination in ACN with dried TMAF derived from its tetrahydrate yielded almost no conversion to pentafluorophosphates in the crude, leading to the apparent observation that dried TMAF cannot replace the commercially available rigorously anhydrous one. (Entry 3)

Summarizing, the first pentafluorinated amino acid was synthesized and isolated in pure form with satisfactory yield. However, the long reaction time, the big yield difference between the reaction mixture and the isolated product, as well as the cost of fluorination agent were serious issues that urged to be addressed. These problems will be discussed in the following chapter.

3.3 Optimization of the perfluorination reaction

In general, the design of new conditions allowing to perform a specific transformation require a deep understanding and broad overview of the chemical species involved, their physical characteristics and accessibility, together with extensive literature research. Only afterwards the different parameters and variables can be combined into one smooth-working, solid mechanism.

Being satisfied with the performance showed by the reaction allowing the insertion of the difluorophosphonate via Cu mediated organocadmium coupling, attention was moved to the inefficiency observed with the pentafluorination reaction, the causes of which were discussed in the previous chapter. Hence, the optimization process started with the analysis of the deprotection of the phosphonate and the formation of the dichloride.

3.3.1 Improving conversion to phosphonic acid dichloride

Previous research with different silylating reagent allowed to identify as optimal the conditions reported by Wagner.^[150] Accordingly, this step was planned to be performed with TMSBr, in ACN at 70 °C for 3 hours. (Table 4, Entry 2).

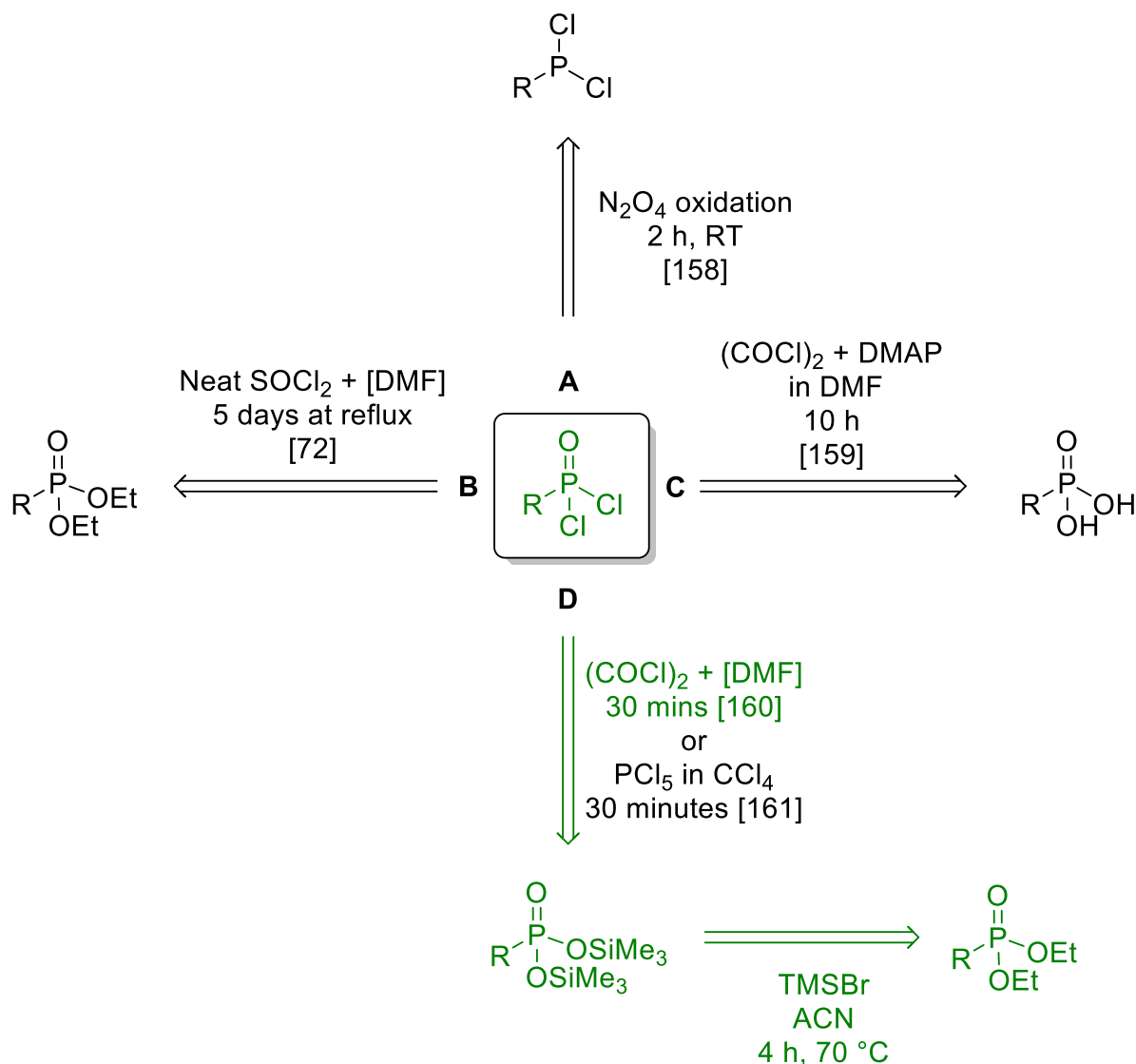
The second problem addressed was the slow synthesis of the phosphonic acid dichloride and consequently, the chlorination reaction was looked a bit more in the details. In the literature, phosphonic acid dichloride preparation was described from different starting material. (Scheme 16)

Griffith et al. in 1968 reported the oxidation of trifluoromethyl dichloro phosphine with nitrogen dioxide to obtain the corresponding phosphonic acid dichloride, but this procedure was not suitable for both the used starting material and the inconvenient experimental set up.^[158] (Scheme 16A)

Boutselis et al. attempted dichlorination of the protected gemdifluoromethylen phosphonate with neat thionyl chloride and catalytic amount of DMF at reflux for 5 days. This approach turned out to be inconvenient as well.^[72] (Scheme 16B)

Results and Discussion

Starting materials comparable to the present work were reported by Murano et al in 2003. The treated aryl gemdifluoromethylen phosphonic acid with oxalyl chloride in presence of DMAP in DMF at RT, but the desired dichloride was obtained only after 10 h reaction.^[159] (Scheme 16C)



Scheme 16: Examined synthetic possibilities to phosphonic acid dichloride

The most convenient route to gem difluoromethylen phosphonic acid dichloride was reported in 1987 by Bhongle et al. and relies on the reaction between the silyl ester of the phosphonic acid and oxalyl chloride in presence of catalytic amount of DMF, at RT for 30 minutes (Scheme 16D).^[160] This reaction can be seen as an improvement of the conditions described by Morita et al. in 1980, where using the same starting materials in presence of phosphorus pentachloride in tetrachlorometane yielded the desired dichloride with comparable yields and reaction time.^[161]

Results and Discussion

Quite luckily, this significantly simplified the overall synthesis, allowing to skip the preparation of the phosphonic acid, greatly improving the time efficacy (hydrolysis, purification and lyophilization were time consuming processes) and exploiting the increased reactivity of the molecule in the overall transformation. Summarizing, this analysis led to choose the silylation method described by Wagner (TMSBr, ACN, 3 h, 70 °C), followed by the chlorination method described by Bhongle et al. (oxalyl chloride + cat. DMF, 30 minutes).

Additional thoughts were spent on the solvent. Considering that the first silylation step and the last fluorination step were described in ACN, this solvent was tested in the chlorination reaction as well, despite being DCM the usual solvent of choice for this reaction in the previously reported literature. In case of success, this slight modification would be highly convenient in the practical execution because it would avoid the tedious solvent exchange step.

All these considerations allowed the definition of an optimized protocol for phosphonic acid dichloride and allowed to address the synthetic drawbacks present in the early pentafluorinated reaction and are summarized in the following figure and points:

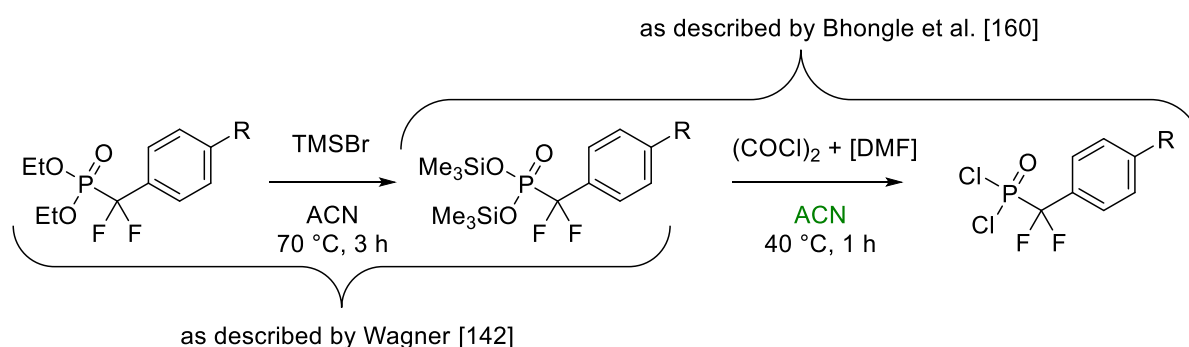


Figure 28: Chosen conditions for the convenient access to the phosphonic acid dichloride

- The logical path to the dichloride could be shortened avoiding the isolation of the phosphonic acid;
- The use the silyl ester as a substrate for the subsequent chlorination reaction would result in milder condition and fast conversion;
- the use of the same solvent in all steps would greatly facilitate the practical execution of overall procedure;

- this reaction combination would greatly improve the time efficiency of the overall conversion of protected phosphonates to pentafluorophosphates, from days to few hours.

After having addressed the first of the three issues presented by the early pentafluorination reaction, it was time to move to the second one: an expensive fluorinating reagent was needed in excess.

3.3.2 Problem 2: costly fluorinating reagent

The use of different fluorinating reagent discussed in previous chapters, such as NfF, PVP HF, Olah's reagent or dried TMAF result in no conversion to the desired pentafluorinated product. Könner in his thesis and other research groups used KF instead, but this reagent present solubility problems in ACN.^[162] Consequently, investigations continued using TMAF also in view of its higher reactivity and stability as fluoride ion source.^[163]

Comparing the early unsuccessful attempt in the use of dried TMAF with the other reactions using the anhydrous reagent reported in Table 8, it was clear that the problem was the excess of water still contained in the former. This time though, with the newly developed one-pot condition, the presence of reactive species from previous steps, such a TMSBr and the more abundant chlorinating agent, would react with the water present in the salt, unleashing the reactivity of TMAF

In order to prove this assumption, the equivalents of oxalyl chloride and DMF were increased, in order to have an excess of unreacted reagent even after the completion of the chlorination reaction. This would react with the water present in the TMAF yielding DMF and HCl in case of the Vilsmeier Haack reagent or CO, CO₂ and HCl in the case of oxalyl chloride.

Following, the perfluorination of the phosphonic dichloride was planned with an excess of TMAF (10 equiv.), obtained by drying the tetrahydrate via the previously described literature procedure ^[157]

3.3.3 Problem 3: loss of yield in the work up

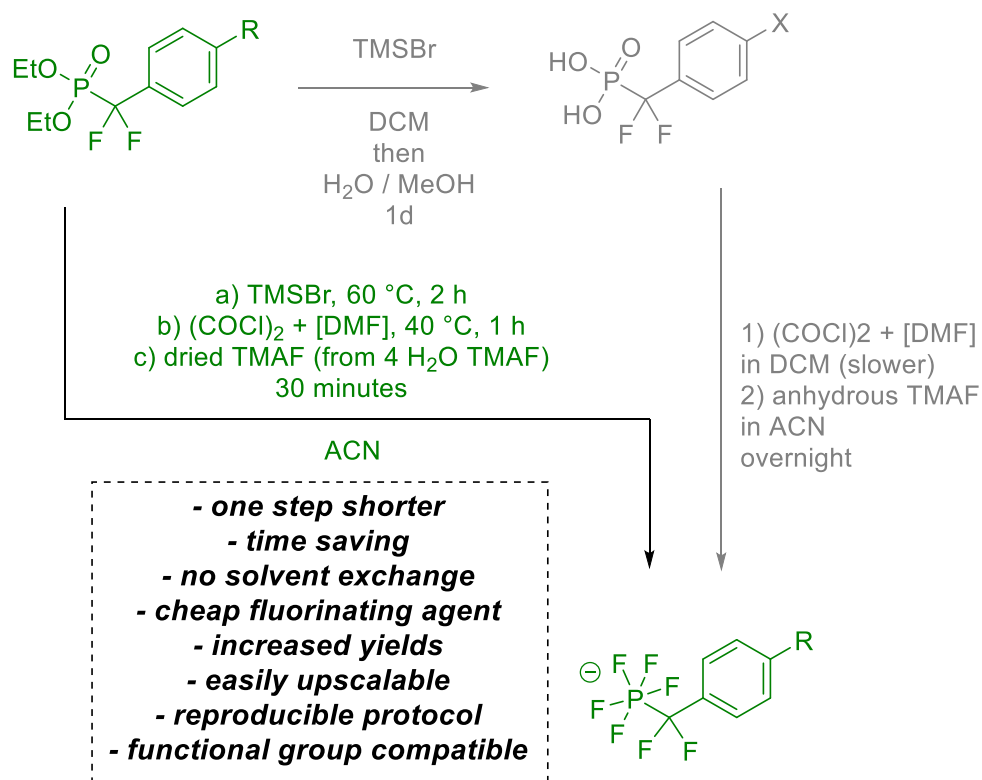
In order to tackle the yield decrease observed during the workup and purification step, the results obtained in the early synthesis of pentafluorophosphates were

Results and Discussion

carefully analyzed. The instability in the crude mixture was rationalized as instability toward acid conditions arising from the chlorination step, whose components could not completely be removed between the steps. In the previous work up, the big amount of salts (tetramethyl ammonium chloride) precipitating from the reaction medium were removed via filtration; the aqueous work up was avoided due to the difficulty in the recovery of useful phosphonic acid as starting material. Hence, the lack of pH neutralization was responsible for the decomposition of the product until its purification causing the irreproducibility that characterized the early reactions' outcome. With these assumptions in mind, the suitable workup procedure was carried out with a saturated aqueous solution of ammonium bicarbonate, in order to quench immediately the acidity of the reagents and avoid steady decomposition.

3.3.4 Development of the fine-tuned perfluorination reaction

Putting all these details together allowed the identification of optimized reaction conditions starting from the easily accessible protected *gem*-difluoromethylen phosphonate directly to the pentafluorophosphate, in a one pot fashion, simply adding step by step the reagents to the flask. The overview of this superior approach is compared with the previously used one in the following scheme.



Scheme 17: Optimized telescopic synthesis of pentafluorophosphates

Results and Discussion

The synthesis of pentafluorophosphates was carried out according to this general scheme and was repeated with different aromatic substrate with extremely satisfying results, which are summarized in the following Table. The first entry described the application of previously described condition including aqueous workup with ammonium bicarbonate. After reacting the diethyl protected phosphonate for 1 h at 60 °C with 5 equivalents of TMSBr, a sample was taken, hydrolyzed and subjected to LCMS analysis confirming the quantitative deprotection. To the reaction mixture 10 equivalents of oxalyl chloride were added, followed by slow dropwise addition of DMF. The reaction was stirred at RT for 2 hours turning of a deep orange color. At this point, a sample of the crude mixture was taken and reacted with MeOH in an Eppendorf tube. Upon this treatment, the presence of the dichloride could be assessed by the formation of the dimethylester, which was observed via LCMS analysis. The flask was then cooled with ice and TMAF was added under inert atmosphere to the complex reaction mixture triggering copious release of gaseous byproducts. After 1 h an aliquote of the reaction was again analyzed at the lcms, where the only mass detected with a direct injection was belonging to the product. Quenching of the resulting heterogenous mixture in a saturated solution of ammonium bicarbonate allowed the prompt neutralization of the acidity. DCM extraction, concentration at rotary evaporator and purification of the crude with column chromatography on reverse material using water and acetonitrile as mobile phase allowed the isolation of the first pentafluorinated amino acid with a yield of 68%.

Results and Discussion

Table 11: Summary on investigation on optimized perfluorination reaction: a) monitored by LC-MS; b) C18 RP-Silica, H₂O/ACN;

Entry	Phosphonate diethylester	TMSBr	(COCl) ₂ + DMF	Reaction conditions	Crude Conv.	Yield of PF ₅
1	Protected amino acid 8	5 eq 60 °C, 1 h ^a ACN	10 + 5 eq. 2 h, RT ^a	TMAF dried (10 eq.) 0 °C to RT, 1h ^a	~100 % ^a	11 68% ^b
2	Protected amino acid 8	3 eq. 60 °C, 1.5 h ^a ACN	10 + 5 eq. 1 h, RT ^a	TMAF dried (8 eq.) 0 °C, 5 mins ^a	~100 % ^a	11 50% ^b
3	Methyl phenylacetate 9	3 eq. 60 °C, 1.5 h ^a ACN	10 + 5 eq. 1 h, RT ^a	TMAF dried (8 eq.) 0 °C, 1.5 h ^a	n.d.	12 49% ^b
4	Phenyl 1	2.2 eq. 60 °C, 1 h ^a ACN	10 + 5 eq. 40 min, RT ^a	TMAF dried (10 eq.) 0 °C to RT, 30 mins ^a	n.d.	5 62% ^b
5	Naphthyl 2	2.2 eq. 60 °C, 1 h ^a ACN	10 + 5 eq. 40 min, RT ^a	TMAF dried (10 eq.) 0 °C to RT, 15 min ^a	n.d.	6 51% ^b

Results and Discussion

These very good results proved the validity of the assumptions that lead to the identification of the one pot multi step procedure.

Entry 2 summarized the investigation aimed to reduce the reaction time and excess of reagents. In the reaction preceding the perfluorination reaction, the equivalent of TMSBr were reduced to 3, and the reaction time was prolonged to 1.5, while reducing the chlorination time to 1 hour. TMAF amount was reduced to 8 equivalent and reacted was carried out for only 5 minutes. Nonetheless it was possible to obtain 50% conversion. This represents a very interesting result proving the efficiency and stability of the newly designed synthetic protocol.

Entry 3 summarized the synthesis of *gem*difluoromethylen pentafluorophosphono phenyl acetate, needed for the synthesis of the bivalent inhibitor. In this case reaction conditions did not change substantially and after the work up 49% of the desired compound could be isolated.

The synthesis of pentafluorinated phenyl and naphthyl was repeated with the new condition and the yield could be increased to 62% and 51% with the perfluorination reaction lasted 30 minutes and 15 minutes, accordingly. (Entry 4 and 5)

The freshly developed synthetic protocol proved to be quite robust. Despite the excess of TMSBr reported in the first entry, the perfluorination was complete in the crude, indicating that the competing reaction between TMSBr and TMAF resulting the stable TMSF and *de facto* reducing the amounts of reactive fluorides was not critical.

Noteworthy, no marked decrease in the isolated yield was observed when the perfluorination reaction was quenched after only 5 minutes after addition of the fluorinating agent, further demonstrating the power of this multi step approach.

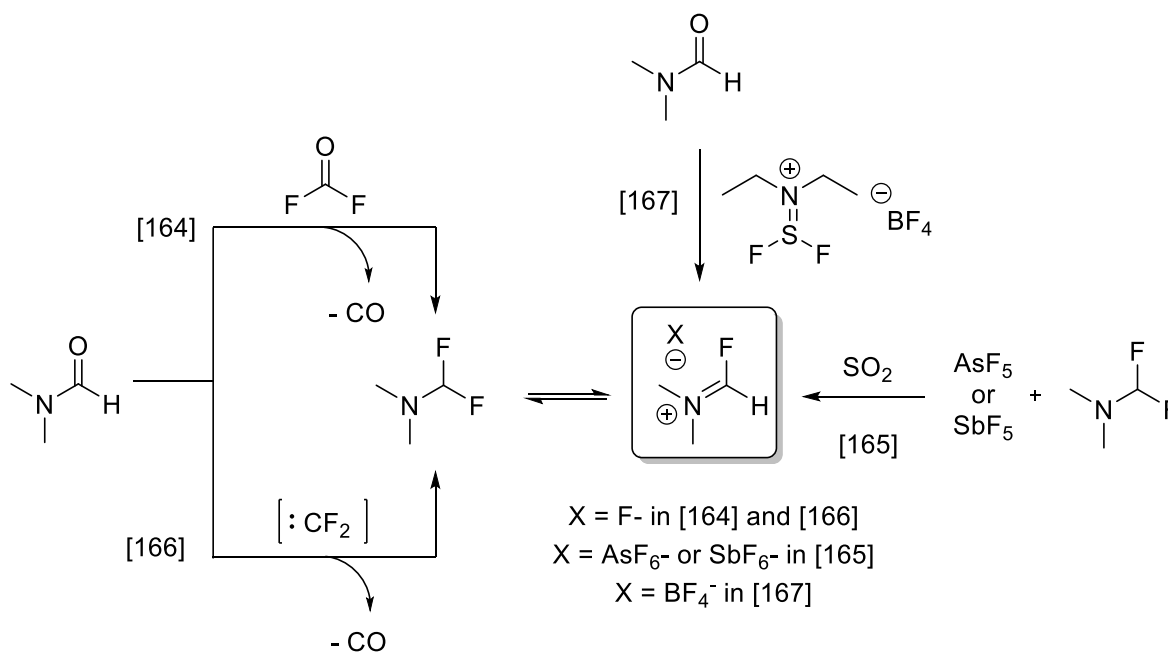
The reaction mechanism is proposed in Scheme 18. After formation of the silyl ester A, reaction with Vilsmeier-Haack reagent yields the dichloride B releasing gaseous byproducts CO₂ and CO as well as the TMSCl.^[160] When adding the TMAF, the first equivalent of fluorinating salt attacks the phosphorus center of B, yielding stepwise the phosphonic difluoride C and releasing tetramethylammonium chloride. The third equivalent of fluorine yields the intermediate D. This is the step where the presence

Results and Discussion

of an electrophile that can remove the last oxygen from the trifluoride is crucial. The Vilsmeier-Haack reagent or the unreacted silylating reagent can accept the oxygen formally allowing the formation of the unstable tetrafluoride under formal release of one equivalent of DMF and tetramethylammonium chloride. The last equivalent of TMAF forms the final product as a tetramethyl ammonium pentafluorophosphate.

The simplified mechanism proposed hereafter does not take into account intermolecular possible reaction among the reagents, such as the formation of TMSF upon reaction with TMSBr and TMAF or the formation of the fluorinated analogue of the Vilsmeier-Haack reagent.

Formation of this α -fluoro dimethyl iminium ion, always in equilibrium with α,α -difluorotrimethylamines, was originally achieved by Fawcett et al. in 1962 by reacting DMF with COF_2 .^[164] Twenty years later, in 1984, investigations by Henle et al. reported the reaction of α,α -difluorotrimethylamines with AsF_5 or SbF_5 .^[165] Burton et al. in 1985 described its preparation from CF_2 carbene from difluorodihalomethanes with DMF in presence of cadmium or zinc metal.^[166] More recently, Roudias et al. reported the reaction with XtalFluor- E (a DAST – diethylaminosulfur trifluoride analogue) in presence of DMF.^[167] Despite all these investigations, its use never appeared to really outclass more classical fluorinating agents.

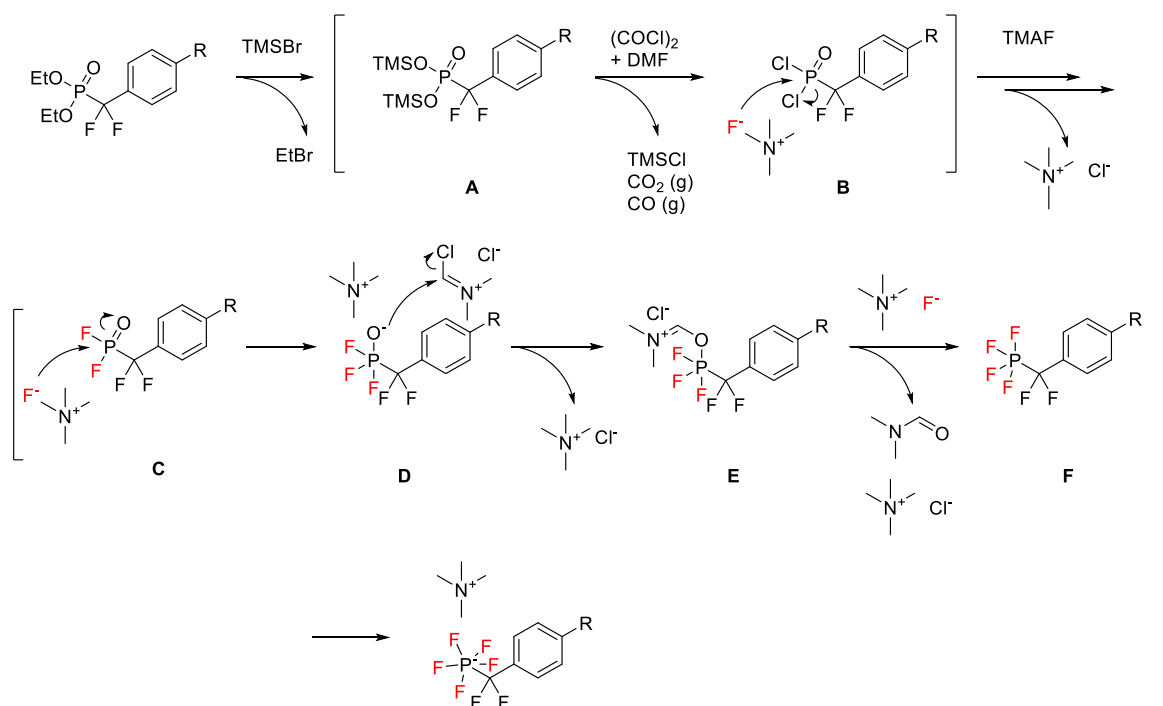


Scheme 18: Reported methods of the formation of the fluorinated analogue of the Vilsmeier Haack reagents, with literature references

Results and Discussion

In order to confirm the formation of such fluorinated analogue of the Vilsmeier, ^{19}F -NMR analysis of the whole mixture over time would yield very interesting insights, including the different intermediates formed and species produced. Even if these side reactions might result in the consumption of the fluorinating reagent in the case of TMSBr (due to the strong affinity of silicon for fluorides), they do not appear to harm the good general outcome of the reaction.

Furthermore, if the formation of fluoroiminium under the conditions developed in this research work would be confirmed by NMR analysis, this method would be a nice alternative to the overview reported in scheme 18, allowing convenient *in situ* formation of such compound starting from commercially available and easy to handle reagents. Its superiority to the employed TMAF as fluoride donor should be verified, but the presence of fluoride instead of chloride is expected to enhance even further the electrophilic character of the compound, which in this case would favor the extraction of the last oxygen from the phosphorus center.



Scheme 19: Proposed mechanism of the perfluorination reaction

The compound after purification with RP C18 MPLC showed the absence of other fluorine or phosphorus containing compounds (monitored by F and P NMR). The absence of salt was ensured via chromatographic separation on reverse phase by 5

Results and Discussion

column volumes of wash with 99% H₂O before reaching the slowly increasing percentage of ACN needed to obtain elution of the desired product (~40% ACN); by doing so the product could be obtained with a high degree of purity. The fluorine and phosphorus NMR of the pentafluorinated moiety is quite interesting. It is possible to divide the fluorine atoms into three groups, according to their different chemical environment. Starting from the left to the right in the following figure, we observe a doublet, which arises from the axial fluorine. The very big J coupling constant measured between the two doublets is to be attributed to the phosphorus, while the much smaller J in the doublet is related to F-F coupling. Right after we it is possible to observe the 4 equatorial fluorines, which couple with the neighboring fluorine with small coupling constants, and as before, with considerable bigger J when coupling with the phosphorus. At the far right, it is possible to observe the CF₂ bridge at ~ -98 ppm. These fluorine atoms in the phosphonate moiety were observed at around -106 ppm, allowing to quantify the conversion and the ratio between the phosphonate to the pentafluorophosphate in the crude.

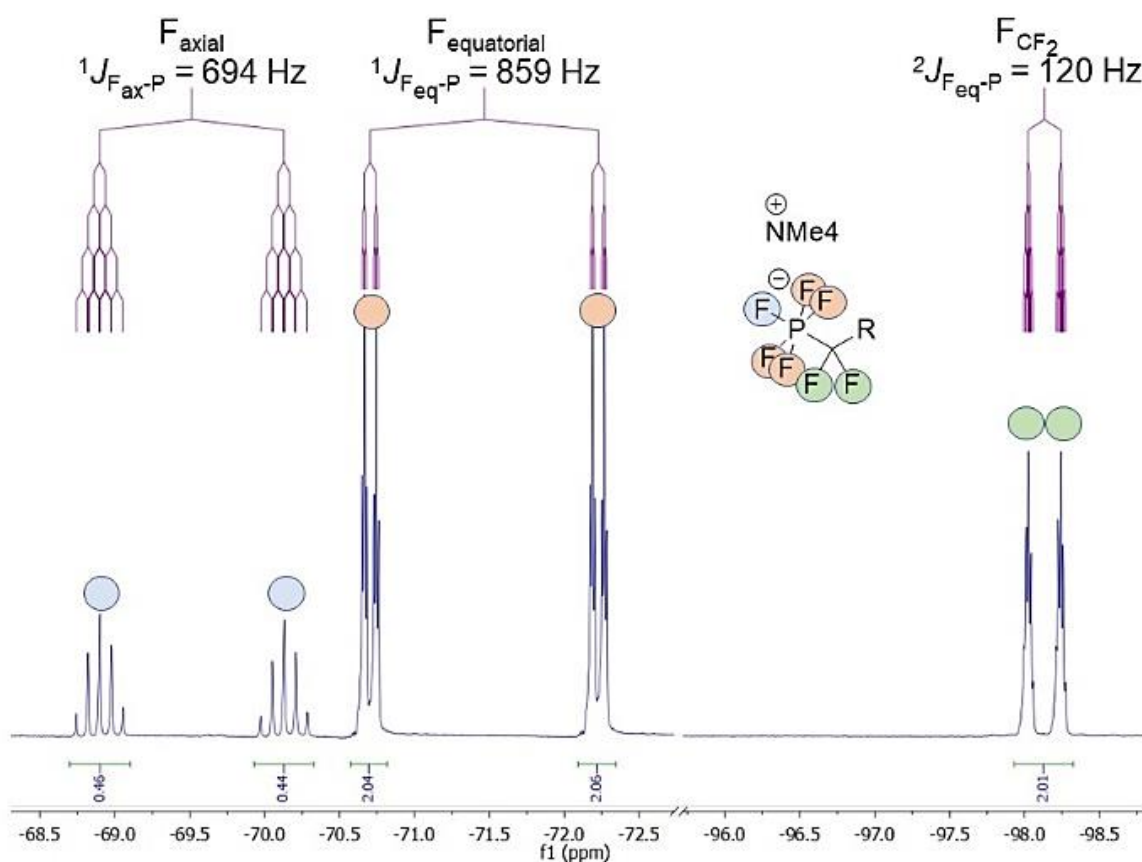


Figure 29: ¹⁹F NMR of the pentafluorophosphate in 11

Results and Discussion

The multiple coupling possibilities are reflected in the P-NMR as well. The complex signal is composed by a doublet of a pentet of a triplet, according to the $n+1$ rule in determining the splitting of signal in nuclear magnetic spectroscopy. (Figure 30)

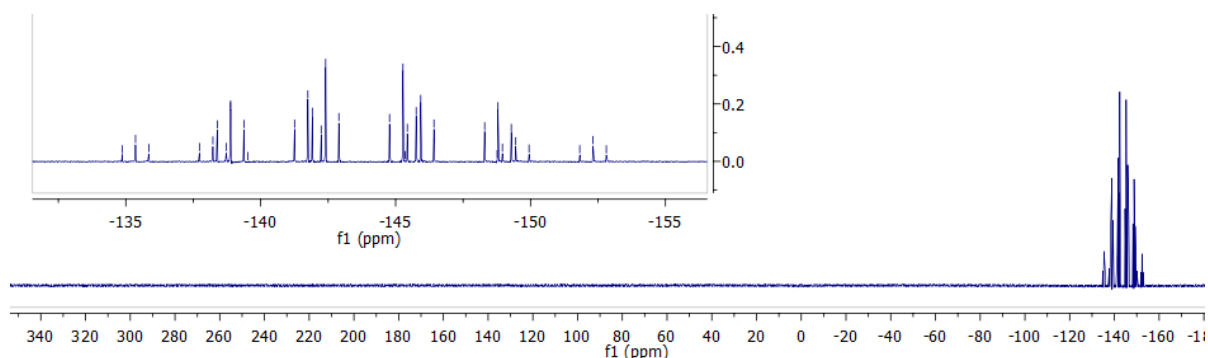


Figure 30: ^{31}P -NMR of pentafluorophosphate **11**

The 3D structure, reported in the following figure, was determined experimentally via x-ray crystallography in collaboration with by Max Rautenberg and Dr. Franziska Hemmerling at the BAM (Bundesanstalt für Materialforschung und –prüfung) Berlin. The pentafluorophosphate group is clearly visible with yellow fluorines and the orange phosphorus atom. The tetramethylammonium cation is adjacent to the PF_5^- moiety.

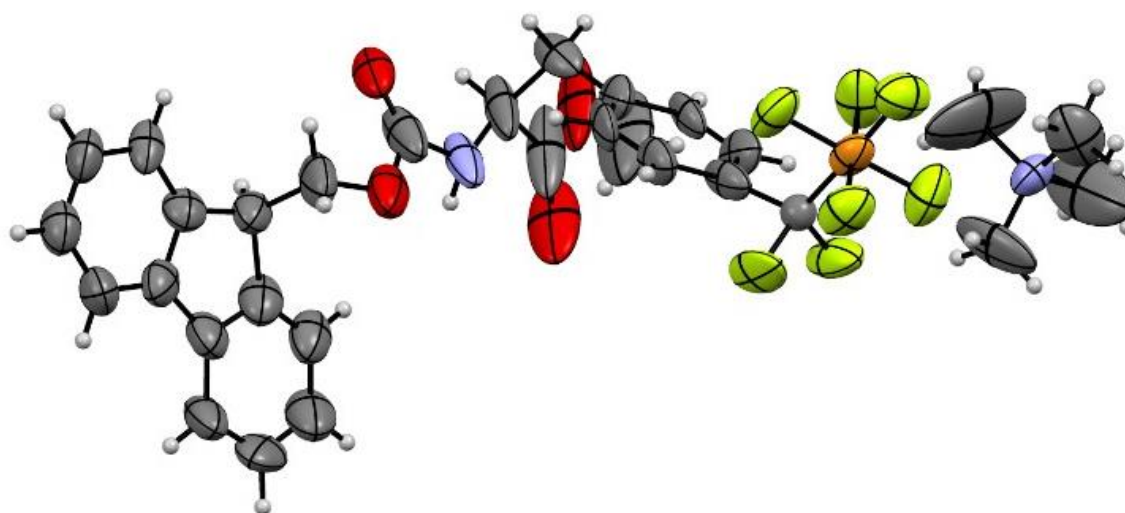


Figure 31: crystal structure of **11** determined experimentally via x-ray crystallography by M. Rautenberg and Dr. F. Hemmerling.

Furthermore, in collaboration with Ruben Cruz at the research group of Prof. Heberle at the Freie Universität Berlin, the infrared spectrum of phenyl *gem*-difluoromethylen

Results and Discussion

pentafluorophosphate and the phosphonate analogue were recorded and characteristic bands were assigned.

In Figure 32 the full spectrum reported here above, the highlighted peaks represent the dangling water signals (3630 and 1628 cm^{-1}) while the characteristics peaks of PF_5^- moiety, restricted in the early fingerprint area, are at around 800 cm^{-1} . The stretching modes responsible for the characteristic band are depicted in the following figure.

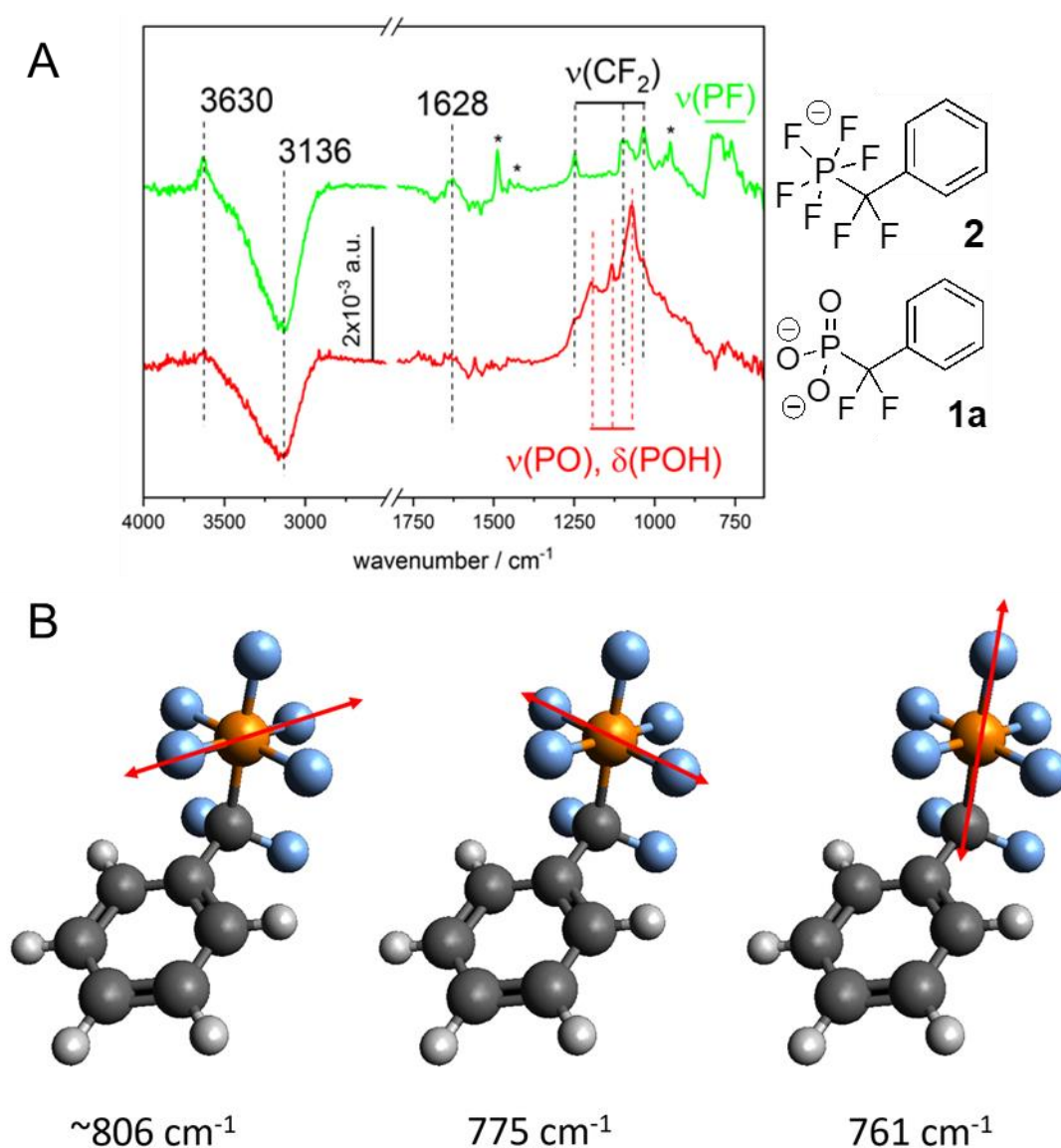
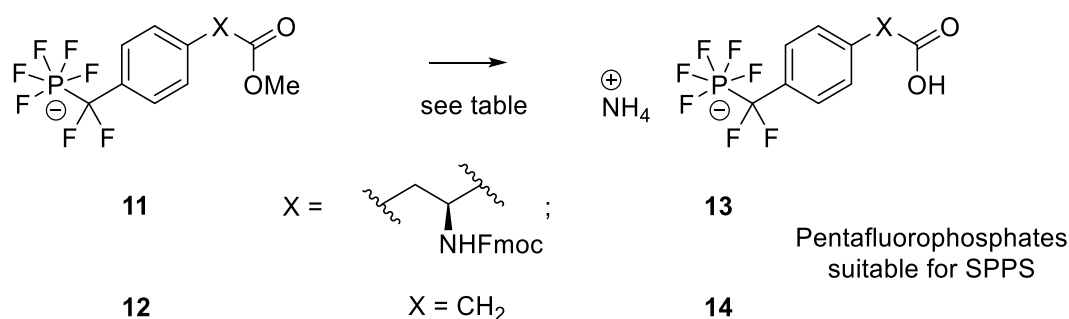


Figure 32: Stretching vibration modes in pentafluorophosphates with band assignment.
Picture by Ruben Cruz

3.4 Preparation of the building block for Fmoc-based solid phase peptide synthesis (SPPS)

3.4.1 Methyl saponification

The saponification of the methyl ester was investigated using two methodologies. The main challenge was to avoid decomposition of the pentafluorophosphate moiety into the corresponding phosphonate under strong basic conditions, as well as the retention of the Fmoc group which is per se base-labile.



Scheme 20: Saponification of the pentafluorinated methyl ester

First, the procedure described by Pascal et al. was followed.^[168] The solvent mixture consists of 0.8 M CaCl₂ in mixed aqueous/organic solvent, which in presence of an alkali hydroxide allows to reduce the strength of the base by forming the less reactive Ca(OH)₂. Furthermore, the Ca²⁺ ion can coordinate to the carboxylate acting as a Lewis acid, resulting in further activation. With a slight excess of base, the procedure was found to be effective and allowed to perform the saponification reaction with high yield. In order to obtain a better understanding of the reaction and try to speed it up, the amount of base was increased to a bigger excess (5 equivalents). In this case, a complex mixture of other products could be observed from LCMS analysis, from the fully unprotected pentafluorophosphato amino acid **15** to the hydrolyzed phosphonic acid Fmoc protected **16** and **18**.

Results and Discussion

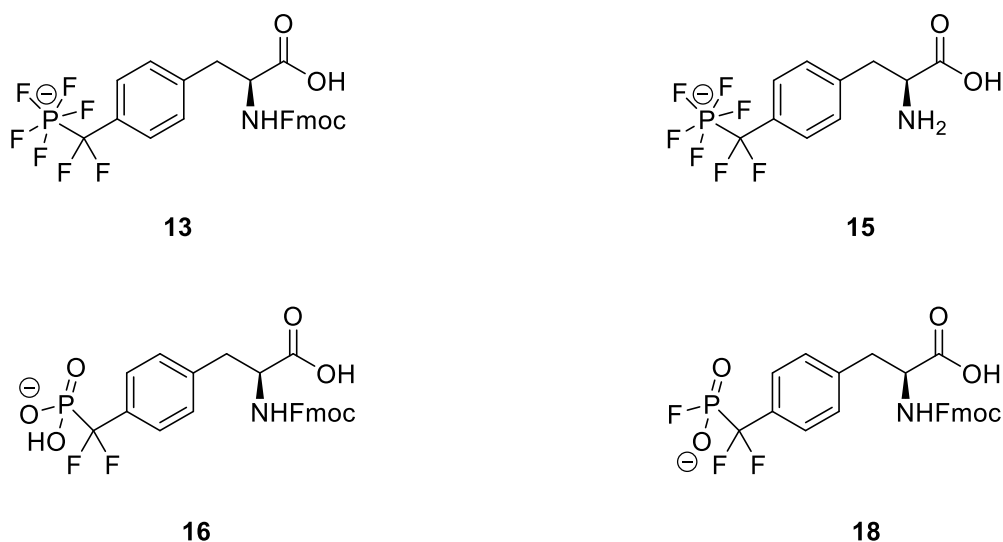


Figure 33: Byproduct of the reaction observed at the LCMS (negative mode)

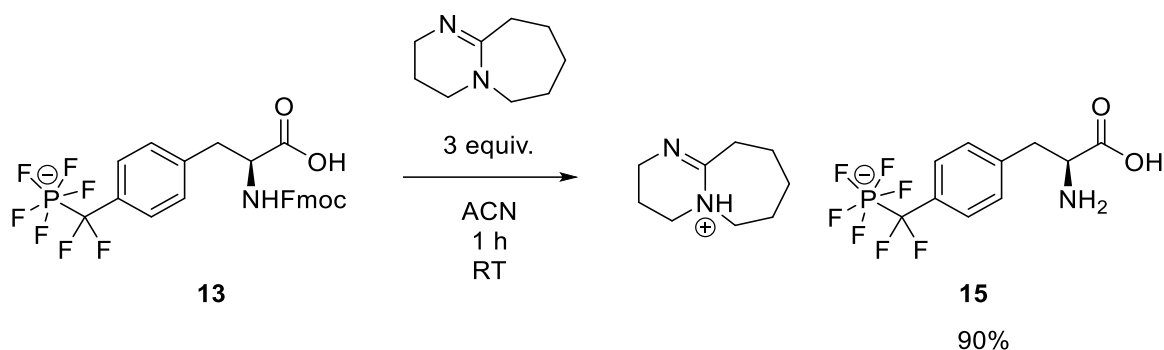
Due to this observation, a milder method based on enzymatic saponification using Subtilisin Carlsberg (EC: 3.4.21.62) from *Bacillus licheniformis*. was investigated as well. The proteolytic enzyme has broad specificity and belong to the family of Serin S8-Endoproteinase. The enzyme was added to the substrate in a basic ammonium bicarbonate buffer and a good conversion was achieved in this case as well. Although this reaction proceeded without formation of byproducts and the desired carboxylic acid could be isolated easily from its precursor via chromatographic procedures, the reaction was slower and the scale up lead to gram scale was not always reproducible in terms of reaction time and yield. The products as ammonium salts could be isolated in a pure form after purification on reverse phase material using water and acetonitrile as mobile phase in a basic ammonium bicarbonate buffer. A summary of the investigations is reported in the following table.

Table 12: Summary of saponification reaction

Entry	Starting material	Conditions	Product Yield
1	11	0.8 M CaCl ₂ + KOH 3 eq. RT, 6 h	13 87%
2	11	Subtilisin Carlsberg 60 °C, 16 h	13 80%
3	12	Subtilisin Carlsberg 60 °C, 16 h	14 83%

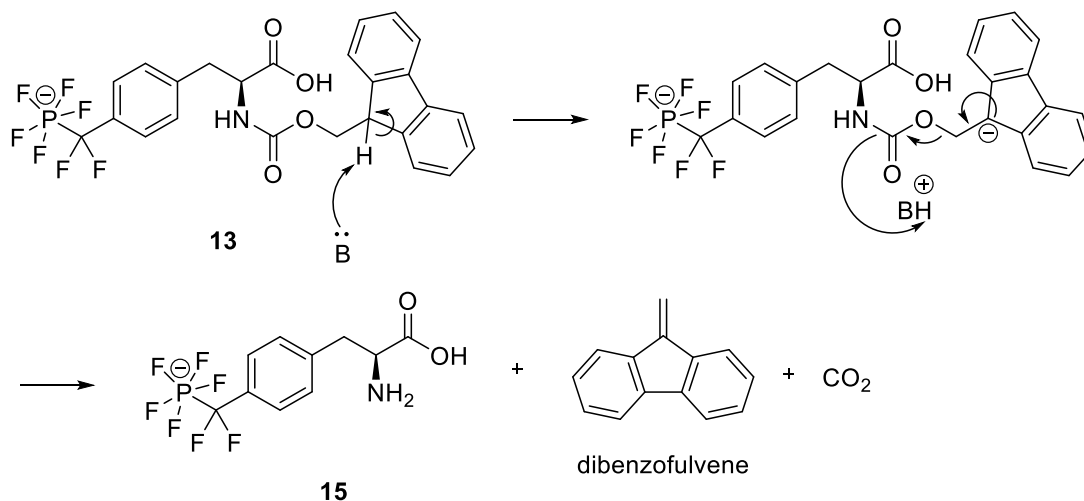
3.4.2 Fmoc deprotection

Fast removal of the Fmoc group can be achieved using a second amine. Similarly effective, despite formally not being secondary amine, is 1,8-diazabicyclo[5.4.0]undec-7-en (DBU), an amidine with high basicity commonly applied for Fmoc deprotection. Stability was investigated also for the deprotection cocktail commonly used in SPPS, such as piperidine in DMF (20%) - Both these reagents showed to be compatible with the pentafluorophosphate moiety.



Scheme 21: Fmoc deprotection of **13**

The reaction mechanism is described in the following figure. After the base deprotonates the tertiary carbon of the fluorenyl species, electronic rearrangements lead to the formation of the desired deprotected amino acid, together with CO_2 and the dibenzofulvene species. DBU does not quench this reactive intermediate but this proved to be not an issue. In case of peptide synthesis, piperidine is preferred since it can react with it via nucleophilic attack to the double bond, avoiding it to react with side chain of amino acid upon the repeated treatments usually employed in solid phase peptide synthesis.



Scheme 22: Mechanism of Fmoc deprotection

3.5 Computational Analysis

The first analysis was performed using Ligand Scout from Inteligand. This software allows a number of computational analyses with 3D modeling which are very useful in drug design. One of the functions allow to download and import protein structures available from protein data bank (PDB), visualize in three dimensions and analyze their features, for example the binding site or the amino acid sequence. The following picture schematizes the H bond interaction between the ligand and the amino acids present in the backbone of the protein's active site: in order to obtain this, the ligand was placed in the active site and energy to in the active site of a given protein after obtaining the related structure of from the protein data bank. (Figure 34)

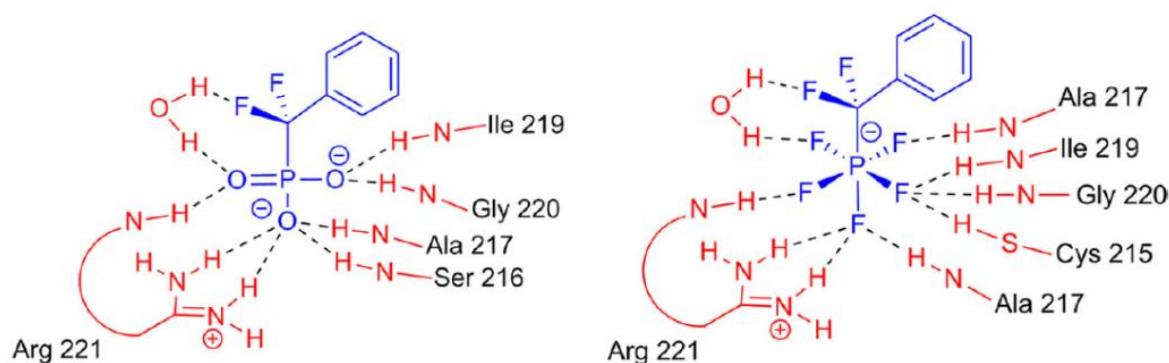


Figure 34: H-bond interaction between the ligand and the amino acids backbone in active site of PTP1B after forcefield minimization: phenyl $\text{CF}_2\text{P}(\text{O})(\text{OH})_2$ **6** (left) and phenyl CF_2PF_5^- **9** (right) (PDB: 4Y14 - Dimer B). Pentafluorophosphates can form a higher number of H-bond interaction than gemdifluoromethylen phosphonates.^[150]

This exemplifies the results from the computational modeling. The increased number of fluorine atoms on the phosphorus center of pentafluorophosphates allows to increase affinity to the receptor by multiple fluorine-hydrogen interaction with the amino acid residue present in protein backbone of the active site.

The same analysis was conducted using the pentafluorinated amino acid as ligand. In this case as well, the multiple favorable interactions of the pentafluorophosphate moiety with the amino acids surrounding the active site are highlighted in red (Figure 35). These results support the use of gem-difluoromethylen pentafluorophosphates

Results and Discussion

as potent inhibitors of phosphatases, acting as phosphotyrosine mimetics stabilized by numerous fluorine – hydrogen interactions.

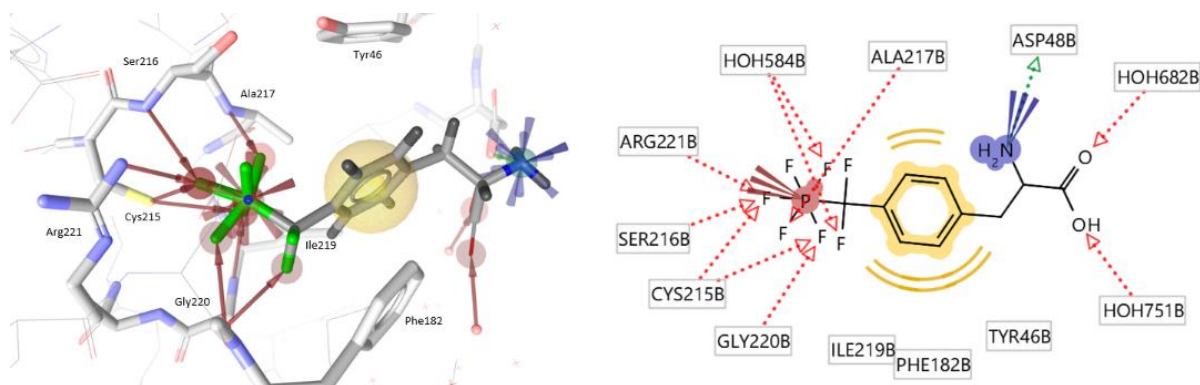


Figure 35: H-bond interactions between *H*-(4- CF_2PF_5)Phe-OH **15** and the protein backbone in the active site of PTP1B obtained from Ligand Scout (PDB: 4Y14 - Dimer B).

In order to further evaluate the physical characteristics of this group and its effect on the electron density, the electrostatic potential surface was evaluated from DFT calculations.

The pKa of the diprotic trifluoro phosphonic acid is 1.16 and 3.93, while the pKa of phenylmethyl phosphonic acid is 3.3 and 8.4.^[169] The value of phenyl *gem*difluoromethylen phosphonic acid can consequently be estimated to be around 2 and 5, for the first and second proton respectively. The electron withdrawing properties of the CF_2 group would favor a double negative charge, which has to be considered in the computation. Considering that pentafluorophosphates are natively single charged, this charge discrepancy between the two results in an increased difficulty in data comparison between the pentafluorophosphates and *gem*difluoromethylen phosphonates.

This being said, Figure 36 highlights how the electron density is delocalized and shared among the seven fluorine atoms of compound **15**, instead of being accumulated of the three oxygen of the phosphonate moiety in compound **17**. This and the following 3 figures have been obtained using the High-Performance Computing (HPC) Service of ZEDAT, Freie Universität Berlin, which is kindly acknowledged for the computing time.

Data support the fact that the higher charge distribution in the fluorine-rich compound is affecting the polarity of the whole molecule and reduces its dipole moment.

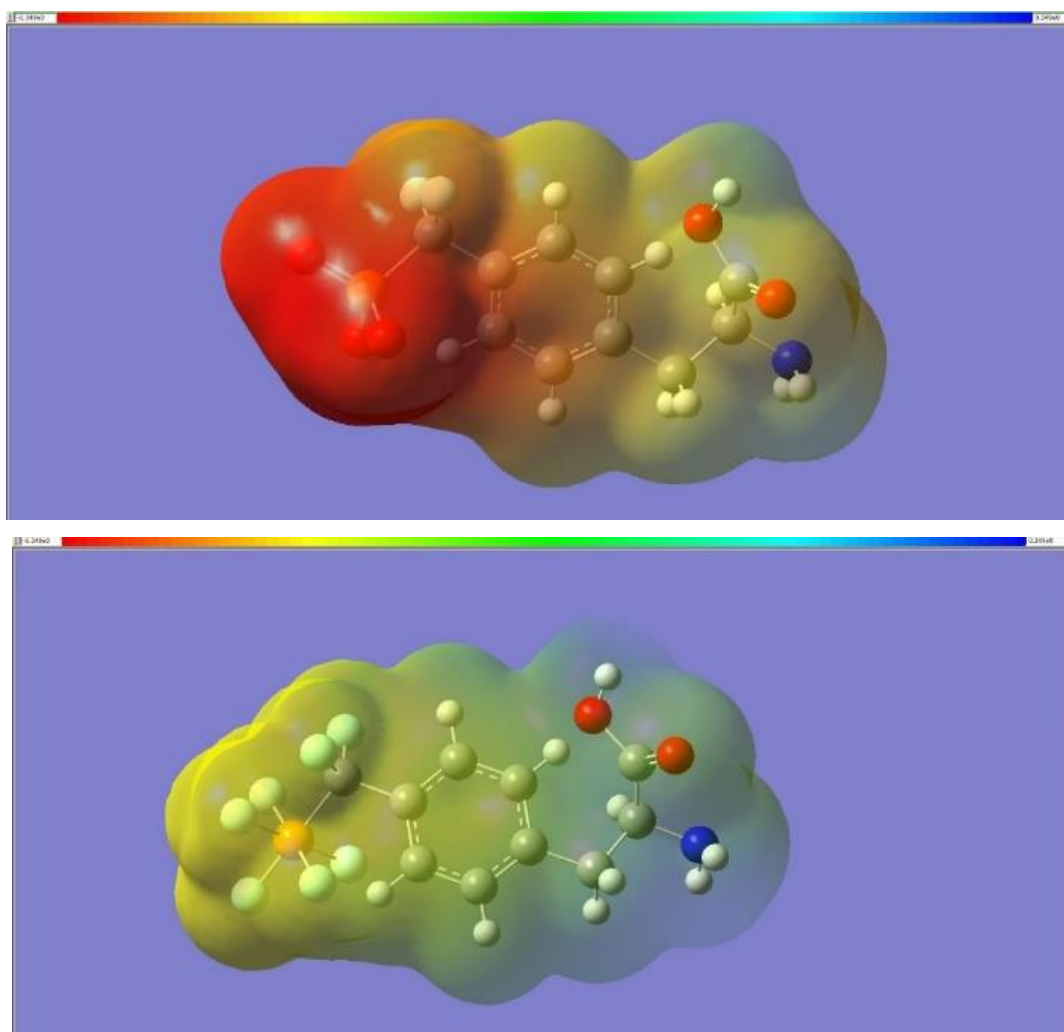


Figure 36: Electrostatic potential surface (ESP) from DFT calculations of 4-phosphono-difluoromethyl phenylalanine **17** and 4-pentafluorophosphato phenylalanine **15**, respectively, with 3-21G basis set with appropriate charge and normalized values (-0.349 (Red) – +0.349 (Blue))

The atomic partial charges were also calculated using the density functional theory (DFT) method. The outcome of such analysis is shown in the following pictures 37 and 38. The atomic charge on the phosphorus appears to be similar when comparing the *gem*-difluoro-methyl-phosphonate phenylalanine **17** (0.854) with the pentafluorophosphono phenylalanine **15** (0.919). The situation changes sensibly when the oxygens of the former are compared to the multiple fluorine of the latter. Indeed, both of them are electronegative and this is reflected by the formal negative charge, but the values of the oxygen in **17** (~ -0.70) are more negative than one on the fluorine of **15** (~ -0.33). This can be attributed to the several fluorine atoms that, even if more electronegative, are present in bigger numbers and somehow equilibrate each other, or due to the double charge of the phosphonate.

Results and Discussion

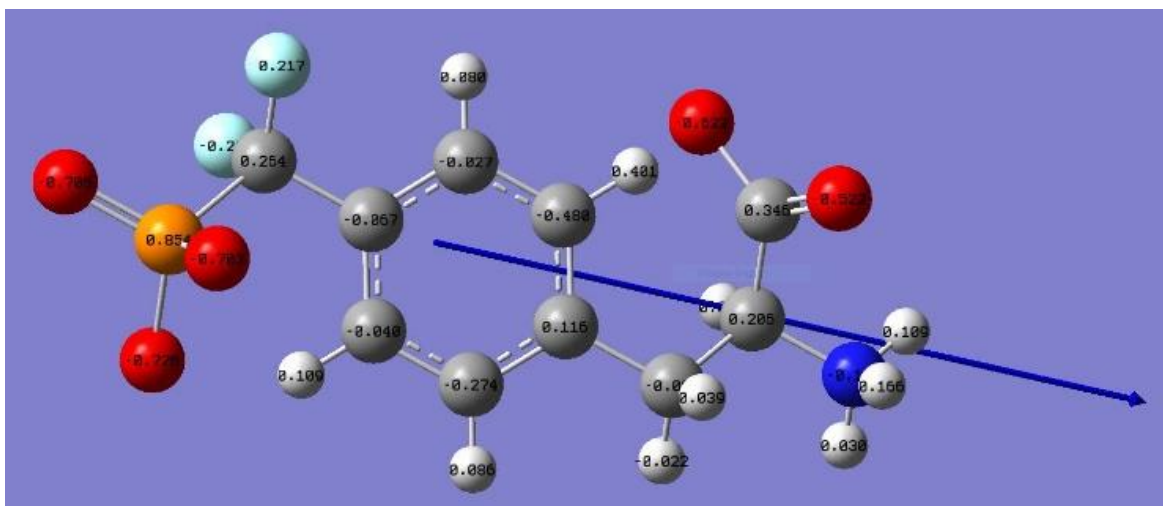


Figure 37: Dipole Moment of unprotected phosphono difluoromethylen-phenylalanine **17** as dianion: 23.5546 D (DFT default spin, B3LYP, cc-pVDZ, charge: -2, Merz-Kollman (ESP) charges)

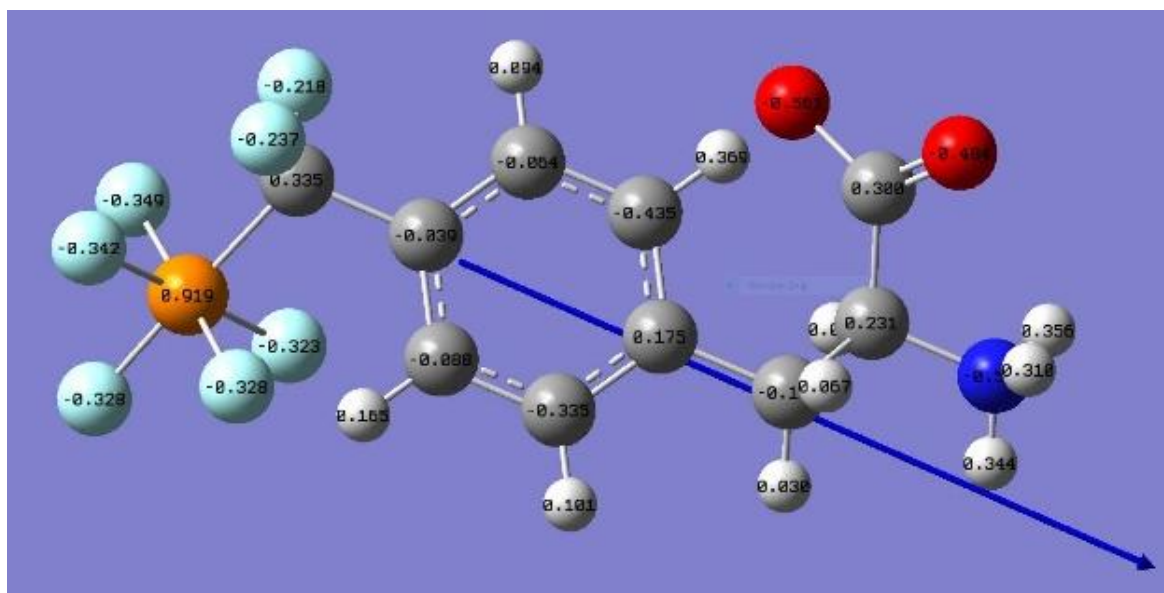


Figure 38: Dipole Moment of pentafluorophosphato-difluoromethyl phenylalanine **15** as mono anion: 20.9242 D (DFT default spin, B3LYP, cc-pVDZ, charge: -1, Merz-Kollman (ESP) charges)

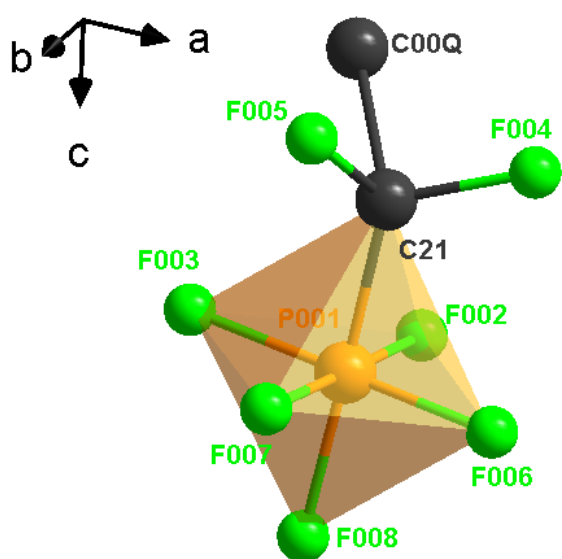
This difference is reflected to the dipole moment, which appears to be higher in intensity in the gemdifluorophosphonate (23.55 D) than in the pentafluorophosphate amino acid (20.92 D), ultimately giving an early idea of the diverse polarity.

It is important to point out that the analysis of the phosphonic acid were based on a molecular charge of -2, while for the pentafluorophosphate this value was -1. A direct comparison would be more accurate with calculations based molecules with identical

Results and Discussion

charge. Nonetheless, the values for the pentafluorophosphate still contribute to a better understanding of this moiety.

Additional consideration may be made regarding the shape and sterical hinderance of the pentafluorophosphate group and compare it with its phosphonic acid analogue. The spatial conformation, reported by previous studies and confirmed via x-ray crystallography,^[135] consist of an octahedral molecular geometry, with the central phosphorus atom (P001) bound to one axial (F008) and 4 equatorial (F002, F006, F007, F003) fluorine atoms (Figure 39). The reported bond lengths were experimentally determined from crystal structure of **11**.



Atom 1	Atom 2	Distance Å
P001	F002	1.6109 ± 0.0093
	F006	1.5485 ± 0.0101
	F007	1.5774 ± 0.0092
	F008	1.6237 ± 0.0115
	F003	1.6191 ± 0.0090
	C21	1.6833 ± 0.0115

Figure 39: Geometry and bond length of pentafluorophosphate group of **11** experimentally determined via x ray crystallography by Dr. F. Hemmerling and M. Rautenberg at BAM (Bundesanstalt für Materialforschung und –prüfung) Berlin.

These length values are in agreement with the one recorded for phosphorus pentafluoride (1.57 ± 0.02 Å).^[170] Similarly, the bond length between phosphorus and oxygen was experimentally determined between 1.43 and 1.67 Å,^[171] with more recent literature reporting values of 1.51 , 1.52 Å.^[172]

Overall, RPF_5 can be considered quite comparable to RP(O)(OH)_2 in the steric hindrance, with P-F and P-O bond length of comparable size. Regarding the shape, the tetrahedral geometry of the phosphonate moiety differs slightly from the octahedral one of the RPF_5^- , but this should not prevent the ligand to reach the active site and interact with it.

3.6 Determination of lipophilicity

The effect of the abundance of fluorine could be directly observed by evaluating the behavior of phenyl *gem*-difluoromethylen phosphonate **6** and phenyl *gem*-difluoromethylen pentafluorophosphate **9** in high-performance liquid chromatography (HPLC).

Figure 40 shows the extracted ion current (EIC) in the negative mode for the phenyl-based compounds where the retention time on C18 material increases from 3 minutes to 10 minutes. (Gradient: (A: H₂O + 0.1 % formic acid / B: ACN + 0.1 % formic acid; gradient: 5-95 % B in 5.5 min, 95% B from 5 to 10 min); 1 mL / min on Zorbax Eclipse plus C-18 RRHD (2.1 x 50 mm, 1.8 μM, 95 Å) column).^[150]

This indicates much stronger interaction with the hydrophobic stationary phase of the column. Similar results were observed when compounds **17** and **15** were subjected to the same analytical method (Figure 41). In this case, the retention time of the amino acid increased from 3.8 minutes for the phosphonic acid to 6 minutes for the corresponding pentafluorophosphate.

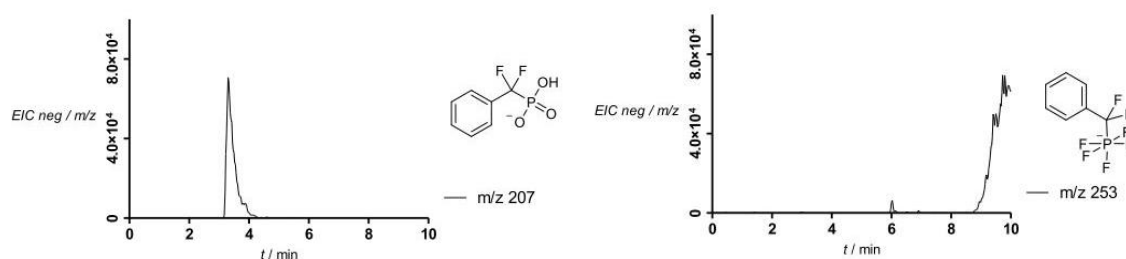
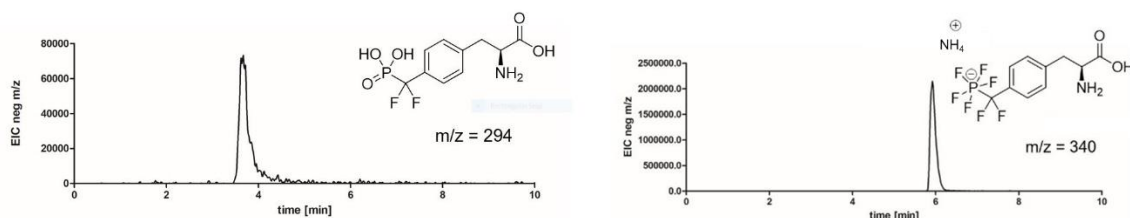


Figure 40: Chromatogram of **3-Na** and **5-TMA** on analytical LCMS equipped with C18 column using H₂O/ACN as mobile phase.



Results and Discussion

*Figure 41: Chromatograms of **17** and **15-NH₄** on analytical LCMS equipped with C18 column using H₂O/ACN as mobile phase.*

A recent collaboration work with Prof. Pagel at the Freie Universität Berlin allowed to investigate the lipophilicity of the new pentafluorinated amino acid from yet another point of view: it was included in the recently published study by Hoffmann et al, reporting the development of a new hydrophobicity scale for canonical and fluorinated amino acid.^[103]

Using a technique called IM-MS, ionized molecules of the sample aggregate in the low permittivity environment of high vacuum forming clusters of different size, which are separated with a drift gas, detected and analyzed. Their collision cross-section (Ω , CCS), which is a measure of the surface that will collide with the gas in the chamber, can be determined. Quantification of the deviation from the theoretical value yields a measure of the packing efficiency of the clusters. In vacuo, hydrophilic molecules form more compact clusters while lipophilic molecules will produce extended agglomerations. The deviation from the theoretically calculated isotopic growth can be quantified with a value called α . Values of α higher than 1 are associated to an expanded cluster size, indirectly giving a quantification of the lipophilicity. On the contrary, α values smaller than 1 indicate a more compact cluster, indicating a more hydrophilic character.

Error! Reference source not found. shows how the pentafluorinated sample **15** (left) results in a slightly decrease packing efficiency compared with the related phosphonate **17**, (right) and this is related in a increased hydrophobicity.

Results and Discussion

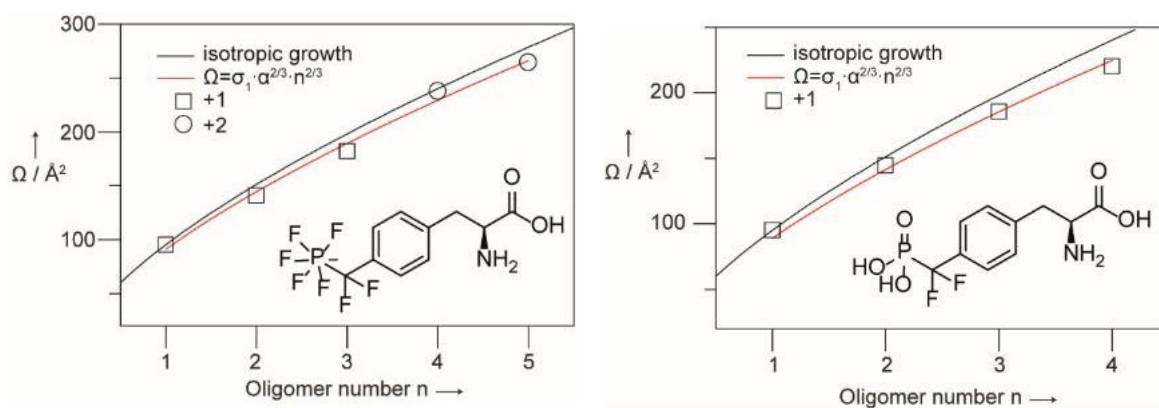


Figure 42: Collision cross section for **17-NH₄** and **15** respectively and deviation from its theoretically calculated isotropic growth

Plotting the results obtained for different amino acids, a hydrophobicity scale was obtained and is reported in Figure 43. Fluorinated amino acids are colored in green.

The high lipophilicity represented by values of α around 1.1 have been determined for pentafluoro isoleucine and leucine. The lowest value at around 0.9, associated to high hydrophilicity, were determined for aspartic acid, serine, glutamic acid and proline, arginine, and the phenylalanine phosphonic acid. In the middle, at α values of around 1, alanine, lysine, tyrosine, and slightly below, at 0.98 the pentafluorinated amino acid, confirming its lipophilicity again from a different point of view.

Interestingly, asparagine and pentafluorophenylalanine are close to that range too, indicating comparable behavior.

The ionizability of functional groups is reflected quite well in the figure. Aspartic acid is more hydrophilic than asparagine, and the same can be said for glutamic acid and glutamine. Quite surprisingly, lysine shows no deviation from theoretical values, maybe indicating that the aliphatic alkyl chain somehow compensates for the easy protonation of the basic primary amine at one if its extremity (pKa 10.53).

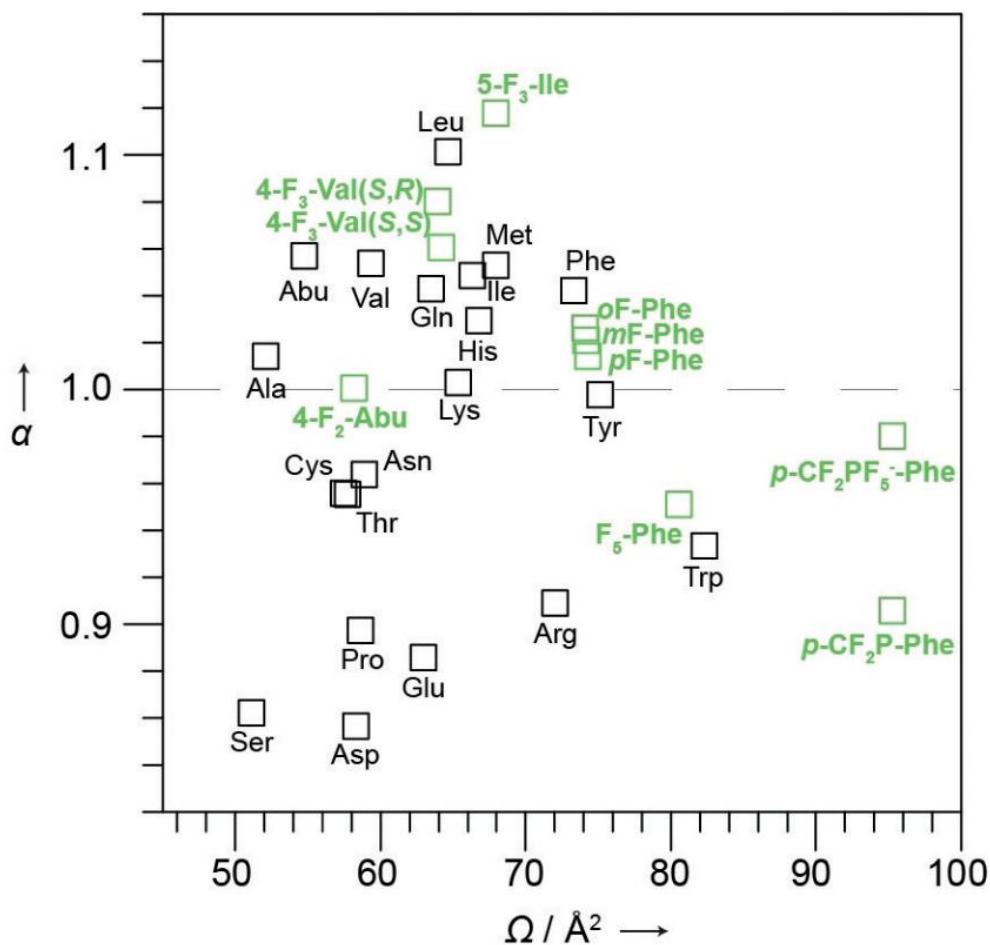


Figure 43: Hydrophobicity table determined by Hoffman et al. for canonical and fluorinated amino acids.^[103]

Exception made for the pentafluorophosphate, it should be noted that none of these molecules are natively charged. This might be the reason of the big discrepancy between value of α for phenylalanine and the corresponding pentafluorophosphate. On the other hand, this fluorine rich fragment appears to be more similar to tyrosine.

Consequently, from this analysis it appears that the pentafluorophosphate is masking the hydrophilicity of the phosphonate analogue, but maybe due to the native charge, its access to the lipophilic area is somehow precluded. This resulted in almost no deviation from theoretical value, which can be rationalized as amphiphilic behavior.

3.7 Stability of aryl *gem*difluoromethylen pentafluorophosphate towards commonly employed SPPS conditions

In order to deepen the knowledge about the properties and the synthetic limit of these new chemical entities, the stability of model perfluorinated compounds towards different conditions were tested, including normally employed solid phase peptide synthesis (SPPS) protocols. Fmoc-based SPPS is a convenient method to produce peptides in a manual or automatized fashion. It consists of repeated cycles of deprotection with a base and coupling reactions performed on solid support, which can be mixed with the coupling solution or conveniently be washed and filtrated right after. The coupling steps are followed by cleavage from the resin, usually with strong acid conditions. In order to identify a possible cleavage cocktail for a pentafluorinated peptide, many different reagents have been tested. The decomposition, if observed, was quantified integrating the CF_2 peaks related to the formation of the *gem*difluoromethylen monofluoro phosphonate or the simple *gem*difluoromethylen phosphonate. As previously discussed, these products are observed at much higher fields (~ -107 ppm instead of ~ -98 ppm). In general, a small amount of the sample (5 mg) was dissolved in the solvent (1 mL) to be tested in an Eppendorf tube and subsequently transferred into an NMR tube for analysis. If present, fluorinated reagents were removed in vacuo before subjecting the sample to ^{19}F -NMR to avoid disturbance in the analysis.

These results are summarized in the following table.

At first, the most common cleavage agent in Fmoc-SPPS was tested. Trifluoroacetic acid (TFA) showed to be incompatible with pentafluorinated amino acid with concentration from 100% down to as little as 0.1 M. In this case, after 2 h 10% decomposition was observed (Entry 1-5). Only concentration of 0.01M TFA or 0.1% were tolerated for 1 and 2 hours respectively, but these conditions are far too mild to promote cleavage on Rink resins to obtain the desired peptide amides (Entry 6-7).

HCl was included to evaluate the stability at different pH values. At pH=1 for 1 h no decomposition was observed but but treatment for over 24 h resulted in 15%

Results and Discussion

hydrolysis (Entry 8-9). At pH=2, stability was observed up to 24 hours (Entry 10-11).

Results and Discussion

Table 13: Stability investigations on PF₅ moiety

Entry	Compound	Conditions	Outcome (analyzed via ¹⁹ F-NMR)
1	Fmoc-(4-PF ₅ ⁻ CF ₂)Phe-OH 13	TFA 100%, 3 h	Decomposition
2	"	TFA 95% (aq.), 2 h	Decomposition
3	"	5% TFA in DCM, 1 h	Decomposition
4	"	0.2% TFA (aq.), 2 h	35% decomposition
5	"	0.1 M TFA (aq.), 1 h	10% decomposition
6	"	0.01 M TFA (aq.), 1 h	stable
7	"	0.1% TFA (aq.), 2 h	stable
8	"	0.1 M HCl (aq.), 1 h	stable
9	"	0.1 M HCl (aq.), 24 h	15% decomposition
10	"	0.01 M HCl (aq.), 1 h	stable
11	"	0.01 M HCl (aq.), 24 h	stable
12	"	AcOH in DCM (1:9), 1.5 h	Decomposition
13	"	Olah' reagent + anisole, 1 h	Stable (analyzed via LCMS)
14	PhenylCF ₂ PF ₅ ⁻ 5	HFIP pure for 1 h	50% degradation (to monofluorophosphate)
15	"	HFIP / DCM 1:4 for 1 h	Stable
16	"	0.1 M HCl in HFIP, 2 h	Decomposition
17	"	TMSBr (100 equiv.) in ACN, 1 h	decomposition
18	"	Sonication in ACN	stable
19	"	SiO ₂ (30 μL/mg) in ACN, 1 h	stable
20	"	piperidine (20%) in DMF, 24 h	stable
21	"	pyridine neat, 1 h	stable

Results and Discussion

22	“	DBU (2%) in DMF, 30 min	stable (analyzed via LCMS)
----	---	-------------------------	----------------------------

In the attempt to identify a suitable cleavage cocktail applicable to Rink resins, acetic acid in DCM (1:9)^[173] was investigated next. After 1.5 hour, complete decomposition was observed (Entry 12).

The last tested protocol suitable for the synthesis of unprotected peptide amides was based on the investigation of Matsuura et al.^[174] Their study reported the successful use of pyridium polyhydrogen fluoride as HF-alternative in the cleavage of amino acids bound to a 4-Benzhydramine (MBHA) resin, an analogue on the Rink support. Indeed these conditions proved to be suitable with the phenyl pentafluorophosphate (Entry 13)

The use of hexafluoroisopropanol (HFIP) was evaluated due to its demonstrated efficacy in peptide synthesis of protected peptide acids on 2-chlorotriyl chloride resins (2-CTC).^[175] These acid sensible resins are commonly used to prepare protected peptide acids with mild cleavage conditions. Pentafluorinated sample were decomposed after 1 hour treatment with the concentrated acid (Entry 14), but its use in commonly employed proportion (1:4 in DCM) results in stability. (Entry 15). Addition of 0.1 M HCl in HFIP, which was reported to be useful in the deprotection of acid labile side chain protecting group of amino acids, not surprisingly resulted in decomposition (Entry 16).

When tested, TMSBr decomposed the PF₅⁻ moiety. This might have occurred because of water molecules in the samples would react with the reagent producing TMSOH and HBr, yielding a harming acidic mixture (Entry 17). Stability was confirmed in case of sonication or in presence of the silica gel commonly employed in chromatographic purifications (Entry 18-19). Compatibility of the PF₅ moiety was assessed in presence of different organic bases as pyridine, piperidine and DBU. (Entry 20-22). In presence of a big excess (>5 equivalents) of aqueous base, hydrolysis was observed (see chapter 3.4.1) but the amount of different byproduct was not quantified.

Summarizing, this investigation led to the identification of two suitable protocols: the use of pyridinium polyhydrogen fluoride for the synthesis of unprotected peptide amides on benzhydramine based resins, and the use of HFIP/DCM (1:4) in the case of protected peptide acids on 2-CTC resins.

Results and Discussion

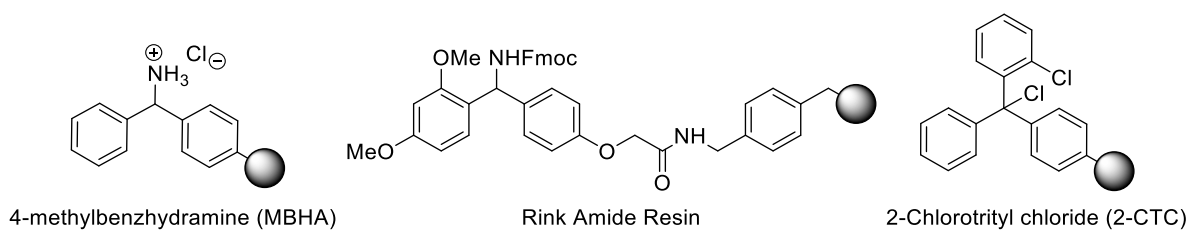


Figure 44: Resins that can be used to obtain peptide amides (MBHA and Rink) and peptide acids 2-CTC

3.8 Peptide synthesis

After achieving the first main objective of this research work by developing the optimized synthesis of pentafluorophosphates, following investigations were aimed to incorporate this moiety into peptides before assessing their biological efficacy against PTP1B. For this purpose, it is common strategy in the literature to use a specific portion of a natural substrate of the protein, opportunely modified at its phosphotyrosine position.^[38b, 176] Hence, the peptide sequence EFGR₉₈₈₋₉₉₈ (Asp-Ala-Asp-Glu-pTyr-Leu-Ile-Pro-Gln-Gln-Gly; K_m PTP1= $2.63 \pm 0.37 \mu\text{M}$; $k_{\text{cat}} = 75.7 \pm 1.0 \text{ s}^{-1}$; $k_{\text{cat}}/K_m = 2.88 \times 10^{-7} \text{ M}^{-1}\text{s}^{-1}$)^[69b] is usually truncated after the leucine residue due to comparable kinetic parameters between the complete undecapeptide and the truncated peptide (Ac-DADEpYL-H; $k_{\text{cat}} = 67.6 \pm 1.2 \text{ s}^{-1}$; K_m PTP1= $3.60 \pm 0.47 \mu\text{M}$; $k_{\text{cat}}/K_m = 1.88 \pm 0.12 \times 10^{-7} \text{ M}^{-1}\text{s}^{-1}$)^[38b]; customizations of the phosphotyrosine residue with synthetically derived analogues were therefore performed on the model substrate sequence DADEpYL. Acetylation and primary amidation of the C-terminus were carried out as well in order to avoid charge-repulsion and results in the final sequence Ac-DADEpLY-H. Such a sequence containing the difluorinated building block F₂pmp is reported to inhibit PTP1B with a IC₅₀ of 0.2 μM .^[68, 176a]

Among all PTP1B inhibitors reported in the literature, the most potent up to now was discovered by Shen in 2001.^[71] This bivalent peptidomimetic, shown in the introductory part in Figure 12 performed very well in vitro assays, revealing a remarkable IC₅₀ value towards the protein in the low nanomolar range. Unfortunately, the presence of two phosphonic acid groups and a carboxylic acid in the side chain of the pseudo tripeptide resulted in a high polarity that strongly disfavored cellular permeability. In order to mask this polarity and favor cellular permeation, different strategies have been described in the literature: this included coupling onto a cell penetrating peptide via disulfide bridge^[177], onto a highly lipophilic fatty acid^[46], and on the functionalization of the phosphonic acid with lipophilic substituents, able to be cleaved by sequential enzymatic reduction within the cell, releasing *in situ* the free phosphonic acids as active species.^[72]

With a new optimized synthesis of the pentafluorophosphate moiety available and after having observed an marked increase in lipophilicity obtained after introduction

Results and Discussion

of this perfluorinated group in fragments, the very last objective of this research work was to prepare these two model peptide inhibitors, the Ac-DADEpYL-H **19** and the pseudo tripeptide **20**, bearing the pentafluorophosphate as phosphotyrosine mimetic. The structures of the two target peptides are summarized in the following figure.

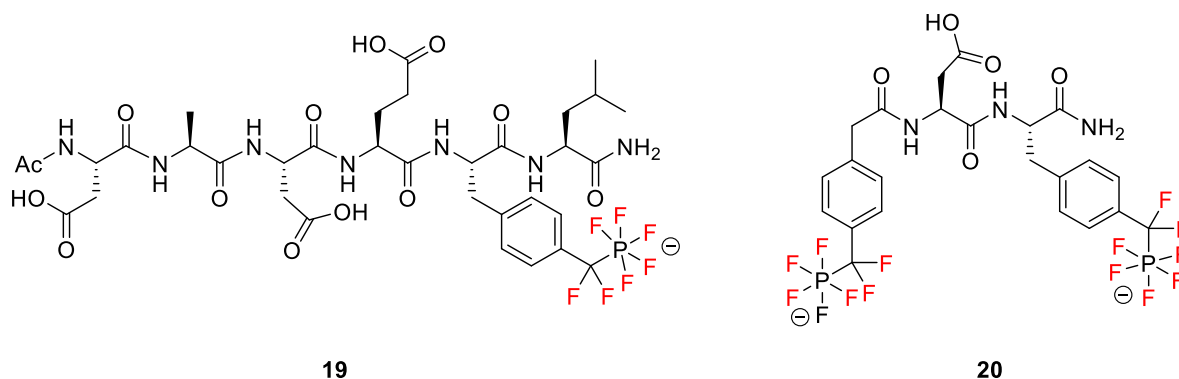


Figure 45: Structure of known model inhibitors of PTP1B as pentafluorophosphates

In principle, to prepare peptides via chemical synthesis, there are two possibilities: solution phase peptide synthesis and solid phase peptide synthesis (SPPS). The convenience of the first approach decreases proportionally with the length of the peptide of interest, due to the necessity to purify the product after each step. In the SPPS approach, the excess of coupling reagents as well as deprotection products are conveniently washed away from the solid support after every reaction, greatly increasing the ease of execution and the time efficiency. This process can be automatized and therefore be conducted even overnight in a peptide synthesizer. The coupling reagents analyzed in the peptide synthesis investigations are summarized in the following figure.

Results and Discussion

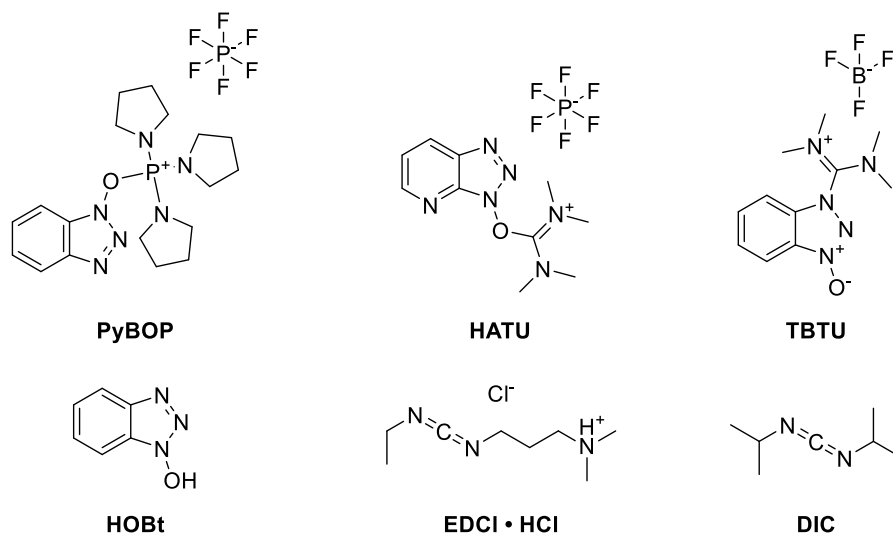
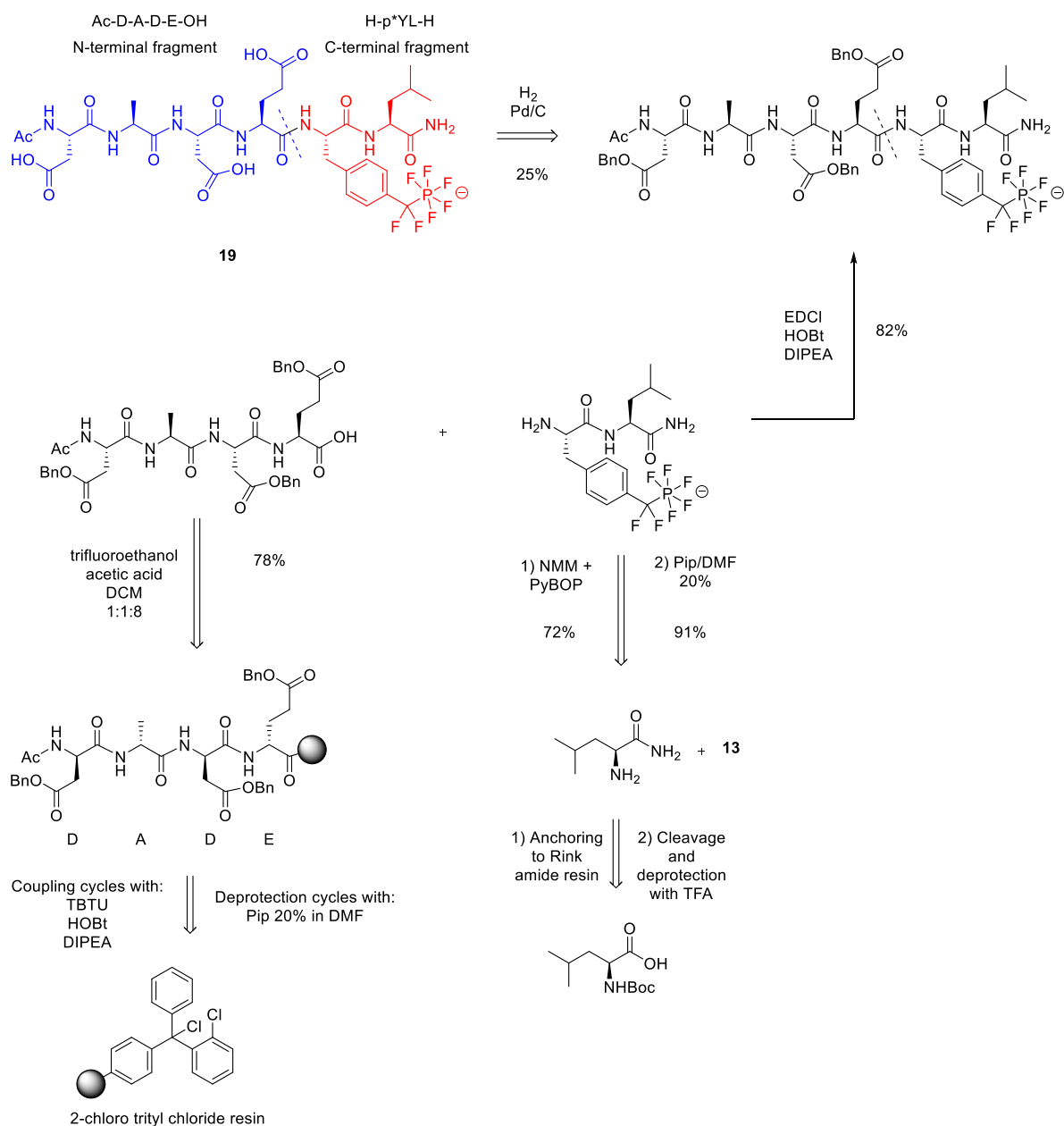


Figure 46: Coupling reagents used in this research work for peptide synthesis in solution or on solid phase

3.8.1 Solution phase peptide synthesis attempt

At first, due to the instability of the pentafluorophosphate toward the acidic condition required by the cleavage step in SPPS, a solution phase peptide synthesis was examined. According to this approach, the coupling steps in presence of the pentafluorophosphate would be performed in solution and the construction of the remaining peptide chain on solid support. This mixed strategy would require the preparation of the many intermediates reported in Scheme 23 with related additional purification steps.



Results and Discussion

Scheme 23: Mixed approach for synthesis of the first pentafluorinated peptide **19**

Results and Discussion

The hexapeptide sequence Ac-DADEpYL-H was ideally divided in two parts, one before (in blue) and one after (in red) the pentafluorinated amino acid. These two fragments were synthesized on solid phase and in solution respectively and final removal of the benzyl esters could be achieved with Pd/C and H₂.

N-Terminal Fragment: The acetylated DADE sequence was prepared on the acid labile resin 2-CTC resin using slightly modified Fmoc-based coupling procedure, alternating cycles of coupling (TBTU, HOBt and DIPEA) and Fmoc deprotection (piperidine in DMF). The instability of the pentafluorophosphate towards acidic conditions hampered the choice of suitable protection group for the other building blocks such as Asp and Glu. The acid labile *tert*butyl ester was therefore unsuitable. Benzylic groups presented the desired orthogonality to base treatments offering cleaving methods relying on hydrogenation, avoiding the need for acid-mediated deprotection. However, these protecting groups offered less protection towards aspartimide formation, an issue that negatively affect yield of the desired product generating byproducts difficult to remove.

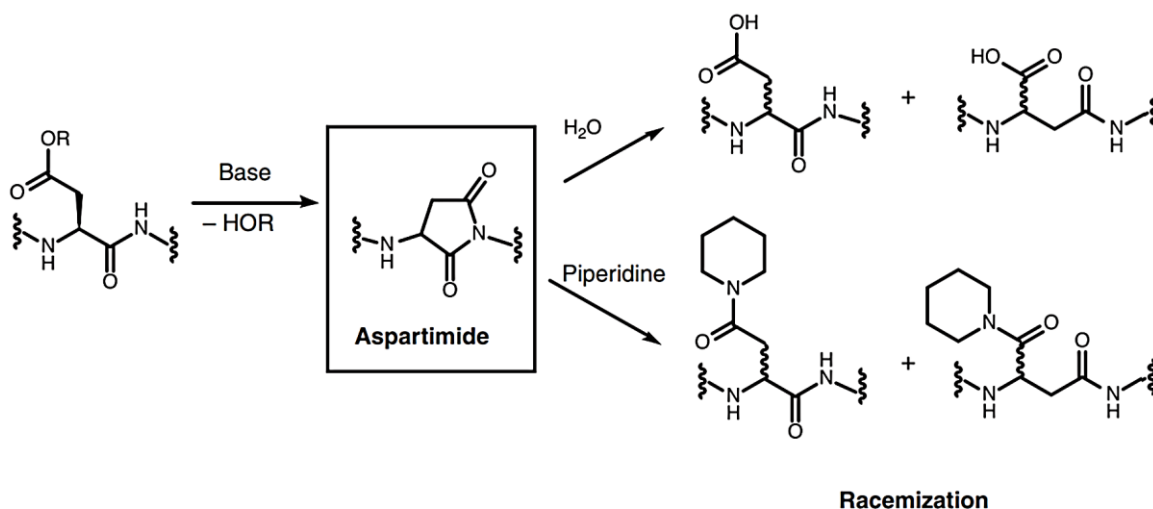


Figure 47: Aspartimide formation leading to a total of 8 byproducts after ring opening. Picture from Neumann et al.^[178]

Aspartimide formation involves the cyclization of amino acids as aspartic acid with the amide nitrogen in the peptide backbone. Ring opening can result in the formation of racemic mixtures of beta amino acids or piperidinyll adduct. This reaction is favored by the strong basic conditions repeated in the cycles of Fmoc deprotection

Results and Discussion

and by sequences where aspartic acid is followed by a small side chain amino acid such as alanine or even glycine. Solution to this problem have been developed by chemical companies by offering more sterically hindered protecting group for these amino acids, specifically designed to address this issue.^[179] Trityl group are protecting groups even more sterically demanding, but the stabilization of the tertiary carbocation by the aromatic groups actually promote the leaving group character of this moiety, resulting in a higher propensity to aspartimide formation.^[180]

Interestingly, performing the piperidine-based Fmoc deprotection in a 0.1M solution of HOBt showed no aspartimide formation.^[181] This technique is reported to prevent formation of aspartimide by keeping the nitrogen in the peptide backbone protonated and non-nucleophilic. Acetylation was carried out with an equimolar mixture of acetic anhydride and pyridine in DMF. Pyridine was added to avoid accidental cleavage of the peptide due to acetic acid formation. Final cleavage was carried out using a mixture of acetic acid, trifluoroethanol in DCM (1:1:8) for 1 hour. The crude wash chromatographically purified with RP C18 yielding the benzyl protected Ac-DADE-OH in 78% yield.

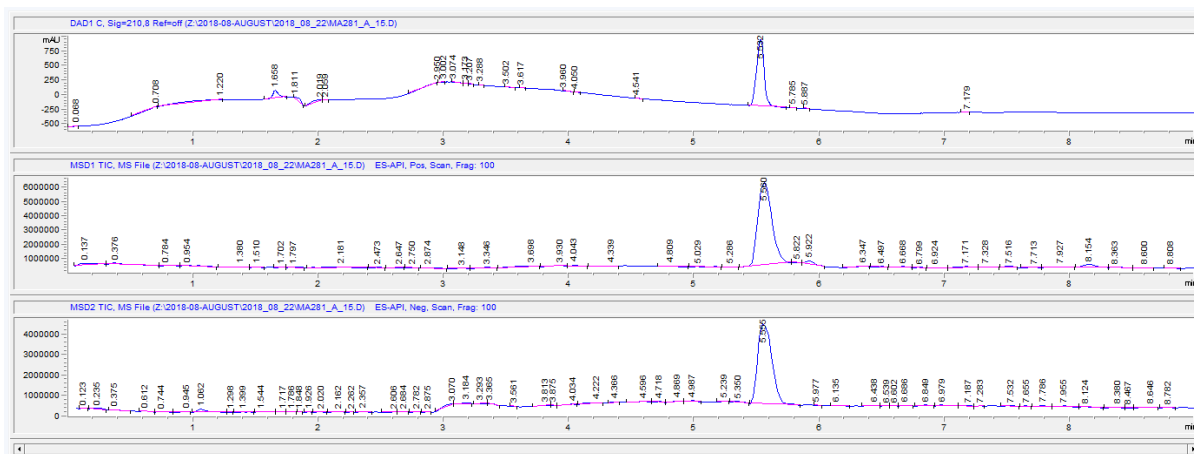


Figure 48: LCMS trace (210 nm absorption, positive total ion current (TIC) and negative TIC) of benzyl protected Ac-DADE-OH after HPLC purification.

C-Terminal Fragment: The dipeptide containing the pentafluorophosphono phenylalanine was obtained via solution phase peptide synthesis by reacting the Fmoc protected amino acid **13** with the amidated leucine building block in a PyBOP - N-Methylmorpholine (NMM) mediated coupling. After 2 hours, aqueous workup and

Results and Discussion

EtOAc extraction, the product was purified from the crude mixture at RP-MPLC (H₂O-ACN, 5 to 99%) yielding 72% of the desired pentafluorinated dipeptide.

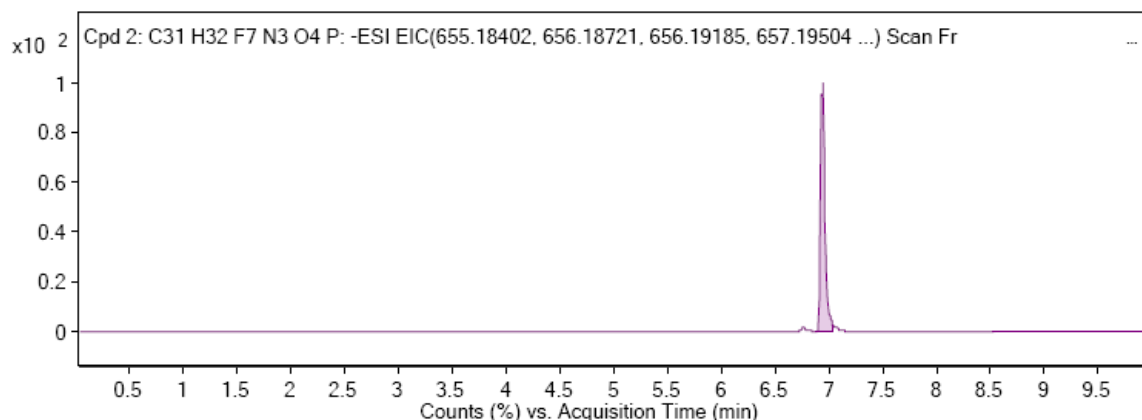


Figure 49: HRMS chromatogram (Extracted ion current) of the C-terminal fragment, Fmoc-pYL-H

Building block leucine amide was obtained via primary amidation of N-Boc-protected Leu carboxylic acid with Rink amide, followed by simultaneous deprotection and cleavage with TFA, yielding the unprotected Leucine amide in 83%.

Benzyl-protected Ac-DADEpYL-H: Solution coupling of the benzyl protected Ac-DADE-OH and Fmoc deprotected H-pYL-H was carried out with DIPEA and EDCI with HOBT. EDCI was chosen because its solubility in water allows its removal in aqueous workup. After 3 hours it was possible to observe completion of the reaction via LCMS. After aqueous workup, purification of the crude via MPLC yielded the desired benzyl protected hexapeptide in 82% yield.

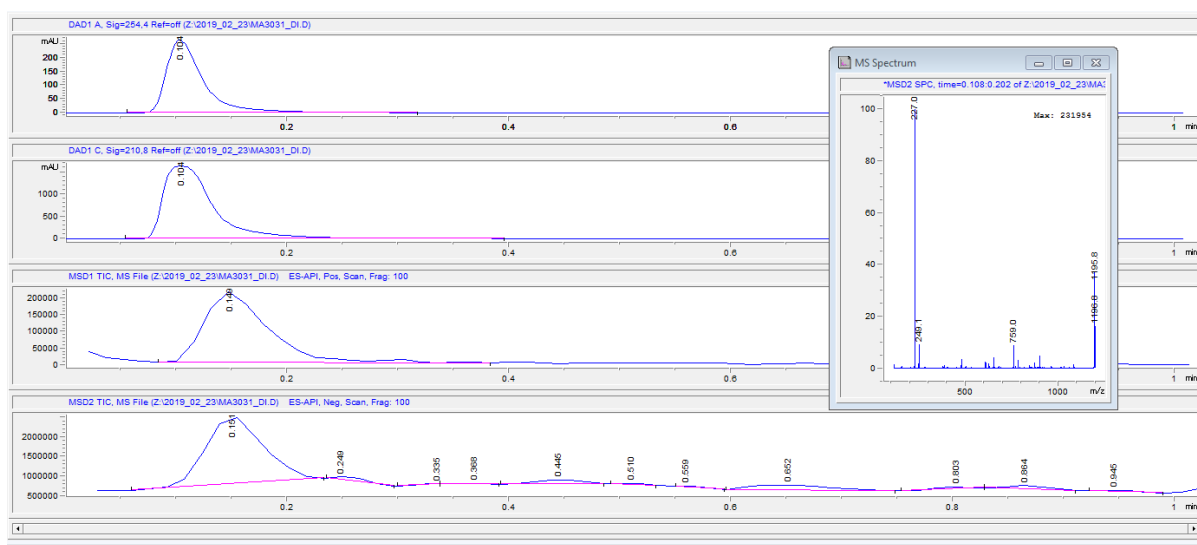


Figure 50: LCMS (DI) of benzyl protected Ac-DADEpYL-H. The mass of the product is 1195 D.

Results and Discussion

Due to its high lipophilicity, this compound could not be observed at LCMS under the standard gradient (5 to 99% ACN in H₂O for 4.5 minutes, followed by to 5.5 min of 99% ACN) on C8 or C18 column; however, the compound could be observed via direct injection, excluding chromatographic separation (Figure 50).

Benzyl deprotection of Ac-DADEpYL-H: The protected peptide was subjected to hydrogenation in presence of Pd on charcoal with a couple of drops of a HCl 0.01 M aqueous solution.

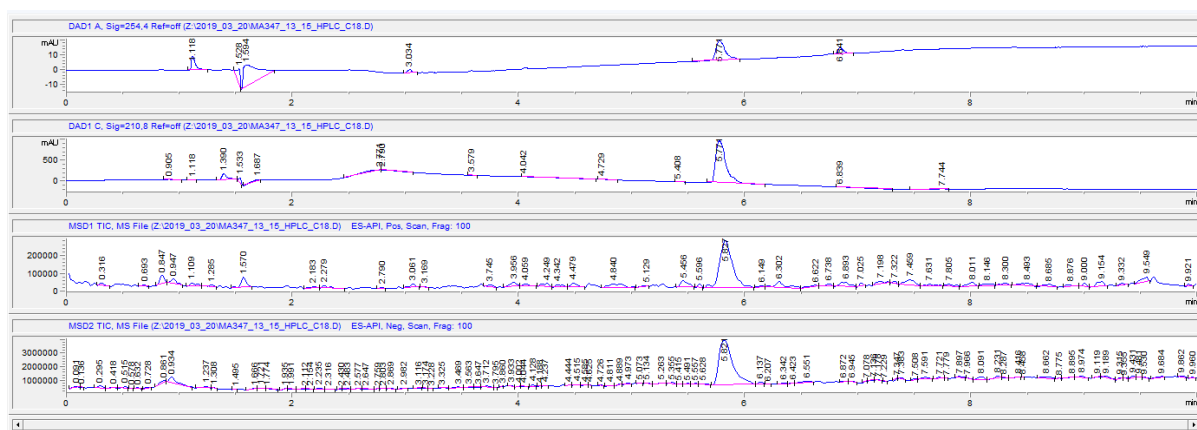


Figure 51: Chromatogram of HPLC purified Ac-DADEpYL-H ($m/z = 924$, $R_t=5.9$ minutes.)

Despite the presence of the product, purification was hampered by the presence of big amounts of ammonium bicarbonate salts coming from the buffer of HPLC purification (50 mM), which could not be steadily removed via lyophilization. A second HPLC with reduced amount of buffer (10 mM) ammonium bicarbonate buffers yielded the peptide with an overall yield of 25%.

Despite being lengthy, this convergent solution phase peptide synthesis allowed the preparation of the first peptide containing a pentafluorinated amino acid.

The development of a SPPS protocol was still highly desirable but identification of suitable cleavage cocktail was not yet identified.

3.8.2 Solid phase peptide synthesis approach

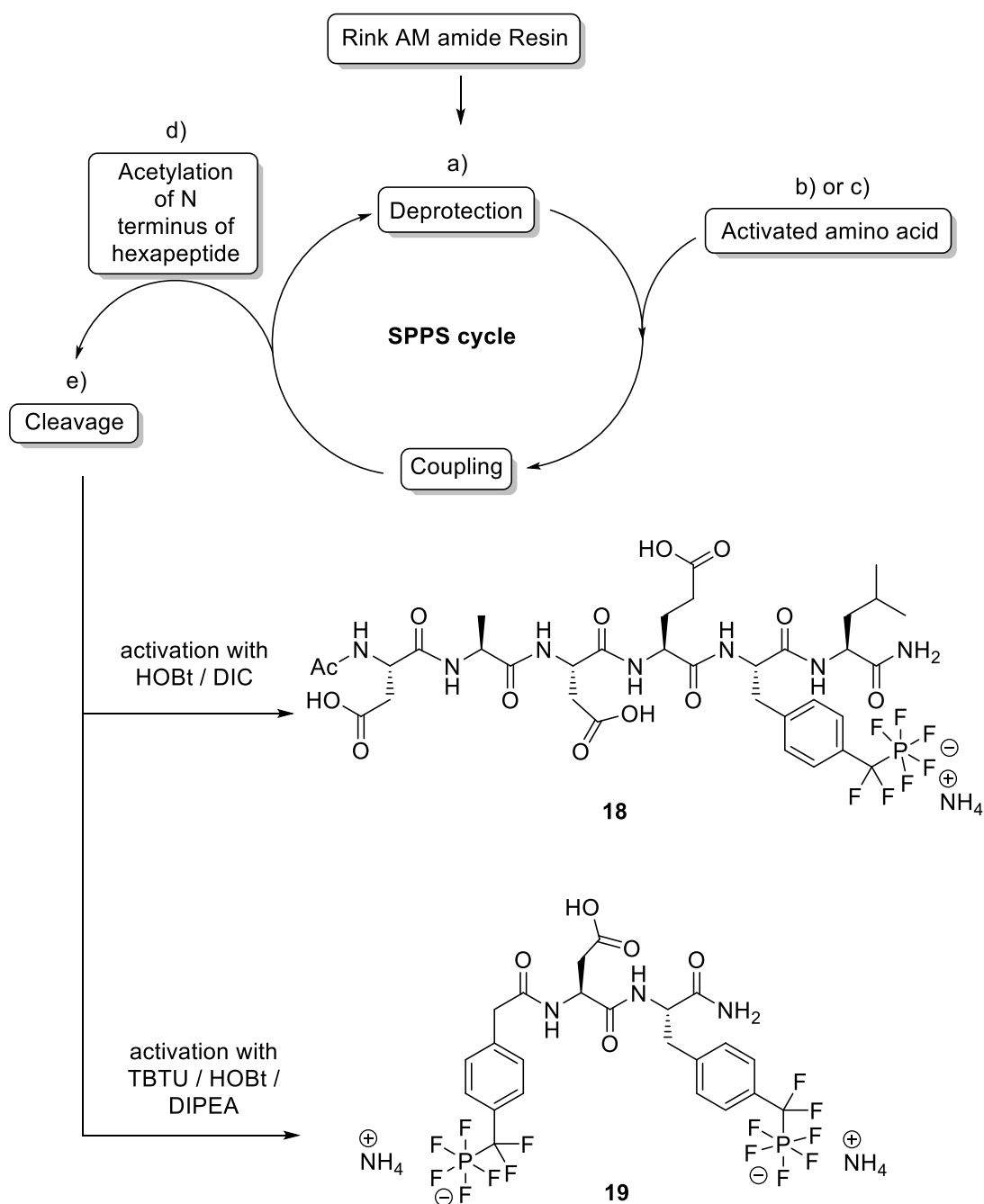
Only after extensive research, this possibility was concretized after assessing the stability of PF₅ towards pyridinium poly hydrogen fluoride, which can be used to obtain peptides amides from Rink resin, and toward HFIP in DCM, for the preparation of protected peptide acids on 2-CTC resin. This discovery forced the reevaluation of the planned peptide synthesis, now to be performed on solid phase.

Since the peptide target was the hexapeptide amide previously shown, the synthesis was carried out using the Rink amide solid support and Olah's reagent; the new synthesis was then planned, taking into account the health hazard and glass etching properties of HF-containing reagent.

As previously seen in the introduction (Figure 19), the most potent *in vitro* PTP1B inhibitor known so far is a bivalent molecule bearing two gemdifluorophosphonate moiety (IC₅₀ = 2.4 nM).^[71] After having identified a convenient procedure for the preparation of peptides containing the pentafluorophosphate moiety, the synthesis of this short chain bearing two pentafluorinated groups was addressed as well.

As shown in Scheme 24, after deprotection of the Rink Amide resin with the common 20% piperidine in DMF mixture, the sequence was built anchoring on the solid support the activated the amino acids DIC / HOBt or TBTU / HOBt / DIPEA. Repeated cycles of deprotection/coupling steps, with washings after each step, were carried out until the peptide sequence was complete. At first the standard DIC / HOBt protocol was used, but due to inefficient coupling of the pentafluorophosphate (monitored via Kaiser test), the more potent TBTU / HOBt / DIPEA mixture was identified as superior.

Results and Discussion



Scheme 24: Reaction conditions: a) Piperidine / DMF 20%; b) canonical amino acids or **13-NH₄** (5 equivalent) DIC / HOBt (5 equiv.); c) canonical amino acid, **13-NH₄** or **14-NH₄** (5 equivalents) TBTU (5 equiv.), HOBt (5 equiv.), DIPEA (10 equiv.); d) Pyridine / Ac₂O in DCM (50 equiv.); e) Pyridinium polyhydrogen fluoride + 10% anisole. Yield of **19**: 18%; Yield of **20**: 46%

Using this method it was possible to obtain the hexapeptide using the carbodiimide-based reagents; however, the final yield was low and no coupling was achieved when trying to react the pentafluorophenylalanine **13** to the resin as first amino acid (monitored via Kaiser test). Therefore, the second peptide was synthesized using only TBTU-based method, which resulted in efficient coupling in all the steps.

Results and Discussion

Acetylation of the N-terminus of the hexapeptide was achieved using acetic anhydride and pyridine in DCM.

The cleavage from the resin was carried out using a minimum volume of Olah's reagent + 10% anisole in the plastic syringe. The workup of this crude needed several optimizations due to the incompatibility of hydrogen fluoride and with usual glass laboratory equipment.

After few attempts a proper handling procedure was developed: the syringe was connected with plastic tubing to a plastic column filled with CaO as neutralizing agent for the hydrogen fluoride gas; this column was connected to one of the manifolds of a Schlenk line. After neutralization of the HF gas, the glass-made Schlenk apparatus could be used without the risk of damaging the equipment and the excess of pyridine was condensed in a second trap cooled with liquid nitrogen. The syringe was then removed from the high vacuum apparatus, the beads were washed with THF, a mixture of THF/H₂O and with ultimately with ACN, according to a decreasing swelling behavior. The washings were collected in a plastic falcon tube containing a saturated aqueous solution of ammonium bicarbonate. The basic mixture was concentrated at rotary evaporation and purified on MPLC equipped with reverse phase C18 column.

This method allowed the preparation of the first two pentafluorinated peptides **19** and **20** in an easy and safe manner. After purification, a small amount of impurity was detected by NMR and was identified as the acyl-PF₅ adduct by Markus Tiemann, who investigated further this interesting byproduct. (Figure 52). Its mechanism of formation relies on the presence of water and aqueous HF: fluoride abstraction followed by a nucleophilic attack of a water molecule on the methylene bridge produces the hydroxy monofluorinated intermediate, which upon formal release of a molecule of HF yields the acylated product.

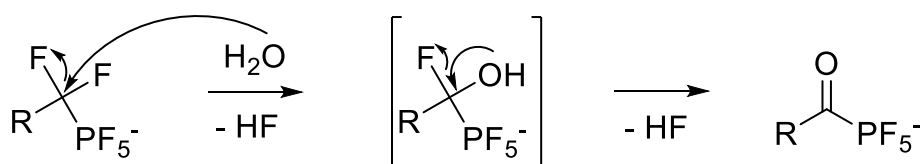


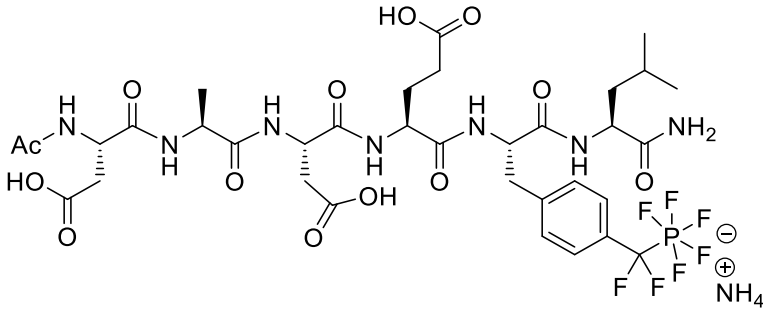
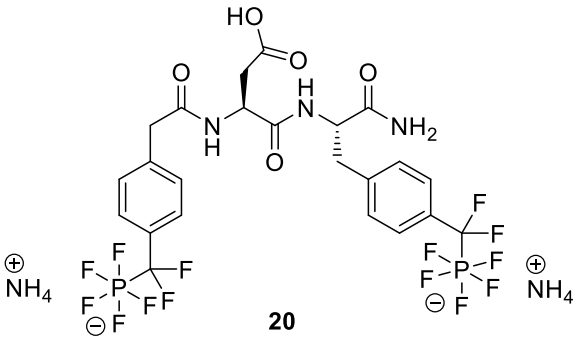
Figure 52: Mechanism of formation of acyl PF₅⁻ byproduct in presence of water

Its removal via chromatographic methods was hampered by the similar retention time on the column used, but a slow gradient allowed to separate it from the desired CF₂PF₅⁻ peptides, yielding the target peptides in high purity (see attached NMR).

3.9 Determination of inhibitory potential

The inhibitory potential of pentafluorinated compounds was measured against PTP1B in a fluorescence-based assay. Results are reported in Table 14.

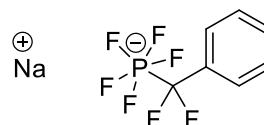
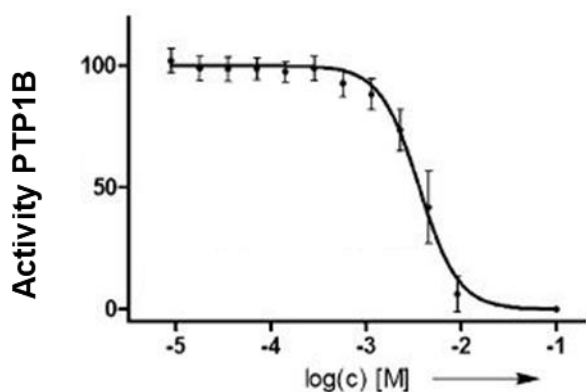
Table 14: Overview of inhibitory potential of chosen phosphonate and pentafluorophosphates

Compound	IC ₅₀
Phenyl gemdifluoromethyl phosphonate 3	3.82 ± 0.456 mM ^a
Phenyl gemdifluoromethyl pentafluorophosphate 5-Na	3.62 ± 0.18 mM ^a
Naphthyl gemdifluoromethyl phosphonate 7	328 ± 6 μM ^a
Naphthyl gemdifluoromethyl pentafluorophosphate 6-Na	52 ± 4 μM ^a
H-4-(CF ₂ PO ₃ H)-Phe-OH 17	3.1 ± 0.3 mM ^b
H-4-(CF ₂ PF ₅)-Phe-OH 15-NH₄	122 ± 14 μM ^b
 Ac-DADE(PF ₅ CF ₂)FL-NH ₂ 19- NH₄	148 ± 12 μM ^b
 20 Pseudo tripeptide 20- NH₄	243 ± 23 μM ^b

Results and Discussion

a: determined in *p*-NPP-based assay by Dr. Stefan Wagner;^[150] b: determined with DiFMUP-based assay by Markus Tiemann

The assays used to determine the biological activity of these samples towards PTP1B were based on spectrophotometric method using pNPP (*para*-nitrophenyl phosphate) as protein substrate. When subjected to enzymatic activity, this phosphorylated aromatic compound is converted into *para*-nitro phenol, whose presence can be observed by monitoring the absorbance at 405 nm and plotting it over time (also known as positive control). On the contrary, the scenario when only the protein is present without substrate is called negative control. Preincubation of the protein with an inhibitor, followed by the addition of the substrate, will result in a line with a decreased slope when compared to what is observed when the protein is free to hydrolyze the substrate: the higher the slope, the lower the inhibitory effect, whereas complete protein activity shutdown will result in a flat line. Associating the slopes with the concentration of the inhibitor allows to quantify the activity of the sample and to calculate the IC₅₀, defined as the concentration required to inhibit 50% of the protein activity. The following graphs were obtained via pNPP based assay carried out by Dr. Stefan Wagner using the software Prism.



Results and Discussion

Figure 53 Inhibition of PTP1B by compound **5**, IC_{50} : 3.62 ± 0.18 mM

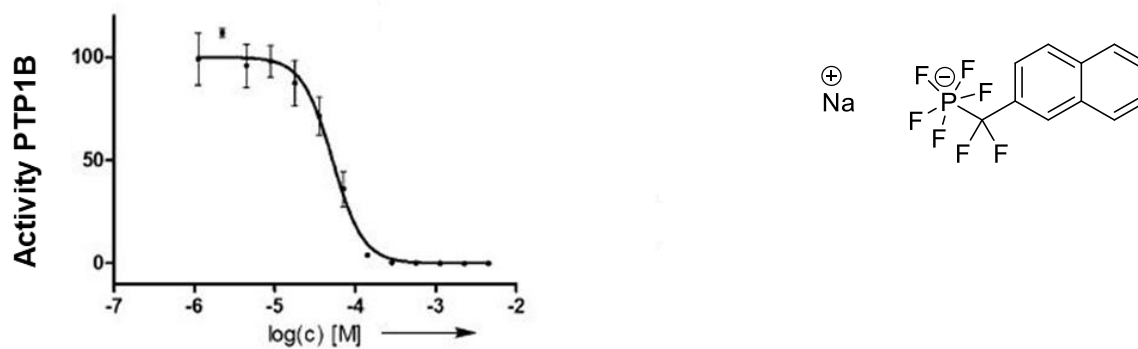


Figure 54 Inhibition of PTP1B by compound **6**, IC_{50} : 0.052 ± 0.004 mM

Results and Discussion

The following curves were determined using a slightly different substrate called DiFMUP (6,8-difluoro-4-methylumbelliferyl phosphate), because the absorbance of the hydrolyzed product can be detected over a wide pH range. The following biological assays have been carried out by Markus Tiemann using the software Prism.

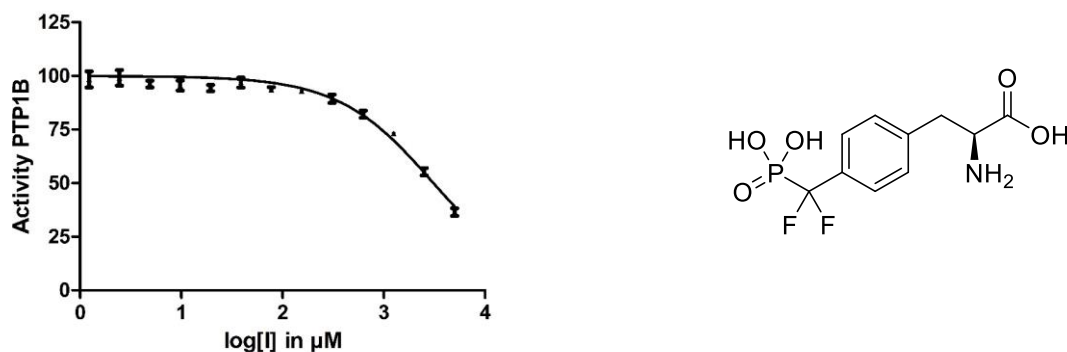


Figure 55 Inhibition of PTP1B by compound **17**, IC_{50} : $3.1 \pm 0.3 \text{ mM}$

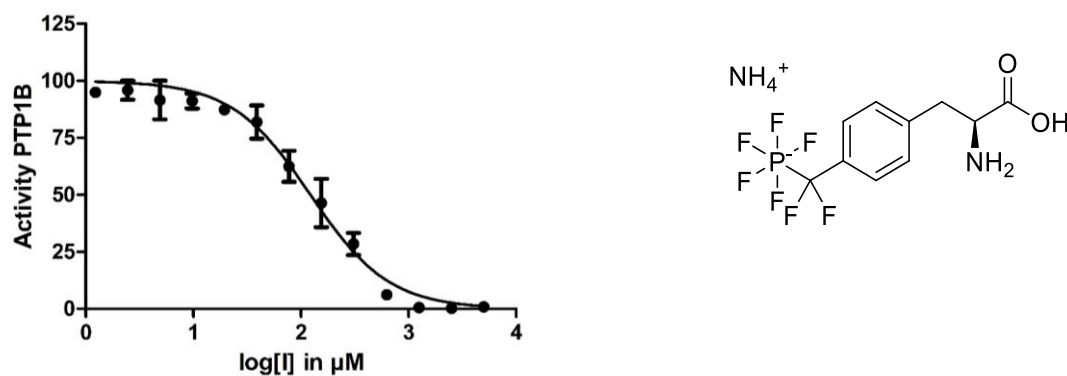


Figure 56 Inhibition of PTP1B by compound **15**, IC_{50} : $122 \pm 14 \mu\text{M}$

Results and Discussion

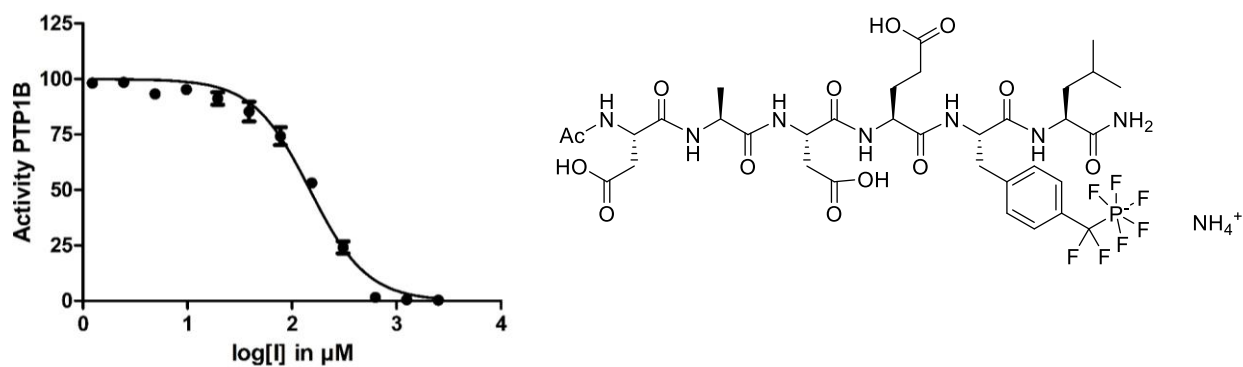


Figure 57 Inhibition of PTP1B by compound **19**, $\text{IC}_{50} = 148 \pm 12 \mu\text{M}$

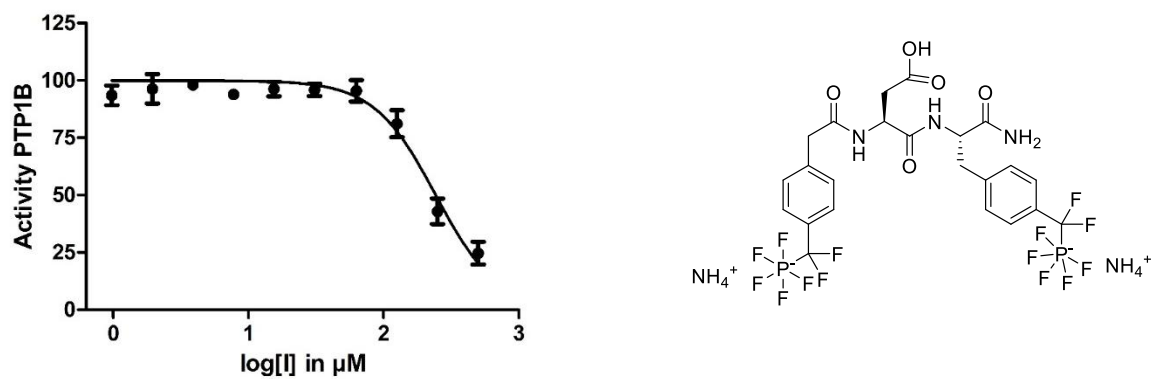


Figure 58 Inhibition of PTP1B by compound **20**, $\text{IC}_{50} = 243 \pm 23 \mu\text{M}$

4 Summary and Outlook and future perspectives

This research work started with investigating a synthetic protocol able to convert phosphonic acids into their corresponding pentafluorophosphates with mild reaction conditions.

After the successful preparation of small pentafluorinated fragments, determination of the biological activity showed encouraging *in vitro* inhibitory potential towards PTP1B. These results supported extensive investigations on the synthesis of pentafluorophosphates, which resulted in the definition of a fine-tuned telescopic reaction, where cheap reagents easily available from commercial sources are sequentially added in a single reactor to starting materials, which are conveniently accessible from robust synthetic procedures (*gem*-difluoromethylen diethyl phosphonates). The time efficient and high-yielding synthesis showed to be compatible with different functional groups and suitable for a scale-up from mg to gram amounts of material.

This, in turn, made possible the preparation of building block suitable for further investigations and collaborations, aimed to study physical properties of the pentafluorophosphate and incorporate the pentafluorinated amino acid into more complex architectures, considering that these studies required millimolar molar amount of building block.

In order to prepare peptides, both solution and solid phase peptide synthesis were studied. These efforts resulted ultimately in the development of a convenient solid phase peptide synthesis (SPPS) protocol, allowing efficient production of pentafluorinated peptides. These were then be tested against PTP1B, producing interesting data. The inhibitory potential for small fragments, as well as mono and bivalent peptides was evaluated by Dr. Stefan Wagner and Markus Tiemann. The expected increase in binding affinity from fragments to peptides was not supported by experimental data, which in fact showed an inhibitory potential with an opposite trend. Excluding the phenyl based fragment, the least active compound appears to be the one which was expected to be the most potent one: the bivalent pseudo tripeptide **20** ($IC_{50} = 243 \pm 23 \mu M$), while the most potent of the compounds tested

Summary and Outlook and future perspectives

remains the naphthyl pentafluorinated fragment **6** ($IC_{50} = 52 \pm 4 \mu M$). Reasons for this observation might be the high increase in lipophilicity of the bidentate ligand, resulting in difficulties in entering the active site (although this was not the case for the hydrophobic naphthyl fragment) or the formation of electrostatic interaction between the PF_5^- and other functional groups present in the molecule, stabilizing specific conformation, disfavoring the binding event. As shown in the introduction, the presence of fluorine offers the possibility for intramolecular H---F bonds, and this might result in precise 3D conformations of peptides which are not ideal for entering the active site. One way to prove this assumption would be the production and sequential testing of small peptide sequences with increasing length, in order to identify a correlation with the inhibition and the chain length. Another option would be the determination of the Ramachandran plot for these inhibitors, which would allow to obtain insights into the structure of peptides. Testing these inhibitors against a wider range of phosphatase would also allow to determine their selectivity, helping to validate their potential as next generation phosphomimetic inhibitors.

This project led to a number of interesting collaborations with interdisciplinary research groups. With Haocheng Qianzhu and Professor Huber from the Australian National University, the incorporation of unprotected pentafluorophosphono phenylalanine **15** into proteins was investigated: very interestingly, after screening a library of different tRNA synthetase via fluorescent activated cell sorting (FACS), they were able to produce a 26kD red fluorescent protein (RFP), which represent the first protein containing pentafluorophosphate moiety ever produced. After the identification of suitable tRNA synthetases, pentafluorinated ubiquitin was produced as well. Further experiments are currently ongoing and the results will be published elsewhere.

In a second collaboration with Dr. Waldemar Hoffmann and Prof. Pagel at FU Berlin, the previously observed lipophilicity of pentafluorinated phenylalanine **15** was measured with an innovative technique. Canonical amino acids, as well as other fluorinated amino acid and the novel pentafluorinated amino acid were analyzed with a method based on Ion Mobility Mass Spectrometry (IM-MS), where molecular aggregation in the low permittivity environment of vacuum was evaluated and correlated with their lipophilicity. Plotting these data allowed the definition of a new hydrophobicity scale for amino acids.

Summary and Outlook and future perspectives

The interpretation of the infrared spectrum was performed by Ruben Cruz and Prof. Heberle at FU Berlin, who correlated the observed vibrational bands to specific P-F stretching modes of **5**.

The 3D structure of the pentafluorinated amino acid **11** was determined by Max Rautenberg and Dr. Hemmerling via X-ray crystallography at Bundesanstalt für Materialforschung und -prüfung. This result allowed to accurately measure the distance between the atoms in the pentafluorophosphate group and compare them with published value of the phosphonate analogue, suggesting size similarity between the two.

Computational analysis was performed by Lauren Finn, Leon Wehrhan and Prof. Keller at FU Berlin. Their contribution included docking studies of **15** aimed to better understand and quantify the fluorine hydrogen interactions between the inhibitor and the active site of the phosphatase.

Summarizing, all these investigations and collaborations with different working groups were aimed to assess the potential of pentafluorophosphates as lipophilic phosphotyrosine mimetics. Analyzing the results, lipophilicity was observed and confirmed by different means but the inhibitory potential proved to be a bit more challenging to rationalize. X-ray analysis allowed to measure the distance between atoms and estimate the sterical hinderance of PF_5^- group, which appeared to be comparable in size with the known phosphonate, enforcing the phosphomimetic properties of this moiety; multiple favorable H-F interactions have been highlighted by computational studies as well. Nonetheless, the inhibitory potential was not always better, and in certain cases was surprisingly lower. The production of more fragments, different peptides with increasing size and expanding the biological target to other phosphatases would allow deeper studies on this moiety and a better understanding of their inhibitory potential.

Furthermore, the conversion of *gem*-difluoromethylen phosphonate to pentafluorinated group can be investigated for the serine analogue, which should be feasible with the proposed method. This would enable a new very interesting and potentially important chapter of studies. In addition to the evaluation of such building block as phosphoserine mimetic inhibitor, pentafluorophosphono serine can be used to further expand the biological potential of pentafluorophosphates as ligands for

Summary and Outlook and future perspectives

sphingosine-1-phosphate receptor (S1PR), which plays a relevant role in the recruitment of lymphocytes and is one of the biomarkers of yet incurable disease as multiple sclerosis (MS).

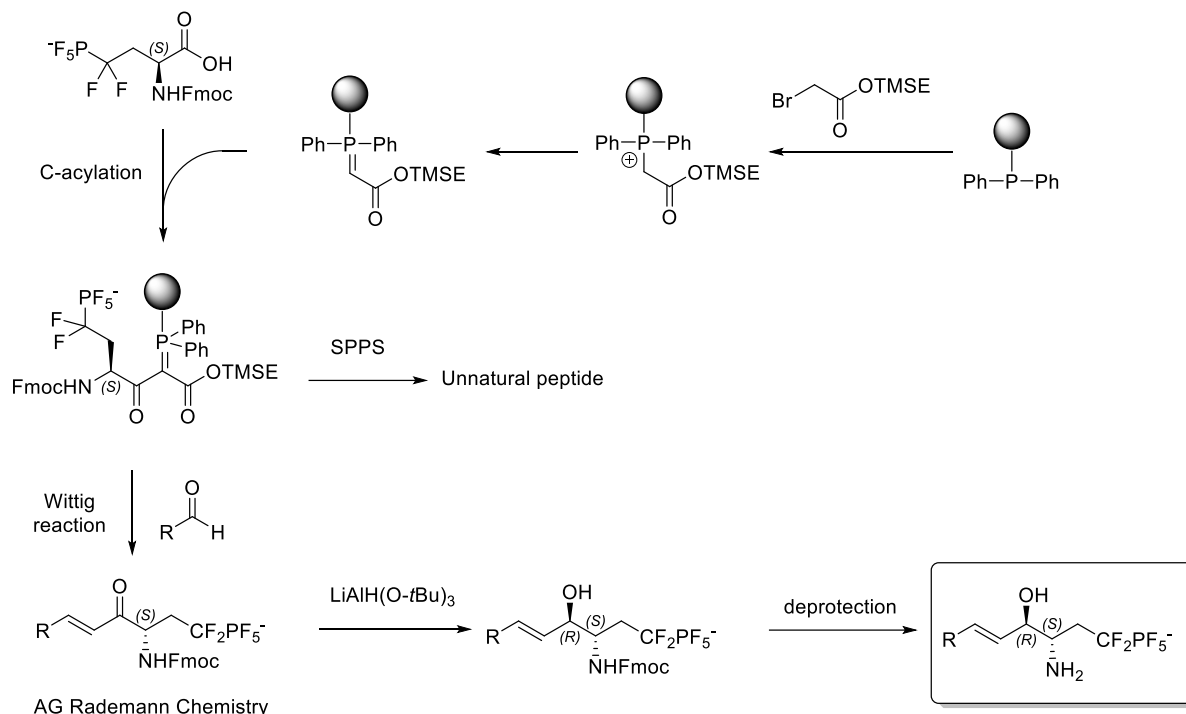


Figure 59: Proposed synthetic pathway to pentafluorinated phosphoserine peptide mimetics and analogue of sphingosine-1-phosphate (S1P) targeting the S1P Receptor, based on a methodology previously developed in the Rademann group^[182]

By developing a convenient synthetic method, this research work paved the road to future investigations on pentafluorinated molecules. The chemical stability observed in aryl *gem*difluoromethylen pentafluorophosphates as well as in the perfluoroalkyl pentafluorophosphates reported in the literature should not change substantially in the case of pentafluorinated serine analogues. If confirmed experimentally, this would represent a very interesting and promising field of studies.

5 Zusammenfassung und Ausblick

Die vorliegende Arbeit begann mit der Untersuchung milder Darstellungsmethoden von Pentafluorosphaten aus Phosphorsäuren.

Nach der erfolgreichen Darstellung kleiner pentafluorierter Bausteine zeigten erste Untersuchungen der biologischen Aktivität *in vitro* vielversprechendes inhibitorisches Potential gegen PTP1B. Diese Ergebnisse wurden unterstützt durch ausgiebige Untersuchungen der Pentafluorophosphat Syntheseroute, welche in einer robusten Mehrstufensequenz aus gut erhältlichen Edukten resultierten. Diese funktionsgruppentolerante Synthesestrategie lieferte im Gramm-Maßstab die Pentafluorophosphate in hohen Ausbeuten mit geringem Zeitaufwand.

Die auf diese Weise etablierte Route erlaubte die Darstellung von Synthesebausteinen für weiterführende Untersuchungen und Kollaborationen zur Erforschung der physikalischen Eigenschaften der Pentafluorophosphate, sowie den Einbau pentafluorierter Aminosäuren in komplexere synthetische Architektur.

Zur Verwendung in der Peptidsynthese wurden Syntheseprotokolle in Lösung und via Festphasensynthese untersucht. Daraus ging ein Festphasen-Syntheseprotokoll hervor für die effiziente Darstellung pentafluorierter Peptide, welche anschließend auf ihre Aktivität gegen PTP1B getestet wurden. Das inhibitorische Potential kleiner Fragmente, mono- und bivalenter Peptide wurde von Dr. Stefan Wagner und Markus Tiemann untersucht. Die erwartete gesteigerte Bindungsaffinität von kleinen Fragmenten hin zu Peptiden wurde dabei nicht festgestellt. Im Gegenteil, wurde mit Ausnahme des Phenylbasierten Bausteins (**5** und **6**) eine Abnahme der Bindungsaffinität für diejenigen Bausteine gefunden, bei denen die höchste Aktivität erwartet wurde. Während für das bivalente Pseudotripeptid **20** ($IC_{50} = 243 \pm 23 \mu M$) die höchste Aktivität erwartet und die Geringste gefunden wurde, war die potenteste getestete Verbindung das Naphthylderivat **6** ($IC_{50} = 52 \pm 4 \mu M$). Eine mögliche Ursache dieser beobachteten Trends könnte die stark erhöhte Lipophilie der Liganden sein, die den Zugang zum aktiven Zentrum erschwert (auch wenn dies für den hydrophobischen Naphthylrest nicht der Fall war). Darüber hinaus könnten elektrostatische Wechselwirkungen zwischen dem Pentafluorophosphat und weiteren

Zusammenfassung und Ausblick

im Molekül vorhandenen funktionellen Gruppen unproduktive Konformationen stabilisieren und die Bindungsaffinität herabsetzen.

Wie bereits in der Einleitung erwähnt wurde, erlaubt die Gegenwart von Fluor die Ausbildung von intramolekularen H-F Brücken, was dreidimensionale Faltungen der Peptide zur Folge haben kann, welche nicht geeignet sind um das aktive Zentrum zu erreichen. Ein Weg, diese Hypothese zu prüfen, wäre die Herstellung und sequenzielle Prüfung kleiner Peptidbausteine mit zunehmender Größe, um Korrelationen zwischen Inhibition und bestimmten Kettenlängen zu identifizieren. Eine Alternative wäre die Bestimmung des Ramachandran Plots für diese Inhibitoren, was einen Einblick in deren Peptidstruktur erlauben würde. Die Inhibitoren gegen eine Vielzahl von Phosphatasen zu testen, würde zudem ermöglichen, ihre Selektivität zu bestimmen und dadurch helfen, ihr Potential als neue Phosphonatmimetika Inhibitoren zu bewerten.

Dieses Projekt führte zu einer Reihe von Kollaborationen mit interdisziplinären Forschungsgruppen. Mit Haocheng Qianzhu und Prof. Huber von der Australian National University wurde der Einbau von ungeschütztem Pentafluorphosphonophenylalanin **15** in Proteine untersucht. Von besonderem Interesse war dabei, dass nach dem Screenen einer Datenbank verschiedener tRNA Synthetase via fluoreszenzmarkierter Durchflusszytometrie (FACS) ein 26kD rotes Fluoreszenz Protein (RFP) erhalten werden konnte, dass das erste pentafluorophosphat-beinhaltende Protein darstellt. Nachdem geeignete tRNA Synthetasen ermittelt werden konnten, wurde zudem pentafluoriertes Ubiquitin hergestellt. Weitergehende Untersuchungen daran laufen momentan und werden andernorts publiziert.

In einer weiteren Zusammenarbeit mit Dr. Waldemar Hoffmann und Prof. Pagel an der FU Berlin wurde die zuvor beobachtete Lipophilie des pentafluorierten Phenylalanins **15** mit einer innovativen Technik untersucht. Kanonische Aminosäuren, fluorierte und neue, pentafluorierte Derivate wurden mit einer Methode basierend auf Ionenmobilitäts Massenspektrometrie (IM-MS) analysiert, bei welcher molekulare Aggregationen im schlecht leitenden Hochvakuum bewertet und mit ihrer Lipophilie in Relation gesetzt wurden. Durch das grafische Auftragen dieser Daten gelang es, eine neue Skala der Hydrophobie von Aminosäuren zu definieren.

Zusammenfassung und Ausblick

Die Interpretation der Infrarotspektren wurde von Ruben Cruz und Prof. Heberle an der FU Berlin durchgeführt, die die beobachteten Vibrationsbanden mit spezifischen P-F Streckschwingungen von **5** in Verbindung brachten.

Die Kristallstruktur der pentafluorierten Aminosäure **11** wurde bestimmt von Max Rautenberg und Dr. Hemmerling durch Röntgenstrukturbestimmung in der Bundesanstalt für Materialforschung und -prüfung. Die Ergebnisse erlaubten es, die Distanz der Atome in der Pentafluorophosphatgruppe zu bestimmen und mit Literaturwerten analoger Phosphonate zu vergleichen und ähnliche Größenordnungen festzustellen.

Quantenchemische Berechnungen wurden durchgeführt von Lauren Finn, Leon Wehrhan und Prof. Keller an der FU Berlin. Ihre Beiträge beinhalten Andockstudien für **15** um die Fluor-Wasserstoff Interaktionen zwischen Inhibitor und der Phosphatase besser zu verstehen und zu quantifizieren.

Zusammenfassend zielten alle Untersuchungen und Kollaborationen darauf ab, das Potential von Pentafluorophosphaten als lipophile Phosphonattyrosin-Mimetika zu ergründen. Die gewünschte Lipophilie wurde beobachtet und durch verschiedene Messmethoden bestätigt, das inhibitorische Potential ließ sich jedoch nur schwer erfassen. Einkristallmessungen erlaubten es, neben der Bestimmung der Bindungslängen, auch die sterische Hinderung der PF_5^- Substituenten abzuschätzen, die vergleichbar mit den bekannten Phosphonaten ist und die phosphormimetischen Eigenschaften dieser Substituenten unterstreicht. Zudem haben quantenmechanische Berechnungen zahlreiche H-F Wechselwirkungen hervorgehoben. Das inhibitorische Potential der pentafluorierten Verbindungen war jedoch nicht immer besser als das der Phosphonate, in einigen Fällen war es sogar überraschend geringer. Die Synthese von mehr Fragmenten, Peptiden mit zunehmender Größe und eine Erweiterung der zu untersuchenden Ziele auf weitere Phosphatasen würde ein besseres Verständnis dieser Substanzklasse und ihres inhibitorischen Potentials erlauben.

Darüber hinaus könnte die Synthese von pentafluorierten Spezies aus gem Difluormethylenphosphonaten für Serinanaloga untersucht werden, welche mit der hier beschriebenen Methodik ebenfalls möglich sein sollte. Zusätzlich zur Bewertung derartiger Bausteine als Phosphonatserinmimetikinhibitor, könnte das

Zusammenfassung und Ausblick

Pentafluorophosphonat von Serin genutzt werden, um das biologische Potential von Pentafluorophosphaten als Liganden für Sphingosin-1-phosphat Rezeptoren (S1PR) zu erweitern, die eine wichtige Rolle im Aufbau der Lymphozyten spielen und ein Typ der Biomarker bisher noch unheilbarer Krankheiten wie Multiple Sklerose (MS) darstellen.

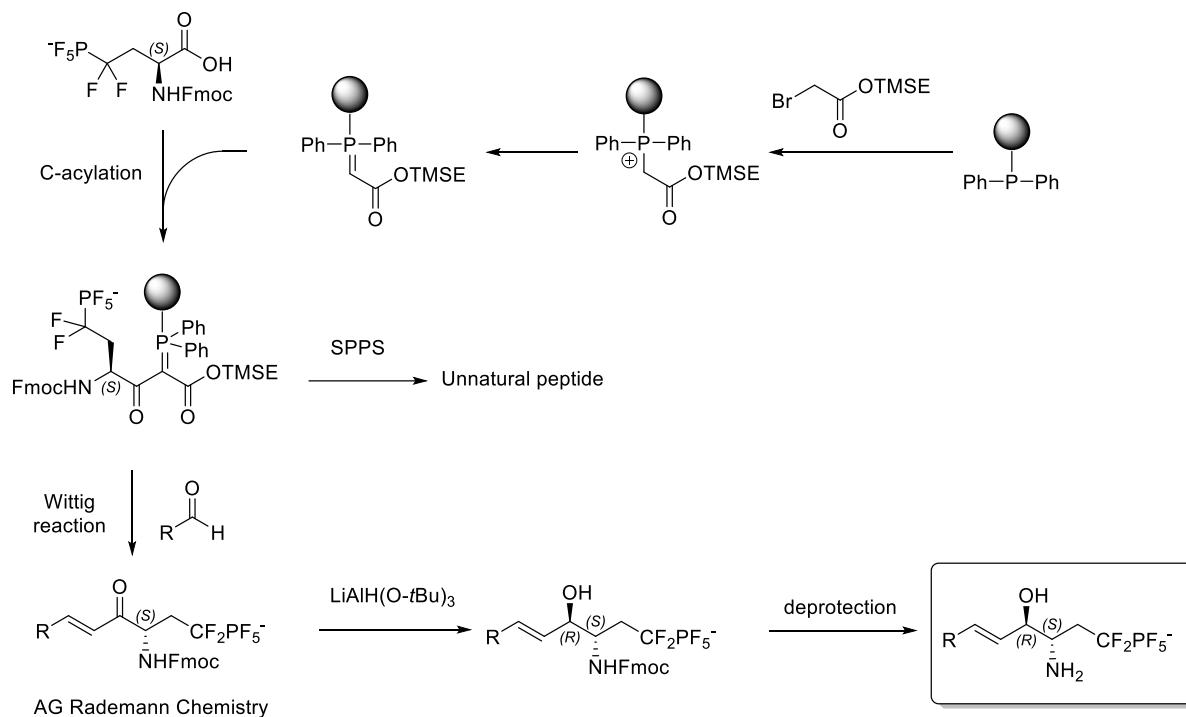


Abbildung 60: Vorgeschlagener Syntheseweg für pentafluorierte Phosphoserin Peptidmimetika und Sphingosin-1-phosphat (S1P), welche den S1P Rezeptor adressieren, basierend auf bereits im Arbeitskreis Redemann entwickelter Methodik

Durch die Entwicklung einer geeigneten Syntheseroute hat die vorliegende Arbeit den Weg bereitet für zukünftige Untersuchungen pentafluorierter Moleküle. Die chemische Stabilität, die für Aryl gem difluormethylierte Pentafluorophosphate und für perfluoralkyl Pentafluorophosphate in der Literatur berichtet wurde, sollte nicht wesentlich abweichen im Falle der pentafluorierten Serinanaloga. Sollte sich dies experimentell bestätigen, würde es ein sehr interessantes und vielversprechendes Forschungsfeld repräsentieren.

6 Experimental Part

6.1 Materials and methods

All moisture sensitive reactions were performed in glassware that was previously vacuum heat dried and flushed with Ar or N₂ using Schlenk technology.

Cadmium powder was activated with HCl (1N) until a metallic shine was observed, washed with H₂O and acetone, dried at high vacuum and stored under inert atmosphere.

NMe₄F was bought as the tetrahydrate from Sigma Aldrich and dried as described in literature ^[183] Accordingly, the reagent was dissolved in dry MeOH. The solution was concentrated to a syrup at the rotary evaporator, re-dissolved 4 times in dry MeOH and concentrated again. Subsequently, the residue was heated at 130 °C for 3 d at high vacuum. The obtained white powder was stored and handled under inert argon atmosphere.

All other chemicals were purchased from Sigma (Merck), ABCR and Fluka and were used without any further purification.

DMF and ACN for the pentafluorination reaction were bought as anhydrous and stored over activated molecular sieves 4A. All other dry solvents were obtained from a column-based solvent system (MBraun, MB-SPS-800).

Removal of volatile components was performed using rotary evaporators from Heidolph with a hot bath of 40 °C, if not otherwise stated. The high vacuum obtained with an oil pump corresponded to 1 µbar or less. Lyophilized fractions were obtained from Christ Alpha 2-4 LD.

Product isolation was conducted on Biotage, IsoleraTM Spektra equipped with KP-Sil or RP-C18 SNAP Cartridges with appropriate HPLC grade solvent mixtures and deionized water, or with HPLC (Agilent Technologies, 1260 series, column Macherey-Nagel, Nucleodur 5 µm C18, 150 x 32 mm, equipped with Agilent 1260 Infinite diode array and multiple wavelength detector and fraction collector).

Experimental Part

Melting points were measured with Büchi Melting point apparatus B-545.

Thin Layer Chromatography analyses were conducted on Merck Aluminum sheets pre-coated with silica gel (Merck, 60 F₂₅₄). Detection was carried out using 254 nm UV-Light, followed by dipping in ceric ammonium molybdate or ninhydrin stains.

The optical rotation was determined using IBZ Messtechnik Polar L μ P (quartz cuvette, optic path 1 cm).

NMR spectra were measured on the following spectrometers: JEOL *ECX400* (9.39 T), JEOL *ECP500* (11.74 T), JEOL *ECZ600* (14.09 T), Bruker Avance III 700 (16.44 T). Chemical shifts (δ) are reported in ppm and coupling constants (J) are given in Hz. ¹H and ¹³C chemical shifts were referenced to the solvent peaks. ¹³C and ³¹P NMR spectra were hydrogen decoupled. Chemical shifts are given in ppm relative to the signal of the used deuterated solvent as internal standard.

MS data were recorded with analytical HPLC-MS from Agilent (1100 Series) equipped with column Luna, 3 μ m C18 100 Å, 100 x 4.6 mm coupled with a ESI single quad spectrometer LCMSD from Agilent.

ESI high resolution mass spectra were recorded with an HPLC system (Agilent Technologies, Infinity II 1290) equipped with Zorbax Eclipse plus C-18 RRHD (2.1 x 50 mm, 1.8 μ m, 95 Å) column, coupled with an ESI-Q-TOF iFunnel mass spectrometer (Agilent Technologies, 6550).

General method of peptide synthesis

Peptide synthesis was conducted using Fmoc-strategy on Rink amide resin 13 from Merck (loading 0.34 mmol/g, 100-200 mesh, 1% divinyl-benzene/polystyrene). PP-PE syringes equipped with a PE-frit were used as reaction vessels.

Coupling of amino acids

N-Fmoc-protected amino acids with suitable side chain protection (5 equiv. with respect to the loading of the resin) were coupled with HOBt (5 equiv.) and DIC (5 equiv.) in a minimal amount of DMF. In the improved protocol, these coupling reagents have been substituted with TBTU (4.9 equiv.), HOBt (5 equiv.) and DIPEA (10 equiv.) in a minimal volume of DMF, added to a pre-swelled resin in DMF. The

Experimental Part

solution was added to the resin pre-swollen in DMF and shaken until completion of the reaction.

The coupling reactions were monitored using the Kaiser test. Coupling effectiveness was quantified via UV-photometric determination of the dibenzofulvene product following to Fmoc cleavage with the following equation:

$$x = \frac{10^5 \cdot E_{\lambda}}{\epsilon_{\lambda} \cdot m_{resin}}$$

x = Loading resin [mmol/g]

ϵ_{λ} = molar extinction coefficient

E_{λ} = Extinction

m_{resin} = mass resin [mg]

$\epsilon_{\lambda 301} = 7800$ l/mol cm

The resin was carefully vacuum dried prior to the Fmoc determination

Washing of the resin

The resin was washed after every coupling and cleavage procedure with 5 syringe volumes of DMF, THF and DCM.

Fmoc cleavage

The Fmoc-group was cleaved by using a mixture of piperidine (20%) in DMF for 20 minutes. After adding the basic cocktail to the resin, the syringe was shaken for 20 minutes and then washed. The cleavage procedure was repeated twice.

End capping of peptide

Before capping, the resin was pre swelled in DMF (2 mL / 100 g of resin). The peptide N-Terminus was capped with an acetic anhydride/pyridine mixture (1:1, 1 mL/200 mg of resin) for 1 hours at RT.

Acidic peptide cleavage

The vacuum-dried resin was treated with Olah's reagent (pyridinium polyhydrogen fluoride) + 10% anisole for 1 hour at RT. The volatile components were removed at high vacuum on a Schlenk line connected to a first trap, loaded with CaO, and then to a second trap cooled with liquid nitrogen. The beads were washed with small portions of THF, THF/ H₂O (1:1) and ACN and the merged washings were neutralized with an aqueous saturated solution of ammonium bicarbonate. The

Experimental Part

mixture was then concentrated to a minimum at the rotary evaporator and the residue was purified at RP MPLC on c18 column with a gradient of ACN / H₂O 10mM NH₄HCO₃ (1 to 100%). Collected fractions were analyzed with LCMS and lyophilized.

Activity determination against PTP1B

para-Nitrophenyl phosphate assay: The phosphatase PTP1B was used as its catalytic domain (amino acid 1 to 321), which was expressed in Escherichia coli Rosetta (DE3) and gratefully provided by Dr. Anja Schütz (Group Prof. Heinemann, MDC Berlin). Stock solutions (10 mM) of the tested substrate mimetics were prepared in H₂O/DMSO (50:50, v / v) and were diluted serially on a microtiter plate (Corning 3544 or 3711) with buffer solution (10 µL). Buffer solution was added (6 µL) followed by the enzyme solution (~ 500 nM, 2 µL) and incubation for 30 min. The assay was started by the addition of pNPP-solution (13 mM in buffer or H₂O, 4 µL). Shaking and centrifugation was performed after every step. The final concentration of PTP1B was ~ 50 nM, the concentration of the enzyme stock solution was determined by photometry.

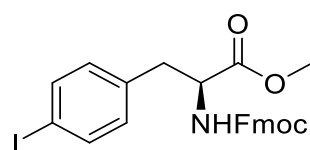
DiFMUP assay: Recombinant human PTP1B was obtained from Abcam (ab51277) at a concentration of 100 µM and used as received, without further purification. An enzymatic 6,8-difluoro-4-methylumbelliferyl phosphate (DiFMUP) assay was used to determine the activity against PTP1B. Test compounds were dissolved in buffer or in dimethyl sulfoxide (DMSO) at a concentration of 20 or 100 mM, and the assay was carried out at a final DMSO concentration 2.5%. The DiFMUP assay buffer contained a final concentration of 50 mM MOPSO (pH 6.5), 200 mM NaCl, 0.03 %Tween-20, 50 µM Tris-(2-carboxyethyl)-phosphin (TCEP) (freshly added prior to each measurement) and 1.5 nM/L SHP2 (final concentration). The final assay volume was 20 µL. Enzyme and test compound in buffer solution were incubated for 30 min at RT. The reaction was started by adding DiFMUP to a final concentration of 67 µM. This substrate concentration matches the experimentally determined K_M value of the enzyme. Measurements were performed on a Genius Pro Reader (SAFIRE II) with the following settings: measurement mode: Fluorescence Top; λ_{ex}: 360 nm (bandwidth 20 nm); λ_{em}: 460 nm (bandwidth 20 nm) ; gain (manual): 60; number of scans: 8; FlashMode: high sensitivity; integration time: 40 µs; lag time: 0 µs; Z-position (manual): 13900 µM; number of kinetic cycles 10; kinetic interval: 60 s; total

Experimental Part

kinetic run time 10 min. Measurements were performed in triplicate. IC_{50} values were calculated with Prism 5 (for Windows, Version 5.01, GraphPad Software Inc.) and were converted into the corresponding K_i values applying the Cheng Prusoff equation.^[184]

6.2 Chemical Synthesis

Methyl N-(fluorenyl-9H-methoxy-carbonyl)-4-iodo-L-phenylalanine **7a**



Fmoc-4-I-Phe-OH (from ABCR, 2988 mg, 10.26 mmol, 1 equiv.) was dissolved in dry MeOH (25 ml) in a heat- and vacuum-dried Schlenk flask under Ar atmosphere. 3 drops of dry DMF were added and the solution was cooled to 0 °C. Oxalyl chloride (2.6 ml, 30.795 mmol, 3 equiv.) was added dropwise under stirring and the reaction was allowed to reach RT for 16 h. The amber solution was then concentrated using a rotary evaporator, diluted with EtOAc and washed with H₂O, saturated NaHCO₃ solution, and brine. The organic layer was dried over Na₂SO₄, filtrated and concentrated in vacuo. Product **7a** (4717 mg, 92%) was obtained as white solid.

$R_f = 0.3$ (EtOAc/Hex, 20%)

¹H NMR (500 MHz, CDCl₃) $\delta = 7.77$ (d, $J=7.6$, 2H, Ar-H), 7.60 (d, $J=8.1$, 2H, Ar-H), $7.61 - 7.51$ (m, 2H, Ar-H), 7.41 (t, $J=7.4$, 2H, Ar-H), 7.32 (t, $J=7.5$, 2H, Ar-H), 6.81 (d, $J=8.1$, 2H, Ar-H), 5.24 (d, $J=7.9$, 1H, NH), 4.64 (q, $J=5.9$, 1H, α -H-Phe), 4.47 (dd, $J=10.5$, 7.2 , 1H, CH_{2 α} -Fmoc), 4.37 (dd, $J=10.4$, 6.9 , 1H, CH_{2 β} -Fmoc), 4.20 (t, $J=6.7$, 1H, CH-Fmoc), 3.73 (s, 3H, OMe), 3.09 (dd, $J=13.9$, 5.6 , 1H, CH_{2 α} -Phe), 3.02 (dd, $J=13.9$, 5.7 , 1H, CH_{2 β} -Phe)

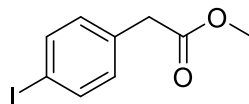
¹³C NMR (126 MHz, CDCl₃) $\delta = 171.7$ (O=C-methyl ester), 155.6 (O=C-Fmoc), 143.9 , 143.8 , 141.5 , 141.4 , 137.8 , 135.5 , 131.4 , 127.9 , 127.2 , 120.1 (17 x Ar-C), 92.8 (C-I), 67.0 (CH₂-Fmoc), 54.6 (CHN), 52.6 (OCH₃), 47.3 (CH-Fmoc), 37.8 (CH₂Phe)

Experimental Part

HRMS (ESI): $[M+H]^+$ calculated for $C_{25}H_{23}INO_4^+$: 528.06663 Da; found: 528.06571 m/z; $[M+Na]^+$ calculated for $C_{25}H_{22}INNaO_4^+$: 550.04857 Da; found: 550.04790 m/z

Spectral data were consistent with published values^[185]

Methyl 4-iodophenylacetate **7b**



4-Iodophenylacetic acid (from ABCR, 5 g, 19.1 mmol, 1 equiv.) was dissolved in dry MeOH (25 ml) in a heat- and vacuum-dried Schlenk flask under Ar atmosphere. 3 drops of dry DMF were added and the solution was cooled to 0 °C. Oxalyl chloride (3.27 ml, 38.2 mmol, 2 equiv.) was added dropwise under stirring and the reaction was allowed to reach RT for 16 h. The amber solution was then concentrated using a rotary evaporator, diluted with EtOAc and washed with H₂O, saturated NaHCO₃ solution, and brine. The organic layer was dried over Na₂SO₄, filtrated and concentrated in vacuo. The crude was purified via column chromatography at MPLC (SiO₂, EtOAc / Hex, 5 to 100%); product **7b** (3.7 g, 70%) was obtained as a colorless oil.

¹H NMR (500 MHz, CDCl₃) δ = 7.64 (d, J=8.4, 2H, Ar-H), 7.02 (d, J=8.5, 2H, Ar-H), 3.69 (s, 3H, OMe), 3.56 (s, 2H, CH₂)

¹³C NMR (126 MHz, CDCl₃) δ = 171.54 (C=O), 137.76, 133.66, 131.37, (Ar-C), 92.73 (C-I), 52.25 (OMe), 40.73 (CH₂Phe)

HRMS (ESI): $[M+H]^+$ calculated for $C_9H_{10}IO_2^+$: 276.97200 Da, found: 276.97089 m/z; $[M+Na]^+$ calculated for $C_9H_9INaO_2^+$: 298.95394 Da, found: 298.95356 m/z

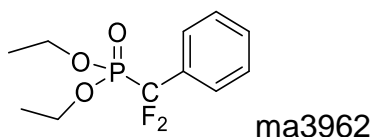
Spectral data were consistent with published value.^[72]

Experimental Part

General procedure for CuBr mediated organo cadmium coupling

A heat - vacuum dried Schlenk flask was charged with previously activated and dried metallic Cadmium (6 equiv.) and dry DMF (4 mL/g of Cd). To the stirred suspension, diethyl bromophosphonate (3.33 equiv.) was added dropwise gently heating the reaction flask. The slightly exothermic reaction was stirred for 3 hours. In another flask, previously dried iodoarene (1 equiv.) was dissolved in dry DMF (1M) and CuBr (3 equiv.) was added. The organocadmium compound was added slowly and dropwise to this stirred mixture under inert atmosphere and the reaction mixture was stirred for 16 hours. After addition of EtOAc (Et₂O in the case of phenyl iodide), the precipitate was filtrated on a bed of Celite and washed with sat. aq. sol. NH₄Cl (3x) and brine. The organic layer was dried over Na₂SO₄, filtrated and concentrated at reduced pressure.

Diethyl difluoro-(phenyl)-methyl phosphonate 1



Iodobenzene	200 mg	0.98 mmol
Cd	661 mg	5.88 mmol
Bromophosphonate	575 μ L	3.24 mmol
CuBr	422 mg	2.94 mmol
DMF	5 mL	

After purification of the crude via chromatography (SiO₂, EtOAc/Hex, 10% to 20%), the product (218 mg, 84%) was isolated as a colorless oil.

R_f = 0.1 (EtOAc/Hex 20%)

¹H NMR (600 MHz, Chloroform-*d*) δ = 7.61 (d, *J*=7.6, 2H, Ar-H), 7.49 – 7.40 (m, 2H, Ar-H), 4.22 – 4.08 (m, 4H, 2xCH₂), 1.29 (t, *J*=7.1, 6H, 2xCH₃)

¹³C NMR (151 MHz, Chloroform-*d*) δ = 132.7 (td, *J*=21.9, 13.7, Ar-C), 131.4 (s, Ar-C), 130.8 (q, *J*=2.1, Ar-C), 128.5 (d, *J*=1.7, Ar-C), 126.3 (td, *J*=6.9, 2.4, Ar-C), 118.6 (dt, *J*=263.2, 218.1, CF₂), 64.85, 64.81 (s, 2x OCH₂), 16.40, 16.36 (s, 2x OCH₂CH₃)

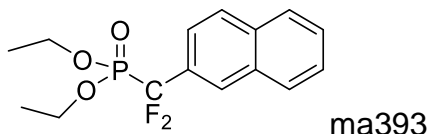
Experimental Part

¹⁹F NMR (565 MHz, Chloroform-*d*) δ = -108.3 (d, $J=116.1$, CF₂)

³¹P NMR (243 MHz, Chloroform-*d*) δ = 7.0 (t, $J=116.5$)

HRMS (ESI): [M+H]⁺ calculated for C₁₁H₁₆F₂O₃P⁺: 265.0800 Da, found: 265.0804 m/z;

Diethyl difluoro-(naphthyl)-methyl phosphonate 2



Iodonaphthalene	1000 mg	3.95 mmol
Cd	2665 mg	23.7 mmol
Bromophosphonate	2320 μ L	13.0 mmol
CuBr	1700 mg	11.85 mmol
DMF	10 mL	

After purification of the crude via chromatography (SiO₂, EtOAc/Hex 10% to 25%), the product (1128 mg, 91%) was isolated as a pale amber oil.

R_f = 0.25 (EtOAc/Hex 1:4)

¹H NMR (600 MHz, Chloroform-*d*) δ = 8.13, 7.91 (d, $J=8.4$), 7.87 (d, $J=7.7$), 7.68 (d, $J=8.7$), 7.60 – 7.48 (m, 11x Ar-H), 4.27 – 4.09 (m, 4H, 2xCH₂), 1.30 (t, $J=7.1$, 6H, 2xCH₃)

¹³C NMR ¹³C NMR (151 MHz, Chloroform-*d*) δ = 134.26, 132.50, 128.87, 128.48, 127.85, 127.66, 126.85, 126.63, 122.82, 119.07, 117.62 (s, 11X Ar-C), 64.9 (d, J = 6.8), 16.4 (d, J = 5.5)

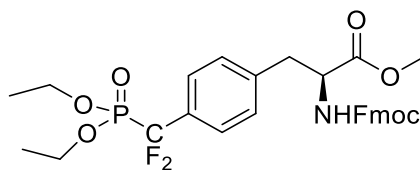
¹⁹F NMR (565 MHz, Chloroform-*d*) δ = -107.70 (d, $J=116.3$)

³¹P NMR (243 MHz, Chloroform-*d*) δ = 7.05 (t, $J=116.3$)

HRMS (ESI): [M+H]⁺ calculated for C₁₅H₁₈F₂O₃P⁺: 315.0956 Da, found: 315.0951 m/z;

Experimental Part

Methyl N-(fluorenyl-9H-methoxy-carbonyl)-4-(diethoxyphosphoryl-difluoromethyl)-L-phenylalanine **8**



7a	2.016 g	3.82 mmol
Cd	2.578 g	22.94 mmol
Bromophosphonate	2.261 mL	12.73 mmol
CuBr	1.645 g	11.47 mmol
DMF	6 mL	

After purification of the crude via chromatography (SiO₂, EtOAc / Hex 1:4 then 1:2), the product (2.256 g, 99%) was isolated as a colorless oil.

$R_f = 0.3$ (EtOAc/Hex, 50%)

¹H NMR (600 MHz, Chloroform-*d*) $\delta = 7.75$ (d, $J=7.5$, 2H, 2 x Ar-H), 7.54 (dd, $J=14.7$, 7.7, 4H, 2 x Ar-H), 7.38 (t, $J=7.4$, 2H, 2 x Ar-H), 7.30 (t, $J=7.5$, 2H, 2 x Ar-H), 7.17 (d, $J=7.9$, 2H, 2 x Ar-H), 5.31 (d, $J=8.2$, 1H, NH), 4.66 (q, $J=6.0$, 1H, α -H-Phe), 4.43 (dd, $J=10.6$, 7.2, 1H, CH₂-Fmoc), 4.36 (dd, $J=10.8$, 7.0, 1H, CH₂-Fmoc), 4.23 – 4.05 (m, 5H, 2xCH₂-ethyl, CH-Fmoc), 3.70 (s, 3H, OMe), 3.17 (dd, $J=13.9$, 5.8, 1H, CH₂-Phe), 3.11 (dd, $J=13.9$, 6.1, 1H, CH₂-Phe), 1.28 (t, $J=7.1$, 6H, CH₃-Et)

¹³C NMR (151 MHz, Chloroform-*d*) $\delta = 171.67$ (O=C-OMe), 155.61 (O=C-Fmoc), 143.87, 143.75, 141.41, 138.99, 131.54 (td, $J=22.2$, 14.0), 129.50, 127.84, 127.16, 126.58 (t, $J=7.6$), 125.7, 125.14, 120.08 (d, $J=3.2$, 18 x Ar-C), 117.21 (dd, $J=262.5$, 218.4, CF₂), 67.02 (CH₂-Fmoc), 64.88 (dd, $J=6.8$, 1.3, 2 x CH₂ Et), 54.72 (CHN), 52.52 (OCH₃), 47.23 (CH-Fmoc), 38.05 (CH₂Phe), 16.40 (d, $J=5.5$, 2 x CH₃ Et)

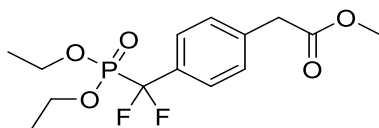
¹⁹F NMR (376 MHz, Chloroform-*d*) $\delta = -108.18$ (d, $J=116.0$)

³¹P NMR (162 MHz, Chloroform-*d*) $\delta = 6.94$ (t, $J=116.1$)

HRMS (ESI): M + H]⁺ calculated for C₃₀H₃₃F₂NO₇P⁺: 588.1957 Da, found 588.1932 m/z; [M+Na]⁺ calculated for C₃₀H₃₂F₂NNaO₇P⁺: 610.1777 Da, found: 610.1765 m/z; [M+K]⁺ calculated for C₃₀H₃₂F₂KNO₇P⁺: 626.1516, found: 626.1493 m/z

Spectral data were consistent with published values^[186]

Methyl 4-(diethyl-phosphonato-difluoromethyl)-phenylacetate 9



7b	750 mg	2.72 mmol
Cd	1832 mg	16.9 mmol
Bromophosphonate	1.595 mL	8.965 mmol
CuBr	1169 mg	8.150 mmol
DMF	8 mL	

After purification of the crude via chromatography (SiO₂, EtOAc / Hex 5 to 100%), the product (836 mg, >99%) was isolated as a colorless oil.

$R_f = 0.4$ (50% EtOAc/hexane)

¹H NMR (500 MHz, Chloroform-*d*) $\delta = 7.57$ (d, $J=7.9$, 2H, Ar-H), 7.37 (d, $J=8.3$, 2H, Ar-H), 4.21 – 4.09 (m, 4H, OCH₂CH₃), 3.69 (s, 3H, OMe), 3.66 (s, 2H, CH₂), 1.30 (t, $J=7.1$, 6H, CH₂CH₃)

¹³C NMR (126 MHz, Chloroform-*d*) $\delta = 171.43$ (C=O), 136.91 (Ar-C), 131.64 (Ar-C), 129.48 (Ar-C), 129.47 (Ar-C), 126.58 (Ar-C), 118.97 (CF₂), 64.88 (2x CH₂ ethyl), 52.25 (OMe), 41.01 (CH₂), 16.43 (2x CH₃ ethyl)

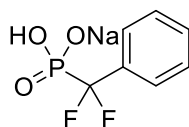
¹⁹F NMR (471 MHz, Chloroform-*d*) $\delta = -108.14$ (d, $J=116.5$)

³¹P NMR (202 MHz, Chloroform-*d*) $\delta = 6.92$ (d, $J=234.3$)

HRMS (ESI): [M+H]⁺ calculated for C₁₄H₂₀F₂O₅P⁺: 337.10109 Da, found: 337.10247 m/z; [M+Na]⁺ calculated for C₁₄H₁₉F₂NaO₅P⁺: 359.08304 Da, found: 359.08386 m/z

Spectral data were consistent with published values^[72]

Difluoro-(phenyl)-methyl-phosphonic acid **3**



The ethyl phosphonate (1429 mg, 5.43 mmol, 1 equiv.) was dissolved in dry DCM (5 mL) and the mixture was cooled to 0°C. TMSBr (10 mL, 81.45 mmol, 15 equiv.) was added dropwise under inert atmosphere. The reaction was stirred and left to reach RT overnight. Volatile components were removed at reduced pressure, the residue was redissolved in a 10% mixture of H₂O in MeOH, Amberlite Na⁺ IR 140 resin (2 g / mmol) was added and stirred overnight. After filtration of the resin beads and lyophilization, 1226 mg (98%) of the desired sodium salt were obtained as a white solid.

Melting Point: (sodium form) > 300 °C

¹H NMR (400 MHz, DMSO-*d*₆) δ = 7.47 (q, *J*=8.0, 7.2, 4H)

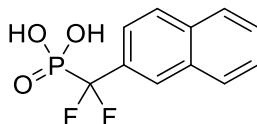
¹³C NMR (101 MHz, DMSO-*d*₆) δ = 130.7, 128.7, 126.6

¹⁹F NMR (376 MHz, DMSO-*d*₆) δ = -107.42 (d, *J*=107.0)

³¹P NMR (162 MHz, DMSO-*d*₆) δ = 3.90 (t, *J*=107.1)

HRMS (ESI): [M+H]⁺ calculated for C₇H₈F₂O₃P⁺: 209.01736 Da, found: 209.01738 m/z

Difluoro-(naphth-2-yl)-methyl-phosphonic acid **4**



Diethyl difluoro(naphth-2-yl)-methyl-phosphonate **3** (109 mg, 0.347 mmol) was dissolved in dry ACN (1 mL) in a microwave vial. TMSBr (114 μL, 0.867 mmol, 2.5 eq.) was added and the solution was heated for 3 h at 70 °C. A mixture of methanol and water (9:1, 4 mL) was added and the solution was lyophilized affording 70 mg, (78%) of the product **4** as a grey powder.

Experimental Part

m.p. 100 °C

¹H NMR (500 MHz, D₂O): δ = 7.93 (s, 1H, H-1), 7.65 (m, 2H, H-4, H6), 7.55 (m, 1H, H-9), 7.49 (m, 1H, H-3), 7.22 (dd, J = 6.3 Hz, J = 3.3 Hz, 2H, H-7, H-8)

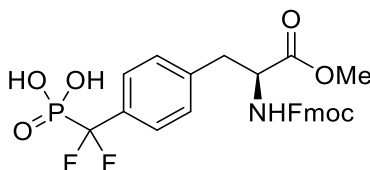
¹³C NMR (126 MHz, D₂O): δ = 133.6, 132.2, 131.4 (td, J = 22.1 Hz, J = 12.6 Hz), 128.5, 128.3, 127.7, 127.5 (d, J = 7.4 Hz), 126.8 (d, J = 7.4 Hz), 126.0 (vbr s), 122.8 (vbr s)

¹⁹F NMR (376 MHz, D₂O): δ = - 108.1 (d, J = 106.8 Hz)

³¹P NMR (162 MHz, D₂O): δ = 5.04 (t, J = 107.6 Hz)

HRMS (ESI): [M+H]⁺ calculated for C₁₁H₁₀F₂O₃P⁺: 259.03301 Da, found: 259.03253 m/z

Methyl N-(fluorenyl-9H-methoxy-carbonyl)-4-(phosphonodifluoromethyl)-L-phenylalanine **10**



The vacuum dried starting material **8** (227 mg, 0.386 mmol, 1 equiv.) was dissolved in dry DCM (2 mL) and cooled with an ice bath. TMSI (266 μL, 1.534 mM, 4 equiv.) was added dropwise to the cooled stirred solution. After 3 h, the mixture was dried in vacuo, redissolved in a mixture of H₂O / ACN (9:1) and stirred overnight. After concentrating the solution at the rotary evaporator, the residue was purified at MPLC (RP c18, ACN / H₂O, 5 to 99%) yielding 194 mg (95%) of the title compound **10** as a white fluffy solid.

R_f = 0.1 (EtOAc/MeOH/H₂O 12:1.5:1)

¹H NMR (400 MHz, Methanol-d₄) δ = 7.76 (d, J=7.5, 2H, 2 x Ar-H), 7.58 (d, J=7.3, 2H, 2 x Ar-H), 7.52 (d, J=8.0, 2H, 2 x Ar-H), 7.35 (t, J=7.5, 2H, 2 x Ar-H), 7.28 (t, J=7.5, 4H, 2 x Ar-H), 4.42 (dd, J=9.4, 5.1, 1H, α-H-Phe), 4.27 (dd, J=6.8, 1.9, 2H, CH₂-Fmoc), 4.14 (t, J=7.0, 1H, CH-Fmoc), 3.68 (s, 3H, OMe), 3.18 (dd, J=13.7, 5.1, 1H, CH_{2α}-Phe), 2.96 (dd, J=13.8, 9.5, 1H, CH_{2β}-Phe)

Experimental Part

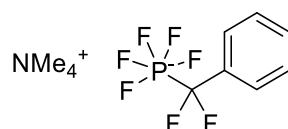
^{13}C NMR (101 MHz, Methanol- d_4) δ = 172.3 (O=C-methyl ester), 157.1 (O=C-Fmoc), 143.9 (C-F₂P), 141.2, 128.9, 127.5, 126.9, 126.2, 124.9, 124.9, 119.6 (18 x Ar), 66.6 (CH₂-Fmoc), 55.4 (CHN), 51.5 (OCH₃), 46.98 (CH-Fmoc), 36.76 (CH₂Phe)

^{19}F NMR (376 MHz, Methanol- d_4) δ = -110.34 (d, $J=112.6$)

^{31}P NMR (162 MHz, Methanol- d_4) δ = 6.79 (br)

HRMS (ESI): [M-H]⁻ calculated for C₂₆H₂₃F₂NO₇P⁻: 530. 11857Da, found: 530. 12098 m/z.

Tetramethylammonium (difluoro-(phenyl)-methyl)-penta-P-fluorophosphate 5



Diethyl phosphonic acid ester **1** (200 mg, 0.757 mmol, 1 equiv.) was dissolved in a Schlenk flask in dry ACN (5 mL). TMSBr (287 μL , 1.67 mmol 2.2 equiv.) was added dropwise under inert atmosphere. The solution was heated at 60°C for 1 hour. After disappearance of the starting material monitored via LC-MS, the vial was equipped with inert gas inlet and outlet to allow the release of the gaseous components developed after addition of dry DMF (293 μL , 3.78 mmol, 5 equiv.) and (COCl)₂ (636 μL , 7.57 mmol, 10 equiv.). After gas development decreased, the reaction was heated in a sealed vessel under inert atmosphere at 40°C with a water bath. After 1.5 hours, the reaction was cooled to 0°C with an ice bath. Previously weighted under inert atmosphere and dried NMe₄F (705 mg, 7.57 mmol, 10 equiv.) was then added slowly under inert atmosphere to the stirred and cooled reaction mixture. After 30 min, the mixture was slowly quenched in a cooled sat. aq. sol. of NaHCO₃ (25 mL/mmol starting material) and extracted with DCM (3 x 30 mL). The collected organic layer was then concentrated at the rotary evaporator, redissolved in H₂O/ACN and purified with RP-MPLC (RP c18, ACN / H₂O, 5 to 99%). After purification the product (119 mg, 62%) was isolated as white fluffy solid.

R_f = 0.5 (EtOAc)

Melting point = 107 °C

Experimental Part

¹H NMR (600 MHz, Acetonitrile- *d*₃) δ = 7.42 (d, *J*=7.6, 2H, Ar-H), 7.35 – 7.27 (m, 3H, Ar-H), 3.02 (s, 12H, NMe₄)

¹³C NMR (151 MHz, Acetonitrile- *d*₃) δ = 127.96, 127.32 (Ar-C), 125.53 (t, *J*=7.8, CF₂), 55.71 – 54.20 (s, NMe₄)

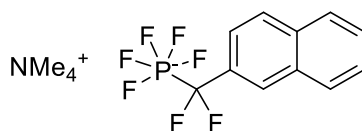
¹⁹F NMR (565 MHz, Acetonitrile- *d*₃) δ = -70.07 (dp, *J*=696.0, 43.5, 1F, F_{ax}), -71.76 (dt, *J*=855.7, 42.9, 9.1, 2F, F_{eq}), -98.59 (dt, *J*=119.9.8, 9.5, 2F, F_{eq})

³¹P NMR (243 MHz, Acetonitrile- *d*₃) δ = -145.27 (dtquin, *J*=864.3, 696.3, 125.2)

HRMS (ESI): [M]⁻ calculated for C₇H₅F₇P⁻: 253.0023 Da, found: 253.0033 m/z

Tetramethylammonium fluorophosphate 6

(difluoro-(naphth-2-yl)-methyl)-penta-P-



Diethyl phosphonic acid ester **3** (300 mg, 0.955 mmol, 1 equiv.) was dissolved in a Schlenk flask in dry ACN (4 mL). TMSBr (277 μ L, 2.10 mmol, 2.2 equiv.) was added dropwise under inert atmosphere. The solution was heated at 60°C for 1 hour. After disappearance of the starting material monitored via LC-MS, the vial was equipped with inert gas inlet and outlet to allow the release of the gaseous components developed after addition of dry DMF (369 μ L, 4.77 mmol, 5 equiv.) and (COCl)₂ (802 μ L, 9.55 mmol, 10 equiv.). After gas development decreased, the reaction was heated in a sealed vessel under inert atmosphere at 40°C with a water bath. After 40 min, the reaction was cooled to 0°C with an ice bath. Previously weighted under inert atmosphere and dried NMe₄F (889 mg, 9.55 mmol, 10 equiv.) was then added slowly under inert atmosphere to the stirred and cooled reaction mixture. After 15 min, the mixture was slowly quenched in a cooled sat. aq. sol. of NaHCO₃ (25 mL/mmol starting material) and extracted with DCM (3 x 30 mL). The collected organic layer was then concentrated at the rotary evaporator, redissolved in H₂O/ACN and purified with RP-MPLC (RP c18, ACN / H₂O, 5 to 99%). After purification the product (184 mg, 51%) was isolated as white fluffy solid.

R_f = 0.65 (EtOAc)

Experimental Part

Melting point: 142 °C

¹H NMR (600 MHz, Acetonitrile-*d*₃) δ = 7.92 – 7.82 (m, 4H, Ar-H), 7.58 – 7.50 (m, 3H, Ar-H), 3.02 (s, 12H, NMe₄)

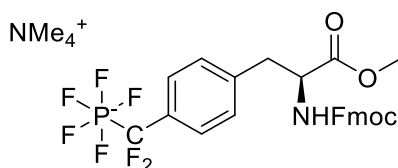
¹³C NMR (151 MHz, Acetonitrile-D₃) δ = 132.56, 128.26, 127.50, 126.78, 126.28, 126.11 (Ar-C), 55.24 (s, NMe₄)

¹⁹F NMR (565 MHz, Acetonitrile-*d*₃) δ = -69.69 (p, *J* = 43.1, 1/2F, F_{ax}), -70.93 (p, *J* = 43.1, 1/2F, F_{ax}), -70.81 (dt, *J*=43.11, 8.74, 2F, F_{eq}), -72.33 (dt, *J*=43.0, 8.5, 2F, F_{eq}), -98.59 (dt, *J* = 119.2, 8.7, CF₂)

³¹P NMR (243 MHz, Acetonitrile-*d*₃) δ = -142.35 (dtquin, *J*=864.3, 696.3, 125.2)

HRMS (ESI): [M]⁻ calculated for C₁₁H₇F₇P⁻: 303.0179 Da, found: 303.0177 m/z

Tetramethylammonium methyl N-(fluorenyl-9H-methoxy-carbonyl)-4-(pentafluorophosphato-difluoromethyl)-L-phenylalanine 11



Diethyl phosphonic acid ester **8** (828 mg, 1.41 mmol, 1 equiv.) was dissolved in a Schlenk flask in dry ACN (5 mL). TMSBr (930 μL, 7.05 mmol, 5 equiv.) was added dropwise under inert atmosphere. The solution was heated at 60°C for 90 mins. After disappearance of the starting material monitored via LC-MS, the vial was equipped with inert gas inlet and outlet to allow the release of the gaseous components developed after addition of dry DMF (545 μL, 7.05 mmol, 5 equiv.) and (COCl)₂ (1.18 μL, 14.09 mmol, 10 equiv.). After gas development decreased, the reaction was heated in a sealed vessel under inert atmosphere at 40°C with a water bath. After 1 h, the reaction was cooled to 0°C with an ice bath. Previously weighted under inert atmosphere and dried NMe₄F (1050 mg, 14.09 mmol, 10 equiv.) was then added slowly under inert atmosphere to the stirred and cooled reaction mixture. After 1 hour, the mixture was slowly quenched in a cooled sat. aq. sol. of NaHCO₃ (25 mL/mmol starting material) and extracted with DCM (3 x 30 mL). The collected organic layer was then concentrated at the rotary evaporator, redissolved in

Experimental Part

H₂O/ACN and purified with RP-MPLC (RP c18, ACN / H₂O, 5 to 99%). After purification the product (619 mg, 68%) was isolated as white fluffy solid.

Melting point = 140-142 °C

[α]_D²⁰ = - 6.9 (c = 1, MeOH)

¹H NMR (600 MHz, Acetonitrile-*d*₃) δ = 7.80 (d, *J*=7.6, 2H, Ar-H), 7.65 – 7.53 (m, 2H, Ar-H), 7.39 (t, *J*=7.5, 2H, Ar-H), 7.38 – 7.23 (m, 4H), 7.15 (d, *J*=7.8, 2H), 4.39 (q, *J*=8.2, 1H, CHN), 4.32 – 4.20 (m, 2H, Fmoc CH₂), 4.18 (t, *J*=6.9, 1H, Fmoc CH), 3.64 (s, 3H, OMe), 3.15 – 3.09 (m, 1H, CH_{2 α} Phe), 3.02 (s, 12H, NMe₄), 2.97 – 2.88 (m, 1H, CH_{2 β} Phe)

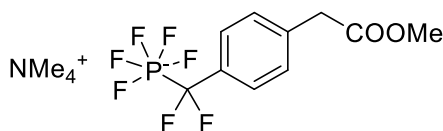
¹³C NMR (151 MHz, Acetonitrile-*d*₃) δ = 172.22 (O=C-methyl ester), 155.93 (O=C-Fmoc), 144.13, 141.19, 136.76, 129.45, 128.24, 127.78, 127.21 (d, *J*=3.2), 125.71 (t, *J*=7.0, CF₂), 125.27 (d, *J*=10.3), 120.05 (18x Ar-C), 66.39 (CH₂-Fmoc), 55.46 (CHN), 55.24 (NMe₄), 51.89 (OMe), 47.03 (CH-Fmoc), 36.87 (CH₂Phe)

¹⁹F NMR (565 MHz, Acetonitrile-*d*₃) δ = -69.65 (p, *J*=42.9, F_{ax}), -70.88 (p, *J*=42.9, F_{ax}), -71.05 (t, *J*=8.8, F_{eq}), -71.12 (t, *J*=8.7, F_{eq}) -98.26 (dt, *J*=120.3, 9.1, CF₂)

³¹P NMR (243 MHz, Acetonitrile-*d*₃) δ = -143.43 (dtquin, *J*=855.99, 696.35, 120.1)

HRMS (ESI): [M]⁻ calculated for C₂₆H₂₂F₇NO₄P⁻: 576.11802 Da, found: 576.11809 m/z

Tetramethylammonium O-methyl-4-(pentafluorophosphato-difluoromethyl)-phenylacetate 12



Diethyl phosphonic acid ester **9** (670 mg, 1.99 mmol, 1 equiv.) was dissolved in a Schlenk flask in dry ACN (10 mL). TMSBr (1.314 μ L, 9.96 mmol, 5 equiv.) was added dropwise under inert atmosphere. The solution was heated at 60°C for 2 hours. After disappearance of the starting material monitored via LC-MS, the vial was equipped with inert gas inlet and outlet to allow the release of the gaseous components developed after addition of dry DMF (766 μ L, 9.96 mmol, 5 equiv.) and

Experimental Part

(COCl)₂ (1.67 μL, 19.92 mmol, 10 equiv.). After gas development decreased, the reaction was heated in a sealed vessel under inert atmosphere at 40°C with a water bath. After 1 h, the reaction was cooled to 0°C with an ice bath. Previously weighted under inert atmosphere and dried NMe₄F (1485 mg, 15.94 mmol, 10 equiv.) was then added slowly under inert atmosphere to the stirred and cooled reaction mixture. After 1 hour, the mixture was slowly quenched in a cooled sat. aq. sol. of NaHCO₃ (25 mL/mmol starting material) and extracted with DCM (3 x 30 mL). The collected organic layer was then concentrated at the rotary evaporator, redissolved in H₂O/ACN and purified with RP-MPLC (RP c18, ACN / H₂O, 5 to 99%). After purification the product (320 mg, 49%) was isolated as white fluffy solid.

¹H NMR (600 MHz, Acetonitrile-*d*₃) δ = 7.40 – 7.32 (m, 2H, Ar-H), 7.21 (d, *J*=8.1, 2H, Ar-H), 3.62 (s, 5H, CH₂, OMe), 3.02 (s, 12H, NMe₄)

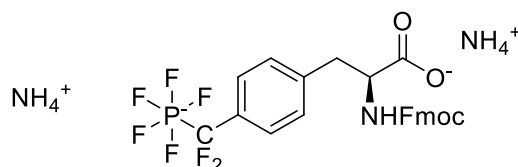
¹³C NMR (151 MHz, Acetonitrile-*d*₃) δ = 172.01 (O=C), 134.40 (d, *J*=2.1), 129.69 (d, *J*=1.2), 128.41 (Ar-C), 125.72 (t, *J*=7.5, CF₂), 55.20 (NMe₄), 51.57 (OMe), 40.14 (CH₂Phe)

¹⁹F NMR (565 MHz, Acetonitrile-*d*₃) δ = -70.09 (dp, *J*=696.7, 43.4, 42.6, F_{ax}), -71.75 (ddt, *J*=855.5, 43.1, 9.4, 4F, F_{eq}), -98.39 (dp, *J*=120.6, 9.3, 2F, CF₂)

³¹P NMR (243 MHz, Acetonitrile-*d*₃) δ = -143.92 (dtquinte, *J*=856.2, 696.6, 120.0)

HRMS (ESI): [M]⁻ calculated for C₁₀H₉F₇O₂P⁻: 325.0234 Da, found: 325.0241 m/z

Ammonium N-(fluorenyl-9H-methoxy-carbonyl)-4-(pentafluorophosphato-difluoromethyl)-L-phenylalanine 13



To the methylester **11** (65 mg, 0.923 mmol) dissolved in 3 mL of an aqueous solution of ammonium bicarbonate (50mM, pH: 7.8), the enzyme (2 mg) was added and gently stirred at 50 °C overnight. All volatile components were removed under reduced pressure and the obtained crude product purified via MPLC (RP C18, ACN / H₂O + 10 mM NH₄HCO₃, 10 to 99%). Fractions containing the product were

Experimental Part

concentrated at a rotary evaporator and lyophilized, yielding 45 mg (80%) of the product **13** as an off white solid.

$[\alpha]_D^{20} = +12.1$ ($c = 1$, MeOH)

^1H NMR (600 MHz, Methanol- d_4) $\delta = 7.78 - 7.70$ (m, 2H, Ar-H), 7.58 (t, $J=7.7$, 2H, Ar-H), 7.39 – 7.29 (m, 4H, Ar-H), 7.32 – 7.21 (m, 2H, Ar-H), 7.14 (d, $J=7.9$, 1H, 2H, Ar-H), 4.37 – 4.26 (m, 2H, CHN, $\text{CH}_\alpha\text{Fmoc}$), 4.26 – 4.15 (m, 1H, $\text{CH}_\beta\text{Fmoc}$), 4.15 (t, $J=7.0$, CH Fmoc), 3.23 – 3.12 (m, 1H, $\text{CH}_{2\alpha}\text{-Phe}$), 2.96 (dd, $J=13.8, 8.2$, 1H, $\text{CH}_{2\beta}\text{-Phe}$)

^{13}C NMR (151 MHz, Methanol- d_4) $\delta = 166.00$ (COOH), 156.88 (C=O Fmoc), 143.93 (d, $J=16.4$), 141.20 (d, $J=2.6$), 137.35, 128.62, 125.45 (t, $J=7.6$), 124.97 (d, $J=16.6$, Ar-C), 66.55, 53.99, 47.00, 37.89, 37.26, 32.38, 28.57, 26.01, 23.45, 18.93

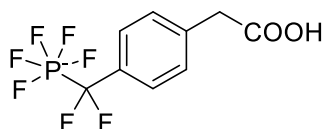
^{13}C NMR (126 MHz, Methanol- d_4) $\delta = 157.07$ (C=O), 141.22, 139.73, 137.08, 127.90, 127.47, 126.94, 124.94, 119.57 (Ar- C), 66.61 (CH_2Fmoc), 54.57 (CHN), 47.02 (CH-Fmoc), 36.86 (CH_2Phe)

^{19}F NMR (565 MHz, Methanol- d_4) $\delta = -71.30$ (dp, $J=693.8, 43.5, 42.9$, 1F, F_{ax}), -73.41 (ddt, $J=861.4, 43.1, 8.5$, 4F, F_{eq}), -99.33 (dt, $J=123.1, 9.2$, 2F, CF_2)

^{31}P NMR (243 MHz, Methanol- d_4) $\delta = -143.16$ (dtquint, $J= 861.5, 694.0, 123.0$)

HRMS (ESI): $[\text{M}]^-$ calculated for $\text{C}_{25}\text{H}_{20}\text{F}_7\text{NO}_4\text{P}^-$: 562.10237 Da, found: 562.10245 m/z

Tetramethyl 4-(pentafluorophosphato-difluoromethyl)-phenylacetic acid **14**



The methylester **12** (320 mg, 0.985 mmol, 1 equiv.) was added to *Bacillus licheniformis* protease (from Sigma Aldrich) (20 mg, 20 mg /mmol) in aqueous buffer (NH_4HCO_3 , 50 mM, pH = 7.8, 30 ml) and stirred at 50 °C overnight. The reaction mixture was concentrated at reduced pressure. The residue was purified via column chromatography at MPLC (RP C18, ACN / H_2O + 10 mM NH_4HCO_3 , 5 to 99%).

Experimental Part

Fractions containing the product were concentrated at rotary evaporator and lyophilized, yielding the product **14** (255 mg, 83%) as a white lyophilisate.

¹H NMR (500 MHz, Methanol-*d*₄) δ = 7.41 (d, *J*=7.7, 2H, Ar-H), 7.26 (d, *J*=7.9, 2H, Ar-H), 3.57 (s, 2H, CH₂Phe), 3.09 (s, 12H, NMe₄⁺)

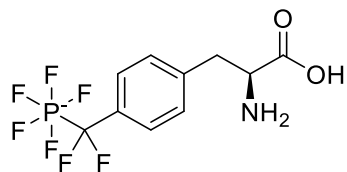
¹³C NMR (126 MHz, Methanol-*d*₄) δ = 176.15 (s, C=O), 135.86, 127.86, 125.55 (s, 6 x Ar-H), 54.53 (s, NMe₄⁺), 42.27 (s, CH₂Phe)

¹⁹F NMR (471 MHz,) δ = -71.18 (dp, *J*=696.1, 43.6, 1F, F_{eq}), -72.30 (d, *J*=43.6, 2F, F_{ax}), -74.13 (d, *J*=41.4, 2F, F_{ax}), -99.54 (d, *J*=124.3, 2F, CF₂)

³¹P NMR (202 MHz,) δ = -143.37 (tdq, *J*=861.4, 694.0, 122.9)

HRMS (ESI): [M]⁻ calculated for C₉H₇F₇O₂P⁻: 311.00774 Da, found: 311.00795 m/z

Ammonium 4-(pentafluorophosphato-difluoromethyl)-L-phenylalanine 15



The ammonium salt of Fmoc-protected amino acid **13** (100 mg, 0.172 mmol, 1 equiv.) was dissolved in ACN (1 ml). DBU (77 μ L, 0.517 mmol, 3 equiv.) was added dropwise to the stirred solution. The reaction was monitored via LCMS. n-Hexane (2 ml) was added to the mixture. The layers were divided and the ACN layer was concentrated at reduced pressure. After purification of the crude via column chromatography on MPLC (RP C18, ACN / H₂O + 10 mM NH₄HCO₃ pH 7.5, 5 to 99%), the product (60 mg, 90%) was isolated as a white lyophilisate.

¹H NMR (700 MHz, Deuterium Oxide) δ = 7.47 (d, J =7.6, 2H, Ar-H), 7.32 (d, J =8.0, 2H, Ar-H), 3.95 (dd, J =8.5, 4.9, 1H, CHN), 3.30 (dd, J =14.5, 4.8, 1H, CH_{2 α} -Phe), 3.12 – 3.04 (m, 1H, CH_{2 β} -Phe)

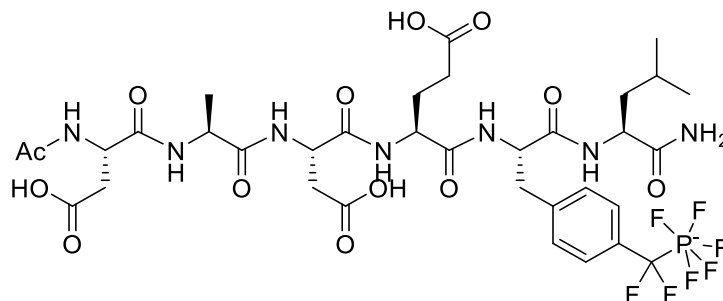
¹³C NMR (176 MHz, Deuterium Oxide) δ = 173.7 (O=C), 138.1, 136.3, 129.1, 129.0, 125.8 (6 x Ar-C), 44.5 (CHN), 36.1 (CH₂Phe)

¹⁹F NMR (376 MHz, Deuterium Oxide) δ = -68.50 (dp, J =693.6, 43.6, 1F, F_{ax}), -72.14 (ddt, J =864.2, 43.0, 8.5, 4F, F_{eq}), -98.27 (dt, J =126.2, 8.3, 2F, CF₂)

³¹P NMR (162 MHz, Deuterium Oxide) δ = -143.00 (dtquin, J =864.8, 171.8, 126.3)

HRMS (ESI): [M]⁻ calculated for C₁₀H₁₀F₇NO₂P⁻ : 340.03429 Da, found: 340.03452 m/z

N-Acetyl-L-aspartyl-L-alaninyl-L-aspartyl-L-glutamyl-4-(pentafluorophosphato-difluoromethyl)-L-phenylalaninyl-L-leucyl-amide **19**



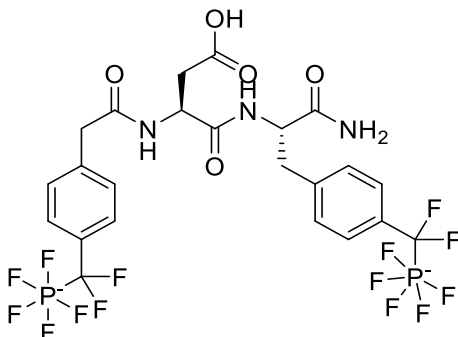
Compound **19** was synthesized applying standard DIC / HOBt coupling procedure. Hence, the amino acid (5 equiv. based on the resin loading) were preactivated with HOBt (5 equiv.) in a minimal amount of DMF. After 5 minutes, DIC (5 equiv.) was added and the reaction mixture was added to the resin preswelled in a minimal amount of DMF. Acetylation, cleavage and purification were carried out as described in the general procedures. From 0.206 mg Rink amide resin, 9.1 mg (18%) of the product **19** were obtained as white fluffy solid.

¹H NMR (600 MHz, Deuterium Oxide) δ = 7.43 – 7.26 (m, 2H, Ar-H), 7.25 – 7.15 (m, 2H, Ar-H), 4.52 – 4.11 (m, 6H, CHN), 3.15 – 2.89 (m, 2H, CH₂Phe), 2.64 (dd, $J=63.7$, 15.9, 4H, 2xCH₂Asp), 2.17 (m, 2H, CH₂Glu), 1.91 (s, 3H, Ac), 1.81 (dd, $J=29.9$, 7.5, 2H, CH₂Glu), 1.56 – 1.37 (m, 3H, CH₂CH) 1.27 (m, 3H, CH₃Ala), 0.76 (d, $J=36.1$, 6H, 2xCH₃Leu)

¹⁹F NMR (565 MHz, Deuterium Oxide) δ = -67.75 (p, $J=42.9$, F_{ax}), -68.97 (p, $J=44.0$, 42.4, F_{ax}), -70.69 – -71.76 (d, $J=42.9$, 2F, F_{eq}), -72.78 (d, $J=42.9$, 2F, F_{eq}), -97.98 (dd, $J=126.4$, 8.7, 2F, CF₂)

HRMS (ESI): [M]⁻ calculated for C₃₄H₄₆F₇N₇O₁₃P⁻: 924.2785 Da, found: 924.2795 m/z

Bis-ammonium 4-(pentafluorophosphato-difluoromethyl)-phenylacetamidyl-L-aspartyl- 4-(pentafluorophosphato-difluoromethyl)-L-phenylalaninyl-amide 20



Compound **20** was synthesized as described in the general methods using TBTU / HOBT / DIPEA, starting from deprotected Rink amide resin (0.159 g, loading 0.34 mmol/g). After Olah´ reagent mediated cleavage and purification on RP MPLC, 11.5 mg (46%) of the product were obtained as white fluffy solid.

¹H NMR (600 MHz, Deuterium Oxide) δ = 7.37 (t, $J=9.5$, 4H, Ar-H), 7.17 (d, $J=7.8$, 4H, Ar-H), 4.52 – 4.43 (m, 2H, CHN), 3.45 (s, 2H, CH₂Phe), 3.10 (d, $J=13.3$, 1H, CH₂Phe), 2.86 (dd, $J=13.2$, 10.2, 1H, CH₂Phe), 2.43 (ddd, $J=96.3$, 15.9, 7.2, 2H, CH₂Asp)

¹⁹F NMR (565 MHz, Deuterium Oxide) δ = -67.53 – -68.13 (m), -69.00 (h, $J=43.2$, 42.7, 2F, F_{ax}), -72.04 (dddd, $J=864.7$, 42.9, 25.4, 7.9, 8F, F_{eq}), -98.00 (dd, $J=126.4$, 8.7, 4F, 2xCF₂)

HRMS (ESI): [M]⁻ calculated for C₂₃H₂₁F₁₄N₃O₅P₂²⁻: 373.5372 Da, found: 373.5387 m/z

7 NMR spectra

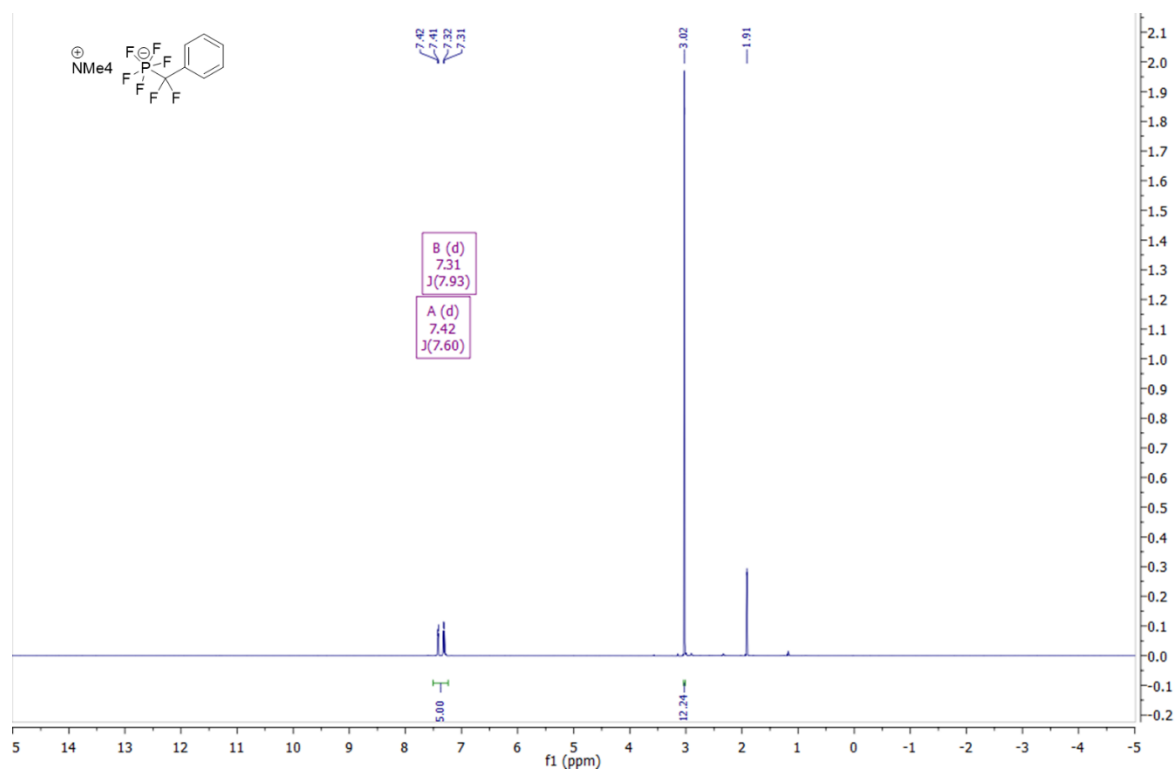


Figure 61 ^1H NMR spectrum (600 MHz, ACN-d_3) of **5**

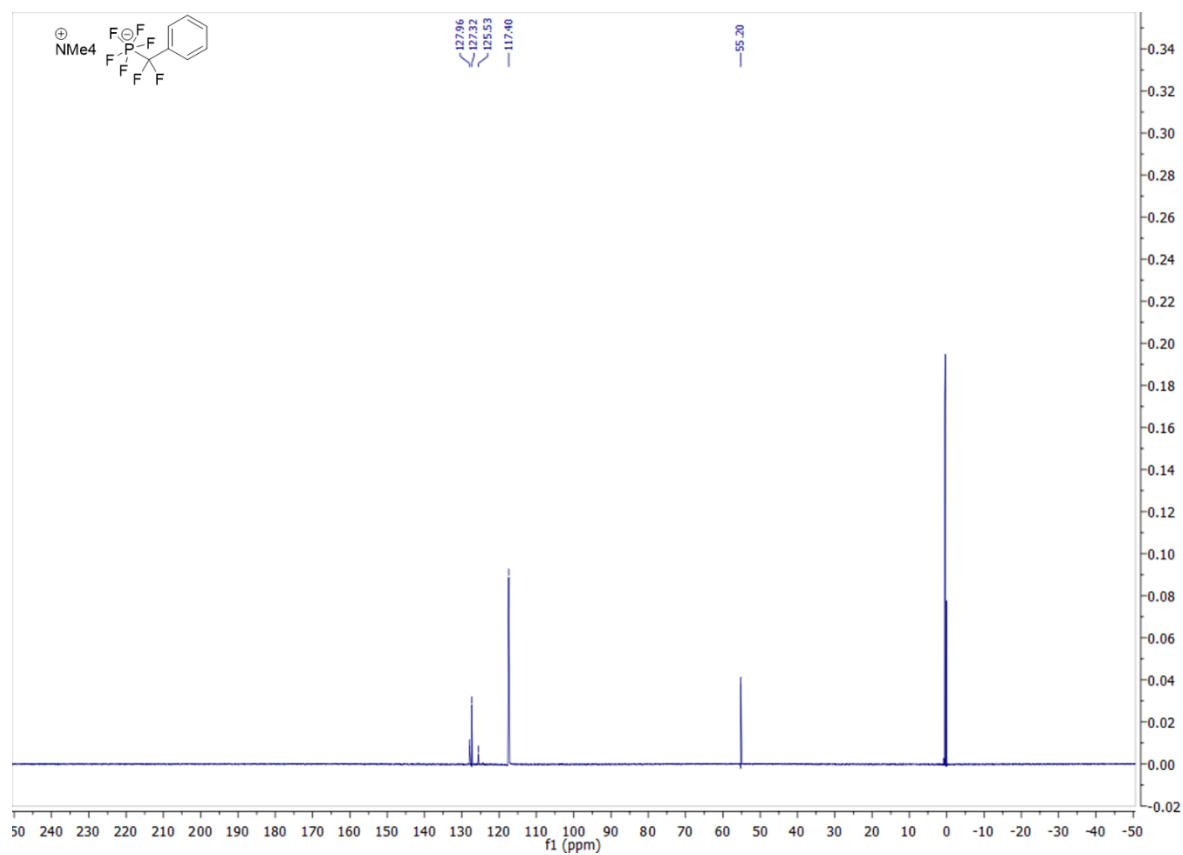


Figure 62 ^{13}C NMR spectrum (150 MHz, ACN-d_3) of **5**

NMR spectra

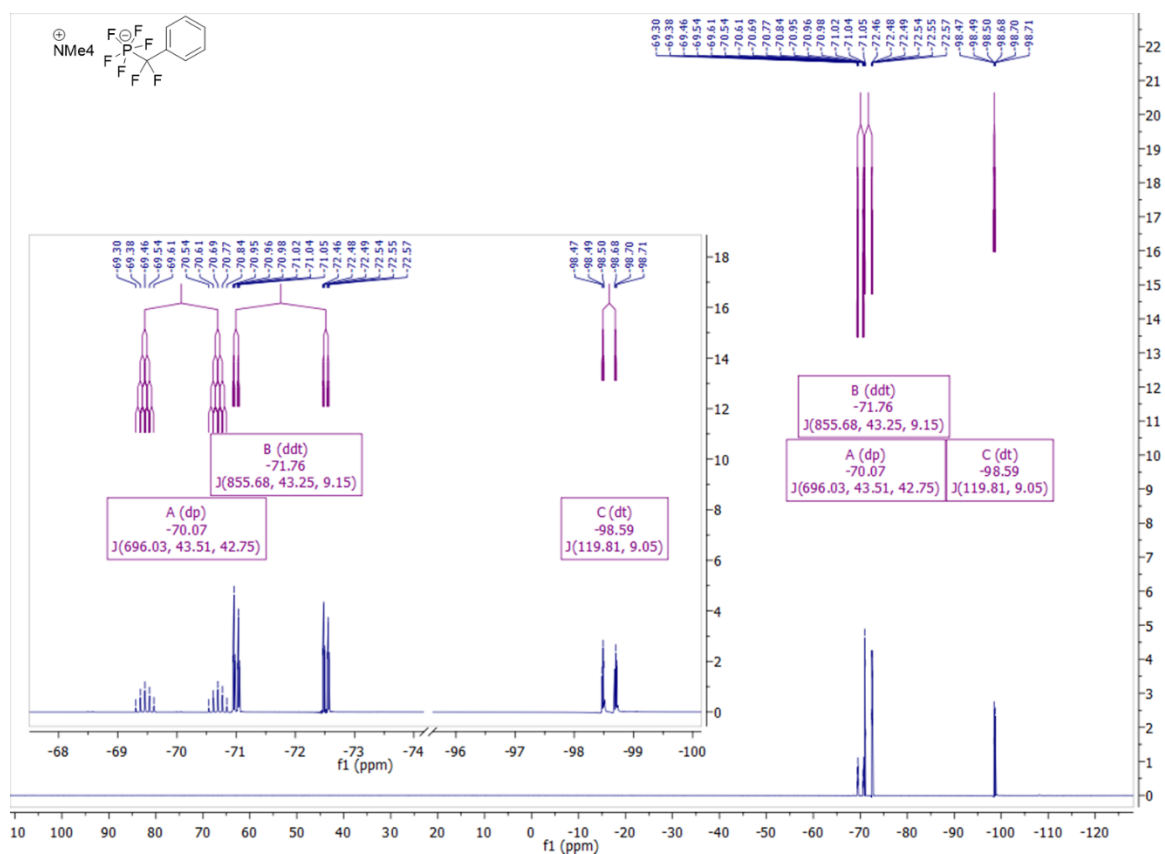


Figure 63 ^{19}F NMR spectrum (565 MHz, ACN-d_3) of **5**

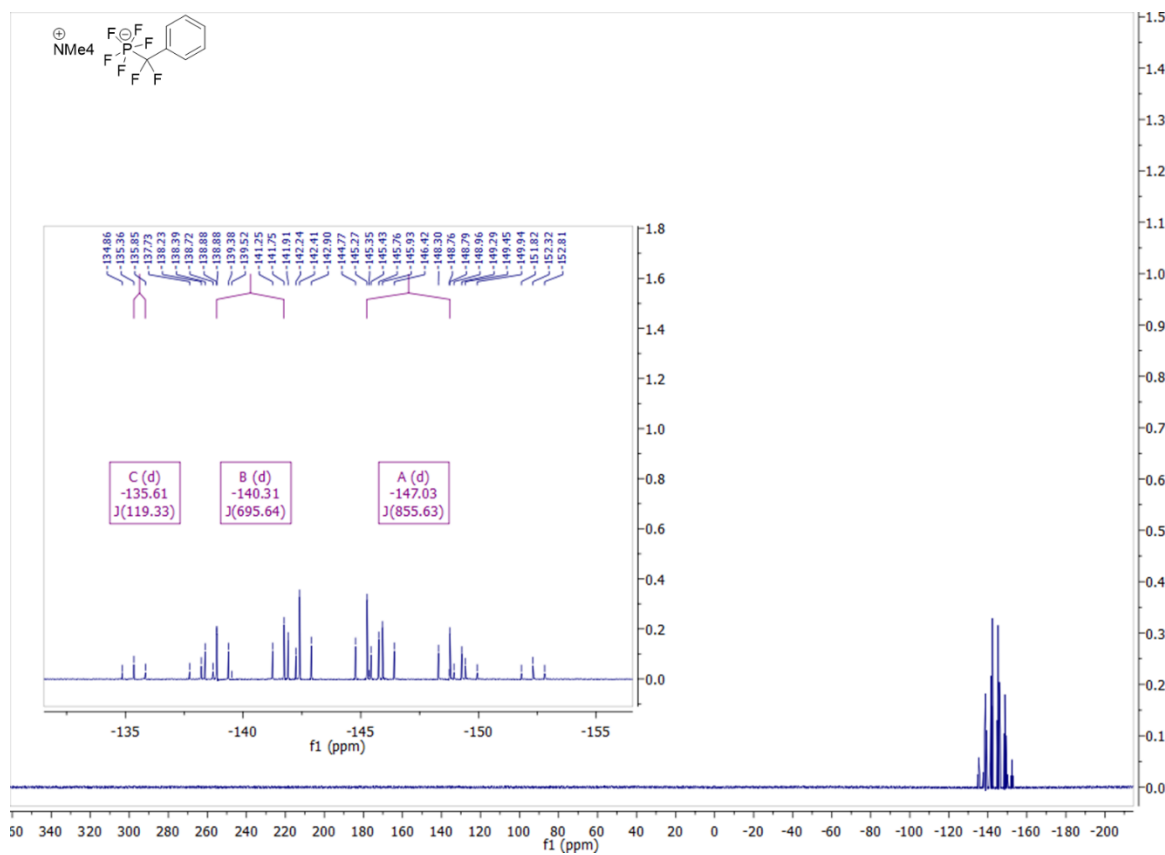


Figure 64 ^{31}P NMR spectrum (242 MHz, ACN-d_3) of **5**

NMR spectra

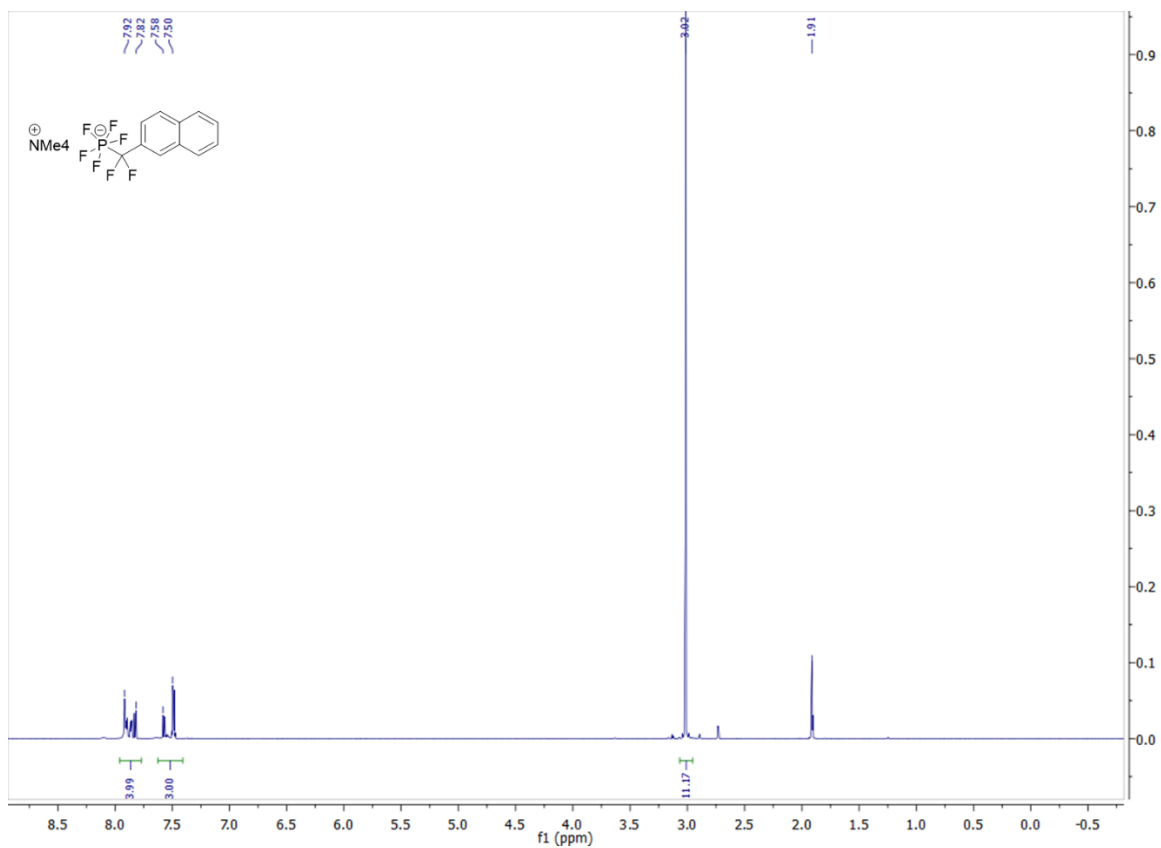


Figure 65 ^1H NMR spectrum (600 MHz, ACN-d_3) of **6**

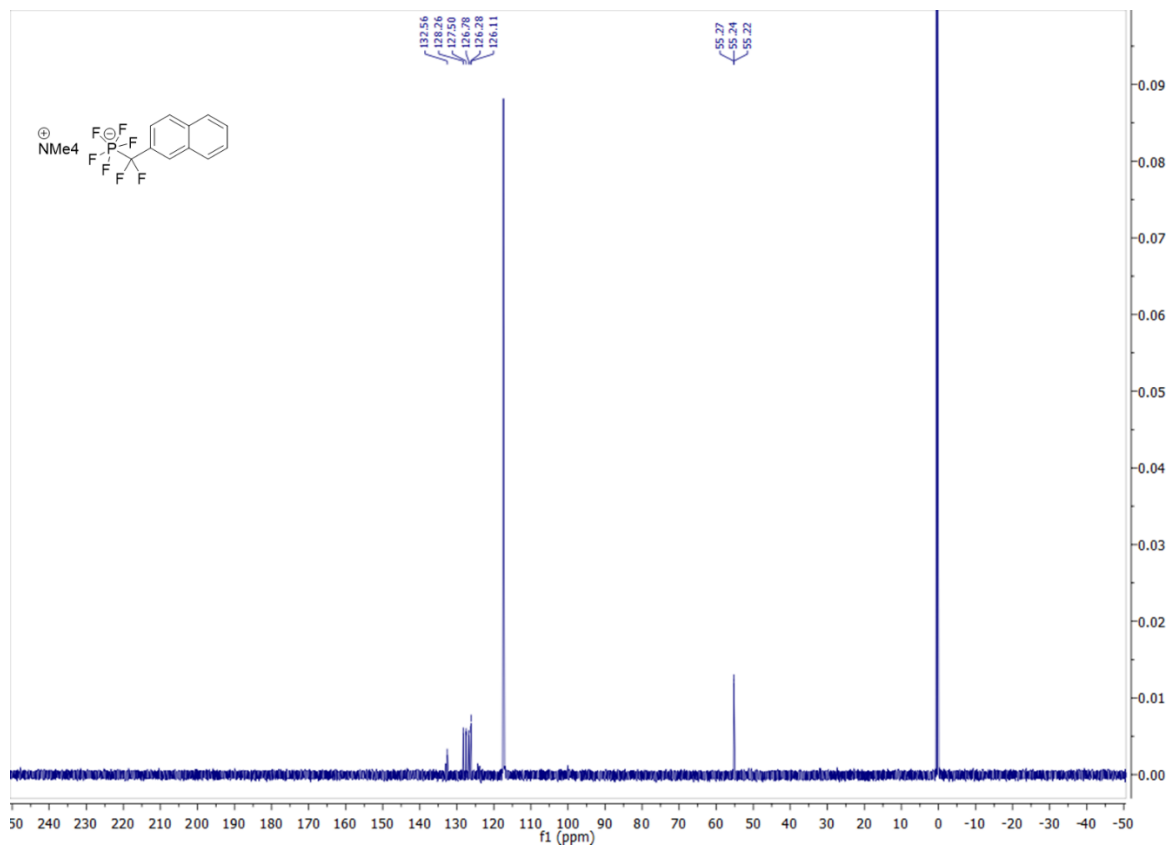


Figure 66 ^{13}C NMR spectrum (150 MHz, ACN-d_3) of **6**

NMR spectra

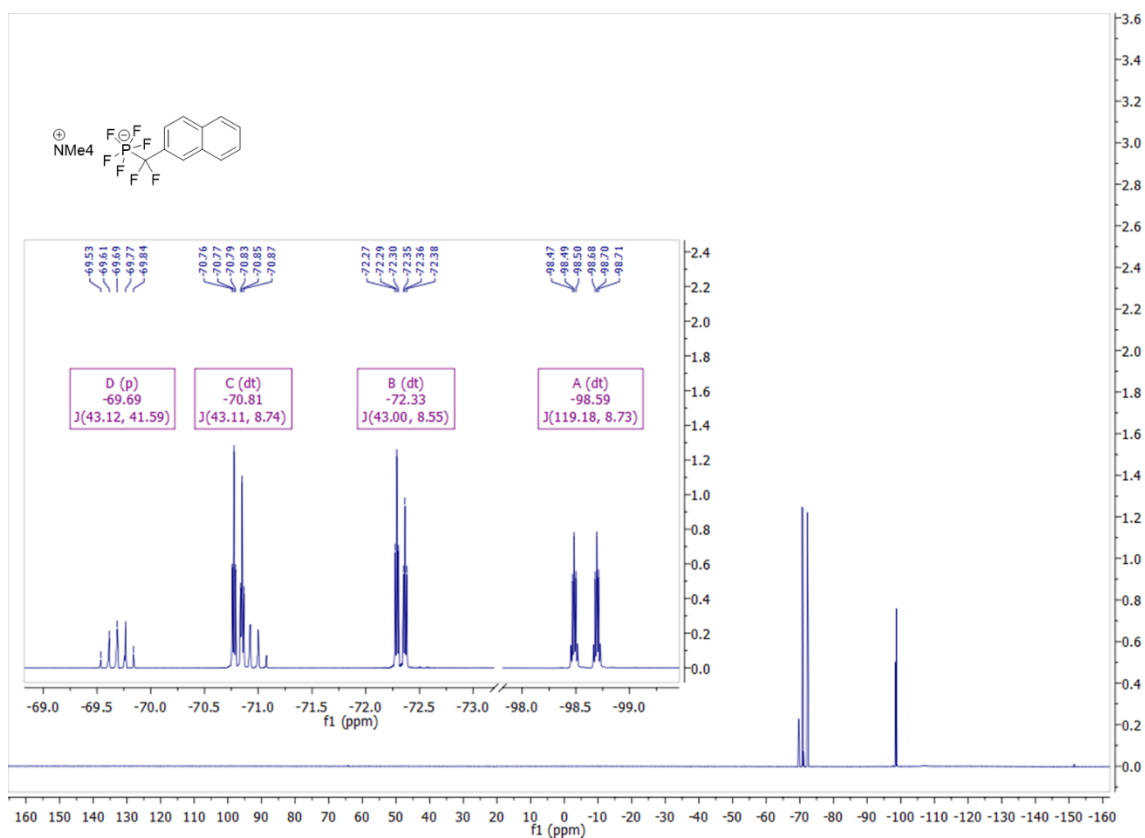


Figure 67 ^{19}F NMR spectrum (565 MHz, ACN-d_3) of **6**

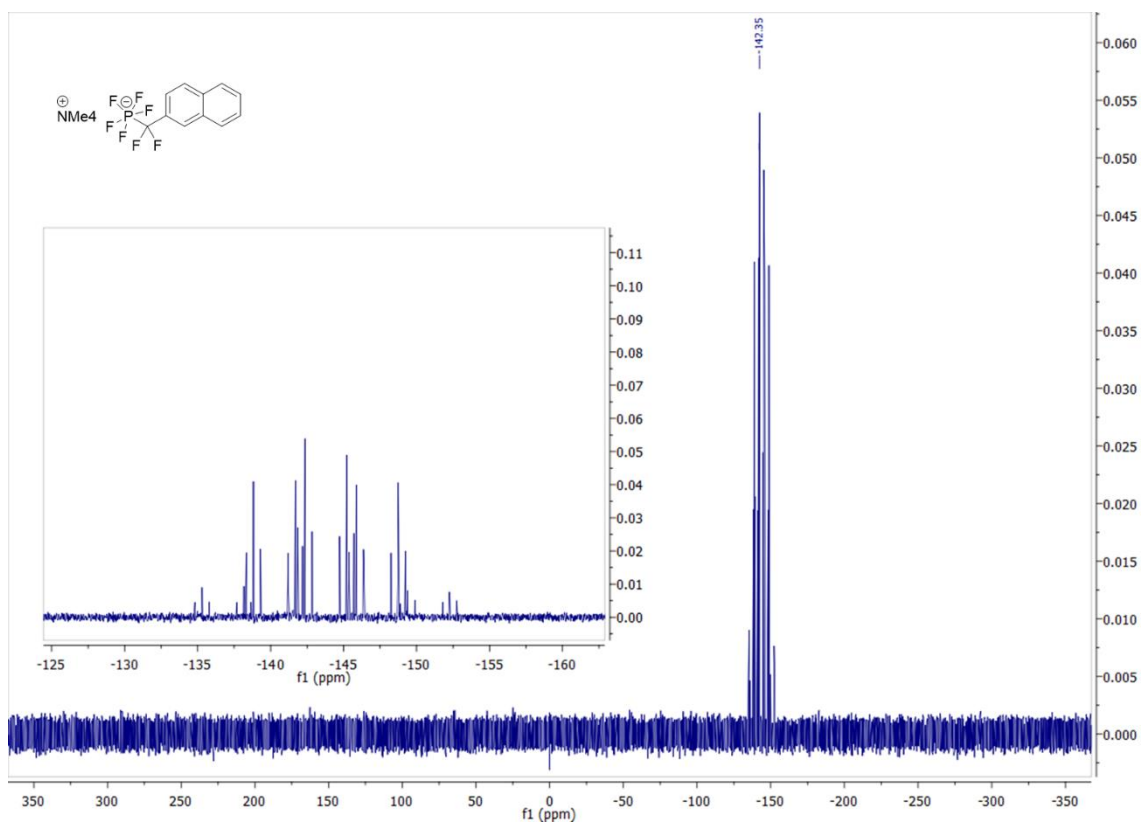


Figure 68 ^{31}P NMR spectrum (242 MHz, ACN-d_3) of **6**

NMR spectra

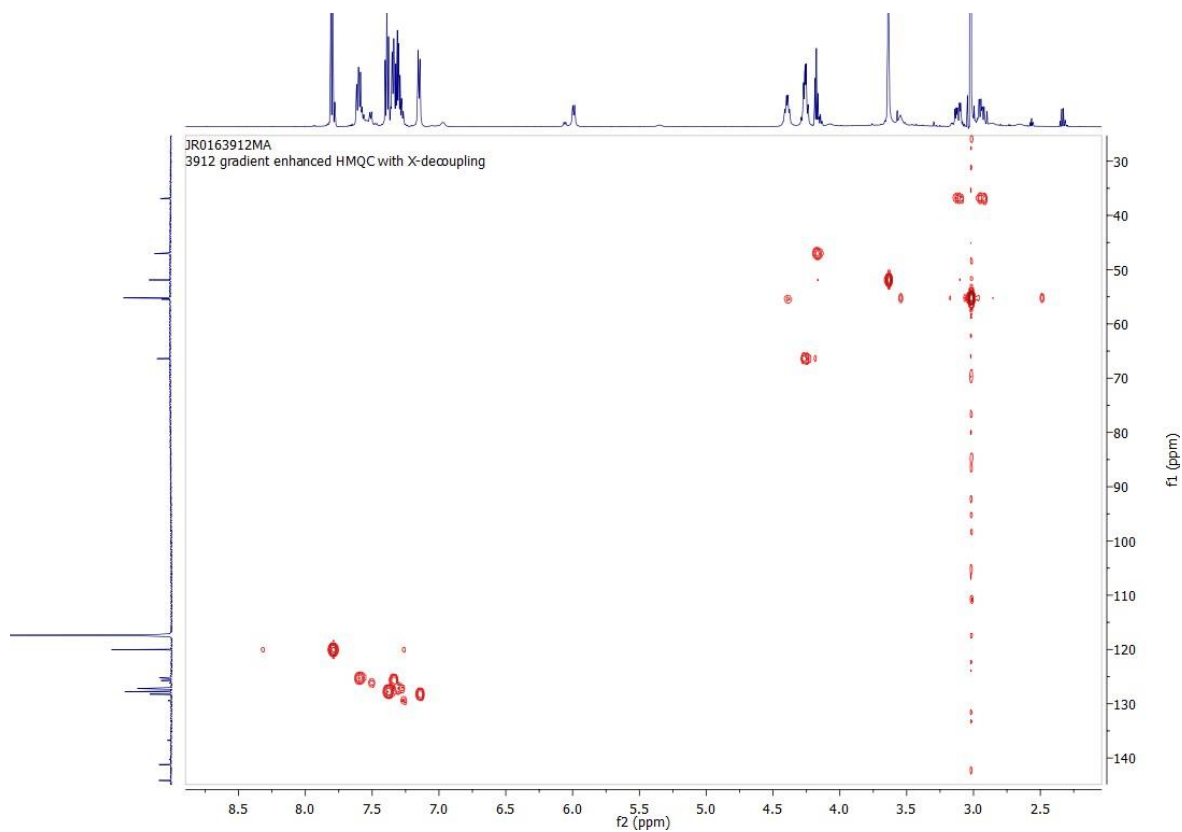


Figure 71 HMQC spectrum (^1H , ^{13}C) in ACN-d_3 of **11**

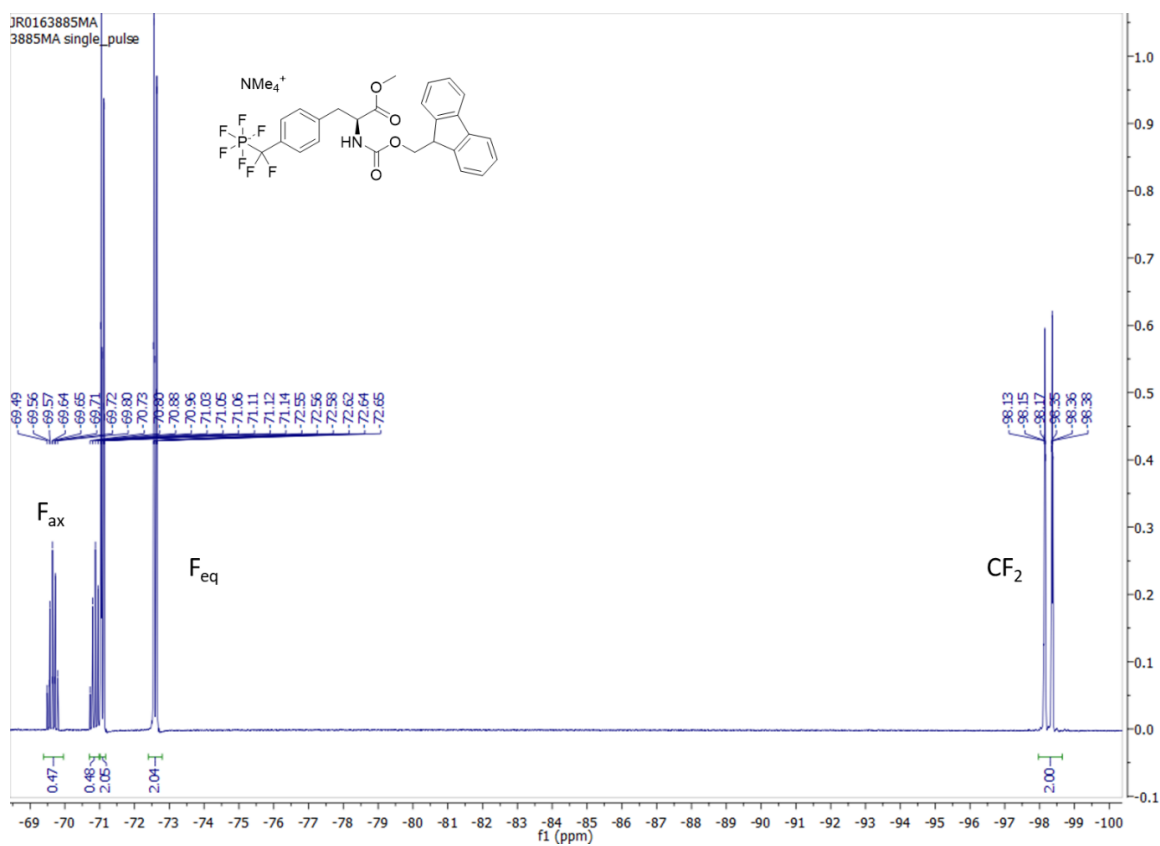


Figure 72 ^{19}F NMR spectrum (565 MHz, ACN-d_3) of **11**

NMR spectra

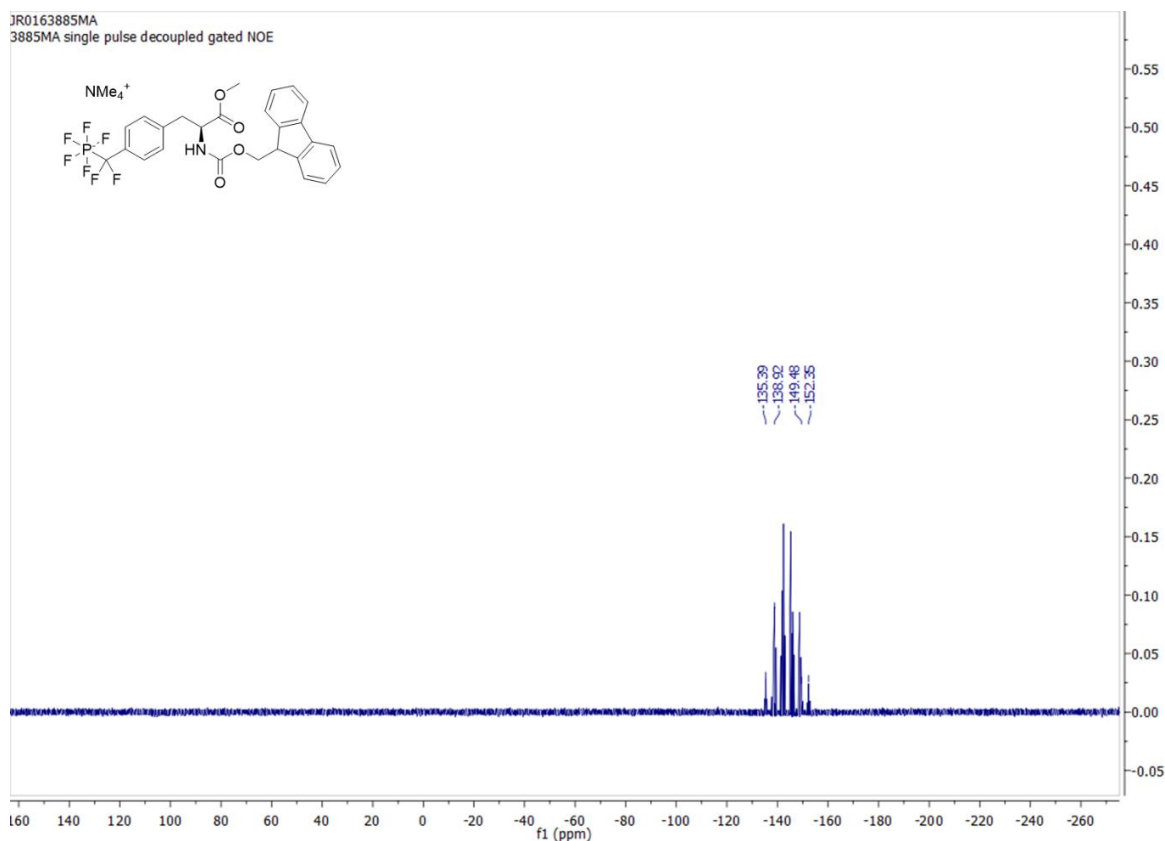


Figure 73 ^{31}P NMR spectrum (243 MHz, ACN-d₃) of **11**

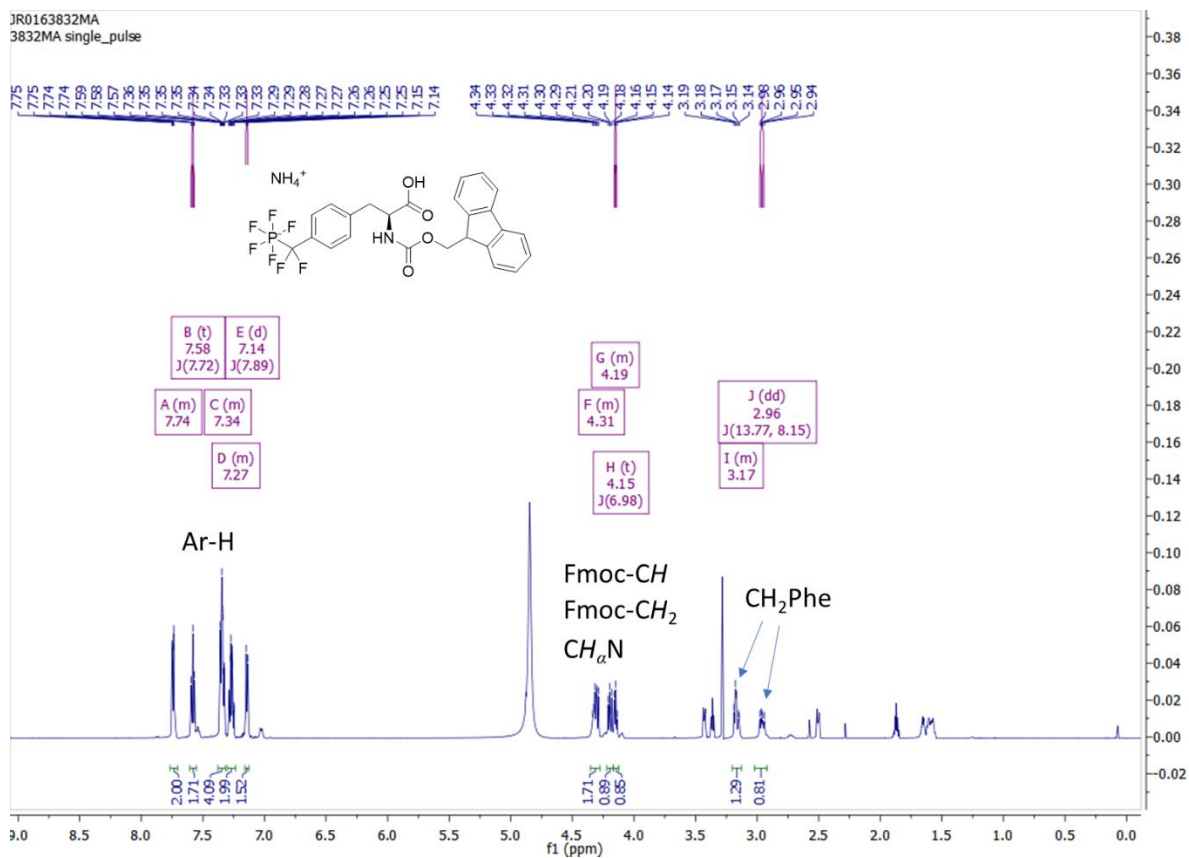


Figure 74 ^1H NMR spectrum (600 MHz, MeOD-d₄) of **13**

NMR spectra

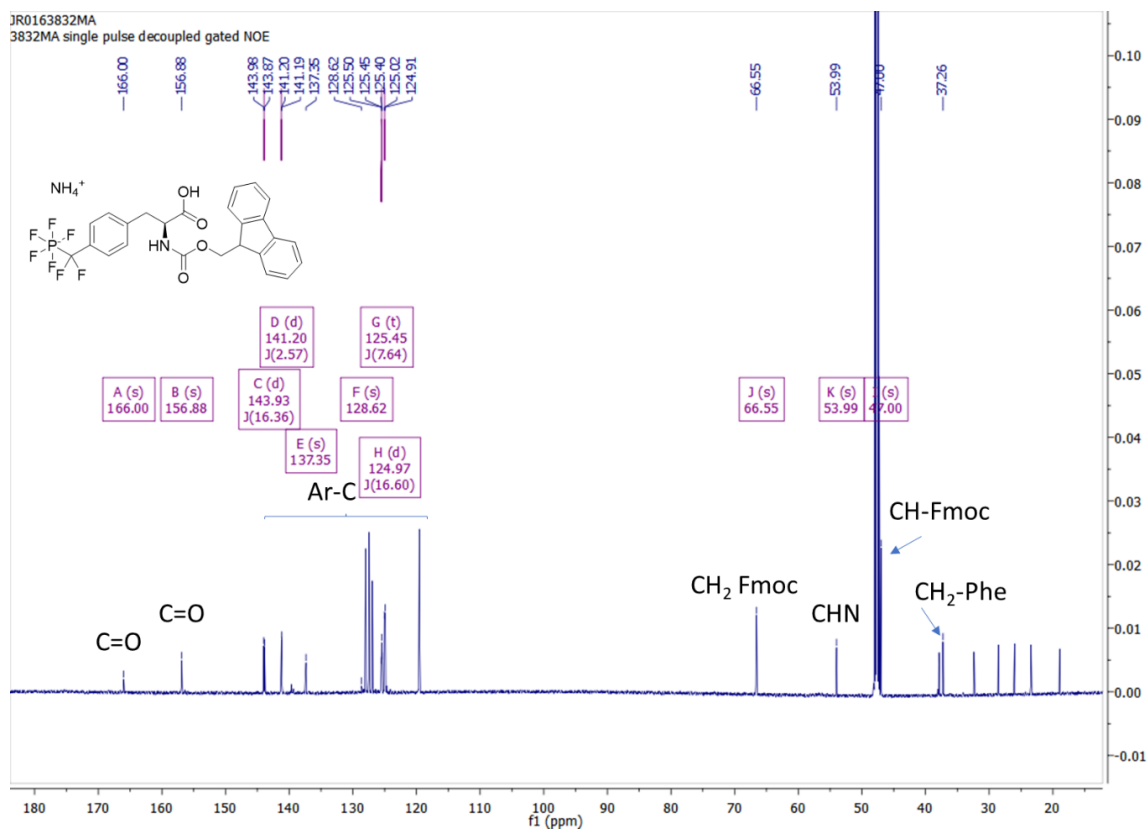


Figure 75 ¹³C NMR spectrum (151 MHz, MeOD-d₄) of **13**

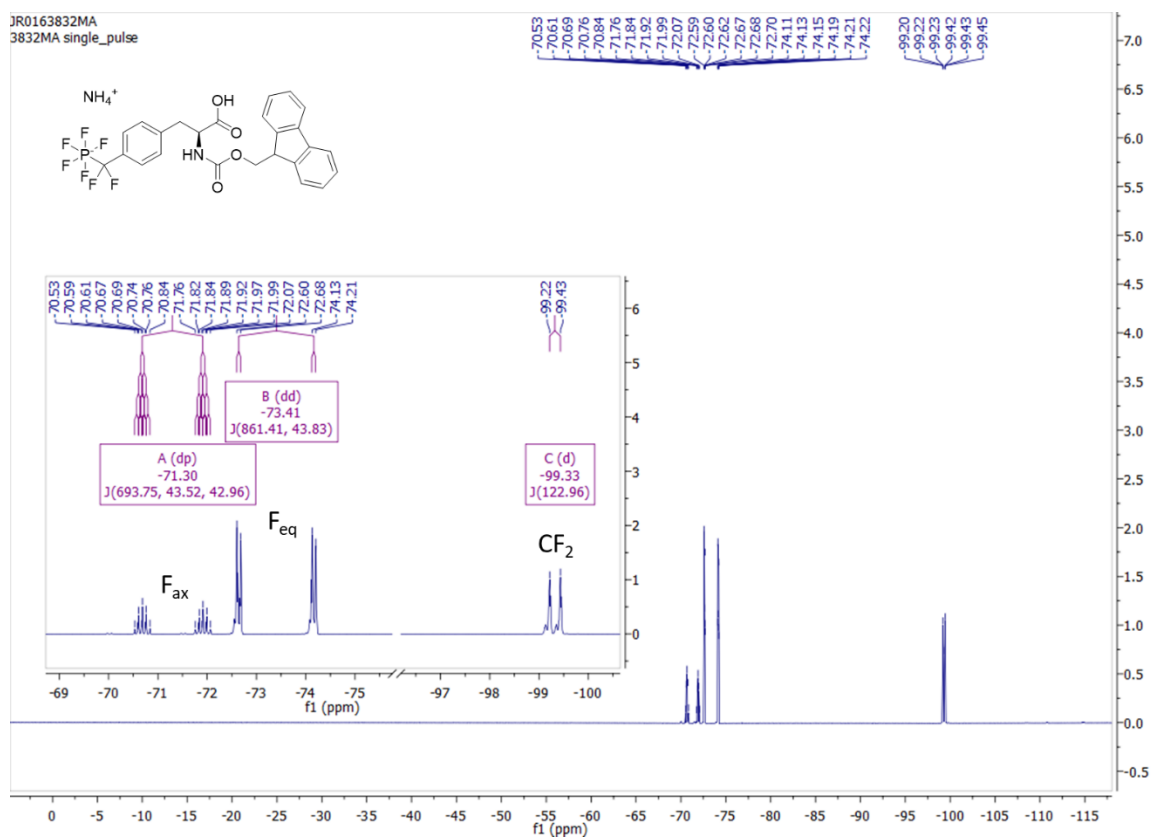


Figure 76 ¹⁹F NMR spectrum (565 MHz, MeOD-d₄) of **13**

NMR spectra

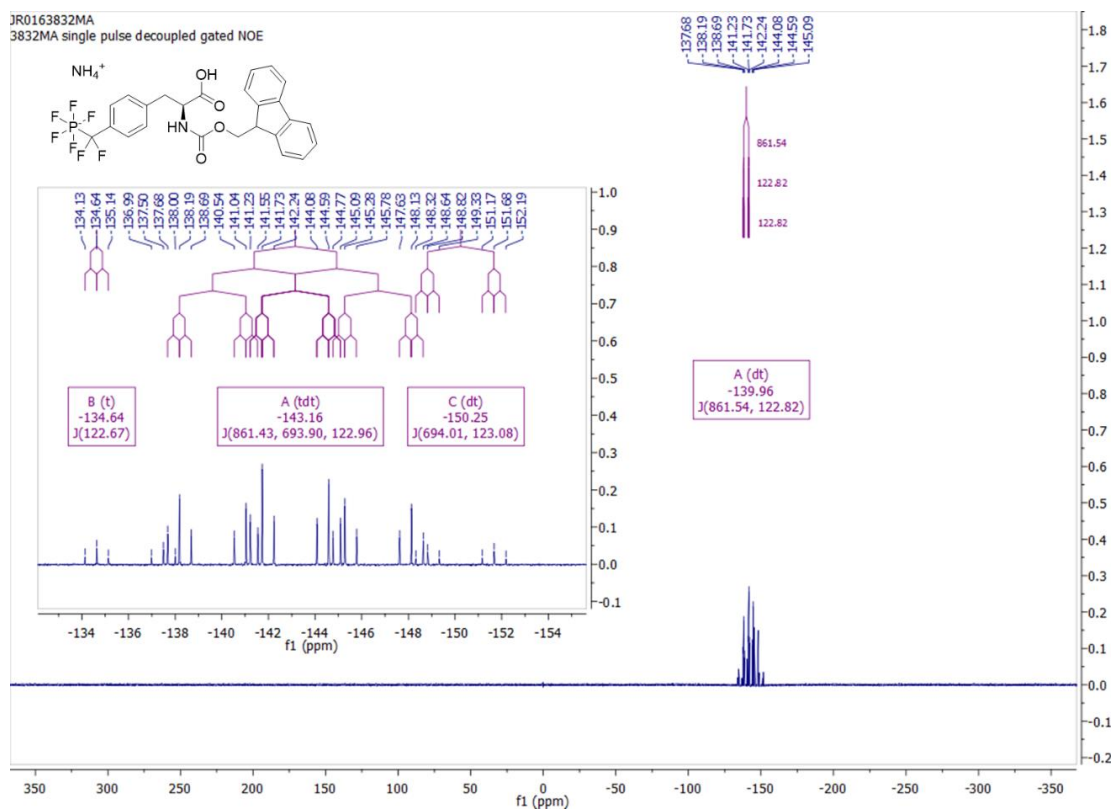


Figure 77 ^{31}P NMR spectrum (243 MHz, MeOD- d_4) of **13**

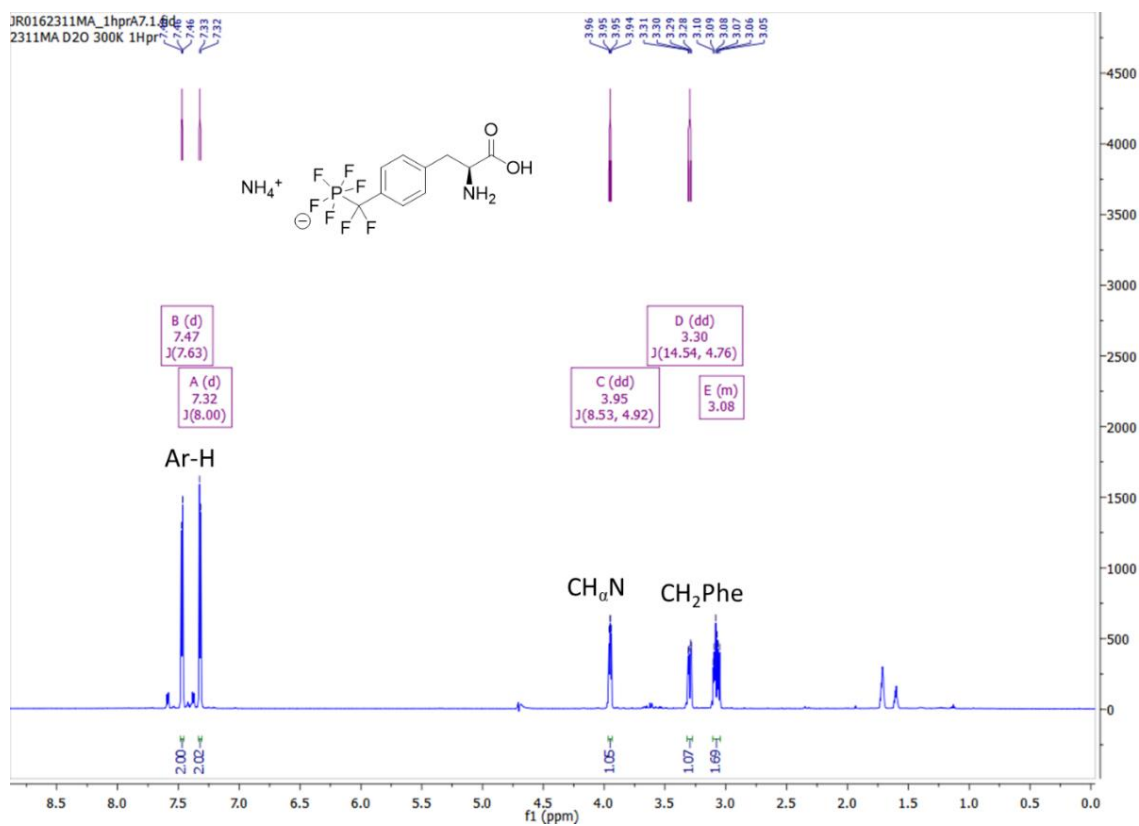


Figure 78 ^1H NMR spectrum (700 MHz, D_2O) of **15**

NMR spectra

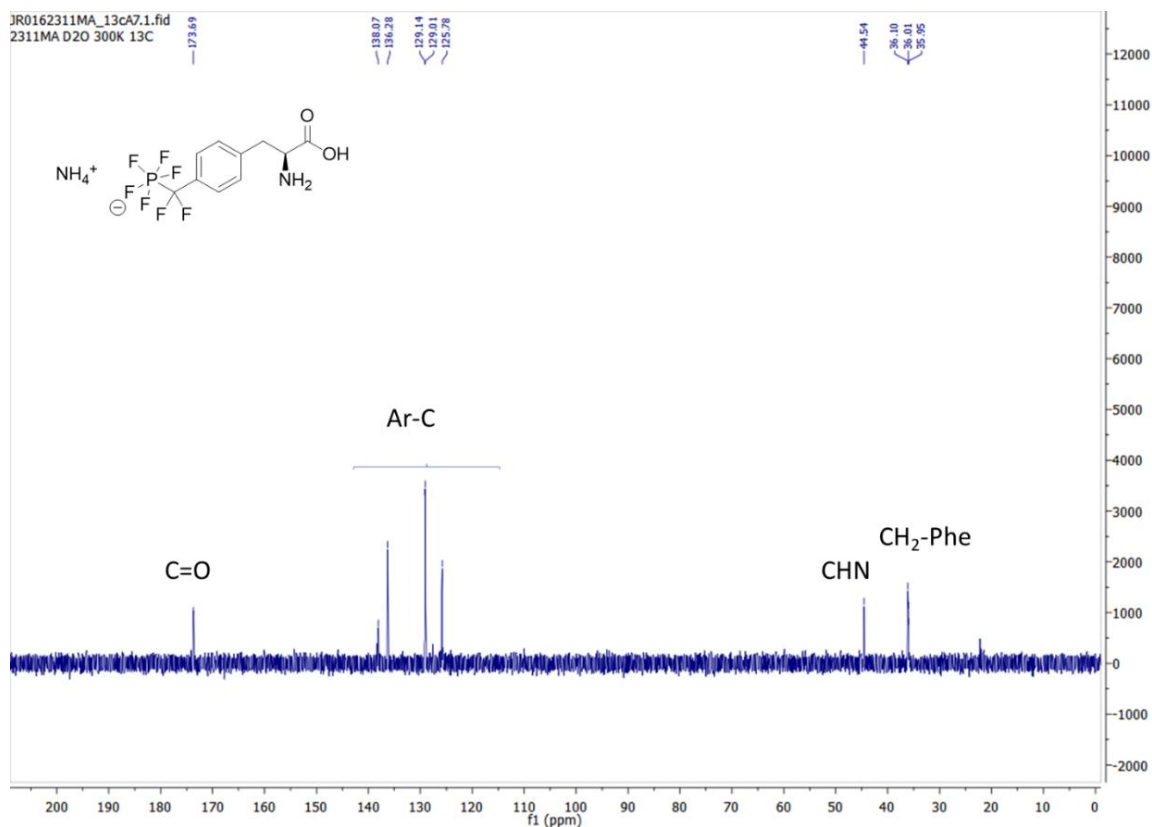


Figure 79 ¹³C NMR spectrum (176 MHz, D₂O) of 15

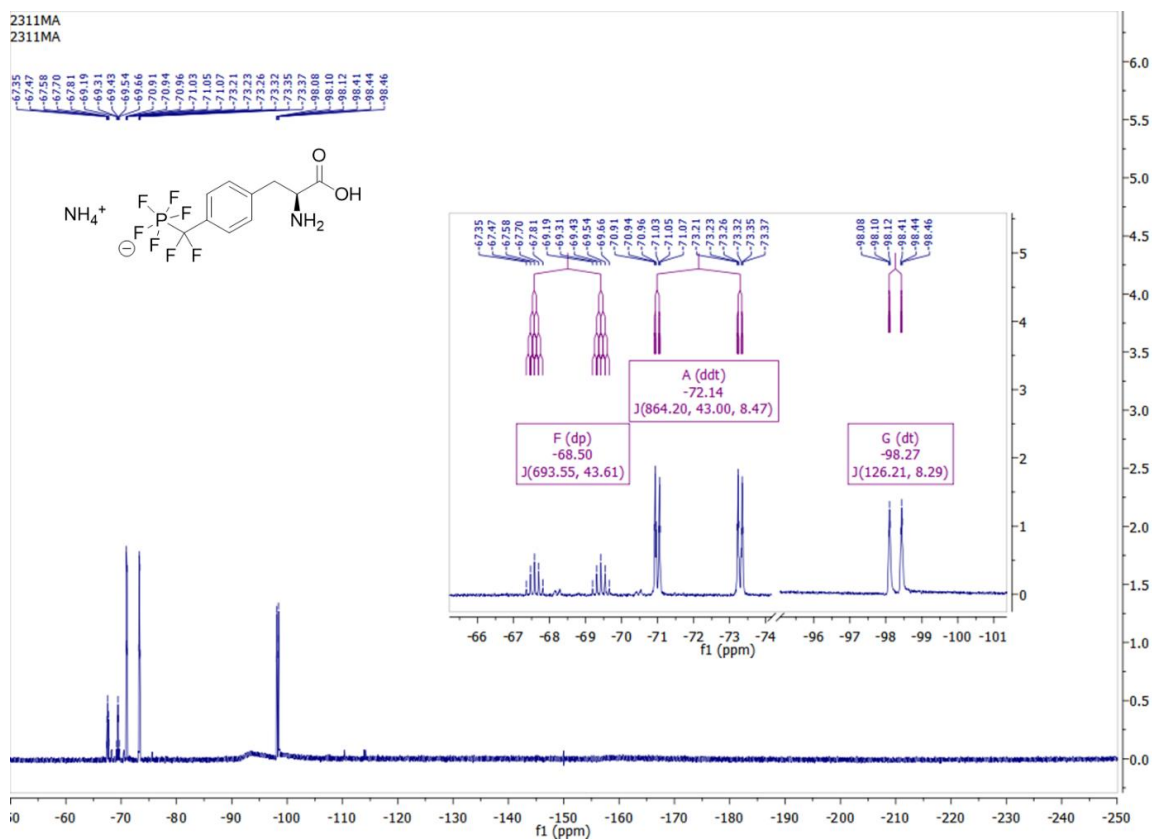


Figure 80 ¹⁹F NMR spectrum (376 MHz, D₂O) of 15

NMR spectra

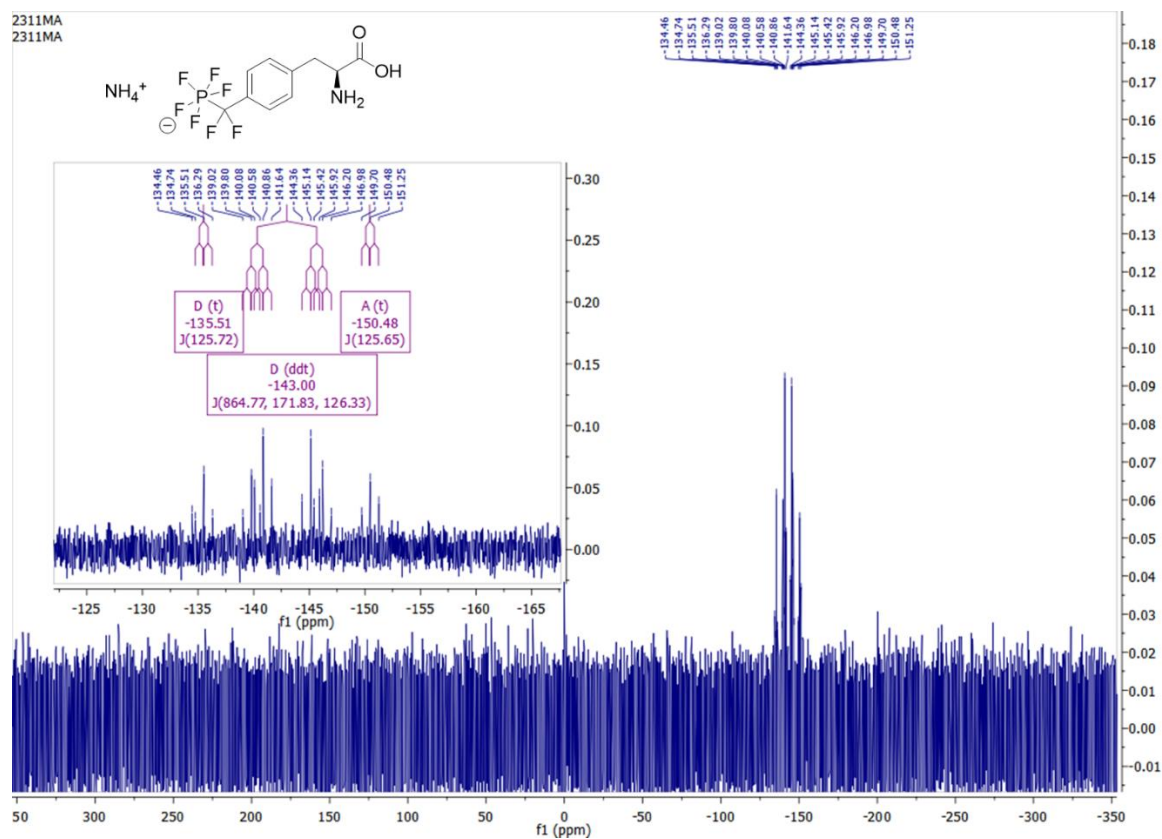


Figure 81 ^{31}P NMR spectrum (161 MHz, D_2O) of **15**

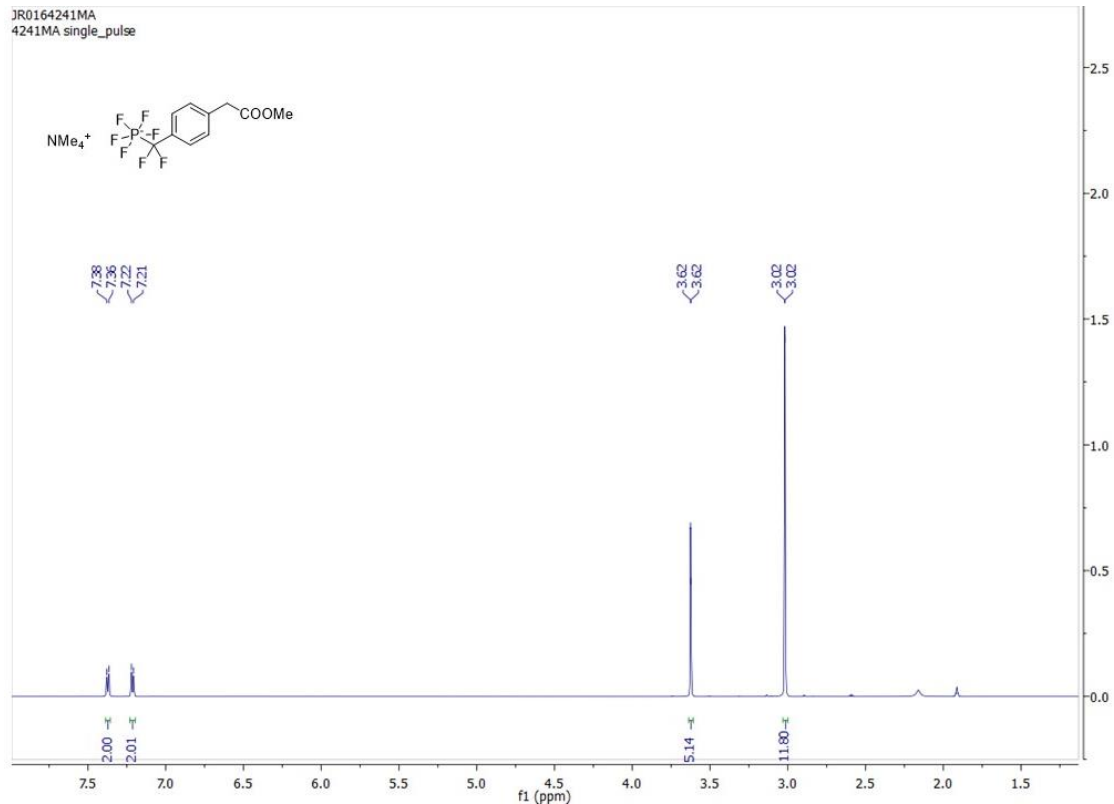


Figure 82 ^1H NMR spectrum (600 MHz, ACN-d_3) of **12**

NMR spectra

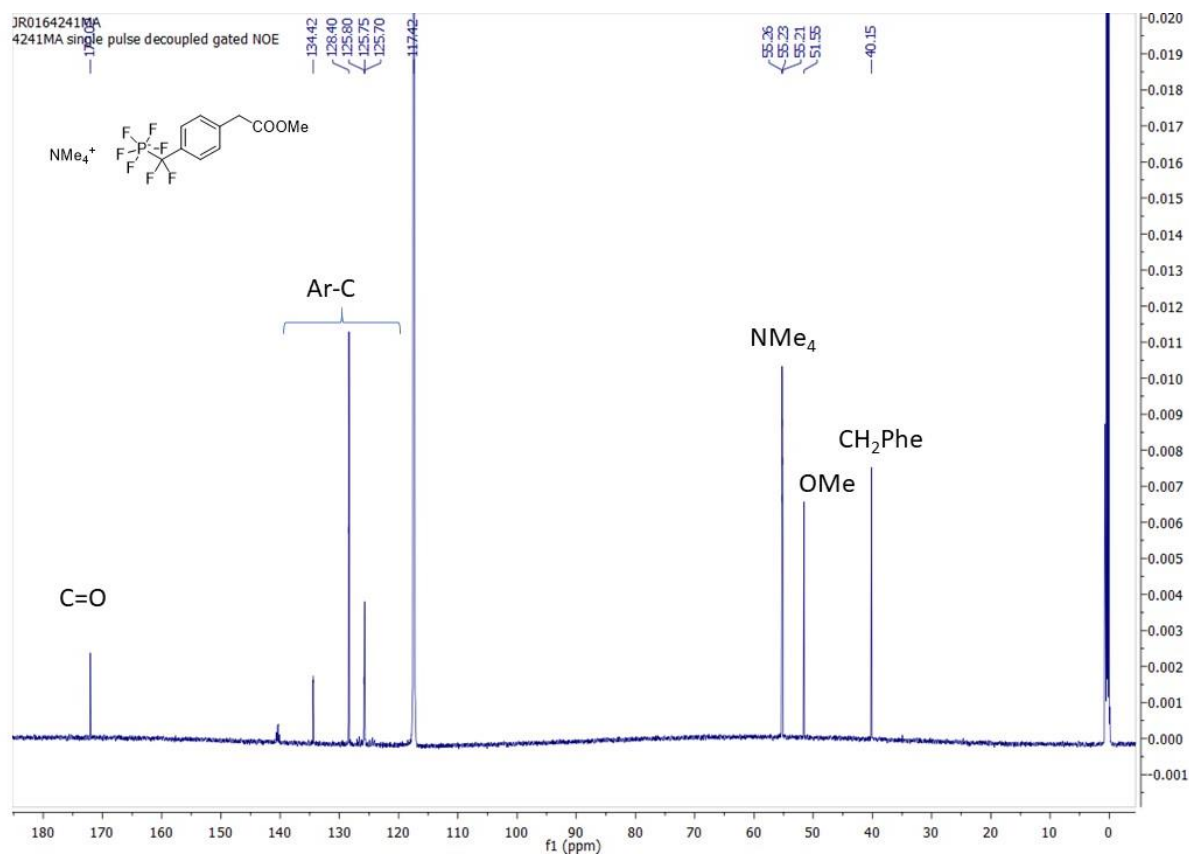


Figure 83 ¹³C NMR spectrum (151 MHz, ACN-d₃) of **12**

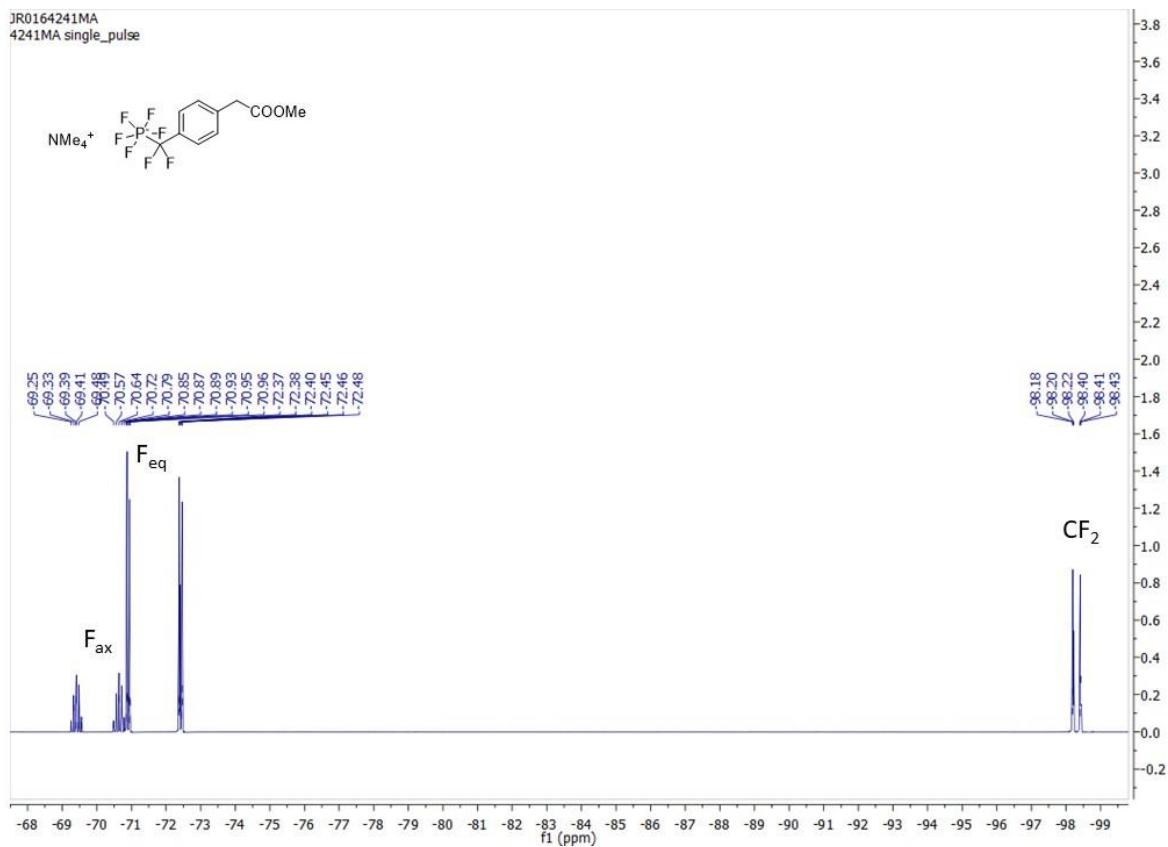


Figure 84 ¹⁹F NMR spectrum (565 MHz, ACN-d₃) of **12**

NMR spectra

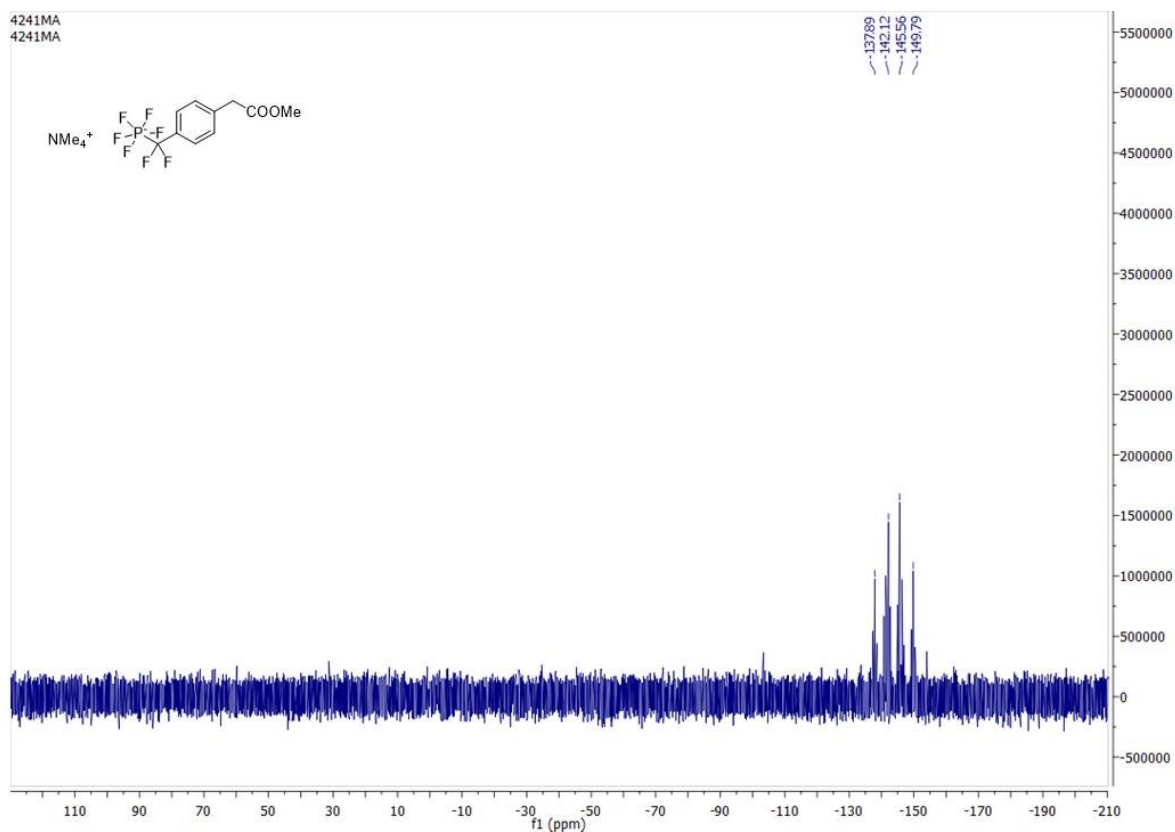


Figure 85 ^{31}P NMR spectrum (243 MHz, ACN-d_3) of **12**

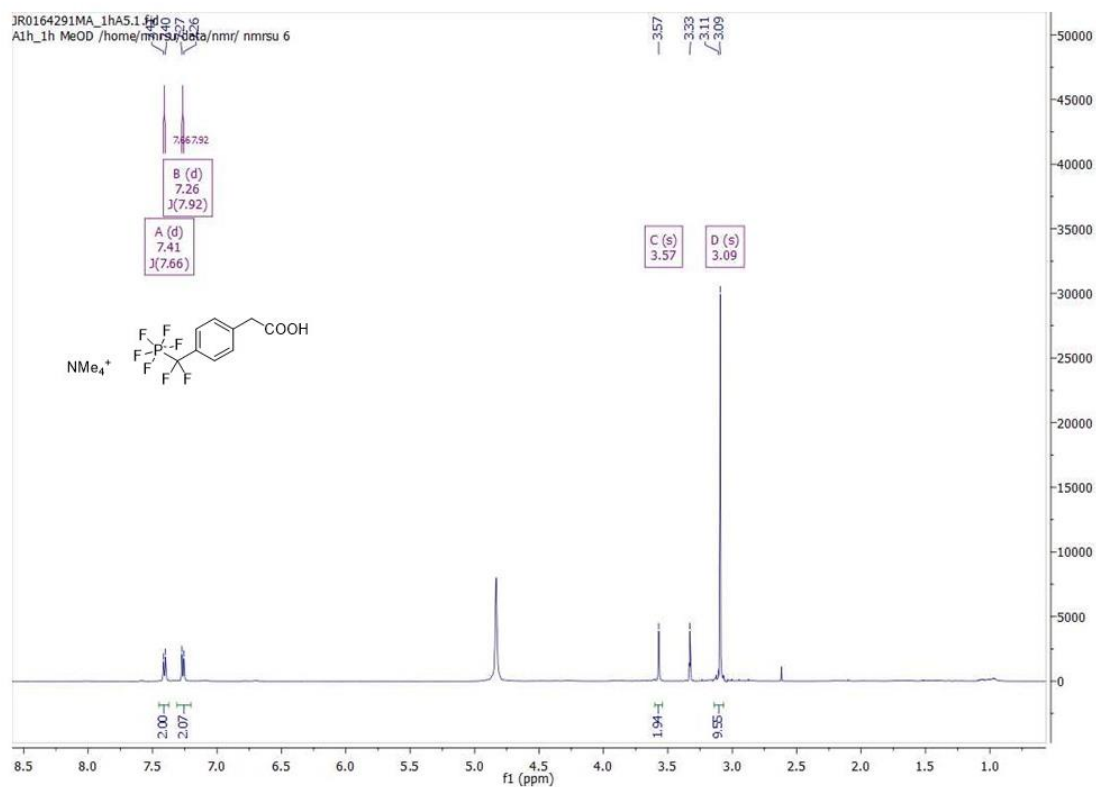


Figure 86 ^1H NMR spectrum (500 MHz, MeOD) of **14**

NMR spectra

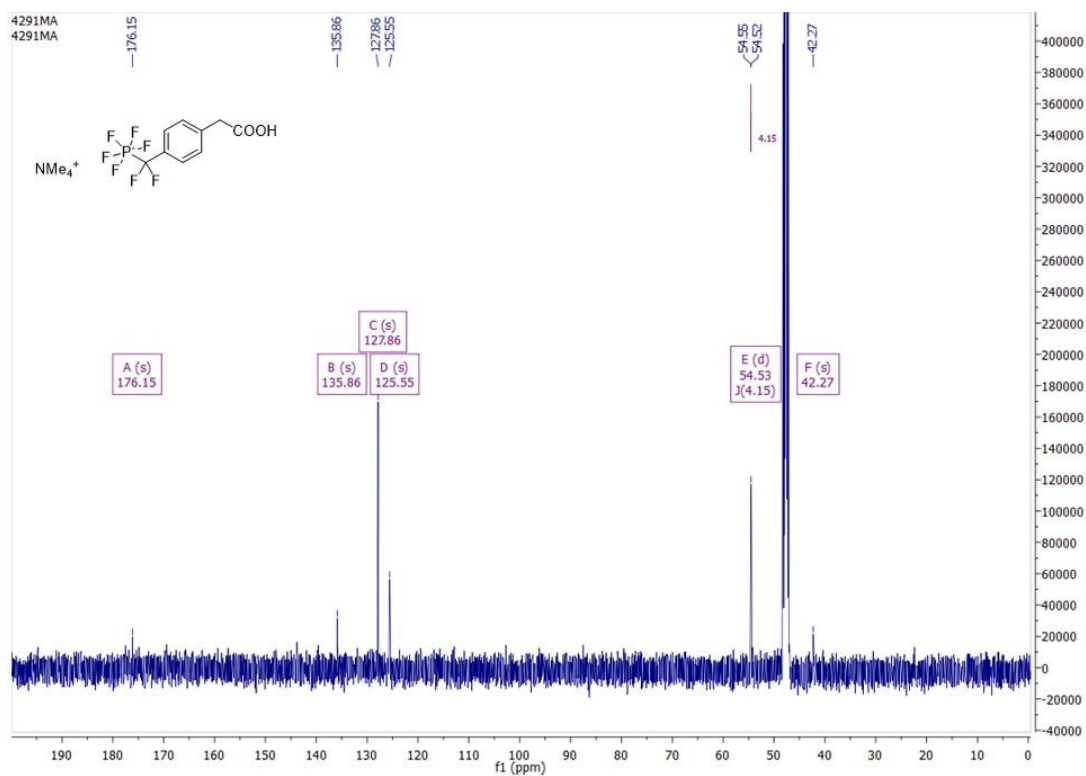


Figure 87 ^{13}C NMR spectrum (125 MHz, MeOD) of **14**

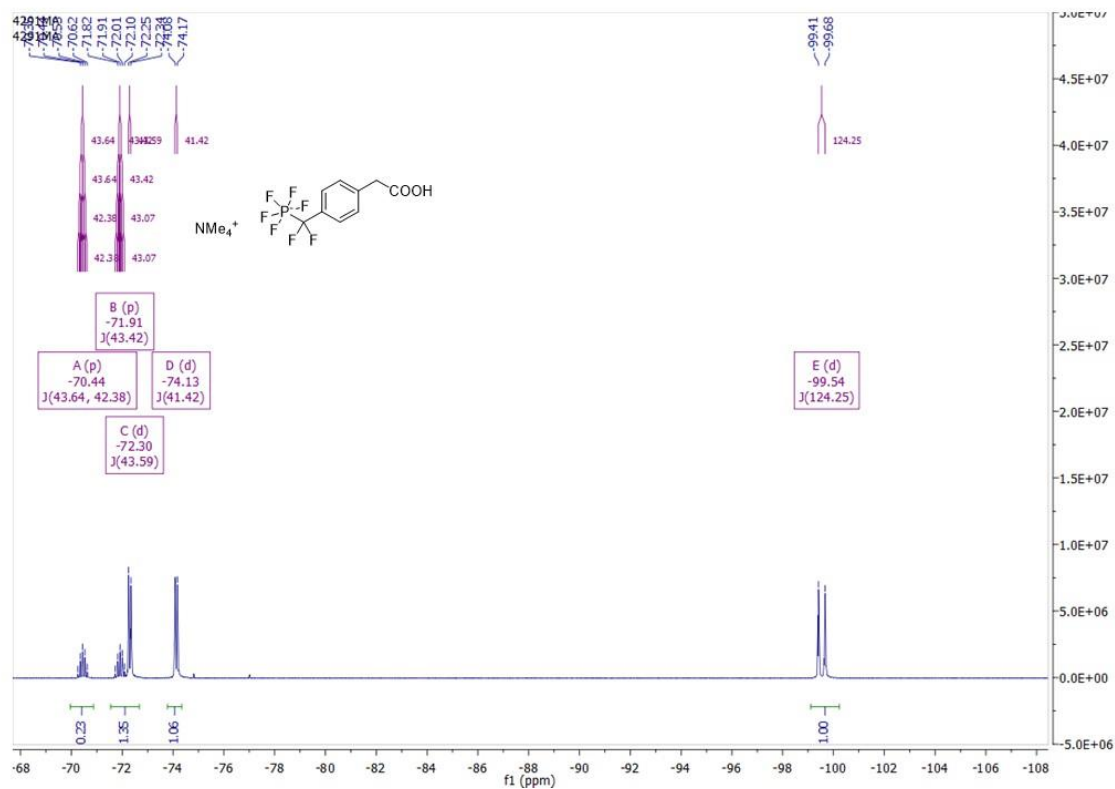


Figure 88 ^{19}F -NMR spectrum (470 MHz, MeOD) of **14**

NMR spectra

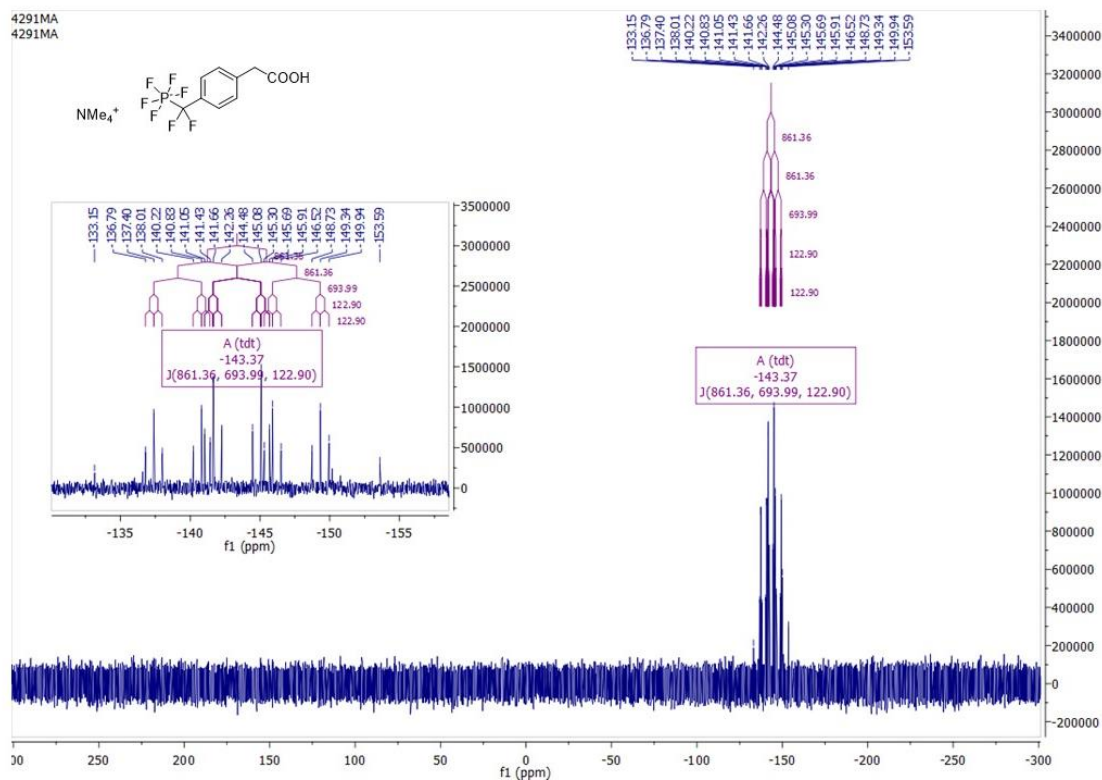


Figure 89 ³¹P-NMR spectrum (202 MHz, MeOD) of 14

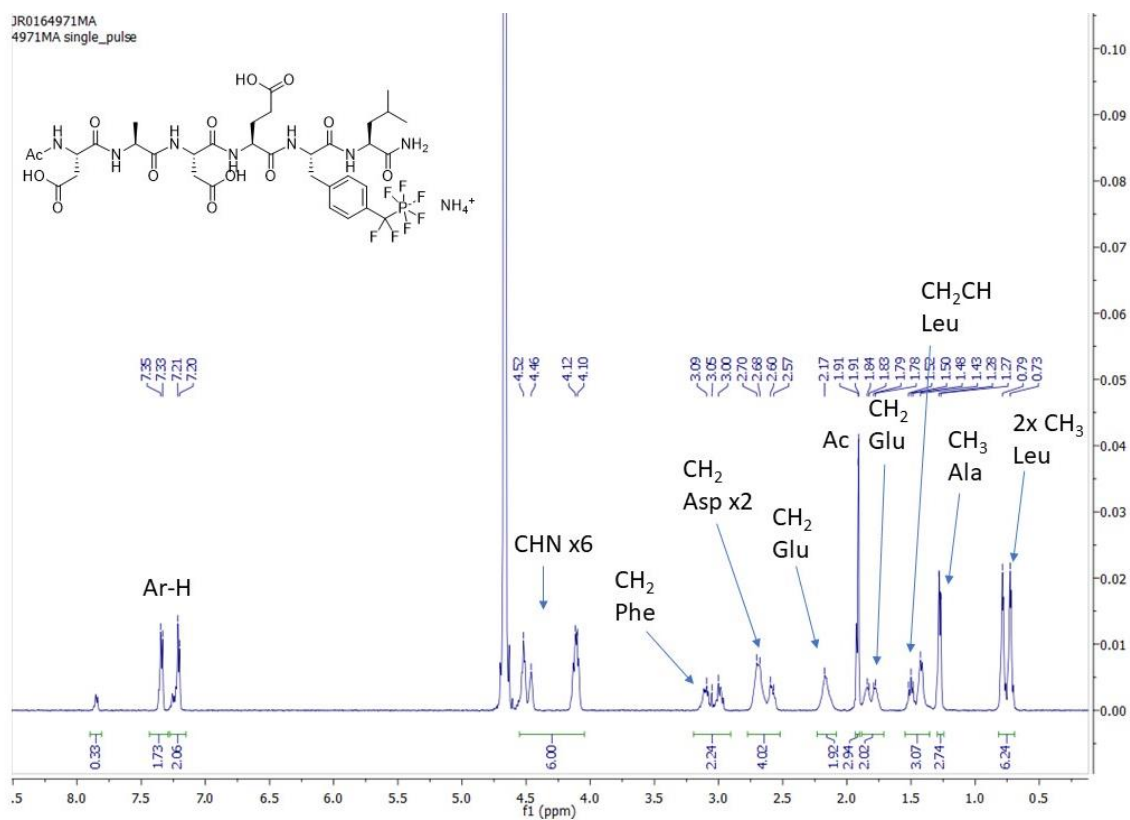


Figure 90 ¹H-NMR spectrum (600 MHz, D₂O) of 19

NMR spectra

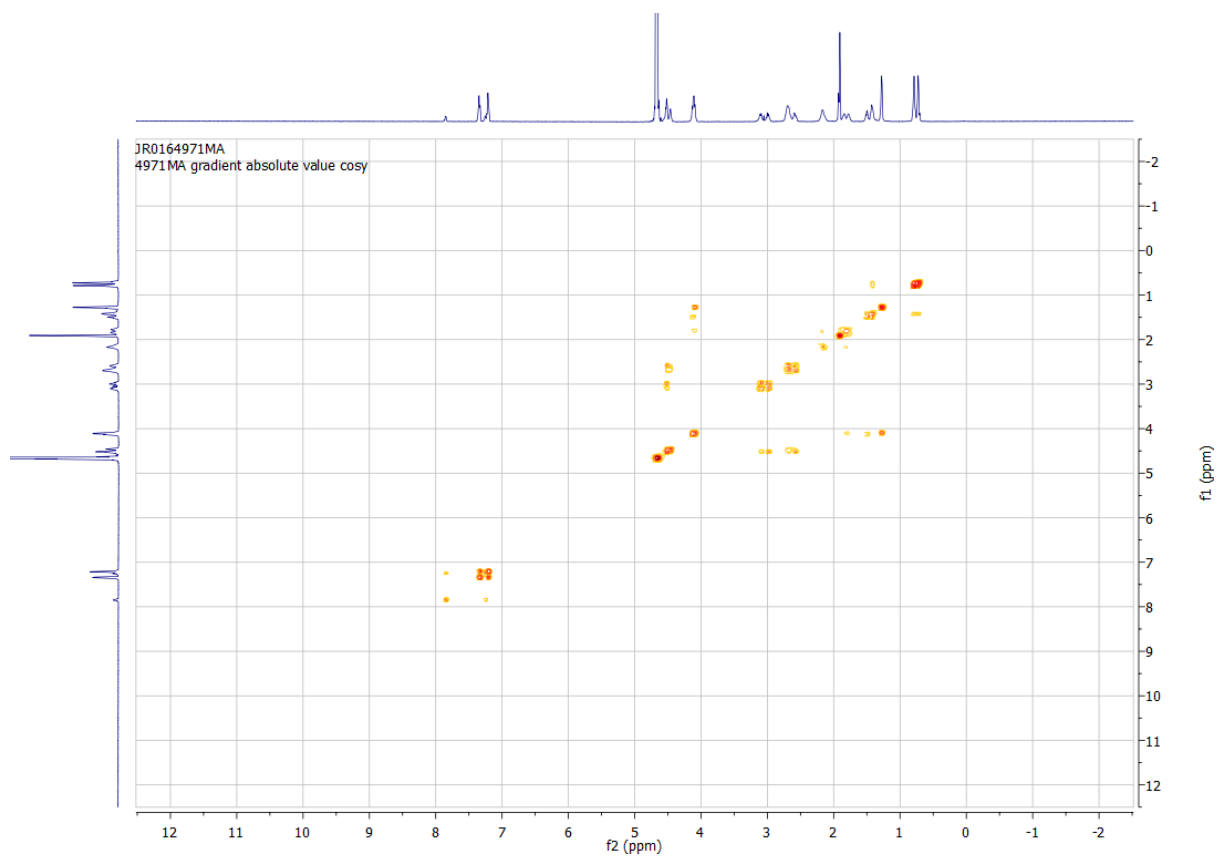


Figure 91 COSY spectrum in D_2O of **19**

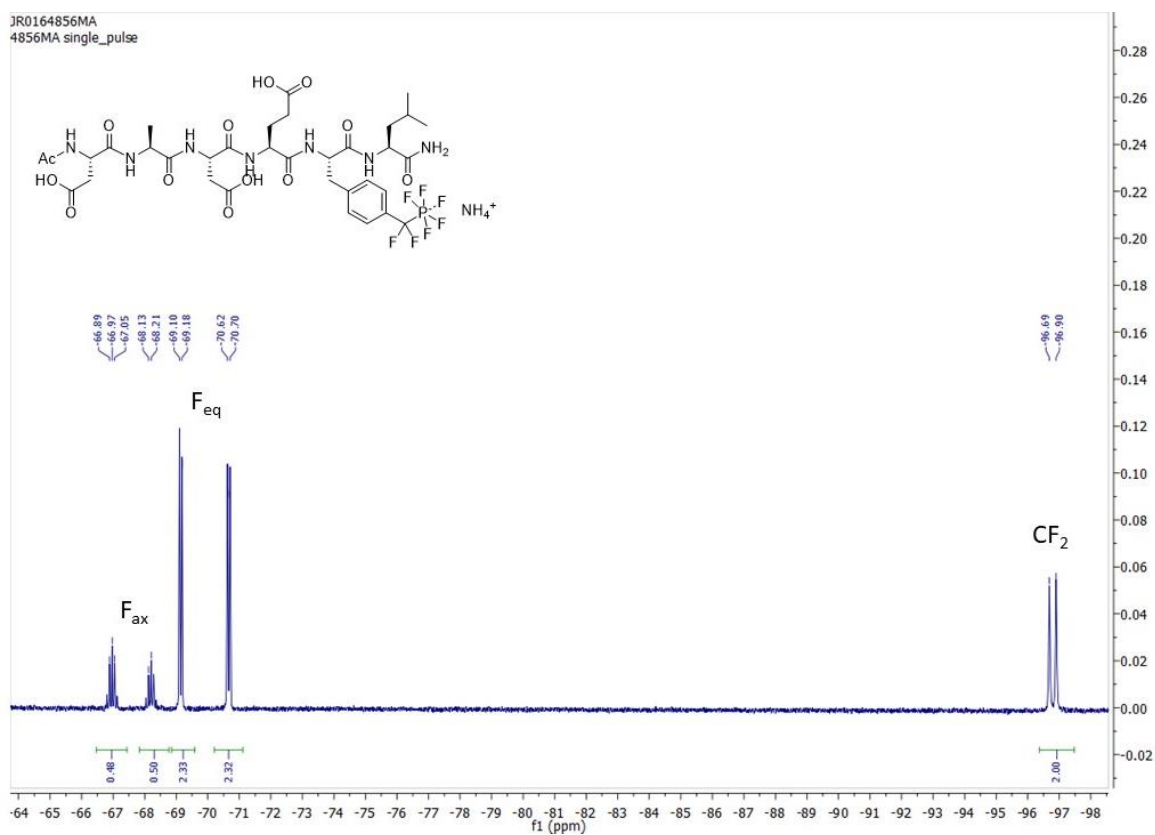


Figure 92 ^{19}F NMR spectrum (565 MHz, D_2O) of **20**

NMR spectra

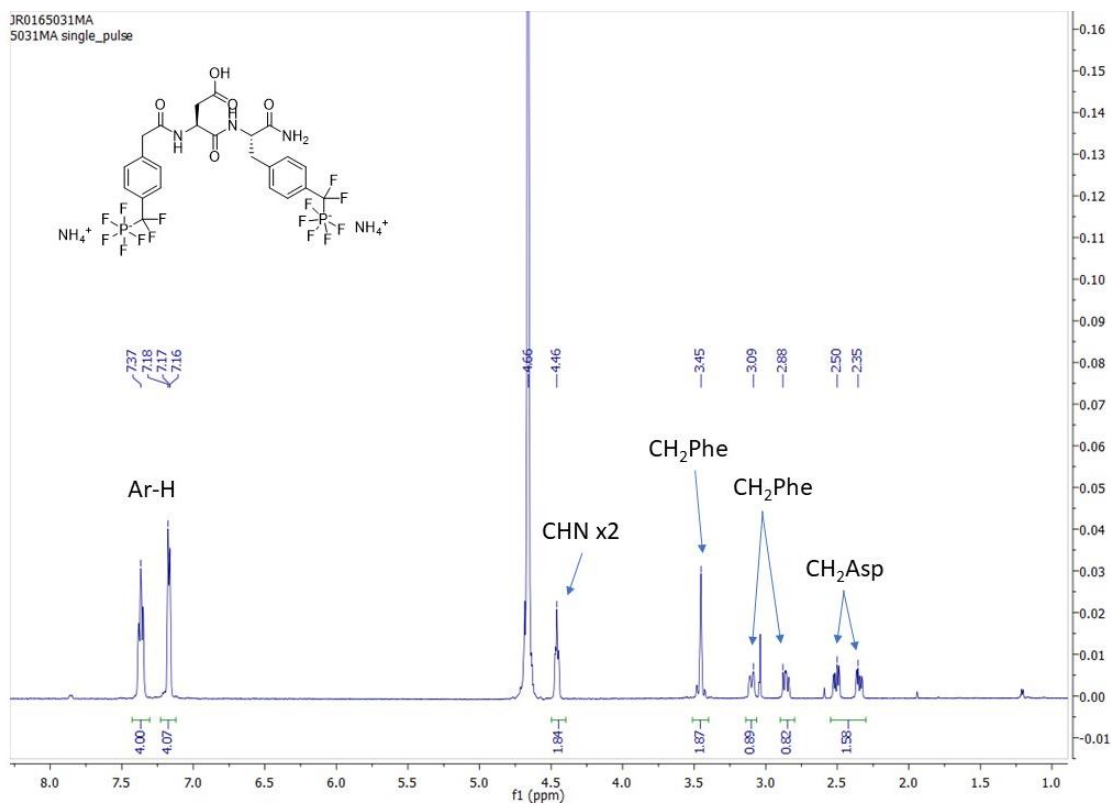


Figure 93 ¹H NMR spectrum (600 MHz, D₂O) of **20**

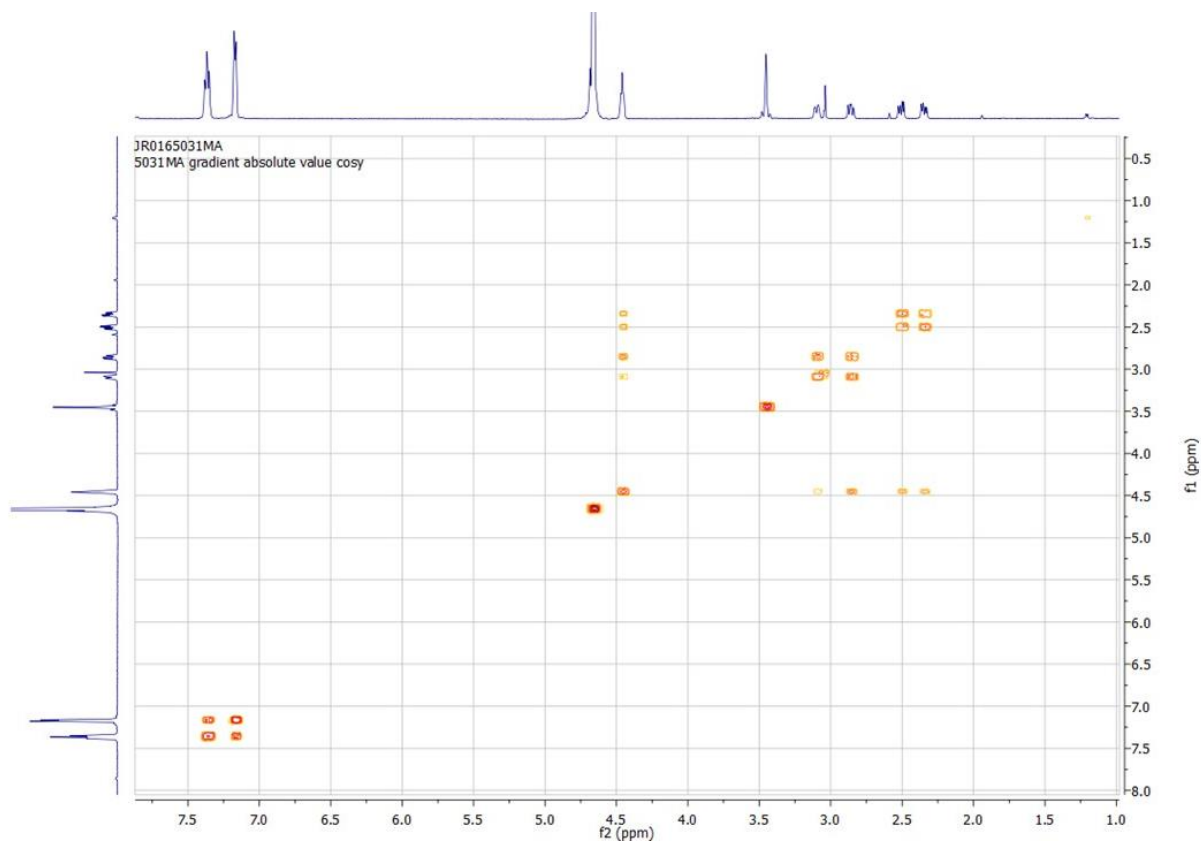


Figure 94 COSY spectrum in D₂O of **20**

NMR spectra

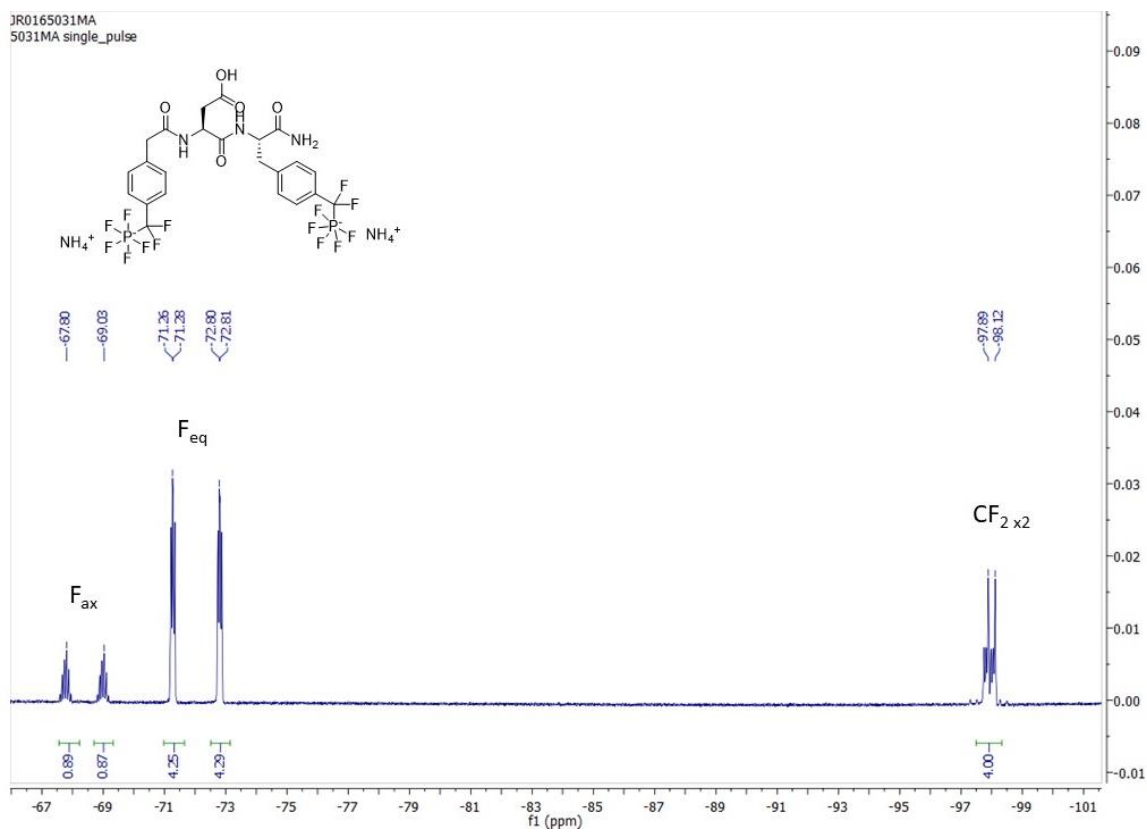


Figure 95 ^{19}F NMR spectrum (565 MHz, D_2O) of **20**

8 References

- [1] P. A. Levene, C. L. Alsberg, *Journal of Biological Chemistry* **1906**, *2*, 127-133.
- [2] F. A. Lipmann, P. A. Levene, *Journal of Biological Chemistry* **1932**, *98*, 109-114.
- [3] G. Burnett, E. P. Kennedy, *Journal of Biological Chemistry* **1954**, *211*, 969-980.
- [4] E. H. Fischer, E. G. Krebs, *Journal of Biological Chemistry* **1955**, *216*, 121-132.
- [5] E. J. Needham, B. L. Parker, T. Burykin, D. E. James, S. J. Humphrey, *Sci. Signal.* **2019**, *12*.
- [6] T. Nosaka, T. Kawashima, K. Misawa, K. Ikuta, A. L. Mui, T. Kitamura, *EMBO J* **1999**, *18*, 4754-4765.
- [7] S. Loughrey Chen, M. J. Huddleston, W. Shou, R. J. Deshaies, R. S. Annan, S. A. Carr, *Mol. Cell. Proteomics* **2002**, *1*, 186-196.
- [8] R. Dajani, E. Fraser, S. M. Roe, N. Young, V. Good, T. C. Dale, L. H. Pearl, *Cell* **2001**, *105*, 721-732.
- [9] a) L. M. Iakoucheva, P. Radivojac, C. J. Brown, T. R. O'Connor, J. G. Sikes, Z. Obradovic, A. K. Dunker, *Nucleic acids research* **2004**, *32*, 1037-1049; b) C. R. Landry, E. D. Levy, S. W. Michnick, *Trends in genetics : TIG* **2009**, *25*, 193-197.
- [10] a) S. J. Humphrey, D. E. James, M. Mann, *Trends Endocrinol. Metab.* **2015**, *26*, 676-687; b) F. Ardito, M. Giuliani, D. Perrone, G. Troiano, L. Lo Muzio, *Int J Mol Med* **2017**, *40*, 271-280.
- [11] G. Hardman, S. Perkins, P. J. Brownridge, C. J. Clarke, D. P. Byrne, A. E. Campbell, A. Kalyuzhnyy, A. Myall, P. A. Eyers, A. R. Jones, C. E. Eyers, *EMBO J* **2019**, *38*, e100847.
- [12] P. Cohen, *Trends in Biochemical Sciences* **2000**, *25*, 596-601.
- [13] T. Hunter, M. A. Hutchinson, W. Eckhart, *Proc. Natl. Acad. Sci. U S A* **1978**, *75*, 5917-5921.
- [14] P. J. Bertics, G. N. Gill, *J Biol Chem* **1985**, *260*, 14642-14647.
- [15] T. Pawson, *Nature* **1995**, *373*, 573-580.

References

- [16] a) W. A. Lim, T. Pawson, *Cell* **2010**, *142*, 661-667; b) L. Li, C. Tibiche, C. Fu, T. Kaneko, M. F. Moran, M. R. Schiller, S. S. Li, E. Wang, *Genome Res.* **2012**, *22*, 1222-1230.
- [17] B. J. Mayer, *FEBS Lett.* **2012**, *586*, 2575-2579.
- [18] G. Manning, D. B. Whyte, R. Martinez, T. Hunter, S. Sudarsanam, *Science* **2002**, *298*, 1912-1934.
- [19] a) B. A. Liu, K. Jablonowski, M. Raina, M. Arce, T. Pawson, P. D. Nash, *Mol. Cell* **2006**, *22*, 851-868; b) B. A. Liu, E. Shah, K. Jablonowski, A. Stergachis, B. Engelmann, P. D. Nash, *Sci. Signal.* **2011**, *4*, ra83.
- [20] C. S. Tan, B. Bodenmiller, A. Pasculescu, M. Jovanovic, M. O. Hengartner, C. Jorgensen, G. D. Bader, R. Aebersold, T. Pawson, R. Linding, *Sci. Signal.* **2009**, *2*, ra39.
- [21] T. Pawson, P. Nash, *Science* **2003**, *300*, 445-452.
- [22] I. Sadowski, J. C. Stone, T. Pawson, *Molecular and Cellular Biology* **1986**, *6*, 4396-4408.
- [23] G. Waksman, D. Kominos, S. C. Robertson, N. Pant, D. Baltimore, R. B. Birge, D. Cowburn, H. Hanafusa, B. J. Mayer, M. Overduin, M. D. Resh, C. B. Rios, L. Silverman, J. Kuriyan, *Nature* **1992**, *358*, 646-653.
- [24] T. Kaneko, R. Joshi, S. M. Feller, S. S. Li, *Cell Commun. Signal.* **2012**, *10*, 32.
- [25] T. Pawson, G. D. Gish, P. Nash, *Trends Cell Biol* **2001**, *11*, 504-511.
- [26] a) W.-Q. Wang, J.-P. Sun, Z.-Y. Zhang, *Current Topics in Medicinal Chemistry* **2003**, *3*, 739-748; b) F. Sacco, L. Perfetto, L. Castagnoli, G. Cesareni, *FEBS letters* **2012**, *586*, 2732-2739.
- [27] A. Alonso, J. Sasin, N. Bottini, I. Friedberg, I. Friedberg, A. Osterman, A. Godzik, T. Hunter, J. Dixon, T. Mustelin, *Cell* **2004**, *117*, 699-711.
- [28] N. K. Tonks, *Nat. Rev. Mol. Cell Biol.* **2006**, *7*, 833-846.
- [29] N. K. Tonks, C. D. Diltz, E. H. Fischer, *J. Biol. Chem.* **1988**, *263*, 6731-6737.
- [30] a) J. V. Frangioni, A. Oda, M. Smith, E. W. Salzman, B. G. Neel, *EMBO J* **1993**, *12*, 4843-4856; b) T. A. Woodford-Thomas, J. D. Rhodes, J. E. Dixon, *J. Cell. Biol.* **1992**, *117*, 401-414.
- [31] D. Barford, A. J. Flint, N. K. Tonks, *Science* **1994**, *263*, 1397-1404.
- [32] S. C. Yip, S. Saha, J. Chernoff, *Trends Biochem Sci* **2010**, *35*, 442-449.
- [33] T. Jin, H. Yu, X. F. Huang, *Sci. Rep.* **2016**, *6*, 20766.

References

- [34] a) T. O. Johnson, J. Ermolieff, M. R. Jirousek, *Nat. Rev. Drug Discov.* **2002**, *1*, 696-709; b) C. Wiesmann, K. J. Barr, J. Kung, J. Zhu, D. A. Erlanson, W. Shen, B. J. Fahr, M. Zhong, L. Taylor, M. Randal, R. S. McDowell, S. K. Hansen, *Nat. Struct. Mol. Biol.* **2004**, *11*, 730-737.
- [35] J. N. Andersen, O. H. Mortensen, G. H. Peters, P. G. Drake, L. F. Iversen, O. H. Olsen, P. G. Jansen, H. S. Andersen, N. K. Tonks, N. P. Moller, *Mol. Cell. Biol.* **2001**, *21*, 7117-7136.
- [36] S. J. Teague, *Nat. Rev. Drug Discov.* **2003**, *2*, 527-541.
- [37] A. P. Kumar, M. N. Nguyen, C. Verma, S. Lukman, *Proteins* **2018**, *86*, 301-321.
- [38] a) N. K. Tonks, *FEBS Lett* **2003**, *546*, 140-148; b) Z. Y. Zhang, D. Maclean, D. J. McNamara, T. K. Sawyer, J. E. Dixon, *Biochemistry* **1994**, *33*, 2285-2290.
- [39] T. A. Brandao, A. C. Hengge, S. J. Johnson, *J Biol Chem* **2010**, *285*, 15874-15883.
- [40] a) F. G. Haj, P. J. Verveer, A. Squire, B. G. Neel, P. I. Bastiaens, *Science* **2002**, *295*, 1708-1711; b) Y. Romsicki, M. Reece, J. Y. Gauthier, E. Asante-Appiah, B. P. Kennedy, *J Biol Chem* **2004**, *279*, 12868-12875.
- [41] N. Boute, S. Boubekour, D. Lacasa, T. Issad, *EMBO reports* **2003**, *4*, 313-319.
- [42] I. Anderie, I. Schulz, A. Schmid, *Cellular signalling* **2007**, *19*, 582-592.
- [43] a) J. H. Choi, H. S. Kim, S. H. Kim, Y. R. Yang, Y. S. Bae, J. S. Chang, H. M. Kwon, S. H. Ryu, P. G. Suh, *Nat Cell Biol* **2006**, *8*, 1389-1397; b) J. Balsamo, T. Leung, H. Ernst, M. K. Zanin, S. Hoffman, J. Lilien, *Journal of Cell Biology* **1996**, *134*, 801-813; c) C. O. Arregui, J. Balsamo, J. Lilien, *J Cell Biol* **1998**, *143*, 861-873.
- [44] M. Elchebly, P. Payette, E. Michaliszyn, W. Cromlish, S. Collins, A. L. Loy, D. Normandin, A. Cheng, J. Himms-Hagen, C. C. Chan, C. Ramachandran, M. J. Gresser, M. L. Tremblay, B. P. Kennedy, *Science* **1999**, *283*, 1544-1548.
- [45] S. Zhang, Z. Y. Zhang, *Drug Discov Today* **2007**, *12*, 373-381.
- [46] L. Xie, S. Y. Lee, J. N. Andersen, S. Waters, K. Shen, X. L. Guo, N. P. Moller, J. M. Olefsky, D. S. Lawrence, Z. Y. Zhang, *Biochemistry* **2003**, *42*, 12792-12804.

References

- [47] C. S. Jiang, L. F. Liang, Y. W. Guo, *Acta Pharmacol. Sin.* **2012**, *33*, 1217-1245.
- [48] a) Y. Akasaki, G. Liu, H. H. Matundan, H. Ng, X. Yuan, Z. Zeng, K. L. Black, J. S. Yu, *J. Biol. Chem.* **2006**, *281*, 6165-6174; b) F. Gu, D. T. Nguyen, M. Stuiblé, N. Dube, M. L. Tremblay, E. Chevet, *J. Biol. Chem.* **2004**, *279*, 49689-49693; c) A. Gonzalez-Rodriguez, O. Escribano, J. Alba, C. M. Rondinone, M. Benito, A. M. Valverde, *J. Cell. Physiol.* **2007**, *212*, 76-88; d) V. Sangwan, G. N. Paliouras, A. Cheng, N. Dube, M. L. Tremblay, M. Park, *J. Biol. Chem.* **2006**, *281*, 221-228.
- [49] S. Zhu, J. D. Bjorge, D. J. Fujita, *Cancer Res.* **2007**, *67*, 10129-10137.
- [50] C. L. Cortesio, K. T. Chan, B. J. Perrin, N. O. Burton, S. Zhang, Z. Y. Zhang, A. Huttenlocher, *J. Cell Biol.* **2008**, *180*, 957-971.
- [51] R. J. Eddy, M. D. Weidmann, V. P. Sharma, J. S. Condeelis, *Trends Cell Biol* **2017**, *27*, 595-607.
- [52] L. V. Ravichandran, H. Chen, Y. Li, M. J. Quon, *Mol. Endocrinol.* **2001**, *15*, 1768-1780.
- [53] D. Bandyopadhyay, A. Kusari, K. A. Kenner, F. Liu, J. Chernoff, T. A. Gustafson, J. Kusari, *J. Biol. Chem.* **1997**, *272*, 1639-1645.
- [54] S. R. Lee, K. S. Kwon, S. R. Kim, S. G. Rhee, *J. Biol. Chem.* **1998**, *273*, 15366-15372.
- [55] R. L. van Montfort, M. Congreve, D. Tisi, R. Carr, H. Jhoti, *Nature* **2003**, *423*, 773-777.
- [56] A. Salmeen, J. N. Andersen, M. P. Myers, T. C. Meng, J. A. Hinks, N. K. Tonks, D. Barford, *Nature* **2003**, *423*, 769-773.
- [57] R. T. Hay, *Mol. Cell* **2005**, *18*, 1-12.
- [58] S. Dadke, S. Cotteret, S. C. Yip, Z. M. Jaffer, F. Haj, A. Ivanov, F. Rauscher, 3rd, K. Shuai, T. Ng, B. G. Neel, J. Chernoff, *Nat. Cell Biol.* **2007**, *9*, 80-85.
- [59] S. M. Kuchay, N. Kim, E. A. Grunz, W. P. Fay, A. H. Chishti, *Mol. Cell. Biol.* **2007**, *27*, 6038-6052.
- [60] J. B. Bliska, K. L. Guan, J. E. Dixon, S. Falkow, *Proc. Natl. Acad. Sci. U S A* **1991**, *88*, 1187-1191.

References

- [61] a) S. Shrestha, B. R. Bhattarai, H. Cho, J. K. Choi, H. Cho, *Bioorg. Med. Chem. Lett.* **2007**, *17*, 2728-2730; b) G. S. Kumar, R. Page, W. Peti, *PLoS One* **2020**, *15*, e0240044.
- [62] M. N. Rao, A. E. Shinnar, L. A. Noecker, T. L. Chao, B. Feibush, B. Snyder, I. Sharkansky, A. Sarkahian, X. Zhang, S. R. Jones, W. A. Kinney, M. Zasloff, *J. Nat. Prod.* **2000**, *63*, 631-635.
- [63] J. George, *Philadelphia Business Journal* **2009**, <https://www.bizjournals.com/philadelphia/stories/2009/2004/2027/daily2031.html>.
- [64] a) A. M. Smith, K. K. Maguire-Nguyen, T. A. Rando, M. A. Zasloff, K. B. Strange, V. P. Yin, *NPJ Regen. Med.* **2017**, *2*, 4; b) N. Krishnan, K. F. Konidaris, G. Gasser, N. K. Tonks, *J. Biol. Chem.* **2018**, *293*, 1517-1525.
- [65] S. M. Domchek, K. R. Auger, S. Chatterjee, T. R. Burke, Jr., S. E. Shoelson, *Biochemistry* **1992**, *31*, 9865-9870.
- [66] a) T. R. Burke, M. S. Smyth, M. Nomizu, A. Otaka, P. P. Roller, *Journal of Organic Chemistry* **1993**, *58*, 1336-1340; b) T. R. Burke, Jr., M. S. Smyth, A. Otaka, M. Nomizu, P. P. Roller, G. Wolf, R. Case, S. E. Shoelson, *Biochemistry* **1994**, *33*, 6490-6494; c) T. R. Burke, Jr., *Curr. Top. Med. Chem.* **2006**, *6*, 1465-1471.
- [67] M. S. Smyth, H. Ford, T. R. Burke, *Tetrahedron Letters* **1992**, *33*, 4137-4140.
- [68] M. Akamatsu, P. P. Roller, L. Chen, Z.-Y. Zhang, B. Ye, T. R. Burke, *Bioorganic & Medicinal Chemistry* **1997**, *5*, 157-163.
- [69] a) J. Montserat, L. Chen, D. S. Lawrence, Z. Y. Zhang, *J. Biol. Chem.* **1996**, *271*, 7868-7872; b) Z. Y. Zhang, A. M. Thieme-Sefler, D. Maclean, D. J. McNamara, E. M. Dobrusin, T. K. Sawyer, J. E. Dixon, *Proc Natl Acad Sci U S A* **1993**, *90*, 4446-4450.
- [70] Y. A. Puius, Y. Zhao, M. Sullivan, D. S. Lawrence, S. C. Almo, Z. Y. Zhang, *Proc. Natl. Acad. Sci. U S A* **1997**, *94*, 13420-13425.
- [71] K. Shen, Y. F. Keng, L. Wu, X. L. Guo, D. S. Lawrence, Z. Y. Zhang, *J Biol Chem* **2001**, *276*, 47311-47319.
- [72] I. G. Boutselis, X. Yu, Z. Y. Zhang, R. F. Borch, *J. Med. Chem.* **2007**, *50*, 856-864.
- [73] Y. T. Chen, J. Xie, C. T. Seto, *J. Org. Chem.* **2003**, *68*, 4123-4125.

References

- [74] C. Leung, J. Grzyb, J. Lee, N. Meyer, G. Hum, C. Jia, S. Liu, S. D. Taylor, *Bioorganic & Medicinal Chemistry* **2002**, *10*, 2309-2323.
- [75] G. Huyer, J. Kelly, J. Moffat, R. Zamboni, Z. Jia, M. J. Gresser, C. Ramachandran, *Anal. Biochem.* **1998**, *258*, 19-30.
- [76] J. E. Bleasdale, D. Ogg, B. J. Palazuk, C. S. Jacob, M. L. Swanson, X. Y. Wang, D. P. Thompson, R. A. Conradi, W. R. Mathews, A. L. Laborde, C. W. Stuchly, A. Heijbel, K. Bergdahl, C. A. Bannow, C. W. Smith, C. Svensson, C. Liljebris, H. J. Schostarez, P. D. May, F. C. Stevens, S. D. Larsen, *Biochemistry* **2001**, *40*, 5642-5654.
- [77] a) L. F. Iversen, H. S. Andersen, S. Branner, S. B. Mortensen, G. H. Peters, K. Norris, O. H. Olsen, C. B. Jeppesen, B. F. Lundt, W. Ripka, K. B. Moller, N. P. Moller, *J. Biol. Chem.* **2000**, *275*, 10300-10307; b) L. F. Iversen, H. S. Andersen, K. B. Moller, O. H. Olsen, G. H. Peters, S. Branner, S. B. Mortensen, T. K. Hansen, J. Lau, Y. Ge, D. D. Holsworth, M. J. Newman, N. P. Hundahl Moller, *Biochemistry* **2001**, *40*, 14812-14820.
- [78] a) J. A. Nettleton, R. Katz, *J. Am. Diet. Assoc.* **2005**, *105*, 428-440; b) T. R. Koves, J. R. Ussher, R. C. Noland, D. Slentz, M. Mosedale, O. Ilkayeva, J. Bain, R. Stevens, J. R. Dyck, C. B. Newgard, G. D. Lopaschuk, D. M. Muoio, *Cell. Metab.* **2008**, *7*, 45-56; c) D. N. Obanda, W. T. Cefalu, *J. Nutr. Biochem.* **2013**, *24*, 1529-1537.
- [79] D. Steinmann, R. R. Baumgartner, E. H. Heiss, S. Bartenstein, A. G. Atanasov, V. M. Dirsch, M. Ganzera, H. Stuppner, *Planta Med.* **2012**, *78*, 219-224.
- [80] a) Y. Xu, S. Ventura, *J. Ethnopharmacol.* **2010**, *127*, 196-199; b) R. Ghosh, H. Graham, P. Rivas, X. J. Tan, K. Crosby, S. Bhaskaran, J. Schoolfield, J. Banu, G. Fernandes, I. T. Yeh, A. P. Kumar, *Anticancer Res.* **2010**, *30*, 857-865.
- [81] E. Fremy, *Journal de Pharmacie et de Chimie* **1842**, *XII*, 757.
- [82] B. Na, P. H. Nguyen, B. T. Zhao, Q. H. Vo, B. S. Min, M. H. Woo, *Pharm. Biol.* **2016**, *54*, 474-480.
- [83] J. L. Li, L. X. Gao, F. W. Meng, C. L. Tang, R. J. Zhang, J. Y. Li, C. Luo, J. Li, W. M. Zhao, *Bioorg. Med. Chem. Lett.* **2015**, *25*, 2028-2032.

References

- [84] Y. Wang, X. Y. Shang, S. J. Wang, S. Y. Mo, S. Li, Y. C. Yang, F. Ye, J. G. Shi, L. He, *J. Nat. Prod.* **2007**, *70*, 296-299.
- [85] Y. Feng, A. R. Carroll, R. Addepalli, G. A. Fechner, V. M. Avery, R. J. Quinn, *J Nat Prod* **2007**, *70*, 1790-1792.
- [86] a) M. Liu, P. E. Hansen, X. Lin, *Mar. Drugs* **2011**, *9*, 1273-1292; b) N. Xu, X. Fan, X. Yan, X. Li, R. Niu, C. K. Tseng, *Phytochemistry* **2003**, *62*, 1221-1224; c) D. Y. Shi, F. Xu, J. Li, S. J. Guo, H. Su, L. J. Han, *Zhongguo Zhong yao za zhi = Zhongguo zhongyao zazhi = China journal of Chinese materia medica* **2008**, *33*, 2238-2240.
- [87] a) Y. Wang, H. J. Yuk, J. Y. Kim, D. W. Kim, Y. H. Song, X. F. Tan, M. J. Curtis-Long, K. H. Park, *Bioorg. Med. Chem. Lett.* **2016**, *26*, 318-321; b) Z. Guo, X. Niu, T. Xiao, J. Lu, W. Li, Y. Zhao, *Journal of Functional Foods* **2015**, *14*, 324-336; c) J. Cai, L. Zhao, W. Tao, *Pharm. Biol.* **2015**, *53*, 1030-1034.
- [88] S. Ji, Z. Li, W. Song, Y. Wang, W. Liang, K. Li, S. Tang, Q. Wang, X. Qiao, D. Zhou, S. Yu, M. Ye, *J. Nat. Prod.* **2016**, *79*, 281-292.
- [89] B. T. Zhao, D. H. Nguyen, D. D. Le, J. S. Choi, B. S. Min, M. H. Woo, *Arch. Pharm. Res.* **2018**, *41*, 130-161.
- [90] a) A. Bondi, *The Journal of Physical Chemistry* **1964**, *68*, 441-451; b) M. Mantina, A. C. Chamberlin, R. Valero, C. J. Cramer, D. G. Truhlar, *J. Phys. Chem. A* **2009**, *113*, 5806-5812.
- [91] A. L. Allred, *Journal of Inorganic and Nuclear Chemistry* **1961**, *17*, 215-221.
- [92] Zumdahl, *Chemistry*, 5th ed.
- [93] F. H. Allen, O. Kennard, D. G. Watson, L. Brammer, A. G. Orpen, R. Taylor, *Journal of the Chemical Society, Perkin Transactions 2* **1987**.
- [94] D. E. Raines, F. Gioia, R. J. Claycomb, R. J. Stevens, *J. Pharmacol. Exp. Ther.* **2004**, *311*, 14-21.
- [95] J. Fried, E. F. Sabo, *J. Am. Chem. Soc.* **2002**, *76*, 1455-1456.
- [96] M. Inoue, Y. Sumii, N. Shibata, *ACS Omega* **2020**, *5*, 10633-10640.
- [97] H. Mei, J. Han, S. Fustero, M. Medio-Simon, D. M. Sedgwick, C. Santi, R. Ruzziconi, V. A. Soloshonok, *Chemistry* **2019**, *25*, 11797-11819.
- [98] B. K. Park, N. R. Kitteringham, P. M. O'Neill, *Annu. Rev. Pharmacol. Toxicol.* **2001**, *41*, 443-470.
- [99] K. Panigrahi, D. L. Nelson, D. B. Berkowitz, *Chem. Biol.* **2012**, *19*, 666-667.

References

- [100] a) D. E. Bergstrom, P. W. Shum, *The Journal of Organic Chemistry* **2002**, *53*, 3953-3958; b) D. E. Bergstrom, A. W. Mott, E. De Clercq, J. Balzarini, D. J. Swartling, *ChemInform* **2010**, *24*, no-no; c) G. M. Blackburn, F. Eckstein, D. E. Kent, T. D. Perrée, *Nucleosides and Nucleotides* **2006**, *4*, 165-167.
- [101] a) A. Arrendale, K. Kim, J. Y. Choi, W. Li, R. L. Geahlen, R. F. Borch, *Chem. Biol.* **2012**, *19*, 764-771; b) K. Panigrahi, M. Eggen, J. H. Maeng, Q. Shen, D. B. Berkowitz, *Chem. Biol.* **2009**, *16*, 928-936.
- [102] L. Gabrielli, C. Airoidi, P. Sperandeo, S. Gianera, A. Polissi, F. Nicotra, L. Cipolla, *European Journal of Organic Chemistry* **2013**, *2013*, 7776-7784.
- [103] W. Hoffmann, J. Langenhan, S. Huhmann, J. Moschner, R. Chang, M. Accorsi, J. Seo, J. Rademann, G. Meijer, B. Kokschi, M. T. Bowers, G. von Helden, K. Pagel, *Angew. Chem. Int. Ed. Engl.* **2019**, *58*, 8216-8220.
- [104] a) C. B. Millard, G. Koellner, A. Ordentlich, A. Shafferman, I. Silman, J. L. Sussman, *J. Am. Chem. Soc.* **1999**, *121*, 9883-9884; b) C. B. Millard, G. Kryger, A. Ordentlich, H. M. Greenblatt, M. Harel, M. L. Raves, Y. Segall, D. Barak, A. Shafferman, I. Silman, J. L. Sussman, *Biochemistry* **1999**, *38*, 7032-7039.
- [105] I. P. Street, C. D. Poulter, *Biochemistry* **1990**, *29*, 7531-7538.
- [106] M. B. van Niel, I. Collins, M. S. Beer, H. B. Broughton, S. K. Cheng, S. C. Goodacre, A. Heald, K. L. Locker, A. M. MacLeod, D. Morrison, C. R. Moyes, D. O'Connor, A. Pike, M. Rowley, M. G. Russell, B. Sohal, J. A. Stanton, S. Thomas, H. Verrier, A. P. Watt, J. L. Castro, *J. Med. Chem.* **1999**, *42*, 2087-2104.
- [107] Y. Kokuryo, K. Kawata, T. Nakatani, A. Kugimiya, Y. Tamura, K. Kawada, M. Matsumoto, R. Suzuki, K. Kuwabara, Y. Hori, M. Ohtani, *J. Med. Chem.* **1997**, *40*, 3280-3291.
- [108] J. F. DeBernardis, D. J. Kerkman, M. Winn, E. N. Bush, D. L. Arendsen, W. J. McClellan, J. J. Kyncl, F. Z. Basha, *J Med Chem* **1985**, *28*, 1398-1404.
- [109] F. Lopez-Munoz, C. Alamo, *Brain Res. Bull.* **2009**, *79*, 130-141.
- [110] WHO, *List of Essential Medicines – 22nd List (2021)*.
- [111] B. K. Park, N. R. Kitteringham, *Drug Metab. Rev.* **1994**, *26*, 605-643.
- [112] <https://www.nhs.uk/mental-health/talking-therapies-medicine-treatments/medicines-and-psychiatry/ssri-antidepressants/overview/>.

References

- [113] R. Huddart, J. K. Hicks, L. B. Ramsey, J. R. Strawn, D. M. Smith, M. Bobonis Babilonia, R. B. Altman, T. E. Klein, *Pharmacogenet. Genomics* **2020**, *30*, 26-33.
- [114] C. Dollery, *Therapeutic Drugs*, Churchill Livingstone, Edinburgh, UK, **1999**.
- [115] <https://www.gelbe-liste.de/wirkstoffgruppen/ssri>.
- [116] J. G. Liehr, G. M. Stancel, L. P. Chorich, G. R. Bousfield, A. Ari Ulubelen, *Chemico-Biological Interactions* **1986**, *59*, 173-184.
- [117] A. C. Stalford, J. L. Maggs, T. L. Gilchrist, B. K. Park, *Steroids* **1997**, *62*, 750-761.
- [118] T. D. Penning, J. J. Talley, S. R. Bertenshaw, J. S. Carter, P. W. Collins, S. Docter, M. J. Graneto, L. F. Lee, J. W. Malecha, J. M. Miyashiro, R. S. Rogers, D. J. Rogier, S. S. Yu, G. D. Anderson, E. G. Burton, J. N. Cogburn, S. A. Gregory, C. M. Koboldt, W. E. Perkins, K. Seibert, A. W. Veenhuizen, Y. Y. Zhang, P. C. Isakson, *Journal of Medicinal Chemistry* **1997**, *40*, 1347-1365.
- [119] S. Dugar, N. Yumibe, J. W. Clader, M. Vizziano, K. Huie, M. Van Heek, D. S. Compton, H. R. Davis, *Bioorg. Med. Chem. Lett.* **1996**, *6*, 1271-1274.
- [120] a) P. Shah, A. D. Westwell, *J Enzyme Inhib Med Chem* **2007**, *22*, 527-540; b) S. Purser, P. R. Moore, S. Swallow, V. Gouverneur, *Chemical Society Reviews* **2008**, *37*, 320-330; c) E. P. Gillis, K. J. Eastman, M. D. Hill, D. J. Donnelly, N. A. Meanwell, *Journal of Medicinal Chemistry* **2015**, *58*, 8315-8359; d) S. Swallow, *Prog. Med. Chem.* **2015**, *54*, 65-133.
- [121] a) P. R. Savoie, J. T. Welch, *Chemical reviews* **2015**, *115*, 1130-1190; b) J. G. Kim, O.-Y. Kang, S. M. Kim, G. Issabayeva, I. S. Oh, Y. Lee, W. H. Lee, H. J. Lim, S. J. Park, *Molecules (Basel, Switzerland)* **2020**, *25*, 5536; c) V. Debrauwer, I. Leito, M. Lõkov, S. Tshepelevitsh, M. Parmentier, N. Blanchard, V. Bizet, *ACS Organic & Inorganic Au* **2021**, *1*, 43-50.
- [122] A. Abula, Z. Xu, Z. Zhu, C. Peng, Z. Chen, W. Zhu, H. A. Aisa, *Journal of Chemical Information and Modeling* **2020**, *60*, 6242-6250.
- [123] W. M. Haynes, D. R. Lide, T. J. Bruno, *CRC Handbook of Chemistry and Physics*, 2016–2017 ed.
- [124] M. F. Sowaileh, R. A. Hazlitt, D. A. Colby, *ChemMedChem* **2017**, *12*, 1481-1490.

References

- [125] Y. Zhang, Y. Wang, C. He, X. Liu, Y. Lu, T. Chen, Q. Pan, J. Xiong, M. She, Z. Tu, X. Qin, M. Li, M. D. Tortorella, J. J. Talley, *Journal of Medicinal Chemistry* **2017**, *60*, 4135-4146.
- [126] J.-A. Ma, D. Cahard, *J. Fluor. Chem.* **2007**, *128*, 975-996.
- [127] a) P. R. Savoie, J. T. Welch, *Chemical reviews* **2015**, *115*, 1130-1190; b) L. Grigolato, W. D. G. Brittain, A. S. Hudson, M. M. Czyzewska, S. L. Cobb, *J. Fluor. Chem.* **2018**, *212*, 166-170.
- [128] R. Schmutzler, *Inorganic Chemistry* **1963**, *3*, 410-415.
- [129] R. Schmutzler, *J. Am. Chem. Soc.* **1964**, *86*, 4500-4502.
- [130] a) L. Lunazzi, S. Brownstein, *Journal of Magnetic Resonance* **1969**, *1*, 119; b) F. N. Tebbe, E. L. Muetterties, *Inorganic Chemistry* **1967**, *6*, 129-132; c) R. W. Rudolph, C. W. Schultz, *J. Am. Chem. Soc.* **1971**, *93*, 1898-1903; d) R. Schmutzler, *Angewandte Chemie* **1965**, *77*, 530-541.
- [131] in *Kirk-Othmer Encyclopedia of Chemical Technology, Vol. 1*, 4th ed. ed., John Wiley and Sons., New York, NY, **1991**, pp. V11 405-406.
- [132] a) E. L. Muetterties, T. A. Bither, M. W. Farlow, D. D. Coffman, *J. Inorg. Nucl. Chem.* **1960**, *16*; b) W. Mahler, E. L. Muetterties, *J. Chem. Phys.* **1960**, *33*.
- [133] X. Chen, W. Xu, M. H. Engelhard, J. Zheng, Y. Zhang, F. Ding, J. Qian, J.-G. Zhang, *Journal of Materials Chemistry A* **2014**, *2*, 2346-2352.
- [134] H. Bode, G. Teufer, *Zeitschrift für anorganische und allgemeine Chemie* **1952**, *268*, 20-24.
- [135] W. S. Sheldrick, *Journal of the Chemical Society, Dalton Transactions* **1974**, 1402-1405.
- [136] N. V. Pavlenko, L. A. Babadzhanova, I. I. Gerus, Y. L. Yagupolskii, W. Tyrra, D. Naumann, *Eur J Inorg Chem* **2007**, *2007*, 1501-1507.
- [137] N. Ignatyev, P. Barthen, K. Koppe, W. Frank, *Vol. WO 2016/074757 A*, **2016**.
- [138] C. Tian, W. L. Nie, M. V. Borzov, P. F. Su, *Organometallics* **2012**, *31*, 1751-1760.
- [139] B. Vabre, K. Chansaenpak, M. Wang, H. Wang, Z. Li, F. P. Gabbai, *Chem. Commun. (Camb)* **2017**, *53*, 8657-8659.
- [140] O. I. Guzyr, S. V. Zasukha, Y. G. Vlasenko, A. N. Chernega, A. B. Rozhenko, Y. G. Shermolovich, *Eur J Inorg Chem* **2013**, *2013*, 4154-4158.
- [141] M. Könner, Freie Universität Berlin (Berlin), **2012**.

References

- [142] S. Wagner, Freie Universität Berlin (Berlin), **2016**.
- [143] L. Wang, X. J. Wei, W. L. Lei, H. Chen, L. Z. Wu, Q. Liu, *Chem. Commun. (Camb)* **2014**, 50, 15916-15919.
- [144] D. J. Burton, R. Takei, S. Shinya, *J. Fluor. Chem.* **1981**, 18, 197-202.
- [145] D. J. Burton, T. Ishihara, M. Maruta, *Chem Lett* **1982**, 11, 755-758.
- [146] a) W. Qiu, D. J. Burton, *J. Fluor. Chem.* **2013**, 155, 45-51; b) W. Qiu, D. J. Burton, *Tetrahedron Letters* **1996**, 37, 2745-2748.
- [147] L. G. Sprague, D. J. Burton, R. D. Guneratne, W. E. Bennett, *J. Fluor. Chem.* **1990**, 49, 75-85.
- [148] C. Meyer, M. Köhn, *Synthesis* **2011**, 2011, 3255-3260.
- [149] C. E. McKenna, M. T. Higa, N. H. Cheung, M.-C. McKenna, *Tetrahedron Letters* **1977**, 18, 155-158.
- [150] S. Wagner, M. Accorsi, J. Rademann, *Chemistry* **2017**, 23, 15387-15395.
- [151] a) T. R. Burke, M. S. Smyth, A. Otaka, P. P. Roller, *Tetrahedron Letters* **1993**, 34, 4125-4128; b) T. R. Burke, Jr., *Curr Top Med Chem* **2006**, 6, 1465-1471; c) J. T. R. Burke, P. Russ, B. Lim, *Synthesis* **1991**, 1991, 1019-1020.
- [152] H. H. Bosshard, R. Mory, M. Schmid, H. Zollinger, *Helvetica Chimica Acta* **1959**, 42, 1653-1658.
- [153] L. Mohammadkhani, M. M. Heravi, *ChemistrySelect* **2019**, 4, 6309-6337.
- [154] A. J. Gutierrez, E. J. Prisbe, J. C. Rohloff, *Nucleosides Nucleotides Nucleic Acids* **2001**, 20, 1299-1302.
- [155] a) W. Q. Liu, B. P. Roques, C. Garbay, *Tetrahedron Letters* **1997**, 38, 1389-1392; b) O. M. Green, *Tetrahedron Letters* **1994**, 35, 8081-8084; c) S. A. Biller, C. Forster, E. M. Gordon, T. Harrity, W. A. Scott, C. P. Ciosek, Jr., *J Med Chem* **1988**, 31, 1869-1871.
- [156] G. M. Blackburn, D. Ingleson, *Journal of the Chemical Society, Perkin Transactions 1* **1980**.
- [157] F. Klanberg, Muettert.El, *Inorganic Chemistry* **1968**, 7, 155-&.
- [158] J. E. Griffiths, *Spectrochimica Acta Part A: Molecular Spectroscopy* **1968**, 24, 303-310.
- [159] T. Murano, H. Takechi, Y. Yuasa, T. Yokomatsu, I. Umesue, S. Soeda, H. Shimeno, S. Shibuya, *Arkivoc* **2003**, 2003, 256-266.

References

- [160] N. N. Bhongle, R. H. Notter, J. G. Turcotte, *Synthetic Communications* **1987**, *17*, 1071-1076.
- [161] T. Morita, Y. Okamoto, H. Sakurai, *Chem Lett* **1980**, *9*, 435-438.
- [162] D. Wynn, *Talanta* **1984**, *31*, 1036-1040.
- [163] J. H. Clark, C. W. Jones, H. Smith, N. Boechat, *J. Fluor. Chem.* **1991**, *54*.
- [164] F. S. Fawcett, C. W. Tullock, D. D. Coffman, *J. Am. Chem. Soc.* **1962**, *84*, 4275-4285.
- [165] H. Henle, M. Geisel, R. Mews, *J. Fluor. Chem.* **1984**, *26*, 133-148.
- [166] D. J. Burton, D. M. Wiemers, *J. Am. Chem. Soc.* **1985**, *107*, 5014-5015.
- [167] M. Roudias, F. Vallee, J. Martel, J. F. Paquin, *J Org Chem* **2018**, *83*, 8731-8738.
- [168] R. Pascal, R. Sola, *Tetrahedron Letters* **1998**, *39*, 5031-5034.
- [169] L. D. Freedman, G. O. Doak, *Chemical reviews* **1957**, *57*, 479-523.
- [170] L. E. Sutton, H. J. M. Bowen, *Tables of Interatomic Distances and Configuration in Molecules and Ions*, Chemical Society, London, **1958**.
- [171] L. S. Bartell, L.-S. Su, H. Yow, *Inorganic Chemistry* **1970**, *9*, 1903-1912.
- [172] B. Gamoke, D. Neff, J. Simons, *J Phys Chem A* **2009**, *113*, 5677-5684.
- [173] B. A. Bunin, *The combinatorial Index*, Elsevier, **1998**.
- [174] S. Matsuura, C. H. Niu, J. S. Cohen, *J Chem Soc Chem Comm* **1976**, 451-452.
- [175] R. Bollhagen, M. Schmiedberger, K. Barlos, E. Grell, *J Chem Soc Chem Comm* **1994**, 2559-2560.
- [176] a) T. R. Burke, Jr., H. K. Kole, P. P. Roller, *Biochem Biophys. Res. Commun.* **1994**, *204*, 129-134; b) H. K. Kole, M. Akamatsu, B. Ye, X. Yan, D. Barford, P. P. Roller, T. R. Burke, Jr., *Biochemical and biophysical research communications* **1995**, *209*, 817-822; c) T. R. Burke, Jr., B. Ye, M. Akamatsu, H. Ford, Jr., X. Yan, H. K. Kole, G. Wolf, S. E. Shoelson, P. P. Roller, *J Med Chem* **1996**, *39*, 1021-1027; d) Z. Jia, D. Barford, A. J. Flint, N. K. Tonks, *Science* **1995**, *268*, 1754-1758; e) T. R. Burke, Z.-J. Yao, H. Zhao, G. W. A. Milne, L. Wu, Z.-Y. Zhang, J. H. Voigt, *Tetrahedron* **1998**, *54*, 9981-9994; f) Y. Gao, L. Wu, J. H. Luo, R. Guo, D. Yang, Z.-Y. Zhang, T. R. Burke, *Bioorg. Med. Chem. Lett.* **2000**, *10*, 923-927.

References

- [177] S. Y. Lee, F. Liang, X. L. Guo, L. Xie, S. M. Cahill, M. Blumenstein, H. Yang, D. S. Lawrence, Z. Y. Zhang, *Angew Chem Int Ed Engl* **2005**, *44*, 4242-4244.
- [178] K. Neumann, J. Farnung, S. Baldauf, J. W. Bode, *Nat. Commun.* **2020**, *11*, 982.
- [179] R. Behrendt, S. Huber, R. Marti, P. White, *J. Pept. Sci.* **2015**, *21*, 680-687.
- [180] M. Mergler, F. Dick, B. Sax, P. Weiler, T. Vorherr, *J. Pept. Sci.* **2003**, *9*, 36-46.
- [181] T. Michels, R. Dölling, U. Haberkorn, W. Mier, *Organic letters* **2012**, *14*, 5218-5221.
- [182] K. Holland-Nell, M. I. Fernandez-Bachiller, Ahsanullah, J. Rademann, *Org Lett* **2014**, *16*, 4428-4431.
- [183] K. O. Christe, W. W. Wilson, R. D. Wilson, R. Bau, J. A. Feng, *J. Am. Chem. Soc.* **1990**, *112*, 7619-7625.
- [184] C. Yung-Chi, W. H. Prusoff, *Biochemical Pharmacology* **1973**, *22*, 3099-3108.
- [185] J. Ge, H. Wu, S. Q. Yao, *Chem. Commun. (Camb)* **2010**, *46*, 2980-2982.
- [186] M. N. Qabar, J. Urban, M. Kahn, *Tetrahedron* **1997**, *53*, 11171-11178.